



TECHNISCHE UNIVERSITÄT MÜNCHEN

FAKULTÄT CHEMIE

LEHRSTUHL ORGANISCHE CHEMIE II

ELUCIDATING THE MECHANISM OF ACTION OF THE NATURAL
PRODUCT XANTHOCILLIN X

TAILORED COFACTOR TRAPS FOR THE *IN SITU* DETECTION OF
HEMITHIOACETAL-FORMING PYRIDOXAL KINASES

DISSERTATION ZUR ERLANGUNG DES AKADEMISCHEN GRADES
EINES DOKTORS DER NATURWISSENSCHAFTEN VON

INES HÜBNER

MÜNCHEN 2020



TECHNISCHE UNIVERSITÄT MÜNCHEN

FAKULTÄT CHEMIE

LEHRSTUHL ORGANISCHE CHEMIE II

ELUCIDATING THE MECHANISM OF ACTION OF THE NATURAL
PRODUCT XANTHOCILLIN X &

TAILORED COFACTOR TRAPS FOR THE *IN SITU* DETECTION OF
HEMITHIOACETAL-FORMING PYRIDOXAL KINASES

Ines Hübner

Vollständiger Abdruck der von der Fakultät für Chemie der Technischen Universität
München zur Erlangung des akademischen Grades eines
Doktors der Naturwissenschaften (Dr. rer. nat.)

genehmigten Dissertation.

Vorsitzender: Prof. Dr. Franz Hagn
Prüfer der Dissertation: 1. Prof. Dr. Stephan A. Sieber
2. Prof. Dr. Cathleen Zeymer
3. Assoc. Prof. Dr. William Wuest

Die Dissertation wurde am 27.11.2020 bei der Technischen Universität München eingereicht und
durch die Fakultät für Chemie am 26.01.2021 angenommen.

Danksagung

An dieser Stelle möchte ich mich bei den Personen bedanken, die diese Arbeit überhaupt möglich gemacht haben.

Mein erster Dank geht an meinen Betreuer Prof. Dr. Stephan A. Sieber. Ich möchte mich bei ihm nicht nur für das Angebot der Promotionsstelle und die gute Betreuung bedanken, sondern auch für das entgegengebrachte Vertrauen, die wissenschaftliche Freiheit und die Unterstützung bei der Realisierung meines Forschungsaufenthaltes an der Emory University in Atlanta. Hierbei möchte ich mich auch sehr bei Prof. William M. Wuest bedanken, der mich für drei Monate in seiner Arbeitsgruppe sehr herzlich und offen aufgenommen und mich und mein Projekt immer enthusiastisch unterstützt hat. Vielen Dank!

Ebenfalls danke ich meinen Kooperationspartnern Jörn Hoßmann sowie Justin Shapiro für die gute Zusammenarbeit. Ich möchte mich außerdem bei Markus Lakemeyer für seine großartige Unterstützung während meiner Masterarbeit und auch für alle Tipps & Tricks danach bedanken. Ein großes Dankeschön geht auch an meine zahlreichen Praktikanten Markus Schwarz, Alexander Henrici, Maximilian Zierke, Marija Sorokina, Benedikt Winkler, Michaela Fiedler und Denis Rühmann sowie Masteranden Julia Friederich, Jan-Niklas Dienemann und Markus Schwarz (ja, noch einmal) für die tatkräftige Unterstützung in den Projekten.

Außerdem ein riesiges Dankeschön an Patrick Zanon, Carolin Gleißner, Martin Pfanzelt, Robert Maccsics, Dietrich Mostert, Isabel Wilkinson und Stuart Ruddell für die Korrektur dieser Arbeit!

Mona Wolff möchte ich für ihre großartige Unterstützung und ihren unermüdlichen Einsatz in den Laboren danken – das hilft uns wirklich sehr! Katja Bäuml und Nina

Bach mitsamt dem MS-Team danke ich für die Wartung unserer MS-Diven. Bei Barbara Eyermann und Angela Weigert Muñoz möchte ich mich für die unkomplizierte und effiziente Zusammenarbeit bei unserem Group-Job bedanken.

Während der gesamt Zeit bin ich wirklich sehr gerne in die Arbeit gegangen, was natürlich auch an den großartigen Mitgliedern dieses Arbeitskreises liegt, mit denen man auch gerne nach Feierabend noch mehr Zeit verbringt. Viele lustige Momente und lange Abende mit diversen Diskussionen und zweideutigen Witzen haben die letzten vier Jahre zu einer unvergesslichen Zeit gemacht. Dafür möchte ich mich bei den Patricks A bis Z, Till Reinhardt, Stuart Ruddell, Robert Macsics, Angela Weigert Muñoz, Carolin Gleißner, Martin Pfanzelt, Theresa Rauh, Dóra Balogh, Franziska Mandl, Josef Braun, Jan-Niklas Dienemann, Konstantin Eckl, Alexandra Geißler, Thomas Gronauer, Dietrich Mostert, Isabel Wilkinson, Stephan Hacker, Michael Zollo und Christina Brumer bedanken! Erwähnen möchte ich auch die „ältere Generation“, die während meiner Zeit den Arbeitskreis verlassen haben, Mathias Hackl, Christian Fetzner, Anja Fux, Volker Kirsch, Annabelle Hoegl, Barbara Eyermann, Pavel Kielkowski, Philipp Le und Markus Lakemeyer.

Mein größter Dank gilt jedoch meiner Familie, die mich unglaublich geduldig bei den vielen Stationen meiner Ausbildung unterstützt haben, und Jonas Drechsel, der mir immer verständnisvoll zur Seite steht.

Vielen Dank!

Abstract

The family of isonitrile natural products, such as xanthocillin X (Xan), exhibits promising antibacterial properties. Despite this exceptional trait, their cellular targets are largely unknown. Based on the nanomolar potency of Xan against diverse difficult-to-treat Gram-negative bacteria, including the critical priority pathogen *Acinetobacter baumannii*, in-depth studies to decipher its mechanism of action were performed in the scope of this work. While initial studies into Xan's ability to bind metals and the search for cellular protein targets did not yield conclusive results, resistant mutants for genome sequencing could be generated. Strikingly, only one conserved mutation in the heme biosynthesis enzyme porphobilinogen synthase (PbgS) was uncovered, leading to reduced enzymatic efficiency. Corresponding upregulation of heme degrading enzymes in the mutants suggested a mechanism by which the cell downregulates heme levels. In contrast, Xan-treated wild type cells exhibited upregulated transport systems for acquisition of heme precursors along with highly elevated levels of porphyrin suggesting an uncontrolled heme biosynthesis. It was demonstrated that this previously unknown mechanism is based on the direct sequestration of heme by Xan preventing its accessibility to cognate binding sites, a prerequisite for regulated heme biosynthesis. As a consequence, elevated levels of porphyrins induce reactive oxygen species which are deleterious for cell viability. Thus, Xan represents a promising antibiotic lead compound displaying activity even against multidrug resistant strains, while exhibiting low toxicity to human cells and to greater wax moth larvae (*Galleria mellonella*).

Pyridoxal kinases (PLK) are important enzymes for the biosynthesis of pyridoxal phosphate, an essential cofactor of numerous enzymatic reactions. The evolution of PLKs resulted in enzymes with structural diversity. In a subclass of these kinases, the

role of a cysteine embedded within a distant flexible lid region has recently been deciphered. This lid cysteine forms a hemithioacetal with the aldehyde of pyridoxal and is essential for its phosphorylation. Despite the presence of these enzymes in various organisms, no tool to investigate the relevance of this lid residue has been available to date. In this work, probes based on the pyridoxal core structure were developed, each equipped with a cysteine-reactive warhead instead of the aldehyde. These probes mimic the cofactor and irreversibly intercept the nucleophilic attack of the lid cysteine. An alkyne-tag placed at two different positions within the pyridoxal structure enables the enrichment of PLKs from living cells. Importantly, these probes showed a preference for either Gram-positive or Gram-negative PLKs depending on the position of the alkyne-tag. The cofactor mimics were used to validate not only the previously studied PLKs of *Staphylococcus aureus* and *Enterococcus faecalis*, but also the PLKs of *Escherichia coli* and *Pseudomonas aeruginosa*, thus deciphering a crucial role of the lid cysteine in catalysis. Overall, these tailored probes allowed a reliable identification of reactive lid cysteines, which qualifies them as chemical tools for the detection of further representatives of this enzyme class in various organisms.

Zusammenfassung

Die Naturstoffklasse der Isonitrile weist vielversprechende antibakterielle Aktivitäten auf. Trotz dieser außergewöhnlichen Eigenschaft sind ihre zellulären Ziele weitgehend unbekannt. Basierend auf der nanomolaren Aktivität von Xanthocillin X (Xan) gegen verschiedene schwer behandelbare Gramnegative Bakterien, einschließlich des kritischen Erregers *Acinetobacter baumannii*, wurde im Rahmen dieser Arbeit eine umfassende Studie durchgeführt, um den Wirkmechanismus zu entschlüsseln. Da sich bei ersten Studien weder Metallbindungen noch zelluläre Proteinziele als relevant für die antibiotische Aktivität von Xan erwiesen, wurden resistente Kolonien für die Genomsequenzierung generiert. Diese identifizierte eine konservierte Mutation in einem Enzym der Häm-Biosynthese, nämlich der Porphobilinogen-Synthase (PbgS), die zu einer verminderten enzymatischen Effizienz führte. Eine entsprechende Hochregulierung der Häm-abbauenden Enzyme in den Mutanten deutete auf einen Resistenzmechanismus hin, durch den die Zelle das Häm-Niveau reduziert. Umgekehrt wiesen mit Xan behandelte Wildtypzellen hochregulierte Transportsysteme für die Aufnahme von Häm-Vorläufern auf, was zusammen mit stark erhöhten Porphyrinspiegeln auf eine unkontrollierte Häm-Biosynthese hindeutete. Es konnte gezeigt werden, dass dieser bisher unentdeckte Mechanismus auf der direkten Sequestrierung von Häm durch Xan beruht, wodurch dessen Zugang zu regulatorischen Bindungsstellen verhindert wird, was eine Voraussetzung für eine kontrollierte Häm-Biosynthese ist. Infolgedessen führten erhöhte Porphyrinkonzentrationen zu reaktiven Sauerstoffspezies, die für die Vitalität der Zellen schädlich sind. Xan stellt somit eine vielversprechende antibiotische Leitstruktur dar, die sogar gegen multiresistente Stämme aktiv ist und gleichzeitig eine geringe Toxizität für menschliche Zellen und Larven der Großen Wachsmotte (*Galleria mellonella*) aufweist.

Pyridoxalkinasen (PLK) sind wichtige Enzyme für die Biosynthese von Pyridoxalphosphat, einem essentiellen Kofaktor zahlreicher enzymatischer Reaktionen. Die Evolution brachte Enzyme mit struktureller Vielfalt hervor. Bei einer Unterklasse dieser Kinasen wurde kürzlich die Rolle eines Cysteins, das in einer entfernten flexiblen Deckelregion eingebettet ist, demonstriert. Dieses Deckel-Cystein bildet mit dem Aldehyd ein Hemithioacetal und ist für die Phosphorylierung essentiell. Trotz der Präsenz dieser Enzyme in verschiedenen Organismen standen bisher keine Methoden zur Verfügung, um die Relevanz dieses Deckelrestes zu untersuchen. Im Rahmen dieser Arbeit wurden Sonden basierend auf dem Grundgerüst des Pyridoxals entwickelt, die jeweils mit einer Cystein-reaktiven Gruppe anstelle des Aldehyds ausgestattet wurden. Diese Sonden imitieren den Kofaktor und fangen den nukleophilen Angriff des Deckel-Cysteins irreversibel ab. Ein Alkin-Rest, der an zwei verschiedenen Positionen innerhalb der Pyridoxalstruktur platziert wurde, ermöglicht die Anreicherung von PLKs aus lebenden Zellen. Interessanterweise zeigten die Sonden je nach Position des Alkin-Rests eine Präferenz für entweder Grampositive oder Gramnegative PLKs. Durch Anwendung der Kofaktor-Imitatoren konnten nicht nur die zuvor bereits erforschten PLKs von *Staphylococcus aureus* und *Enterococcus faecalis* validiert werden, sondern auch die PLKs von *Escherichia coli* und *Pseudomonas aeruginosa*, wodurch eine entscheidende Rolle des Deckel-Cysteins für ihre Katalyse entschlüsselt werden konnte. Insgesamt ermöglichten diese maßgeschneiderten Sonden einen zuverlässigen Nachweis des Deckel-Cysteins in diesen PLKs, was sie als chemische Werkzeuge für die Identifikation weiterer Vertreter dieser Enzymklasse in diversen Organismen qualifiziert.

Introductory remarks

Results of this work have been published as follows:

Hübner, I., Shapiro J. A., Hoßmann, J., Drechsel J., Hacker, S. M., Rather, P. N., Pieper, D. H., Wuest, W. M., Sieber, S. A., The broad spectrum antibiotic xanthocillin X effectively kills *Acinetobacter baumannii* via dysregulation of heme biosynthesis, *ACS Cent. Sci.* 2021, 7, 3, 488–498.

Hübner, I.*, Dienemann, J.-N.*, Friederich, J., Schneider, S., Sieber, S. A., Tailored cofactor traps for the *in situ* detection of hemithioacetal-forming pyridoxal kinases. *ACS Chem. Biol.* 2020, 15, 12, 3227–3234.

Table of Contents

I. Introduction	1
1. Natural Products as Source for Novel Antibiotics.....	3
1.1. Antibiotic Crisis.....	3
1.2. Natural Products in Antibacterial Drug Discovery.....	5
2. Target Identification of Natural Products	9
2.1. Macromolecule Biosynthesis Assay	10
2.2. Activity-Based Protein Profiling (ABPP).....	12
2.3. Selection of Resistant Mutants	15
II. Elucidating the Mechanism of Action of the Natural Product Xanthocillin X.....	19
1. The Natural Product Class of Xanthocillin X	21
2. Results and Discussion.....	24
2.1. Synthesis of Xanthocillin and its Derivatives	24
2.2. Antibacterial Screen	26
2.3. Metal Binding Studies	27
2.4. Protein Target Identification by Chemical Proteomics.....	29
2.5. Target Identification by Selection of Resistant Mutants	34
2.6. Porphobilinogen Synthase	36
2.7. Whole Proteome Analysis	42
2.8. Heme Binding	45
2.9. Extraction and Quantification of Porphyrins.....	48
2.10. Time-Kill Experiments.....	49
2.11. Checkerboard Assay	50
2.12. Toxicity and <i>Galleria mellonella</i> Infection Model.....	51
2.13. Summary – Mechanism of Action	54
2.14. Outlook.....	57
3. Experimental Section.....	58
3.1. Media	58
3.2. Stock Solutions	58
3.3. Overnight Cultures	59
3.4. Minimum Inhibitory Concentration (MIC)	59
3.5. Metal Chelation Assay	59
3.6. Gel-free ABPP and AfBPP	60
3.7. Gel-based ABPP	64
3.8. Cloning.....	65
3.9. Catalases-Peroxidases (<i>AbcCAT</i> , <i>EcCAT</i>)	74
3.10. Generation and Sequencing of Xan-resistant <i>A. baumannii</i> ATCC19606.....	75
3.11. Porphobilinogen Synthase (<i>PbgS</i>)	77
3.12. Whole Proteome Analysis	81
3.13. UV-Vis Spectroscopy	84
3.14. Hemin Decomposition.....	84

3.15.	Measuring Regulatory Heme (RH).....	85
3.16.	Porphyrin Quantification.....	87
3.17.	Time-kill Assays.....	87
3.18.	Checkerboard Assay.....	88
3.19.	MTT Assay.....	89
3.20.	<i>Galleria mellonella</i> Assay.....	90
3.21.	Chemical Synthesis.....	91
III.	<i>Tailored Cofactor Traps for the in Situ Detection of Hemithioacetal-Forming Pyridoxal Kinases</i>	107
1.	Vitamin B₆	109
2.	Results and Discussion	114
2.1.	Synthesis and Biological Evaluation of Inhibitors and Probes.....	115
2.2.	<i>In situ</i> Profiling in Gram-positive Bacteria.....	120
2.3.	<i>In situ</i> Profiling in Gram-negative Bacteria.....	122
2.4.	Conclusion and Outlook.....	125
3.	Experimental Section	128
3.1.	Bacterial Cultures.....	128
3.2.	Cloning of Pyridoxal Kinases.....	128
3.3.	Protein Overexpression and Purification.....	130
3.4.	Intact Protein Mass Spectrometry (IPMS).....	131
3.5.	Activity-based Protein Profiling.....	132
3.6.	PLK Inhibition Assay.....	135
3.7.	PLK Activity Assay in Lysate.....	136
3.8.	Computational Modeling.....	137
3.9.	Chemical Synthesis.....	138
IV.	<i>Bibliography</i>	149
V.	<i>Appendix</i>	169

I. Introduction

1. Natural Products as Source for Novel Antibiotics

1.1. Antibiotic Crisis

Since the discovery of penicillin by Alexander Fleming about 100 years ago,¹ antibiotics have not only saved the lives of patients with bacterial infection, they have also enabled surgery for patients with other conditions. In cancer therapy or for organ transplantation, for example, effective antibiotics are needed to protect immunocompromised patients from infections. However, the rapid emergence of antimicrobial resistance endangers those life-saving medical measures, leading to predictions of 10 million deaths yearly by 2050 if no action is taken.² There are already strains of bacteria that are resistant to all or almost all available antibiotics, such as multidrug-resistant (MDR) *Pseudomonas* or *Acinetobacter* species.³ Reasons for this resistance development are manifold. For example, the excessive use of antibiotics in agriculture as well as inappropriate prescriptions of these drugs, leading to sub-inhibitory and sub-therapeutic doses, which support genetic alterations and promote the development of resistance.⁴ In the past, the pharmaceutical industry continuously developed new antibiotics, ensuring a supply of therapies against resistant bacteria. However, 15 of the 18 largest pharmaceutical companies have now discontinued antibiotics research, as strict approval requirements must first be met and thereafter the drug is available on the market only for a short time due to resistance development.⁵ The remaining companies have focused mainly on synergistic antibiotic combinations or on optimizing existing antibiotic scaffolds,^{6,7} which explains the innovation gap in new broad-spectrum compound classes since the discovery of fluoroquinolones 50 years ago.⁸ This is particularly problematic given the increasing prevalence of resistance mechanisms that affect an entire class of antibiotics, so-called cross-resistance. These include the expression of drug-inactivating enzymes, the modification of the target molecule, and modifications to reduce the cellular drug

concentration.⁹⁻¹² For example, several cross-resistance mechanisms are known to inactivate β -lactam antibiotics, characterised by their β -lactam ring, which is crucial for their activity. These antibiotics acetylate penicillin-binding proteins (PBP), which belong to the transpeptidase family and catalyse the cross-linking of the peptide side chains of adjacent glycan strands.^{13,14} Enzymes have been developed, so-called β -lactamases, which hydrolytically cleave the β -lactam ring, whereby the antibiotic loses its activity.¹²⁻¹⁴ Further, many of the β -lactam antibiotics target the same enzymes of the PBP family. The result of this selection pressure was the development of structurally modified PBPs, such as PBP 2a, which can no longer be inhibited by the respective β -lactams, leading to resistance to a large number of approved β -lactam antibiotics.¹² It should be noted that this is not the individual fate of β -lactams, but almost every class of antibiotics suffers from cross-resistance.^{10,15}

Modifications of a target protein are of particular concern since the antibiotics currently on the market mainly have only five different cellular targets, namely the biosynthesis of the cell wall, proteins, DNA/RNA and folate, or alternatively they lead to membrane disruption, each of which is attacked by several different antibiotic groups (Figure I-1).¹⁶⁻¹⁸ Thus, modifications of target proteins can cause cross-resistance to even chemically different classes of compounds which have overlapping binding sites. One example is the dimethylation of a single adenine in the nascent 23S rRNA, which is part of the large (50S) ribosomal subunit, that leads to cross-resistance to macrolides and lincosamide antibiotics.¹⁹ These examples illustrate that novel structures with new mechanism of action (MoA) are indispensable in the fight against resistant bacteria.

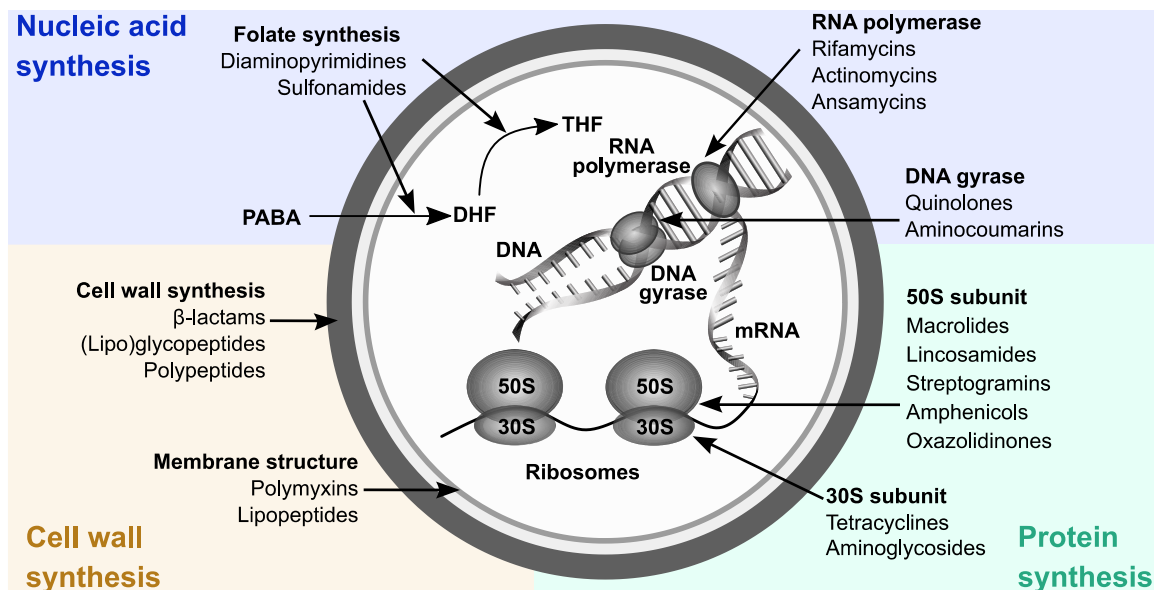


Figure I-1: Schematic overview of common antibiotic targets. Nucleic acid synthesis targets can be divided into DNA/RNA precursor synthesis, namely folate synthesis, and DNA/RNA synthesis (blue). Antibiotics that address the cell wall either inhibit cell wall synthesis or disrupt the membrane (orange). Within protein synthesis, 30S and 50S ribosomal subunits are the major targets of antibiotics (green).

1.2. Natural Products in Antibacterial Drug Discovery

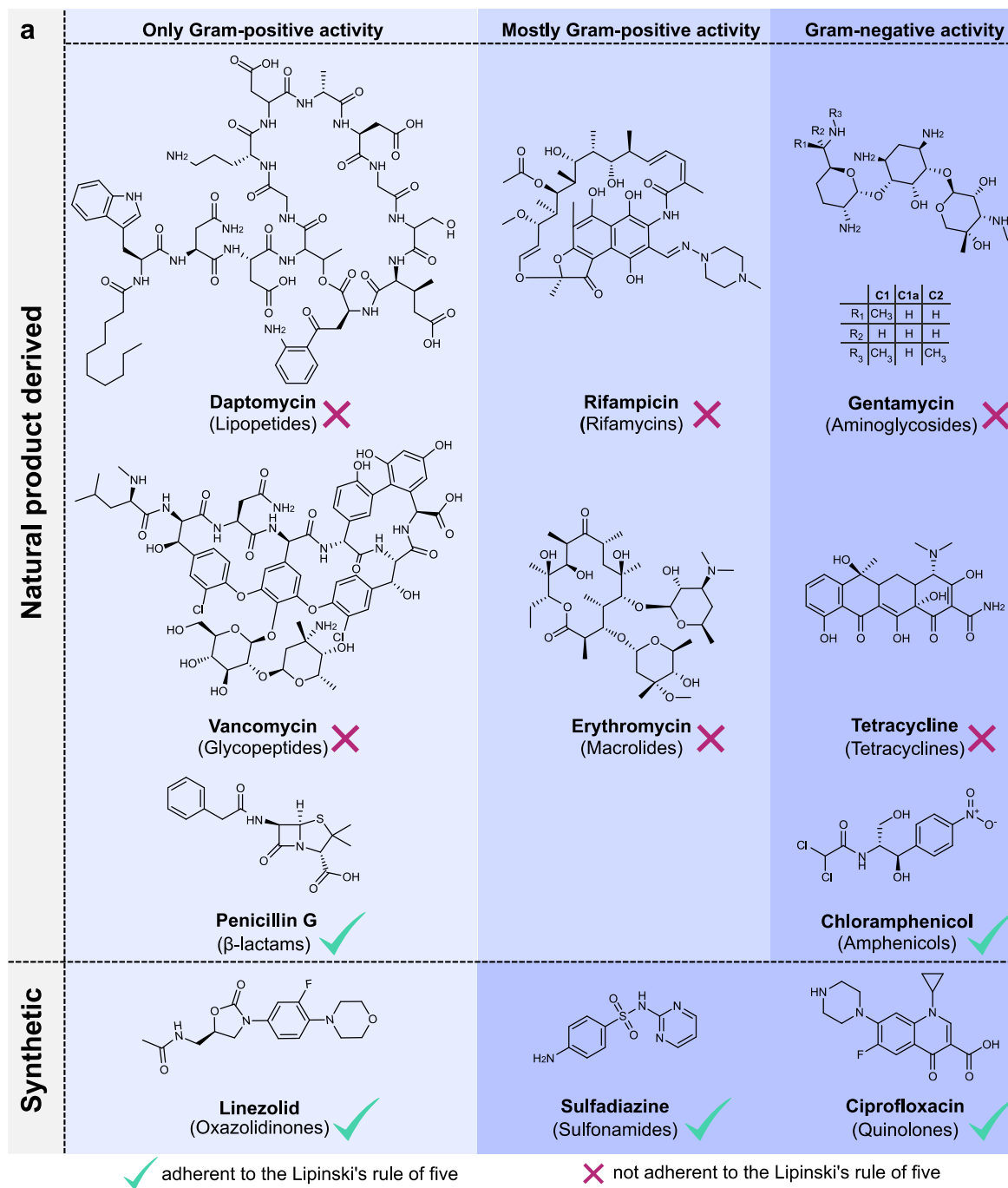
Nature has been an unsurpassed source for new lead compounds for antibacterial drug discovery.⁷ This is not surprising, since the properties of natural products (NP), such as cell permeability and target specificity, are fine-tuned by evolutionary processes to give the producing organism a survival advantage. Until the early 2000s, many pharmaceutical companies owned or worked with fully integrated NP groups that were able to perform fermentation, isolation, characterization and semi-synthesis on a large scale (e.g., Merck, Bayer). Thus, 74% of small molecules used of antibacterial therapy are derived from NPs, like rifampicin, or are NPs, such as erythromycin, daptomycin, and penicillin G (Figure I-2a).^{1,20-24} In addition, NP mixtures are also used, as is the case with the drug gentamicin, whose main components are gentamicin C₁, gentamicin C_{1a} and gentamicin C₂.^{25,26} Only a few classes are of purely synthetic origin, such as fluoroquinolones (e.g., ciprofloxacin) and sulfonamides (e.g.,

sulfadiazine), which is reflected in their very simple and synthetically accessible structures.

Despite the success of NPs in drug discovery, most companies have abandoned the field of NP research because many of the sources of cultivatable soil microorganisms have already been investigated and the risk of expending considerable resources on the "rediscovery" of old NPs is too high to justify further investments.⁷ Companies shifted their focus towards the screening of collections of synthetic compounds, that are easy to assemble, and can be synthesised *via* automated, combinatorial, or parallel synthesis.²⁷ These libraries for high-throughput screening (HTS) contain mainly molecules that follow Lipinski's rule of five, which defines the physiochemical requirements of small molecules for good oral bioavailability.²⁸ However, antibacterial compounds have always been considered an exception to these rules, as they occupy a distinct property space that is very different from drugs used in other therapeutic fields (Figure I-2).²⁹ The most probable reason for this is bacteria's different cell architecture, which strongly influences the permeability and efflux of antibacterial agents.^{30,31} Considering this fact, it is not very surprising that compounds with either only Gram-positive or only Gram-negative activity have very different properties, since the cell wall structures of these organisms differ considerably.^{29,31} Compounds with activity against Gram-negative organisms have to penetrate not only the inner membrane and the peptidoglycan layer, but also an outer membrane, which represents an impermeable barrier for many small molecules and the main reason why most antibiotics are ineffective against these bacteria.³² Porins, which create cylindrical openings (β -barrels) in the outer membrane with polar amino acid side chains coating the inside of the opening, have been shown to be major entry pathways for antibacterial compounds into these organisms.^{29,33} Therefore, highly polar molecules can preferentially penetrate the bacteria through these hydrophilic channels. This is in line with a study by O'Shea and Moser, which reports a mean

calculated logarithm of the partition coefficient between n-octanol and water ($\text{clog}P$) of -0.1 for compounds with Gram-negative activity, which is significantly lower than a reference pharmaceutical compound library that on average follows Lipinski's rule of five (mean $\text{clog}P$ of 2.7, Figure I-2b).²⁹ The importance of this property space is best exemplified by aminoglycosides (e.g., gentamycin) and fluoroquinolones (e.g., ciprofloxacin), which are highly polar antibiotic classes.^{28,29} In addition, this study revealed a mean molecular weight for these compounds of 414 Da with a clear molecular weight threshold of 600 Da, below which approximately 95% are found. However, for antibiotics that only act against Gram-positive bacteria, this threshold does not exist, with high molecular weight examples including macrolides, streptogramins, the lipopeptide daptomycin and cell wall active glycopeptides. The $\text{clog}P$ of these molecules differs only slightly from the reference library but they have highly complex structures, which are almost not found in HTS libraries.²⁹

These very different properties of antibiotics compared to the reference compound library can explain why HTS has had little success in discovering new antibiotics. It is therefore important to continue research on NPs and their MoA in order to successfully combat the increasing number of resistant bacteria. In the "golden age" of antibiotic discovery, a plethora of different NP scaffolds with antibacterial activity were discovered. However, their mechanistic and biological characterization is still in the fledgling stages. Therefore, the systematic investigation of these neglected structures for new MoAs represents an unexploited source for new drugs.



b

	Lipinski's rule of five	Reference pharm. cmpds.	Antibiotics (only Gram-positive activity)	Antibiotics (Gram-negative activity)
MW (Da)	< 500	338	813	414
clogP	< 5	2.7	2.1	-0.1
H-bond donors	< 5	1.6	7.1	5.1
H-bond acceptors	< 10	4.9	16.3	9.4

Figure I-2: Structures of antibiotics and their physicochemical properties. a) Structure of antibiotics classified by their activity and origin. b) Table contains Lipinski's rule of five, as well as a comparison of the physicochemical

properties of antibiotics (divided into only Gram-positive or Gram-positive and -negative activity) of a reference library of pharmaceutical molecules used for non-infection therapies.^{28,29}

2. Target Identification of Natural Products

Target identification of a bioactive substance, whether synthetic or natural, is a notoriously difficult task, but one that is of great value for drug discovery and development. Identifying the full spectrum of targets of a small molecule can help to optimize the lead structure more quickly and simultaneously minimize unwanted side effects caused by off-targets.³⁴ The toolbox for target discovery has developed rapidly in recent years and numerous methods are now available, each with its advantages and disadvantages.³⁵⁻³⁷

Traditional methods for discovering the target of an antibiotic small molecule include macromolecule biosynthesis assay, affinity chromatography and the generation of resistant mutants, which, due to technical advancements and improvements, are still the most commonly used techniques and will be discussed in the following sections.^{35,37}

Drug discovery of NPs faces the additional challenge of low compound availability, which complicates the application of some target identification strategies requiring compounds in milligram quantities. While laboratory cultures can produce compounds only at the microgram-per-litre scale, large-scale cultivation technologies can overcome this problem but are rarely available in the academic environment. In addition, the ease for the subsequent isolation and cleaning of the NP highly depends on its structure, stability and quantity. Also synthetic production is often very difficult, if at all possible, since many metabolites have very complex structures.³⁷

2.1. Macromolecule Biosynthesis Assay

The macromolecular biosynthesis assay (MBA) can be a good starting point to elucidate the MoA of an antibiotic agent. The method examines the effect of sub-inhibitory or sub-bactericidal concentrations of an antibiotic on the biosynthesis rate of macromolecules, thereby identifying the inhibition of cellular processes.^{38,39}

For this purpose, radiolabelled precursors, such as ³H-thymidine, ³H-uridine, ³H-leucine, ¹⁴C-*N*-acetylglucosamine specific for DNA, RNA, protein and cell wall synthesis, respectively, are used and the incorporation of these into the macromolecules is monitored (Figure I-3). While the radioactive count of a control without antimicrobial treatment is used as 100% incorporation of precursors, treatment with the corresponding control antibiotic serves as a positive control for inhibition of this biosynthetic pathway.^{34,38} In general, this method provides a first hint whether the compound specifically inhibits one of the four major biosynthetic pathways (DNA, RNA, protein and cell wall). If all cellular processes are affected by a compound at once, this is an indication of an unspecific mechanism, which can be very valuable additional information.³⁷

Although macromolecular assays are informative and have been used by pharmaceutical companies for years, they have limitations. The MBA was originally developed for large culture volumes, which made this method unsuitable for elucidating the MoA of natural substances, which are often only available in very limited quantities. This drawback has been overcome by optimizing this method for microplates, which now makes it applicable to NPs, and also increased the throughput.^{34,40} In fact, macromolecular assays have recently been used to obtain an initial hint of the MoA of the novel NP teixobactin. It has been shown that the antibiotic has a strong effect exclusively on the synthesis of the cell wall, which suggests an inhibition of peptidoglycan synthesis.⁴¹ However, MBAs always require in-depth studies to clarify the exact MoA. In the case of teixobactin, an inhibition mechanism was revealed by binding to a highly conserved motif of lipid II, which validated the MBA results.⁴¹ Another disadvantage of this assay is that it is limited to

the major biosynthetic pathways. Therefore, this assay cannot be used to uncover a totally novel MoA.³⁷

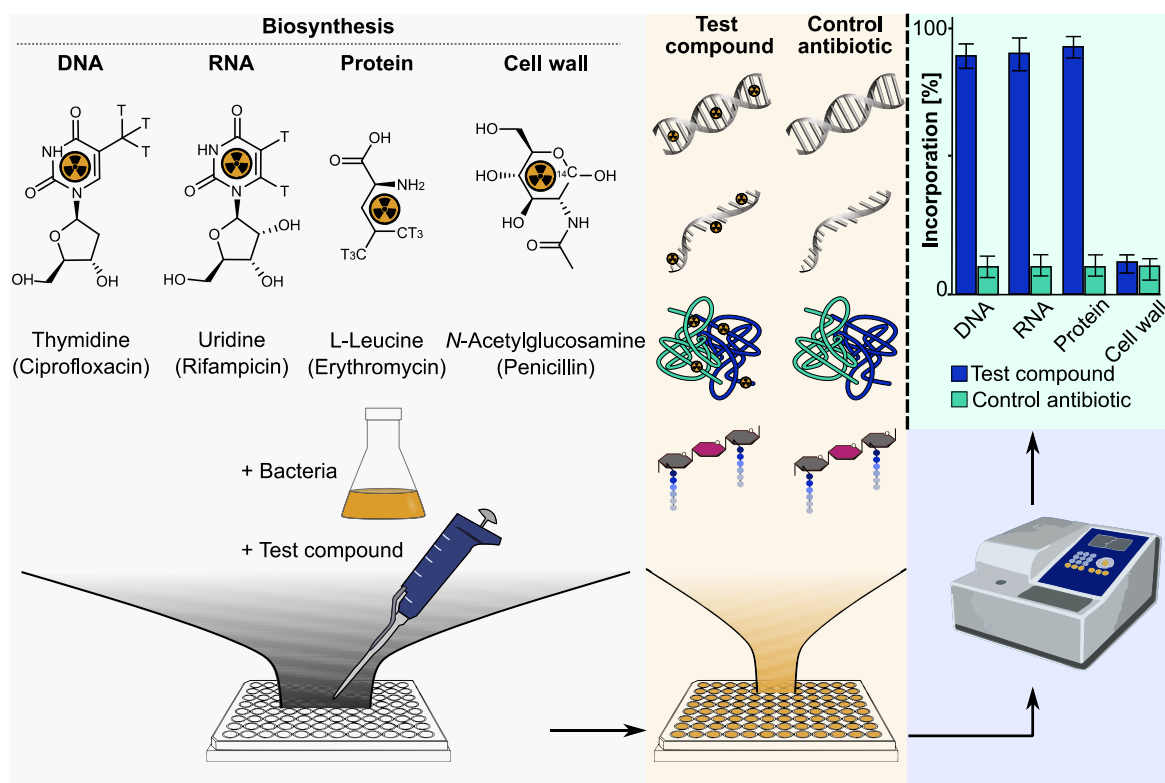


Figure I-3: Schematic workflow of a macromolecular biosynthesis assay (MBA). Radiolabeled precursors, specific for the major metabolic pathways, namely DNA, RNA, protein and cell wall synthesis, are used to study the effect of a NP on macromolecular biosynthesis and thus to elucidate the MoA. Control antibiotics (examples in parentheses) with known MoA are used as positive controls for the inhibition of the respective pathway.

2.2. Activity-Based Protein Profiling (ABPP)

Affinity chromatography enables the identification of the cellular target(s) that directly bind the molecule of interest. The traditional method was to screen the chromatographic fractions for enzyme activity after the cell lysate was subjected to a compound immobilized on a solid matrix. Afterwards, the eluted bound proteins were analysed for their protein sequence and characterised.^{35,37,42} The success of this method is best illustrated by the classical pulldown of penicillin-binding proteins (PBP).⁴³ However, this method is very labour-intensive and requires large quantities of extracts. In addition, the small molecule must be modified for immobilization, which in turn requires information about its structure-activity relationship in order to maintain the activity of the compound. Moreover, this method can only be applied in artificial *in vitro* settings and is only suited for high-affinity ligands that bind target proteins with a comparatively high abundance.³⁷

Over the last 30 years, advances in affinity reagents and in quantitative and high-resolution mass spectrometry analysis (MS) have overcome these major drawbacks and contributed to the development of modern affinity purification strategies, including activity-based protein profiling (ABPP).³⁶

ABPP is an established proteomic method introduced by Powers and Walkers and further developed by Bogoy and Cravatt.⁴⁴⁻⁴⁸ This strategy allows the analysis of enzyme function, activity and regulation *in vitro* and *in vivo* as well as the identification of target proteins of a biologically active substance.

Generally, the concept of ABPP relies on the treatment of a complex protein sample or live cells with a chemical probe functionalized with a reporter tag for subsequent analysis. Initially, reporter tags were attached directly to the molecule of interest, which limited the methodology to *in vitro* experiments, as many commonly used tags are too polar or bulky to penetrate cells. The bioorthogonal Huisgen-[3+2] azide alkyne cycloaddition (click-reaction; CuAAC), however, enabled the late introduction of the reporter tag, thus overcoming this limitation.⁴⁹⁻⁵³ In this case, the compound is

modified with a terminal alkyne tag to which an azide-equipped fluorescent dye (e.g., rhodamine azide) or an affinity tag (e.g., biotin azide) is attached. While a fluorescent tag enables quick and easy analysis of probe-labelled proteins *via* gel electrophoresis, an affinity tag allows enrichment of target proteins (Figure I-4). After enrichment using avidin-coated beads, probe-bound proteins are tryptically digested and analysed by liquid chromatography-coupled tandem mass spectrometry (LC-MS/MS).

This method requires a covalent bond between the compound and its binding partners. Where the compound and protein target interact non-covalently, an additional functionalization is required to enable covalent cross-linking before the aforementioned analysis. A photoreactive group, such as benzophenone and diazirine, can be attached to the bioactive molecule in addition to the alkyne tag, which will form a covalent bond to the binding partner upon UV irradiation.⁵⁴ For example, the diazirine moiety will form, upon nitrogen release a carbene that will readily insert into nearby CH, NH and SH bonds, e.g., from an amino acid of the bound protein target.⁵⁵ The diazirine group in particular has received considerable attention because it is comparatively small, chemically stable and requires only a very short irradiation time as opposed to the alternatives. Yao *et al.* developed a series of "minimalist" photo-crosslinkers consisting of a linking group (amine, carboxylic acid or halide) to allow facile attachment to NPs, the photoreactive diazirine, and an alkyne tag as a bioorthogonal enrichment handle.^{56,57} The reaction of such a probe is then affinity-based rather than activity-based, since the binding to the target molecule does not depend on the activity of the protein itself - as is the case for covalent probes - but rather on the affinity between protein and probe. Hence this approach is also called affinity-based protein profiling (ABPP).

Thus, ABPP is a powerful technique for studying MoA and has already been successfully used for target identification of various NPs, such as vancomycin.^{58,59} However, it has to be kept in mind that this technique can almost exclusively be used to identify protein targets, so non-protein targets can often be overlooked. In addition, ABPP requires a probe which has to be synthesised first and which should

have an activity comparable to that of the parent compound. Especially in the case of NPs, which are often only available in limited quantities, this can be a great challenge. Furthermore, photoreactive groups can have a high background, making validation experiments mandatory to exclude false positive hits.⁶⁰

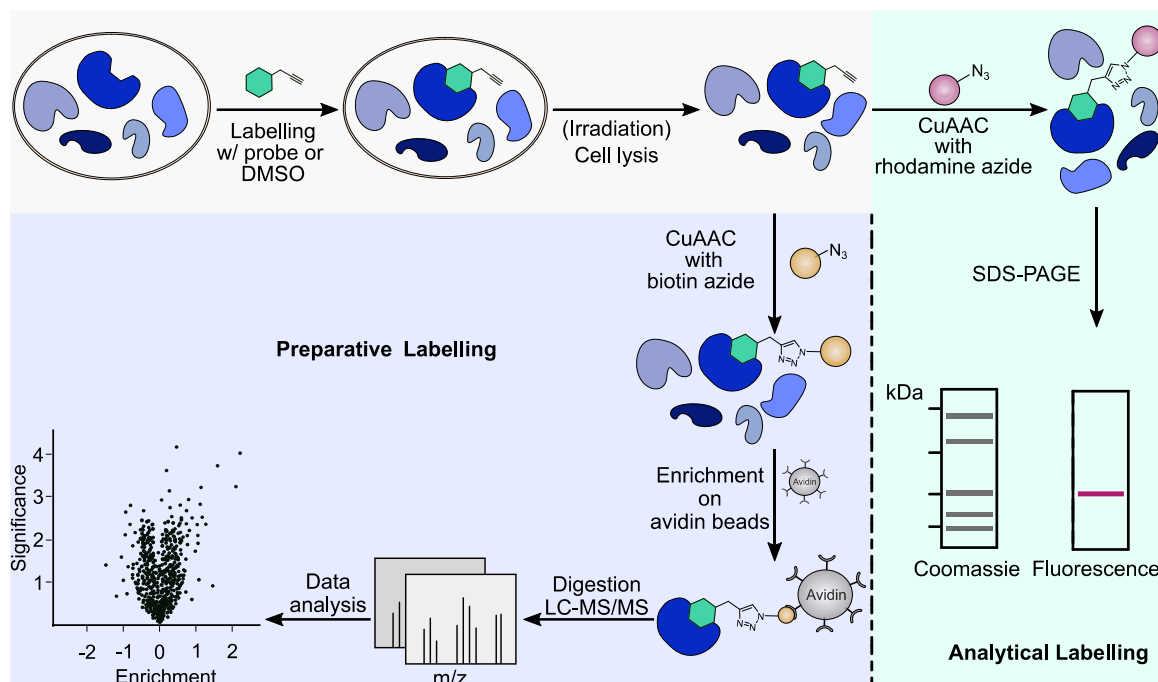


Figure I-4: Schematic workflow for target identification by ABPP and A/BPP. Intact cells are treated with a probe or DMSO (as control), ultraviolet (UV) light irradiated (only for photoprobe (A/BPP)) and lysed. For analytical labelling, rhodamine azide is clicked to the labelled proteins and analysed by SDS-PAGE. For identification of targets, the labelled proteins are clicked to biotin azide, enriched on avidin beads, enzymatically digested and analysed by LC-MS/MS measurements.

2.3. Selection of Resistant Mutants

The traditional "old school" method of selecting mutants capable of growing in the presence of a lethal concentration of the compound of interest is still a useful tool for drug development and target identification. The principle of this method is that the identification of the gene causing the resistant phenotype can reveal the MoA of the compound. Yet this particular step was traditionally a labour-intensive task that took several months, often years, and thus limited the success of this method. With the advent of the next-generation-sequencing (NGS) technology, however, genome research has been revolutionized and whole genomes of resistant strains can thus be sequenced within one day. NGS technologies employ massive parallel resequencing of DNA fragments; often more than one billion short reads per instrument run are generated, which are then aligned to a reference genome and genetic variations of the mutated strains are identified.^{37,61,62}

Typically, resistant bacteria can be obtained in two different ways. The first method, which is the most commonly used, involves the serial passage of bacteria in media containing the antibiotic of interest at concentrations close to the MIC, which are progressively increased over the course of the experiment with the accumulation of resistant mutants (Figure I-5). Since selection is not lethal and growth often occurs over several hundred generations, naturally occurring mutations are always acquired that are not related to antibiotic selection.⁶³ Therefore, a parallel experiment must be carried out, in which the bacteria are passaged under the same conditions but without the antibiotic. Overall, this method is very simple and demands only small amounts of the compound. One drawback is, however, that only mutants with high fitness are selected (e.g., the mutant spectrum is biased), and since selection is gradual, mutants often contain more than one mutation, requiring labour-intensive follow-up studies to confirm the role of each mutation.^{64,65}

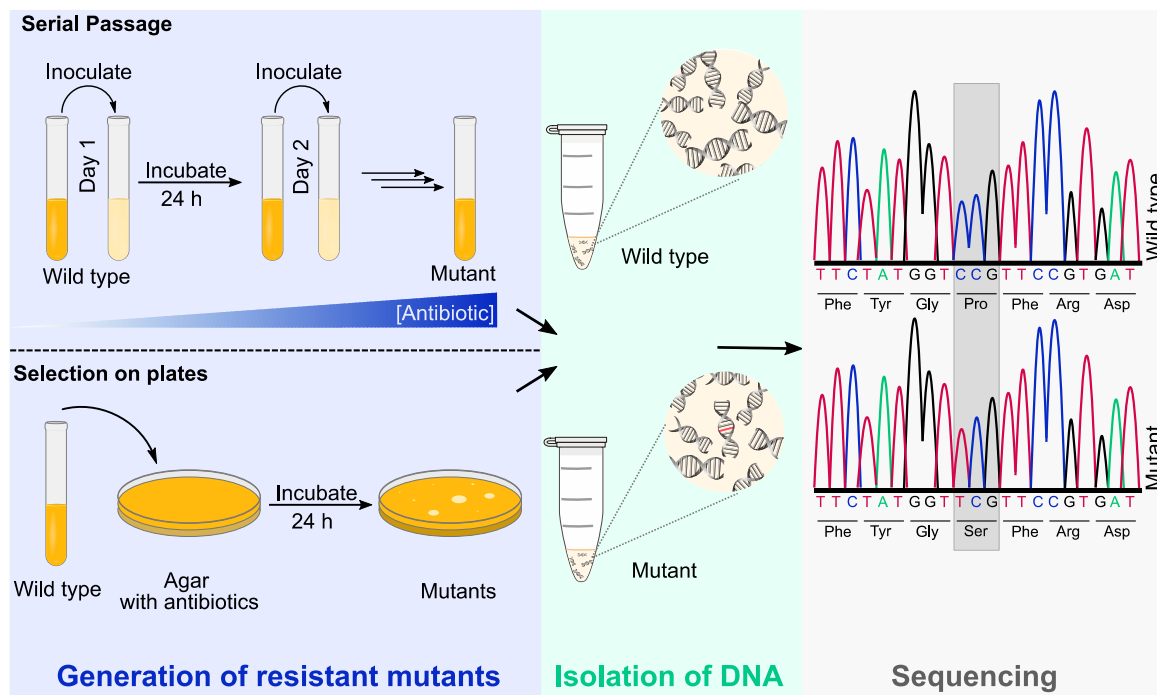


Figure I-5: Schematic workflow for target identification by generation and sequencing of resistant mutants. Bacteria, resistant to an antibiotic, can be obtained by serial passage or selection on agar plates. After isolation, DNA is sequenced and compared to wild type DNA in order to identify altered genes.

The second approach, which is preferable if possible, is to perform a selection on agar plates containing antibiotic concentrations above the MIC. The advantages of this approach are that mutants usually contain only one mutation and that resistant mutants with strong fitness reductions can also be selected. Using this method, the bacterial type I signal peptidase (SPase) LepB was successfully identified as the target of Gram-negative active arylomycins.⁶⁶ The main problem when using agar plate selections is that large amounts of antibiotics are required.⁶⁴

Although the NGS technology makes sequencing of resistant mutants indispensable for target identification, in some cases it is impossible to create variants that are resistant to a compound.⁶⁷ Furthermore, it is imperative for the success of this method that the resistance is caused by changing the target. However, this is only one of many resistance mechanisms. For example, multidrug efflux pumps and transporters can be overexpressed due to mutations in regulatory regions.^{11,30} These mutations, however,

do not allow conclusions to be drawn about the cellular target. In the case of target modification as a resistance mechanism, however, even specific amino acid residues can be inferred, which are important for understanding the compound-protein interactions.³⁷

II. Elucidating the Mechanism of Action of the Natural Product Xanthocillin X

Results of this work have been published as follows:

Hübner, I., Shapiro J. A., Hoßmann, J., Drechsel J., Hacker, S. M., Rather, P. N., Pieper, D. H., Wuest, W. M., Sieber, S. A., The broad spectrum antibiotic xanthocillin X effectively kills *Acinetobacter baumannii* via dysregulation of heme biosynthesis, *ACS Cent. Sci.* 2021, 7, 3, 488–498.

1. The Natural Product Class of Xanthocillin X

One class of NPs, the isonitrile family, has received very little attention so far, although it has an impressive spectrum of activity. The first compound of this class, xanthocillin X (Xan, Figure II-1), was isolated from the fungus *Penicillium chrysogenum* by W. Rothe in 1948.⁶⁸ He also reported the broad antibacterial activity spectrum of Xan. This includes a number of Gram-positive bacteria, numerous Gram-negative bacteria and some pathogenic fungi.^{68,69} Later, Xan was also introduced as an antibiotic onto the market, but, because of its poor absorption, its use was limited to local treatments.^{68,70} Although the median lethal dose (LD₅₀) of Xan in mice and guinea pigs is comparable to antibiotics that have become important for local treatment (tyrothricin, gramicidin S), increased reports of skin irritation have led to Xan being withdrawn from the market very quickly.^{69,71} However, it is interesting to note that, compared to sulfonamides and penicillin, bacteria have developed resistance very slowly and cross-resistance was not observed, suggesting a novel MoA.^{68,70}

Despite the fact that Xan is known to have a broad spectrum of activity, a quantitative evaluation of its antibiotic properties against various bacterial species, such as the current clinically relevant pathogens *Acinetobacter baumannii* and *Klebsiella pneumoniae*, is missing.⁷² Only Shang *et al.* published a minimal inhibitory concentration (MIC) of Xan against *Staphylococcus aureus* and *Escherichia coli* of 2 µg/mL and 1 µg/mL, respectively, confirming its highly potent antibiotic properties.⁷³

In nature, there is a number of Xan-like compounds in which vinyl isonitrile groups are present, all of which have an impressive spectrum of activity. In 1968, Takatsuki *et al.* isolated methyl derivatives of Xan from strains of *Aspergillus* (Figure II-1):

Xanthocillin X mono (XanMME) and dimethyl ether (XanDME) as well as methoxy-xanthocillin X dimethyl ether (M-XanDME). These compounds were shown to have particularly antiviral and antitumoral effects.⁷⁴ In addition, Tsunakawa *et al.* extracted BU-4704 (Figure II-1), a NP from a strain of *Aspergillus*, which showed an MIC in *E. coli* of 1.6 µg/mL and in *K. pneumoniae* of 0.4 µg/mL.⁷⁵ In search of new active compounds against Gram-negative bacteria, the NP MDN-0057 was recently discovered (Figure II-1), which exhibits an MIC in the range of 0.25 to 64 µg/mL against a large number of Gram-negative bacteria such as *E. coli*, *K. pneumoniae*, *Pseudomonas aeruginosa* and *A. baumannii*, the latter ranked as critical pathogen with highest priority according to the WHO.^{7,76} The structure of this NP is quite different from Xan, but also has (vinyl) isonitrile groups, which demonstrates the presence of this functional group in numerous highly active antibacterial NPs.

To date, about 200 members of this class have been isolated from various sources, including fungi (e.g., Xan, MK4588), bacteria (e.g., SF2768) and sponges (e.g., kalihinol A, axisonitrile-3), all of which exhibit broad activity against bacteria, viruses, fungi and parasites with comparatively low human toxicity (Figure II-1).^{7,68,73-75,77-80} In addition, secondary and tertiary isocyanides have proven to be metabolically stable, making isonitrile a promising pharmacophore in the discovery and development of new antimicrobial drugs.^{7,81}

Despite these characteristics, neither the reactivity of this functional group in the cellular environment has been elucidated, nor is the MoA of a representative of this group known. Until now, binding to transition metals (e.g., Fe, Cu) either directly or complexed in heme has been linked to the bioactivity of isonitriles. For instance, terpene isonitriles have been shown to have antiplasmodial activity by binding to heme, thereby inhibiting the parasite's vital heme detoxification processes.⁸²⁻⁸⁴ Furthermore, SF2768 has been shown to bind to copper, which has been linked to

antibacterial activity.^{78,85} However, a comprehensive study to identify the cellular targets of this compound class is still missing. Xan was chosen as a representative compound for this class to decipher its MoA and provide unprecedented insights into the antibacterial mechanism of isonitriles.

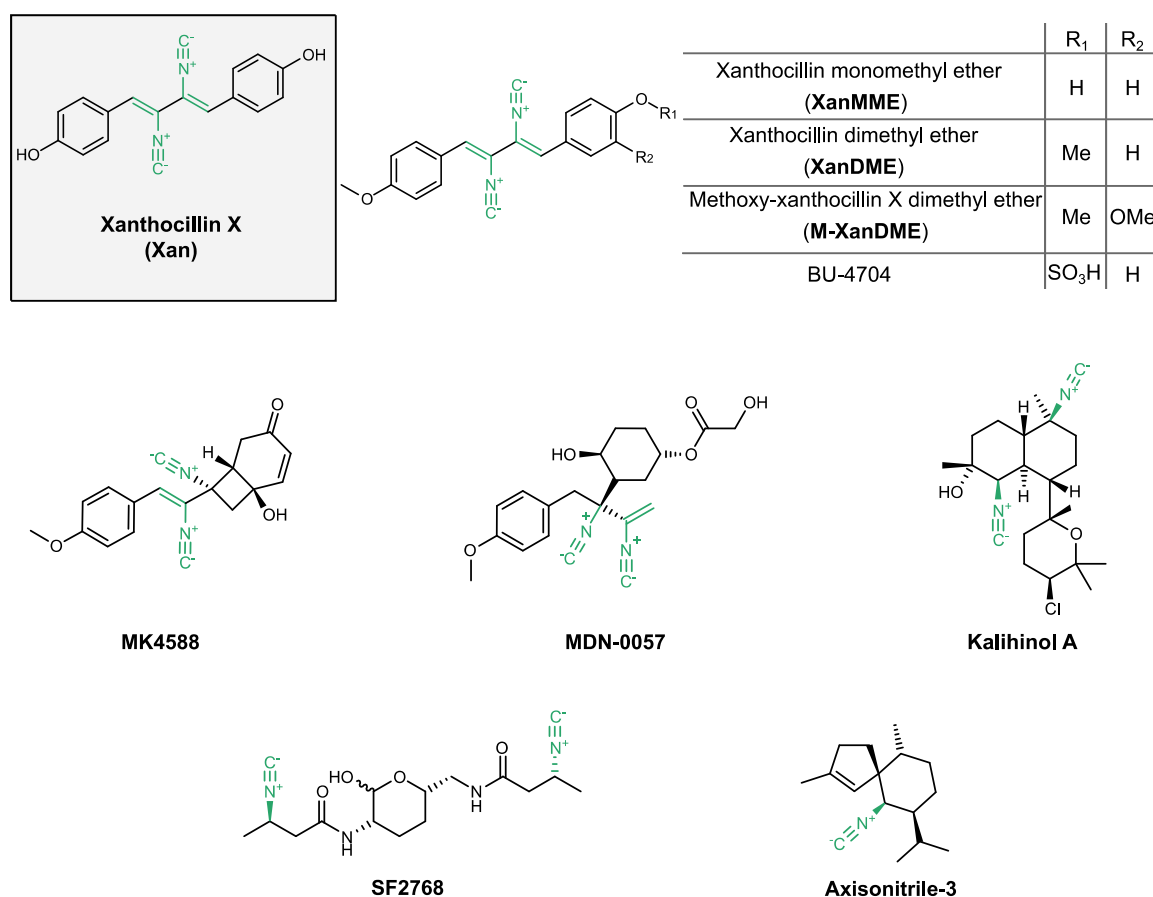


Figure II-1: Structures of representative examples of the isonitrile NP class. In nature, there are numerous isonitrile-containing NPs, some structurally very similar to Xan, others not.^{7,68,74,75,78,86-88}

2. Results and Discussion

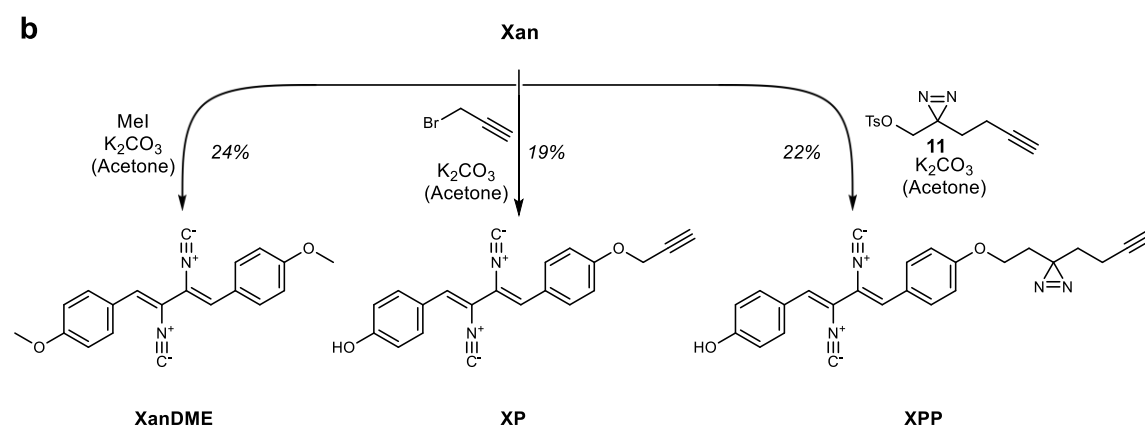
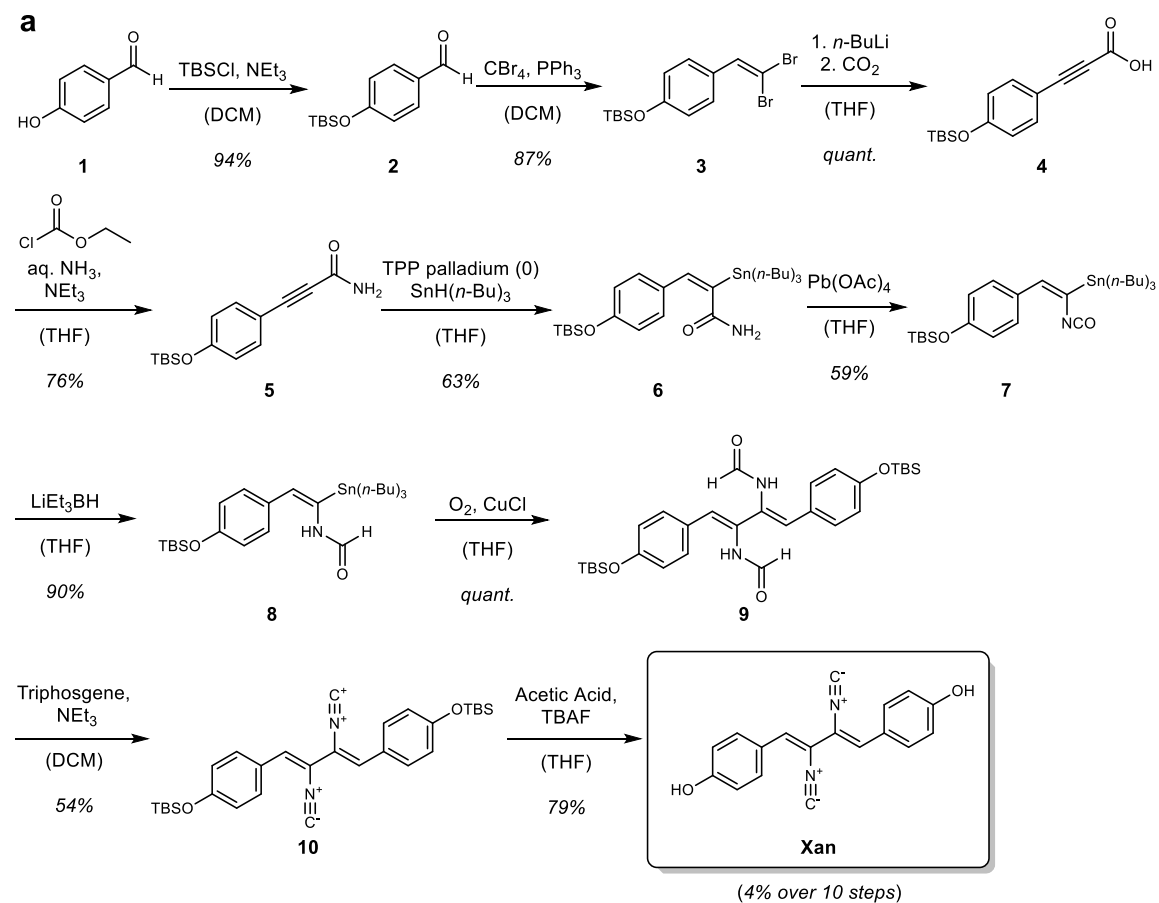
2.1. Synthesis of Xanthocillin and its Derivatives

The literature-known synthesis of Xan represented the first part of the doctoral thesis.^{89,90} Xan was then used to synthesize XanDME as well as the xanthocillin probe (XP) and the xanthocillin photoprobe (XPP) for ABPP and A β BPP, respectively.

In the first step of the Xan synthesis, the *tert*-butyldimethylsilyl (TBS)-protected benzaldehyde (2) was converted in a *Corey-Fuchs* reaction *via* the dibromoolefin (3) into the corresponding propionic acid (4),⁹¹ which was subsequently reacted with ammonia to the corresponding amide (5). The hydrostannation of this amide yielded the (*E*)-vinylstannate (6). By an oxidative rearrangement of compound 6 using $\text{Pb}(\text{OAc})_4$,⁹² the corresponding isocyanate (7) could be obtained, which was directly converted into the *N*-formyl-enamides (8) by reduction with LiEt_3BH . A Cu(I)-catalysed homocoupling of compound 8 led to the symmetrical (*Z,Z*)-diene (9), which was dehydrated with triphosgene to yield the corresponding (*Z,Z*)-diisonitrile (10). In the last step, the TBS protecting group was removed using tetrabutylammonium fluoride (TBAF) and acetic acid to obtain Xan with an overall yield of 4% over 10 steps (Scheme II-1a).^{89,90}

Afterwards Xan was used to synthesize XanDME, which was also tested for its biological activity to obtain first structure-activity relationship (SAR) data. For this purpose, Xan was dimethylated using two equivalents of methyl iodide and XanDME was obtained with a yield of 24%. For XP and XPP, Xan was alkylated using propargyl bromide and the minimal photoprobe (11),⁹³ respectively. To prevent double methylation, the reactions were monitored by mass spectrometry and stopped as soon as a double methylated compound was detected. XP and XPP were obtained

with yields of 19% and 22%, respectively, while Xan could be re-isolated with a recovery of 81% for the XP synthesis and 49% for the XPP synthesis (Scheme II-1b).



Scheme II-1: Synthesis of Xan, XanDME, XP und XPP. a) Xan was synthesised according to a published procedure.^{89,90}

b) For the synthesis of XanDME, XP and XPP, Xan was methylated using the respective methylation reagents.

2.2. Antibacterial Screen

A quantitative evaluation of Xan's antibiotic properties against currently clinically relevant bacteria, such as *A. baumannii* and *K. pneumoniae*, is lacking so far. Thus, activity of Xan was first tested against a panel of Gram-positive and Gram-negative strains.

Table II-1| Activity of Xan against pathogenic bacteria. MIC values were determined in $n = 3$ independent experiments.

	Strain	MIC (24 h) [μ M]
Gram-negative	<i>Acinetobacter baumannii</i> ATCC19606	0.25 – 0.5
	<i>Acinetobacter baumannii</i> ATCC17978	0.25 – 0.5
	<i>Acinetobacter baumannii</i> AB5075 (MDR)	1
	<i>Escherichia coli</i> K12	1
	<i>Escherichia coli</i> 536	1
	<i>Escherichia coli</i> UTI89	1
	<i>Pseudomonas aeruginosa</i> DSM 22644 (PAO1)	3
	<i>Klebsiella pneumoniae</i> DSM 30104	3
	<i>Salmonella typhimurium</i> LT2	3
	<i>Salmonella typhimurium</i> TA98	1
	<i>Salmonella typhimurium</i> TA100	1
Gram-positive	<i>Staphylococcus aureus</i> NCTC 8325 (MSSA)	3
	<i>Staphylococcus aureus</i> Mu 50 (MRSA)	1
	<i>Staphylococcus aureus</i> USA300 FPR3757 (MRSA)	3
	<i>Listeria monocytogenes</i> EGD-e	1
	<i>Enterococcus faecium</i> DSM 17050 (VRE)	> 10
<i>Enterococcus faecalis</i> V583/ATCC 700802 (VRE)	> 10	

The screening revealed a broad bioactivity spectrum for Xan that includes many clinically relevant strains, with the notable exception of *Enterococcal* species (Table II-1). Xan eliminated not only the antibiotic-sensitive (MSSA) and methicillin-resistant (MRSA) *S. aureus* reference strains, but also the difficult to treat Gram-negative pathogens such as *P. aeruginosa*, *K. pneumoniae*, *E. coli* and multi-drug resistant (MDR) *A. baumannii* AB5075 in the low μ M range. Remarkable was the activity of Xan

against *A. baumannii* ATCC19606 and ATCC17989, a critical pathogen with highest priority according to the WHO,⁷⁶ in the nanomolar range, which is why this strain was chosen as a model organism for mechanistic studies.

2.3. Metal Binding Studies

It has already been shown that the activity of isonitriles is related to their copper-binding ability. More specifically, Zhu *et al.* published that the isonitrile compound SF2768 binds copper, which leads to a decrease in the free metal concentration within bacteria and thus possibly to disturbances of essential copper-dependent enzymatic processes.⁸⁵ Hence, the MoA analysis was initiated with metal binding assays to test whether Xan exerts a similar MoA.

A metal-ligand fluorescence titration with different metals of physiological relevance (Cu(II), Fe(II), Fe(III), Ni(II), Co(II), Mn(II), Al(III), Zn(II) and Mg(II)) was performed to investigate Xan's metal binding ability.⁹⁴ This study showed that of the nine metals tested, Cu(II) was the only one that interacted with Xan (Figure II-2a). Based on this result, XanDME's ability to bind copper was tested. Interestingly, under these experimental conditions XanDME showed no significant interaction with Cu(II) (Figure II-2b), suggesting an important role of the two hydroxy groups for metal binding. While XanDME's antiviral activity has been reported,⁷⁴ data on its antibiotic potency is completely lacking. This suggests a low bacterial activity of XanDME, which was corroborated by its inactivity against *A. baumannii* ATCC17978 (MIC >16 μ M, Figure II-2c) and, at least at first glance, confirmed copper-binding as potential MoA. Unexpectedly, however, both compounds showed comparable activity against *A. baumannii* ATCC17978 Δ *adeB* Δ *adeJ*, a knock-out strain of two efflux pumps (*adeB*, *adeJ*). This indicates that the loss of activity of XanDME against wild type *A. baumannii* is predominantly due to a higher efflux rate, which is caused by the efflux pumps *adeB* and *adeJ*. This discrepancy between the inability to bind copper and the comparable

activity in the knock-out strain to Xan suggests that copper binding is not the main MoA and contributes, if at all, only partially to the activity of these compounds.

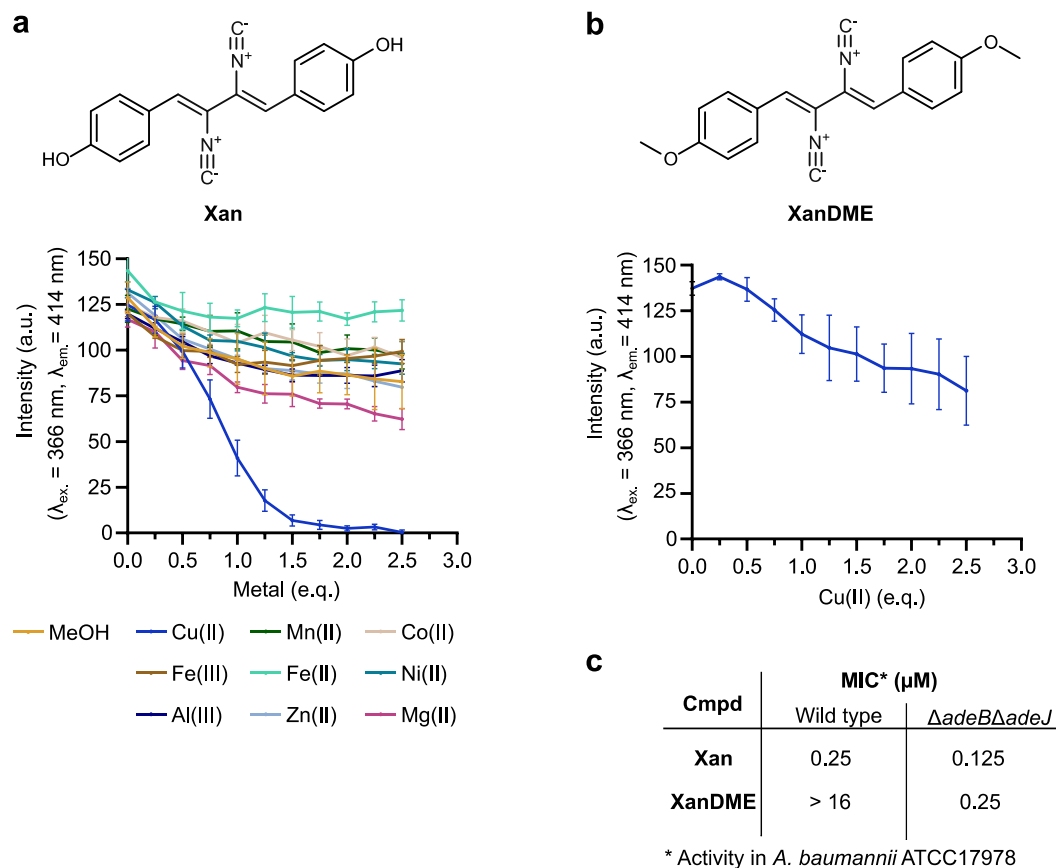


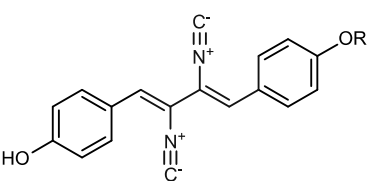
Figure II-2: Metal binding studies using Xan and XanDME. a) Fluorescence titration of Xan with various metals. The data represent average values \pm s.d. of independent experiments ($n = 3$ per group). b) Fluorescence titration of XanDME with Cu(II). The data represent average values \pm s.d. of independent experiments ($n = 3$). c) MIC values of Xan and XanDME in *A. baumannii* ATCC17978 wild type and *A. baumannii* ATCC17978 $\Delta\text{adeB}\Delta\text{adeJ}$,⁹⁵ a knock-out strain of two efflux pumps (*adeB*, *adeJ*). MIC values were determined in $n = 3$ independent experiments.

2.4. Protein Target Identification by Chemical Proteomics

Next, an unbiased method for target identification was performed. Since a large number of antibiotics have proteins as cellular targets,¹⁶ a chemical proteomics approach, more specifically ABPP and A β BPP, was performed. For this, the strains *A. baumannii* ATCC19606, in which Xan shows the highest activity, and *E. coli* K12, the best studied Gram-negative pathogen, were selected.

The design of the respective probes was straightforward. As there are methylated derivatives of Xan in nature (e.g., XanDME, XanMME) which, as know from previous experiments, show comparable activity to Xan in a strain with downregulated efflux pumps, it is assumed that modifications at a phenolic OH group do not alter the MoA. Consequently, Xan was synthetically equipped with an alkyne tag and a minimal photocrosslinker for ABPP and A β BPP, respectively. The synthesis of these probes, XP and XPP, is described in chapter "Synthesis of Xanthocillin and its Derivatives".

In fact, these modifications of Xan resulted in only a slight increase in MIC (~6-fold), rendering the probes suitable for proteomics experiments (Figure II-3).



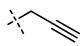
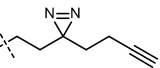
Cmpd	R	MIC in <i>E. coli</i> (μ M)	MIC in <i>A. baumannii</i> (μ M)
Xan	H	1	0.25 - 0.5
XP		3	3
XPP		n.d.	3 - 6

Figure II-3: Bioactivity data of Xan and its probes. In *E. coli* and *A. baumannii*, MICs of XP and XPP increased 3 to 12-fold compared to Xan. MIC values were determined in three independent experiments.

To decipher the identity of the covalently targeted proteins, a quantitative gel and label-free ABPP analysis was performed.⁹⁶ For this purpose, either intact *E. coli* or *A. baumannii* cells were incubated with 3 μ M (MIC concentration) XP for 2 h. After cell lysis, labelled proteins were clicked to biotin-azide, enriched on avidin beads and analysed by mass spectrometry (liquid chromatography-tandem mass spectrometry (LC-MS/MS)). In order to exclude non-specific avidin binding, a dimethyl sulfoxide (DMSO) control was additionally performed. Although Xan and XP exhibit similar activity, the cellular targets may be different. Therefore, competitive labelling experiments were conducted to ensure that the enriched target proteins of XP are also addressed by Xan. For this purpose, either *E. coli* or *A. baumannii* cells were pre-treated with an excess of Xan (30 μ M) before adding XP.

The enrichment of several proteins by XP in both strains revealed considerable covalent binding (Figure II-4a and d). In addition, some of these proteins are significantly less enriched in the corresponding competitive experiments (Figure II-4b and e). Proteins were only considered as targets if they were enriched by XP and out-competed by Xan. Interestingly, all proteins that met both criteria are non-essential for the survival of *A. baumannii* or *E. coli* (Figure II-4c and f). However, it is conceivable that the activity is based on the simultaneous inhibition of several non-essential targets.³²

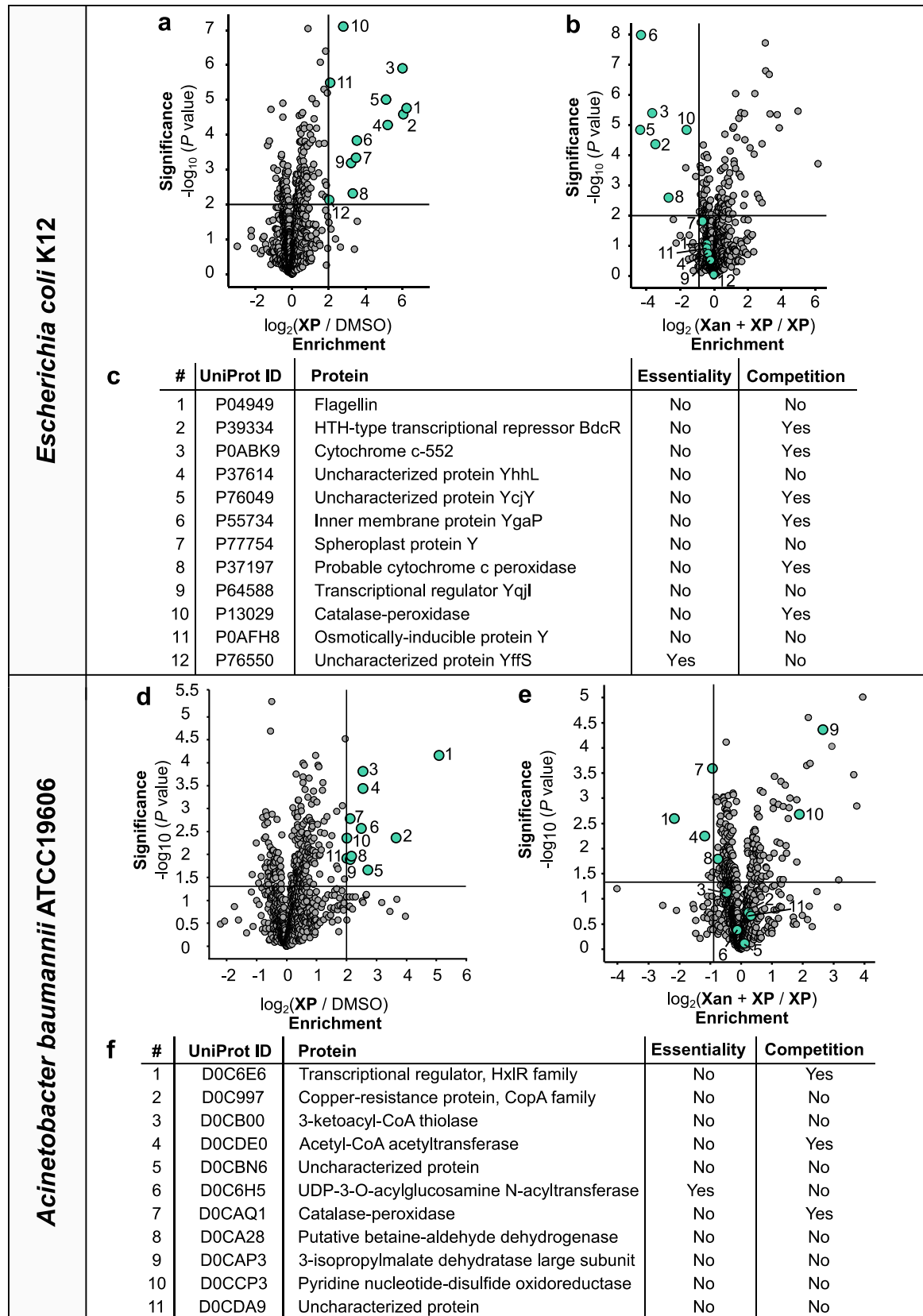


Figure II-4: Target identification in *E. coli* and *A. baumannii* using XP. a) and d) The volcano plots show enrichment of proteins after treatment of respective bacteria with XP (3 μ M) compared to DMSO on a \log_2 scale. The vertical

threshold line represents a \log_2 enrichment ratio of 2 and the horizontal threshold line a $-\log_{10}$ (P value) of 2 and 1.3 (two-sided two-sample t -test) for *E. coli* ($n = 4$ independent experiments) and *A. baumannii* ($n = 3$ independent experiments), respectively. Green dots represent proteins that were significantly enriched by XP compared to DMSO. b) and e) Competitive ABPP experiments using XP. The volcano plots show enrichment of proteins after pre-treatment of intact bacterial cells with Xan ($30 \mu\text{M}$) on a \log_2 scale. The vertical threshold line represents a \log_2 enrichment ratio of -0.9 and the horizontal threshold line a $-\log_{10}$ (P value) of 2 and 1.3 (two-sided two-sample t -test) for *E. coli* ($n = 4$ independent experiments) and *A. baumannii* ($n = 3$ independent experiments), respectively. c) and f) Tables that allocate proteins above the set threshold from the ABPP experiments (a) and d)). Three essential gene databases for *E. coli* K12 were used to determine essentiality.⁹⁷⁻⁹⁹ To determine essentiality for *A. baumannii* proteins, a transposon mutant library generated by Gallagher *et al.* was used.¹⁰⁰ For that, BLAST search was performed to assign homologous proteins in *A. baumannii* AB5075 (Program version BLASTP 2.10.1+, search limited to *A. baumannii* AB5075 (taxid:1116234), the resulting query coverage and percent identity are listed in Supplementary Table 1).^{101,102}

In order to investigate this hypothesis in more detail, validation experiments were conducted, focusing on the catalase peroxidase (CAT) of *A. baumannii* (*AbCAT*; UniProt: D0CAQ1, *katG*) and *E. coli* (*EcCAT*; UniProt ID: P13029, *katG*), which was the only overlapping target protein. For this purpose, the two catalases, were cloned, overexpressed in *E. coli* strains and purified by affinity chromatography.¹⁰³ To confirm the covalent binding of XP to these target proteins, an analytical ABPP experiment was performed in which XP was incubated with each of the two CATs, which were then subjected to the "click-reaction" using rhodamine azide as fluorescent marker and analysed by SDS-PAGE. The dose dependent labelling of the CATs, including the negative heat-inactivated control samples, validated a specific and covalent binding (Figure II-5a). However, a subsequent activity assay showed that this binding does not affect enzyme activities, excluding them as relevant cellular targets (Figure II-5b).

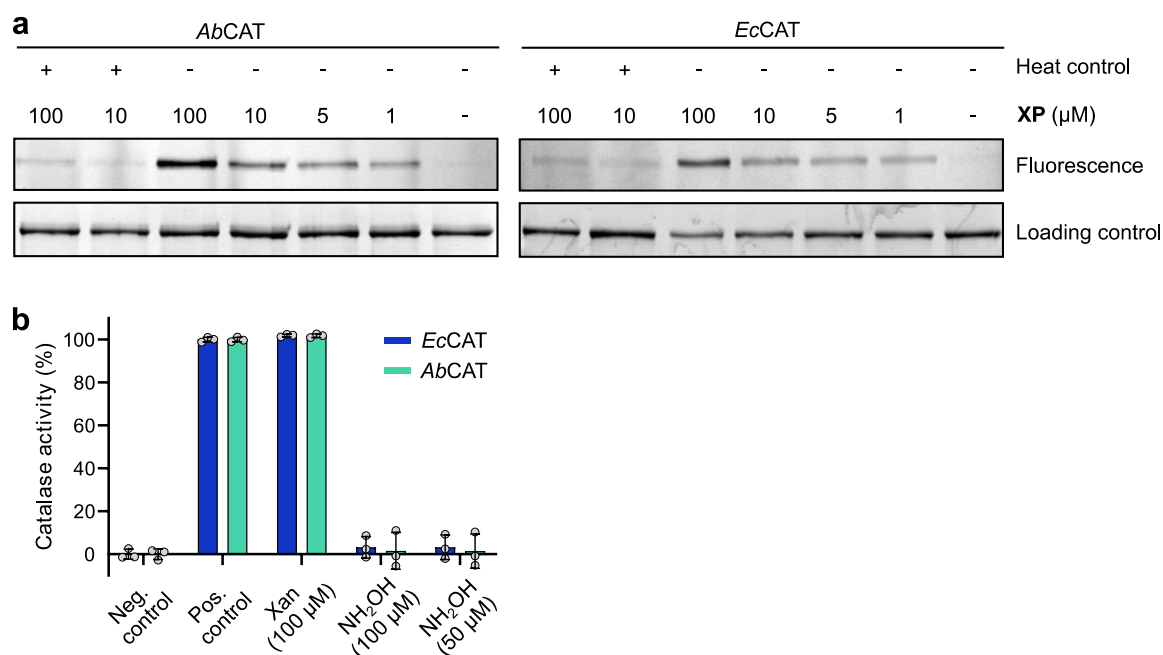


Figure II-5: Validation of CATs as targets of Xan. a) Gel-based labelling of recombinant *AbCAT* and *EcCAT*. Recombinant protein (1 μM) was treated with indicated concentrations of XP or DMSO as control for 1 h. Heat inactivated protein samples were included as control for unspecific binding. After incubation, samples were subjected to click-reaction and analysed by SDS-PAGE with subsequent in-gel fluorescence scanning and Coomassie staining. The gel is representative for three independent experiments. b) Catalase activity assay kit (*BioVision*, catalog number K773-100) was used to investigate Xan's influence on CAT activity. Hydroxylamine was used as positive control for CAT inhibition.¹⁰⁴ Values represent mean \pm s.d. of averaged duplicates of independent experiments ($n = 3$) and are normalised to the DMSO-treated samples (positive control, 100%) and the negative control (without enzymes, 0%).

Since isonitriles are also known as ligands in metal complexes, non-covalent targets may be involved in Xan's MoA.¹⁰⁵ Therefore, an *AfBPP* experiment was performed in *A. baumannii*. For this purpose, intact cells were incubated with 3 μM XPP, irradiated with ultraviolet light to establish a covalent bond with the putative target protein, lysed, clicked to biotin azide, enriched and analysed by LC-MS/MS. However, again there was no essential protein among the enriched hits (Supplementary Figure 1 and Supplementary Figure 2).

In summary, chemical proteomics has not been able to identify a cellular target to explain the MoA, which could have several reasons. Firstly, this method always bears

the risk that the probe cannot address the main target due to the modification. However, both probes show an activity comparable to that of Xan, making this argument rather unlikely. Furthermore, as described in section "Activity-Based Protein Profiling (ABPP)", ABPP as well as AfBPP can only identify protein targets. It is thus conceivable that Xan acts largely *via* a proteome-independent mechanism.

2.5. Target Identification by Selection of Resistant Mutants

2.5.1. Generation of Resistant Mutants

Since previous experiments have not provided evidence that metals or proteins are involved in Xan's MoA, the next step was to generate Xan-resistant mutants. By comparing the gene sequences of mutant and wild type, altered cellular targets that may explain the MoA can be identified.

Initially, attempts to develop resistant colonies by selection on agar plates supplemented with Xan (2× and 4× MIC) have failed. However, serial passage of *A. baumannii* in the presence of sub-inhibitory concentrations of Xan for 11 days was successful. Although the bacteria developed resistance to Xan after only a few passages, this development was significantly slower compared to the control antibiotic ciprofloxacin (Cip; Supplementary Table 2). The slower development of resistance compared to conventional antibiotics is consistent with a previous study in which staphylococci were treated with sub-MICs of Xan for 240 days that did not yield resistant strains.⁶⁸ Since serial passage can result in mutations unrelated to the MoA of Xan, bacteria were passaged for 11 days in the presence of only DMSO to identify these naturally occurring mutations (negative control). In total, nine resistant colonies were isolated from three independent biological experiments (referred to as A-C) as well as three colonies of the negative control.

Whole-genome sequencing of these variants and comparison with the wild type revealed that only the gene *hemB*, which codes for the enzyme porphobilinogen synthase (PbgS), was consistently mutated in response to Xan (Figure II-6).

Interestingly, exactly the same missense mutation within *hemB* was found in all nine colonies that led to the amino acid change P241S (Supplementary Table 3).

All other mutations found consistently in all resistant colonies were also present in the negative control. Consequently, these are presumably of natural origin and were thus not considered as cellular targets.

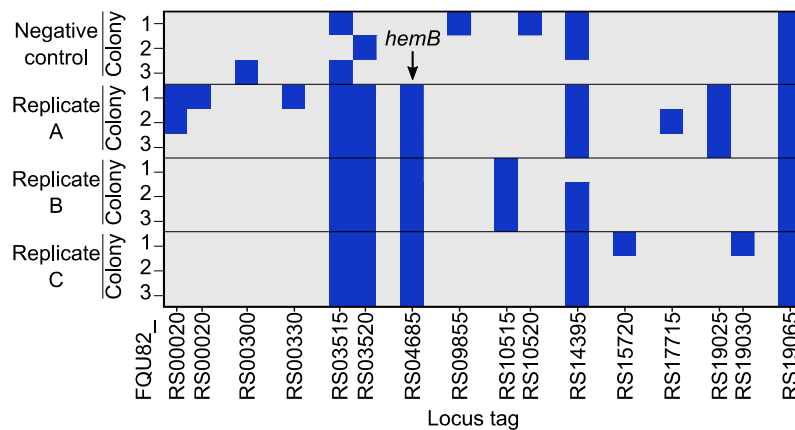


Figure II-6: Sequence analysis of Xan-resistant isolates. Mutants were obtained in three independent experiments by sequential passaging in sub-MIC concentrations of Xan. Three colonies from each independent experiment were sequenced and compared to three colonies of the negative control (passaging in the presence of DMSO). Mutations are ordered according to the recently published genome sequence of *A. baumannii* ATCC19606 (CP045110, chromosome and CP45108 plasmid p1ATCC19606).¹⁰⁶ Space between locus tags was omitted, if adjacent genes were mutated.

2.6. Phorphobilinogen Synthase

2.6.1. Introduction

The class of tetrapyrroles is structurally characterised by its four five-membered pyrrole rings, which are usually connected to each other by single atom bridges. Two classes of cyclic tetrapyrroles occur in nature, the porphyrins and the porphinooids. The former, which include heme as the most important representative, are characterised by their completely unsaturated ring system. In comparison, the porphinooids are more reduced cyclic tetrapyrroles such as vitamin B₁₂, siroheme and heme *d*₁.¹⁰⁷

The common precursor of all tetrapyrroles, 5-aminolevulinic acid (5-ALA), is synthesised in nature by two different, unrelated pathways, which are the C₄ pathway (Shemin pathway) and the C₅ pathway (Figure II-7).^{108,109} The latter, which is present in most bacteria, all archaea and all plants, starts from the C₅ skeleton of glutamate, more specifically glutamyl-tRNA, which is converted to 5-ALA by the catalysis of two consecutive enzymes, namely glutamyl-tRNA reductase (GtrR; *hemA*) and glutamate-1-semialdehyde-2,1-aminomutase (GsaM, *hemL*).^{107,108} In contrast, in humans, animals, fungi and the α -group of proteobacteria, 5-ALA is produced by the condensation of succinyl coenzyme A and glycine, catalysed by the enzyme 5-aminolevulinic acid synthase (*AlaS*, *hemA*).^{109,110} It is important to note that although the 5-ALA synthesis differs between organisms, this always seems to be the rate-limiting step of the porphyrin synthesis.¹¹⁰

The following three enzymes in the tetrapyrrole biosynthesis, porphobilinogen synthase (PbgS), hydroxymethylbilane synthase (HmbS) and uroporphyrinogen synthase (UroS), are highly conserved and can be regarded as a universal trunk, producing the precursor uroporphyrinogen III (UPGIII). UPGIII is used subsequently for the synthesis of numerous tetrapyrrole-based cofactors including heme.^{110,111}

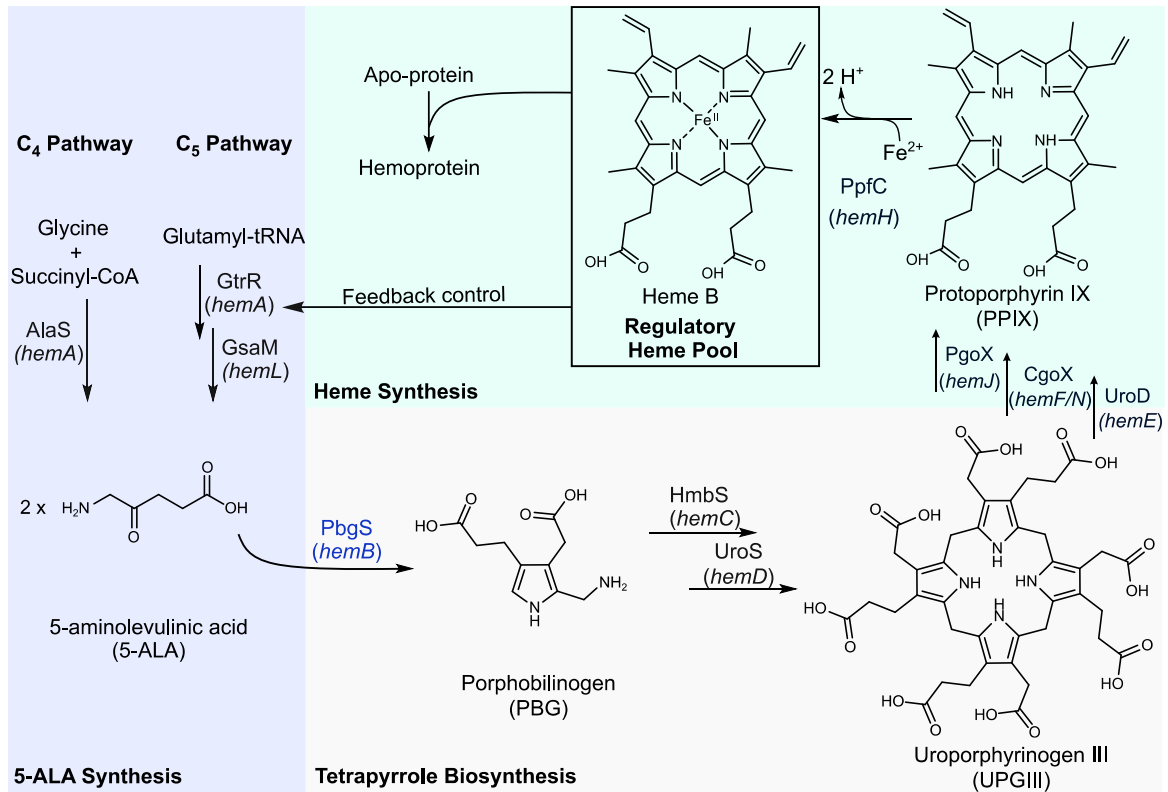


Figure II-7: Schematic overview of heme biosynthesis. In nature, the synthesis of 5-aminolevulinic acid (5-ALA) occurs *via* two different pathways, the C₄ and the C₅ pathway. The latter is the most common in bacteria. The following three enzymatic steps of the tetrapyrrole biosynthesis, catalyzed by porphobilinogen synthase (PbgS, highlighted in blue), hydroxymethylbilane synthase (HmbS) and uroporphyrinogen synthase (UroS), are highly conserved throughout different organisms and produce uroporphyrinogen III (UPGIII), a precursor for numerous cofactors. For the synthesis of heme, UPGIII is converted to protoporphyrin IX, into which the insertion of ferrous iron leads to heme B. Freshly synthesised free heme has several functions such as the regulation of its own biosynthesis by feedback control. Further it serves as a cofactor for hemoproteins.

Heme refers to a group of structurally very similar molecules, of which the most important representatives are heme B and heme C.¹¹² In cells, heme acts as a prosthetic group of many hemoproteins, which are involved in essential biological functions such as oxygen binding and metabolism (e.g., hemoglobin and oxidases) and electron transfer (e.g., cytochromes).¹¹³ Furthermore, heme functions as a regulator for certain proteins (heme-responsive proteins) by binding to the heme regulatory motif in an ON/OFF mechanism. It is assumed that heme-responsive

proteins are regulated by free heme, heme from heme-binding proteins with low affinity, or newly synthesised heme, which are referred to as regulatory heme (RH).¹¹⁴

Although heme plays a crucial role in all organisms, the regulation of its biosynthesis is not well understood and different hypotheses have been published. In bacteria, two regulatory steps were recognized, namely the oxygen dependent expression of the coproporphyrinogen oxidase (CgoX, *hemF* or *hemM*) enzyme and the abundance of the initial enzyme GtrR (*hemA*).¹¹¹ In several strains it was shown that the regulation of GtrR (*hemA*) is characteristically heme-dependent, suggesting that bacteria reduce the synthesis of heme and all intermediates in heme-replete conditions.^{115–117}

2.6.2. Overexpression of Porphobilinogen synthase (PbgS)

Porphobilinogen synthase (PbgS), a homooctamer in both eukaryotes and prokaryotes, catalyses the asymmetric condensation of two 5-ALA molecules to the monopyrrole porphobilinogen (PBG) (Figure II-7).^{107,110,118} There are two 5-ALA binding sites, known as A- and P-sites, each containing an active site lysine. The conserved lysine residue in the P-site forms a Schiff base with 5-ALA.¹¹⁹ The A-site characteristics of PbgS enzymes from different organisms may differ depending on the metal requirements (Zn²⁺, Mg²⁺).^{110,120} These metal requirements vary greatly from organism to organism. While human PbgS (*hPbgS*) and *P. aeruginosa* PbgS (*PaPbgS*) require only Zn²⁺ and Mg²⁺, respectively, for their activity,^{119,121} *E. coli* PbgS (*EcPbgS*) demands both metals.^{110,122}

In *A. baumannii*, PbgS is an essential enzyme, which has not yet been characterised.^{100,107} In order to obtain an initial hint about the relevance of the mutation P241S for the enzyme, a sequence alignment was first performed using Clustal O.¹²³ This clearly illustrated the mutation being close to the active site (Supplementary Figure 3). Given that PbgS might be the cellular target of Xan, this target mutation could possibly prevent the binding of Xan, which would explain the resistance development.

To investigate this, *N*-terminally His-tagged PbgS(wt) (pDest 17-*abhemB*_{wt}) was cloned and transformed into *E. coli* BL21(DE3) and *E. coli* Lemo21(DE3) expression strains and test expressions were performed. However, soluble protein could not be isolated under any condition tested (varying IPTG concentrations, expression time and temperature), as assessed by SDS-PAGE after purification on Ni-NTA resin, which is in line with studies on homologous proteins reporting on the formation of inclusion bodies (Figure II-8a).¹²⁴ Only the expression as *N*-terminally His-tagged maltose-binding protein (MBP) fusion construct either with (pET MBP-1a-*abhemB*_{wt}) or without (pET-41-K-*abhemB*_{wt}) TEV cleavage site in *E. coli* Lemo21(DE3) resulted in a partially soluble protein, which aggregated after cleavage of MBP by TEV protease. The corresponding MBP fusion construct of the mutant protein P241S (pET MBP-1a-*abhemB*_{P241S}) showed a similar expression behaviour. After expression as a partially soluble protein, it proved to be highly unstable after MBP cleavage, making the recombinant proteins unsuitable for further investigations.

Often proteins require their natural environment for correct folding. Thus, PbgS(wt) and PbgS(P241S) were cloned tag-free into plasmid pVRL2, which has been shown to be suitable for gene cloning and expression in *Acinetobacter* species.¹²⁵ The resulting plasmids pVRL2-*abhemB*_{wt} and pVRL2-*abhemB*_{P241S} were transformed into *A. baumannii* ATCC19606. Satisfyingly, PbgS(wt) and the mutant were expressed as soluble, active proteins upon arabinose induction as gauged by an activity assay using the crude cell lysate. The activity assay was performed as previously described.^{120,126}

Under these conditions the Michaelis-Menten parameters, K_m and v_{max} , of the enzymes were determined. *A. baumannii* (wt) lysate was included as control, to subtract the basal activity of the native PbgS(wt), which was considerably lower compared to the activity measured in the overexpressed lysates. For PbgS(wt), the K_m towards the substrate 5-ALA was determined to be 153 μ M for PbgS(wt), which was in line with literature data of homologous proteins (Figure II-8b).^{121,127,128} Notably, PbgS(P241S) was still active, albeit with a 37-fold increase in K_m (5670 μ M), concluding that the mutation led to a significant decrease in affinity for 5-ALA. Further, the

maximum reaction velocity, v_{max} , of the wild type protein (0.027 min^{-1}) was significantly higher compared to the variant (0.015 min^{-1}).

In order to compare the efficiency of the two enzymes,^{129,130} it must be ensured that the cell lysates contained similar amounts of enzyme (k_{cat}/K_m with $k_{cat} = v_{max}/[\text{Enzyme}]$). Since the enzymes were cloned without tag to ensure expression conditions as native as possible, these could not be quantified directly. To make an indirect quantitative estimation, the relative amount of overexpressed proteins was quantified *via* label-free LC-MS/MS analysis. The LFQ intensities revealed that PbgS(wt) and PbgS(P241S) were overexpressed in comparable quantities (Figure II-8c), thus the ratio v_{max}/K_m revealed a significant drop in enzyme efficiency for mutant PbgS(P241S) of about 60-fold.

Next, Xan's influence on the enzyme activity was investigated. Therefore, Xan was pre-incubated with the wild type protein before the addition of the substrate, however, no inhibitory effect was observed under the conditions tested (Figure II-8d). This also supports the results of the chemical proteomic experiments, which indicated a largely proteome-independent MoA and in which PbgS was also not enriched as a target protein.

Thus, the consistent mutation of this essential heme biosynthesis enzyme throughout all resistant mutants may have a more global effect on the tetrapyrrole biosynthesis in general.

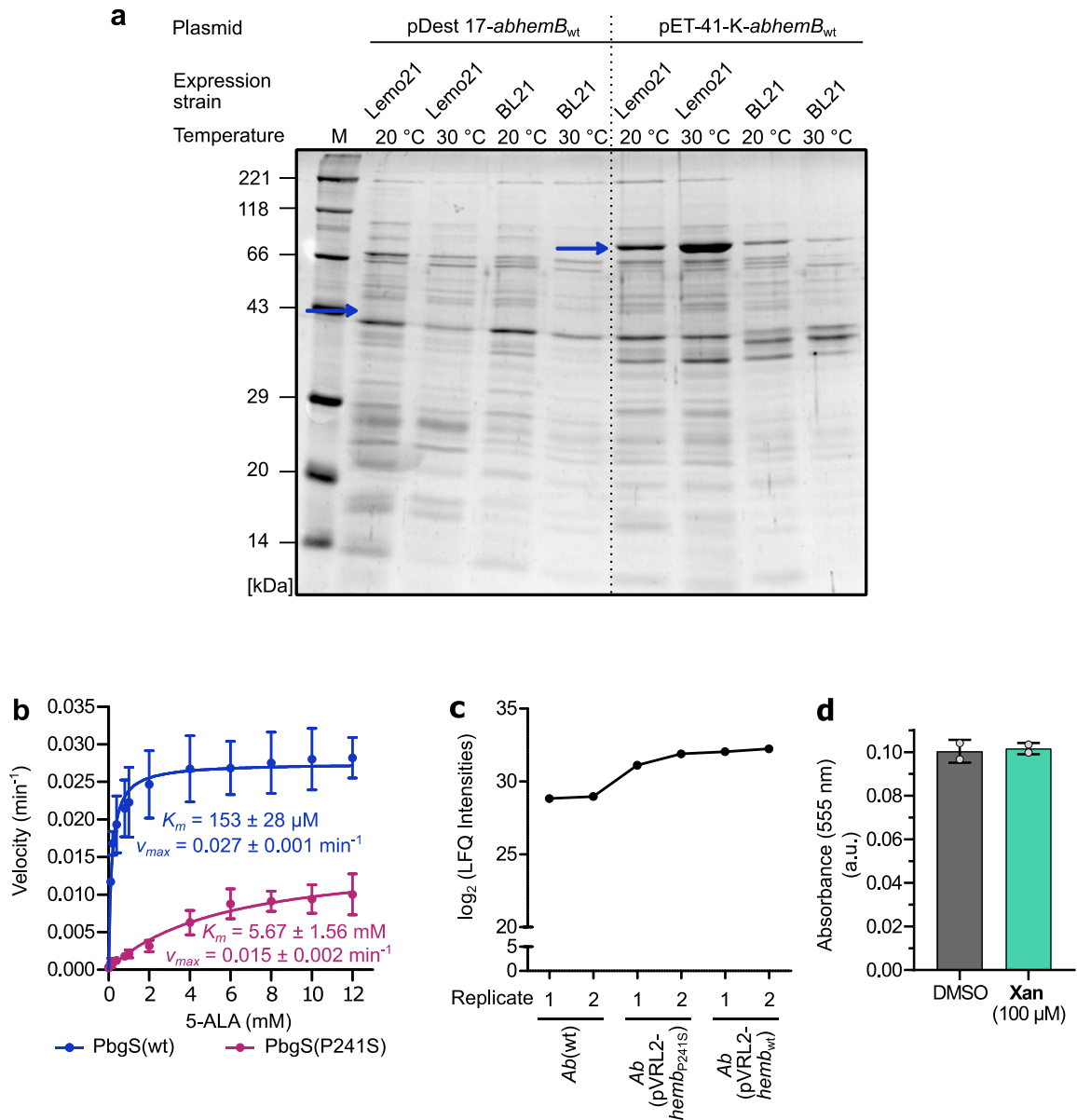


Figure II-8: Overexpression and activity assay of PbgS(wt) and PbgS(P241S). a) SDS-PAGE analysis of test expressions of PbgS(wt). *E. coli* Lemo21(DE3) and *E. coli* BL21(DE3) harbouring plasmids pDest 17-*abh*emB_{wt} or pET-41-K-*abh*emB_{wt} were used for expression of fusion proteins with a molecular weight of 42.6 kDa (6×His-tag-PbgS) and 83.6 kDa (6×His-tag-MBP-PbgS), respectively. This gel is representative for all conditions tested (varying IPTG concentrations, temperature and duration of expression). Here, protein expression was induced with 400 μM IPTG, cells were incubated at indicated temperature (20 °C or 30 °C) for 20 h at 150 rpm. Afterwards, 5 mL of cell culture were purified using Ni-NTA matrix (*Qiagen*) following the manufacturer's protocol. 50 μL of eluted sample was analysed by SDS-PAGE and Coomassie staining. Blue arrows indicate the expected position of the fusion proteins. b) PbgS activity assay with wild type and P241S mutant. Assays were conducted in crude lysates of *A. baumannii* that harbour either pVRL2-*abh*emB_{wt} or pVRL2-*abh*emB_{p241s} for expression of PbgS(wt) and PbgS(P241S), respectively. Lysate of *A. baumannii* (wt) (without plasmid) was used as blank control in order to subtract the basal PbgS activity level. All the data represent mean values \pm s.d. of averaged duplicates of independent experiments ($n = 3$ per group). Data were analysed with GraphPad Prism (version 5.03) using non-linear regression. c) LFQ

intensities of PbgS(wt) and PbgS(P241) in crude lysates, which were used for the activity assay (b). d) The activity assay described in b) was used to test PbgS(wt) inhibition by Xan. For that, 100 μ M Xan was pre-incubated with the crude lysate for 15 min at 37 °C before 5-ALA (100 μ M) was added. Enzymatic reaction was stopped after 30 min. Data represent mean values \pm s.d. of averaged duplicates of independent experiments ($n = 2$ per group).

2.7. Whole Proteome Analysis

To further investigate the impact of the mutation of this essential enzyme on the cellular level, the mutant strains were compared with wild type *A. baumannii* in a whole proteome analysis. For this purpose, *A. baumannii* wild type and three mutants (A-3, B-3 and C-3) were grown in the absence of Xan until the mid-exponential phase (OD_{600} of 2.0) was reached and subsequently subjected to label-free LC-MS/MS analysis. Notably, the three mutants showed a high overlap of dysregulated proteins, a large number of which was upregulated compared to the wild type (Figure II-9a and b). Among these proteins were those involved in protection against oxidative stress (catalase, two heme-oxygenase like proteins), biofilm formation (e.g., protein CsuC/E, spore coat protein U domain protein), efflux transporters (RND transporter, efflux transporter (RND family)) and acetoin metabolism (e.g., TPP-dependent acetoin dehydrogenase complex) (Figure II-9a). Biofilm formation and the upregulation of efflux pumps are common methods to evade the antibiotic pressure.^{11,131} Remarkable was the upregulation of two heme-oxygenase like proteins in all mutants, as these enzymes catalyse the degradation of heme. Together with impaired porphobilinogen synthesis by mutated PbgS, their increased expression indicates the need to reduce heme concentration during resistance formation to Xan. It is known that reduced heme levels may limit the electron flow in the electron transport chain and thus shift the metabolism from respiration to fermentation.¹³² In fact, *A. baumannii* is considered strictly aerobic, but a recent paper published first evidence for the survival of *A. baumannii* under anaerobic conditions.¹³³ This is consistent with the upregulation of enzymes that metabolize acetoin, a key fermentation product in bacteria.¹³⁴

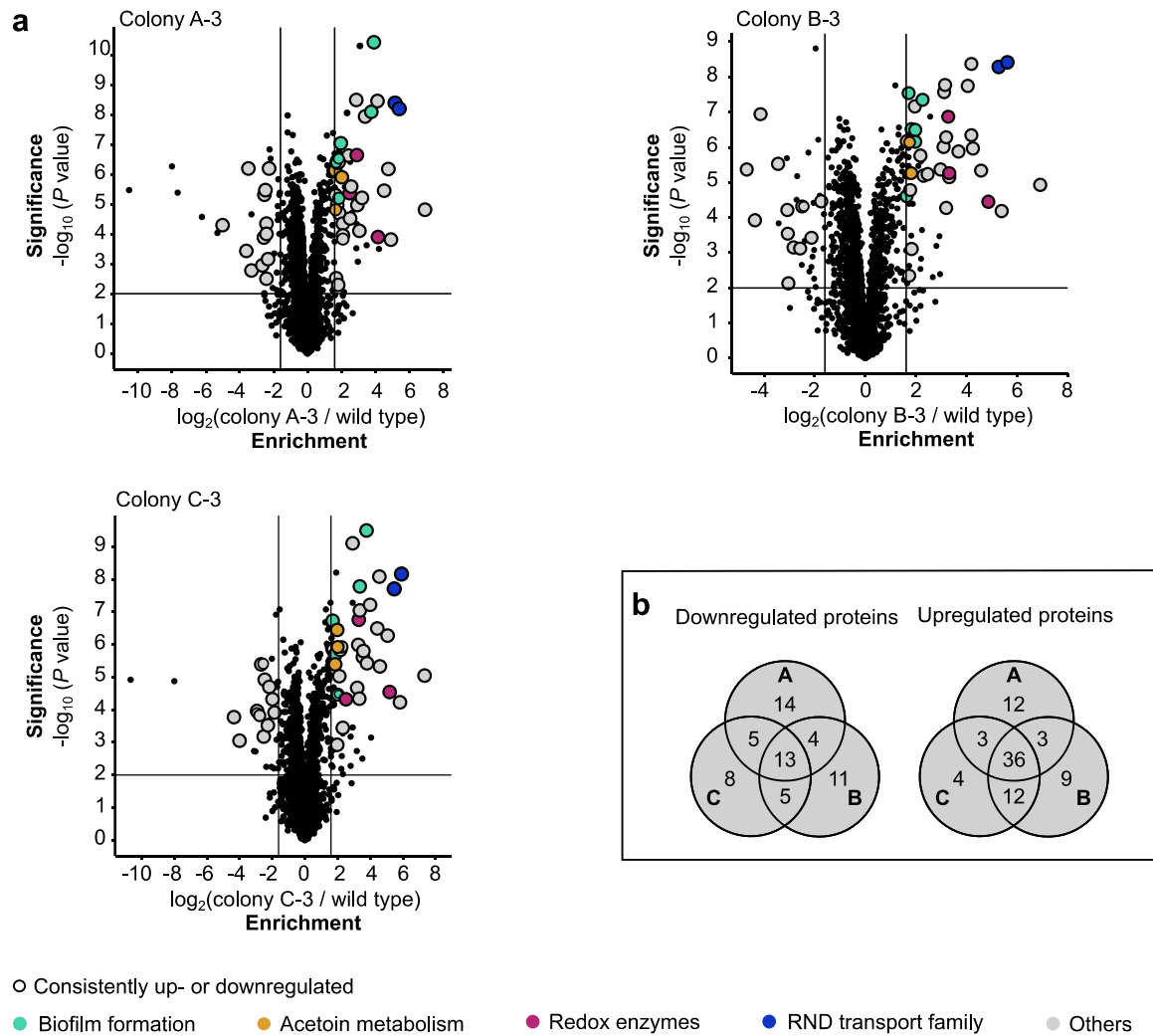


Figure II-9: Whole proteome analysis of Xan-resistant mutants and wild type *A. baumannii*. a) One colony from each independent serial passage experiment was compared to *A. baumannii* wild type. The volcano plots show the change of protein levels in the full proteome on a \log_2 scale. The vertical and horizontal threshold lines represent a \log_2 change of 1.6 and -1.6 and a $-\log_{10}(P \text{ value})$ of 2 (two-sided two-sample t -test, $n = 4$ independent experiments per group), respectively. Black circle represents proteins up- or downregulated consistently in all three colonies compared with the wild type. Green dots represent proteins involved in biofilm formation.^{135,136} Blue dots represent proteins that belong to the resistance-nodulation-division (RND) transporter family.¹³¹ Red dots represent redox enzymes known to protect cells from oxidative stress. Orange dots represent proteins involved in acetoin metabolism.¹³⁷ Supplementary Table 4 and Supplementary Table 5 give details on the dysregulated proteins. b) Venn-diagrams showing consistently up- and downregulated proteins that are above the set thresholds of the full proteome analysis of Xan-resistant colonies.

To better understand the direct impact of Xan on heme biosynthesis, a complementary experiment was performed by comparing the whole proteome of Xan-treated and untreated wild type *A. baumannii*. To this end, the cells were cultured either in the presence of 125 nM Xan ($\frac{1}{2}$ MIC) or DMSO until the mid-exponential phase (OD_{600} of 2.0) was reached. LC-MS/MS analysis revealed the highest change in protein level (> 3 -fold) for a putative proton/sodium glutamate symport protein (Figure II-10).¹³⁸ In bacteria, glutamate is needed for the formation of 5-ALA, the precursor of heme, which is why the upregulation of this symporter points to an increased demand for glutamate and thus to an enhanced heme biosynthesis in the presence of Xan. Additionally, the increased expression of two TonB-dependent siderophore receptors, which transport iron chelates, also supports this assumption, as it suggests elevated uptake of iron, which is the substrate for the final step of heme biosynthesis.¹³⁹

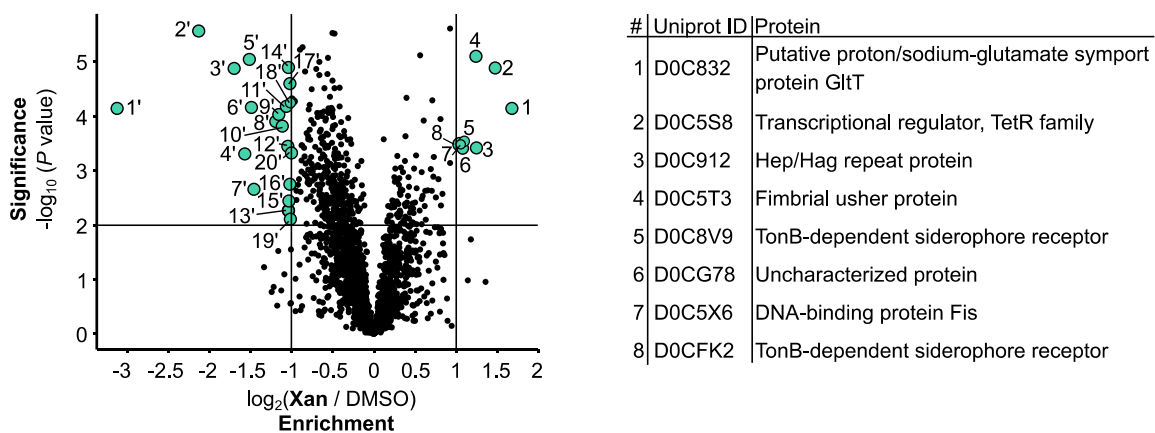


Figure II-10: Full proteome analysis of Xan compared with DMSO-treated *A. baumannii* ATCC19606. Volcano plot shows the change of protein levels in the full proteome on a \log_2 scale. The vertical and horizontal lines represent a \log_2 change of 1 and -1 and a $-\log_{10}(P \text{ value})$ of 2 (two-sided two-sample t -test, $n = 4$ independent experiments per group), respectively. The table allocates upregulated proteins above the set threshold from full proteome analysis of Xan-treated *A. baumannii*. Supplementary Table 6 gives details on the downregulated proteins.

In summary, whole proteome analysis of Xan-resistant and Xan-treated *A. baumannii* indicates that Xan stimulates heme biosynthesis and the resistance strategy is to counteract this activation.

2.8. Heme Binding

Both chemical proteomics and the analysis of the resistant mutants suggest that Xan triggers the activation of heme biosynthesis, which was revealed *via* whole proteome analysis, by a protein-independent mechanism.

A previous study published that the binding of various isonitrile compounds to heme can be linked to their activity against the malaria-causing parasite, *Plasmodium falciparum*, without providing comprehensive data.⁸³ The interaction of the isonitrile compounds and hemin was detected spectroscopically.⁸³

2.8.1. *In vitro* Heme Binding

To further test this hypothesis, the effect of Xan on the visible absorption spectrum of hemin was investigated. Hemin exhibits a Soret absorption band with a peak at 390 nm, which was red-shifted to 438 nm, and a peak at 550 nm appeared upon Xan addition, emphasizing a direct interaction of Xan with hemin (Figure II-11a). Furthermore, this effect was detectable in a concentration dependent manner. No alteration of the absorption spectrum was observed when using resveratrol (Res), a molecule structurally highly similar to Xan, but without isonitrile groups (Figure II-11b), highlighting the relevance of isonitriles for interactions with heme.

In the cells, heme is involved in various cellular processes and reactions. A simple assay based on the degradation of heme by glutathione (GSH) was performed to get a first insight into whether Xan may influence the biochemical behaviour of heme by binding to it.^{83,140} Indeed, heme degradation was inhibited dose-dependently and even equimolar amounts of Xan were sufficient to achieve complete inhibition (Figure II-11c).

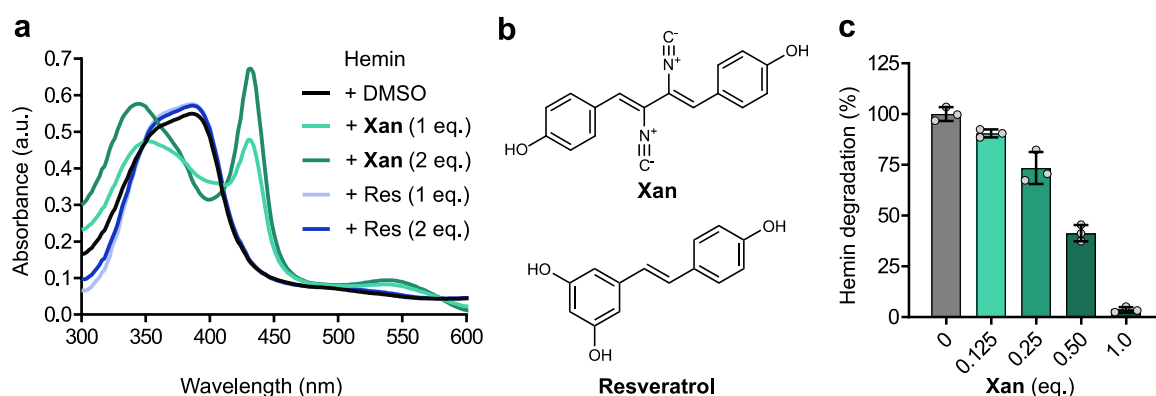


Figure II-11: Validation of Xan's binding to heme. a) UV-Vis spectra of hemin with DMSO (black), Xan (20 μ M, light green, and 40 μ M, dark green) and resveratrol (Res) (20 μ M, light blue, and 40 μ M, dark blue) in 200 mM HEPES (pH 7.0). Data represent averaged technical duplicates and this figure is representative for $n = 3$ independent experiments. b) Structure of Res compared to Xan. c) Inhibition of the GSH-mediated destruction of hemin by Xan. Hemin (20 μ M) was pre-incubated with Xan and the assay was started by the addition of GSH (2 mM). Decomposition was followed spectroscopically at 400 nm. Values represent mean \pm s.d. of averaged triplicates of independent experiments ($n = 3$) and are normalised to the DMSO-treated control.

2.8.2. Measurement of Regulatory Heme (RH) Level

As already described in the previous section "Phorphobilinogen Synthase", RH plays an important role not only in the regulation of hemoproteins, but also in the inhibition of its own biosynthesis.¹⁴¹ It is conceivable that by binding, Xan may unbalance the finely tuned regulatory role of heme in cells and reduce the level of free RH.

To investigate this hypothesis, the RH level was inspected using a colourimetric assay.¹¹⁴ This assay is based on the reconstitution of horseradish peroxidase (HRP) in its cofactor-free form (apoHRP) with RH, monitored by the activity of the resulting active holoHRP. Thus, high activity reflects a high RH level.¹¹⁴ To first prove the applicability of this assay for investigations of reduced RH levels due to Xan binding, hemin was pre-incubated with increasing concentrations of Xan followed by addition of apoHRP (5 μ M) for reconstitution. Indeed, this assay showed a decreasing holoHRP activity with increasing Xan concentration (Figure II-12a, green bars). To rule out that the decrease in activity is due to holoHRP inhibition, Xan was added after reconstitution, which did not affect activity even at high concentrations (Figure II-12a,

blue bars). These results suggest that in the presence of Xan, the holoHRP has less RH available for reconstitution which can be accurately detected with this assay.

Next, this HRP assay was applied to intact *A. baumannii* cells. For this purpose, *A. baumannii* was incubated with Xan for 30 minutes, which is presumably long enough to allow the compound to enter the cell but not sufficiently long to cause stimulation of heme biosynthesis by Xan. DMSO-treated *A. baumannii* served as positive control for the reconstitution. After cell lysis, a clear decrease of RH levels with increasing concentration of Xan was detected (Figure II-12b).

Combined with the heme binding experiments, these results show that Xan effectively sequesters heme and thereby lowers free RH levels. This restricts the ability of hemoproteins to acquire this crucial cofactor, thus impairing their physiological metabolic function, as has been shown for HRP. Furthermore, heme regulates its own synthesis by binding to glutamyl-tRNA reductase (GtrR, *hemaA*) via a feedback mechanism,¹¹⁰ which may also be adversely affected. Such an impairment of feedback inhibition might lead to an uncontrolled heme biosynthesis resulting in excessive production of heme, which is highly toxic for the cells. Remarkably, this stimulation of heme biosynthesis has already been recognized in the whole proteome analysis of Xan-treated *A. baumannii*.

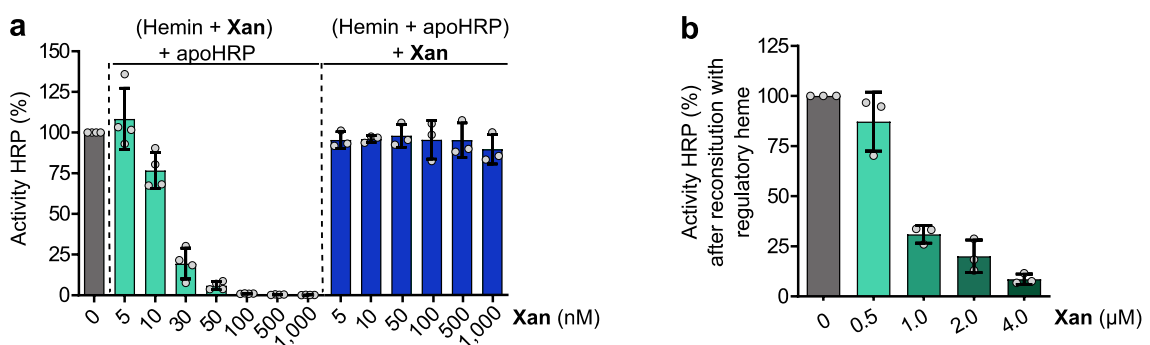


Figure II-12: Measurement of RH level. a) *In vitro* activity assay of reconstituted holoHRP in the presence of various concentrations of Xan. Hemin (5 nM) was pre-incubated with either Xan (green bars) or apoHRP (blue bars, 5 μ M) followed by addition of apoHRP or Xan, respectively and activity of holoHRP was subsequently measured.

Averaged technical duplicates were normalised to the respective DMSO-treated samples and values represent mean \pm s.d. of independent experiments ($n = 3$). b) Reconstitution activity assay of holoHRP in *A. baumannii* cell lysate after treatment of intact cells with various concentrations of Xan for 30 min. ApoHRP (final concentration 10 μ M) was added to cell lysates and activity of holoHRP was measured. Averaged technical quadruplicates were normalised to the respective DMSO-treated samples and values represent mean \pm s.d. of independent experiments ($n = 3$). Noteworthy, at low concentrations of Xan a higher activity, both *in vitro* and in intact *A. baumannii*, was observed for unknown reasons (Supplementary Figure 4).

2.9. Extraction and Quantification of Porphyrins

An upregulated heme biosynthesis caused by restricted feedback inhibition would lead to elevated tetrapyrrole levels. The most direct way to prove this would be to quantify the intracellular heme level. However, since initial tests have shown that such a quantification is not achievable in the presence of Xan, due to its binding to heme, the fluorescent properties of metal-free tetrapyrroles (e.g., protoporphyrin IX) have been exploited.¹⁴²

For this purpose, *A. baumannii* was incubated for 1 h with either Xan or DMSO. Subsequently, the porphyrins were extracted from the cell lysate according to an established protocol and the fluorescence spectra were measured ($\lambda_{\text{ex.}} = 406 \text{ nm}$).^{143–145} It is important to note that the spectra of the Xan- and DMSO-treated samples have the same characteristic features, namely two maxima at about 612 nm and 658 nm (Figure II-13a). Therefore, the fluorescence signal at $\lambda_{\text{ex.}} = 406 \text{ nm}$ and $\lambda_{\text{em.}} = 612 \text{ nm}$ was used to compare the fluorescence intensities. As expected for upregulated heme biosynthesis, the fluorescent signal of Xan-treated *A. baumannii* was significantly higher (Figure II-13b), indicating the accumulation of fluorescent porphyrins. Furthermore, incubation of the bacteria over a longer period of time with Xan (4 h) resulted in a reddish-brown colour of the bacterial pellet (Figure II-13c), which is very characteristic for the accumulation of porphyrins.^{146–148}

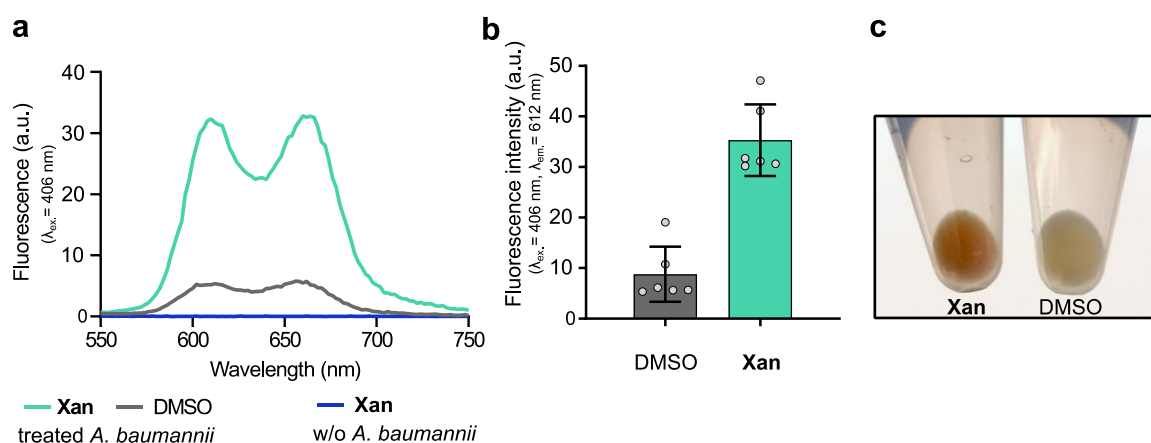


Figure II-13: Accumulation of porphyrins. a) Fluorescence spectrum of extracted porphyrins. Intact *A. baumannii* ATCC19606 was incubated with Xan ($1 \mu\text{M}$) or DMSO for 1 h. After cell lysis, porphyrins were extracted and fluorescence spectra were recorded ($\lambda_{\text{ex.}} = 406 \text{ nm}$). Samples containing Xan without added bacteria ($1 \mu\text{M}$, violet) served as fluorescence control. Figure is representative for $n = 6$ independent extractions. b) Detection of accumulated porphyrins by fluorescence spectroscopy. Intact *A. baumannii* ATCC19606 was incubated with Xan ($1 \mu\text{M}$) for 1 h. After cell lysis, porphyrins were extracted and fluorescence intensities ($\lambda_{\text{ex.}} = 406 \text{ nm}$, $\lambda_{\text{em.}} = 612 \text{ nm}$) were measured. Data represent mean values \pm s.d. of fluorescence intensities of independent experiments ($n = 6$). c) Pellets of *A. baumannii* treated with either Xan ($1 \mu\text{M}$, left) or DMSO (right) for 4 h.

2.10. Time-Kill Experiments

The accumulation of porphyrins potentially produces reactive oxygen species (ROS), which is known to be deleterious to bacteria.¹⁴⁹ In order to explore the biological effect of the elevated porphyrin level caused by Xan, time-kill experiments were performed. *A. baumannii* was incubated either with Xan ($1\times$ MIC and $16\times$ MIC) or DMSO and colony forming units (CFU) were determined after several time points on LB agar plates.

While the bacterial population in the DMSO control increased to 10^9 CFU/mL, Xan exhibited bacteriostatic activity over a period of 7 hours at both concentrations tested (Figure II-14a). However, after 24 h, Xan at 250 nM ($1\times$ MIC) no longer affected bacterial growth and CFU/mL were comparable to the DMSO control, whereas at a concentration of $4 \mu\text{M}$ ($16\times$ MIC) the bacteria were completely eliminated, showing a bactericidal effect. The bacterial growth after 24 h at $1\times$ MIC is most likely due to the

known inoculum effect of antibiotics, as the starting CFU/mL for MIC determination and the time-kill experiment were approximately 10^5 and 10^7 , respectively.¹⁵⁰

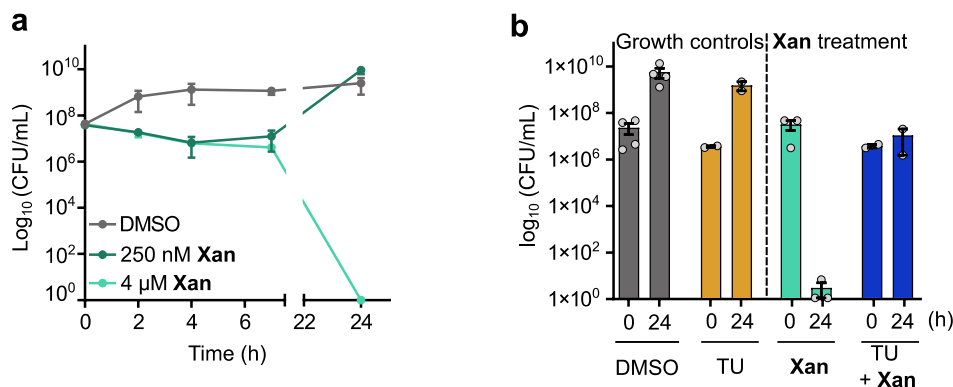


Figure II-14: Time-kill experiments. a) Time-dependent killing of exponentially growing *A. baumannii* ATCC19606 ($\sim 10^7$ CFU/mL) by Xan (1 \times MIC and 16 \times MIC). After various time points viable cells (CFU/mL) were determined in quadruplicates. The data represent average values \pm s.d. ($n = 3$ independent experiments per group). b) Protective effect of thiourea (TU) on Xan-treated *A. baumannii* ATCC19606. DMSO (grey bars), TU (150 mM, orange bars), Xan (4 μ M, green bars) as well as TU (150 mM) and Xan (4 μ M, blue bars) were added to *A. baumannii* ATCC19606 ($\sim 10^7$ CFU/mL) and cells were incubated for 24 h. After 0 h and 24 h CFU/mL were determined in quadruplicates. Data represent mean values \pm s.e.m of $n = 4$ (DMSO), $n = 3$ (Xan) and $n = 2$ (TU, TU and Xan) independent experiments.

Next, it was investigated whether the bactericidal effect was caused by ROS. For this purpose, the time-kill experiment was performed in the presence of the known radical scavenger thiourea (TU).¹⁵¹ Indeed, TU was able to counteract the deleterious activity of Xan (Figure II-14b), which is demonstrated by the bacteriostatic effect. This suggests that the bactericidal activity of Xan is caused by ROS.

2.11. Checkerboard Assay

The synergistic combination of two antibiotics is generally an effective strategy to combat resistant strains.⁶ Since the activity of aminoglycoside antibiotics, such as gentamicin (Gen), is known to be influenced by altered heme biosynthesis, the synergistic effect of Xan and Gen was investigated next.^{132,147,152} Fractional inhibitory

concentrations (FICs) in a Gen-sensitive (ATCC19606) and Gen-resistant (AB5075)¹⁵³ *A. baumannii* strain were determined by checkerboard assays. In fact, Xan potentiated the activity of Gen not only in the Gen-sensitive, but also in the Gen-resistant strain. This was manifested by FIC indices in the range of 0.3125 – 0.375 (Table II-2), which means that Xan (0.25× MIC) resensitized the Gen-resistant *A. baumannii* AB5075, resulting in a reduction of the MIC of Gen from 800 µM to 50 – 100 µM.

Table II-2| Antimicrobial synergy study with Gen and Xan in *A. baumannii*. checkerboard assay was performed in $n = 3$ (ATCC19606) and $n = 2$ (AB5075) independent experiments.

<i>A. baumannii</i>	Gen MIC (µM)	FIC Index
ATCC19606	8 – 16	0.3125 – 0.375
AB5075	800	0.3125 – 0.375

2.12. Toxicity and *Galleria mellonella* Infection Model

Xan has already been studied in animals and humans without exhibiting high toxic effects.^{68–71} In addition, Shang *et al.* published a half maximal inhibitory concentration (IC₅₀) in HeLa cells of approximately 35 µM, which provides a therapeutic window.⁷³ In order to validate these results, Xan's toxicity was tested in HeLa cells, which didn't show significant toxicity in HeLa cells up to its solubility limit of 10 µM (Figure II-15).

Encouraged by these results, *in vivo* models were next used to study Xan. In addition to testing the toxicity of Xan in these models, Xan's ability to eliminate *A. baumannii in vivo* was investigated.

The murine model is the most frequently used model for the investigation of microbial infections. However, there are ethical, financial and logistical hurdles associated with the use of rodents as an infection model, preventing them from being used in many

laboratories.¹⁵⁴ *Galleria mellonella* has proved to be an alternative model, as the larvae can be obtained easily, cheaply and in large numbers.^{154,155} Although insects have no adaptive immune defence, their innate immune response resembles the immune system in vertebrates.¹⁵⁶ Furthermore, there are no ethical restrictions and no additional laboratory equipment is required, making it a viable infection model for many research groups.¹⁵⁴

For this model, injection is the most common way of administration, for which, however, the compound has to be dissolved. Since the solubility of Xan was repeatedly a limiting factor in previous experiments, the DMSO tolerance of *Galleria mellonella* larvae was first investigated. Injections of various concentrations of DMSO in PBS into the larvae revealed a DMSO tolerance of up to 10% (Figure II-15a), which was thus used as a solvent for Xan. To study the toxicity, different concentrations of Xan were injected, which was found to be not lethal to the larvae up to 1 mM, the highest concentration tested (Figure II-15b). However, it should be noted that Xan was not completely dissolved at the highest concentration but was administered as a suspension.

To investigate the *in vivo* efficacy of Xan against *A. baumannii*, the larvae were infected with a lethal dose of *A. baumannii* AB5075 (approximately 10⁵ total CFUs). However, administration of Xan 1.5 h later did not enhance the survival rate of the larvae (Figure II-15c).

Several standard antibiotics have already been tested in similar infection models. Cefotaxime, tetracycline, gentamicin and meropenem were used at concentrations of 150 mg/kg, 50 mg/kg, 6 mg/kg and 60 mg/kg, respectively.¹⁵⁷ The highest concentration at which Xan was completely dissolved was 100 µM, equivalent to 0.6 mg/kg, and thus significantly lower than the concentrations of standard antibiotics, which could be a potential reason for the lack of activity.

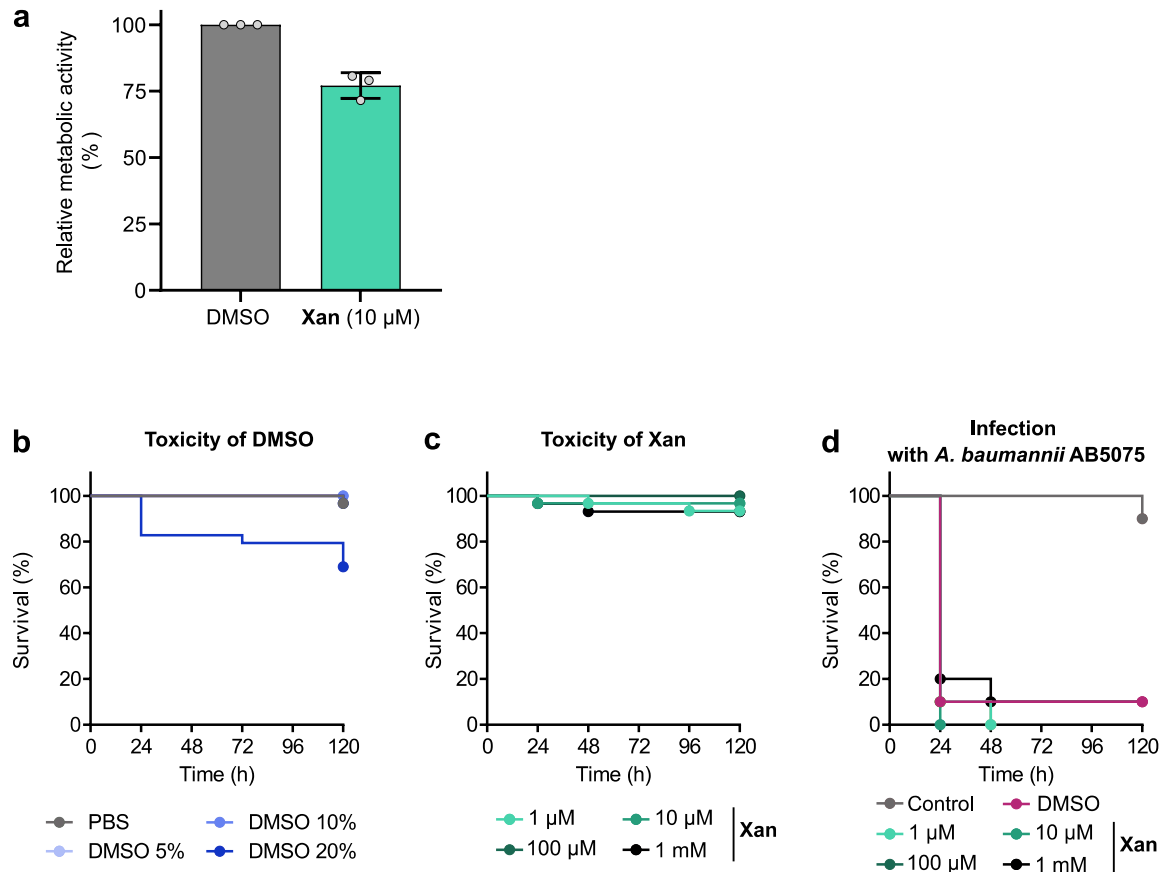


Figure II-15: Toxicity of Xan and activity of Xan tested in *Galleria mellonella*. Cytotoxicity of Xan against human cells (HeLa). Averaged technical sextuplicates were normalised to DMSO-treated samples and value represents mean \pm s.d. of independent experiments ($n = 3$). b) Various concentrations of DMSO were injected into *Galleria mellonella* larvae to study the maximum DMSO tolerance. c) Various concentrations of Xan, dissolved in PBS + 10% DMSO, were injected (5 μ L) into the worms to study the toxicity. The reported values in b) and c) represent the averages of $n = 3$ independent experiments with at least 10 worms per group for each experiment. d) *Galleria mellonella* larvae were infected with *A. baumannii* ($\sim 10^5$ CFU). After 1.5 h, various concentrations of Xan, dissolved in PBS + 10% DMSO, were injected (5 μ L). The control group (grey) was not infected with *A. baumannii* and PBS + 10% DMSO was injected 1.5 h later. The reported values represent one independent experiment with 10 worms per group.

2.13. Summary – Mechanism of Action

Based on the fascinating activity of Xan against a variety of pathogenic bacteria, including *A. baumannii*, a multidisciplinary target analysis was performed to unravel the MoA. A metal binding assay and chemical proteomic methods, ABPP and A/BPP, suggest that neither metal complexation nor protein binding is the major contributor to the MoA. The generation and subsequent sequencing of Xan-resistant mutants identified PbgS as the only consistently mutated enzyme among all variants. Interestingly, an identical missense mutation was found in all mutants, resulting in the amino acid modification P241S near the active site. Activity studies revealed a significantly lower efficiency (k_{cat}/K_m) for the mutated PbgS for substrate 5-ALA, which presumably entails a lower tetrapyrrole synthesis rate. Notably, inhibition experiments excluded PbgS as a direct target of Xan, which was consistent with ABPP and A/BPP results.

A whole proteome analysis of Xan-resistant mutants *versus* wild type as well as Xan-*versus* DMSO-treated wild type *A. baumannii* was performed to explain the causes and consequences of Xan treatment. With the addition of Xan, the upregulation of putative proton/sodium glutamate symport protein as well as TonB-dependent siderophore receptors demonstrated enhanced heme biosynthesis, which was validated by elevated porphyrin levels. In contrast, resistant mutants have made adaptations, besides the mutation in PbgS, aiming to reduce heme levels. These include the upregulation of heme degrading as well as acetoin metabolizing enzymes. The latter indicate a change in metabolism from respiration to fermentation. In addition, the direct binding of Xan to heme results in a corresponding reduction in free RH levels and impedes access to RH by heme-dependent enzymes.

How does Xan trigger heme biosynthesis and eliminate bacteria? In summary, the results refer to a MoA in which Xan penetrates bacterial cells and binds to free RH (spectroscopic analysis, Figure II-16). This complexation impairs the binding of RH to

essential hemoproteins (as shown in the HRP assay), which consequently cannot carry out their biological function due to the lack of their crucial cofactor. Examples of essential heme dependent proteins are those of the electron transport chain (e.g., succinate dehydrogenase cytochrome *b₅₅₆* subunit, cytochrome *bo₃* ubiquinol oxidase subunit).¹⁵⁸ Another important function of RH is the feedback inhibition of its own biosynthesis, which might be compromised by the binding of Xan to heme. As a result, uncontrolled heme biosynthesis leads to an increased demand for its substrates (upregulation of glutamate symporter and TonB-dependent siderophore receptors) and ultimately to increased porphyrin levels (fluorescence analysis). This dysregulation can have multiple detrimental consequences for the bacteria. The elevated porphyrin level causes deleterious ROS (time-kill experiment). It is also conceivable that the increased demand for glutamate leads to a glutamate deficiency within the bacteria. To escape this antibiotic pressure, the bacteria have evolved a resistance strategy in which a single mutation in a regulatory enzyme of heme biosynthesis, PbgS, significantly reduces the porphobilinogen synthesis rate, an intermediate in the tetrapyrrole biosynthesis. Together with the expression of heme-degrading enzymes and the upregulation of efflux pumps (whole proteome analysis), the effects of Xan can be balanced. The binding of Xan to heme and the down-regulation of heme production may result in an insufficient supply of the electron transport chain with the cofactor, forcing bacteria to switch to fermentative metabolism, as indicated by the upregulation of acetoin metabolizing enzymes (whole proteome analysis). This MoA, which is based on binding to a cofactor, also explains the broad spectrum of activity of Xan, with the exception of *E. faecalis* and *E. faecium*. Interestingly, both strains represent natural heme auxotrophs that do not synthesize their own heme. They take up heme from the environment, but can also survive without this cofactor due to their metabolically diverse fermentation pathways.¹⁵⁹

In summary, this multidisciplinary study has succeeded in understanding the MoA of the NP Xan, which has been known for over 70 years.

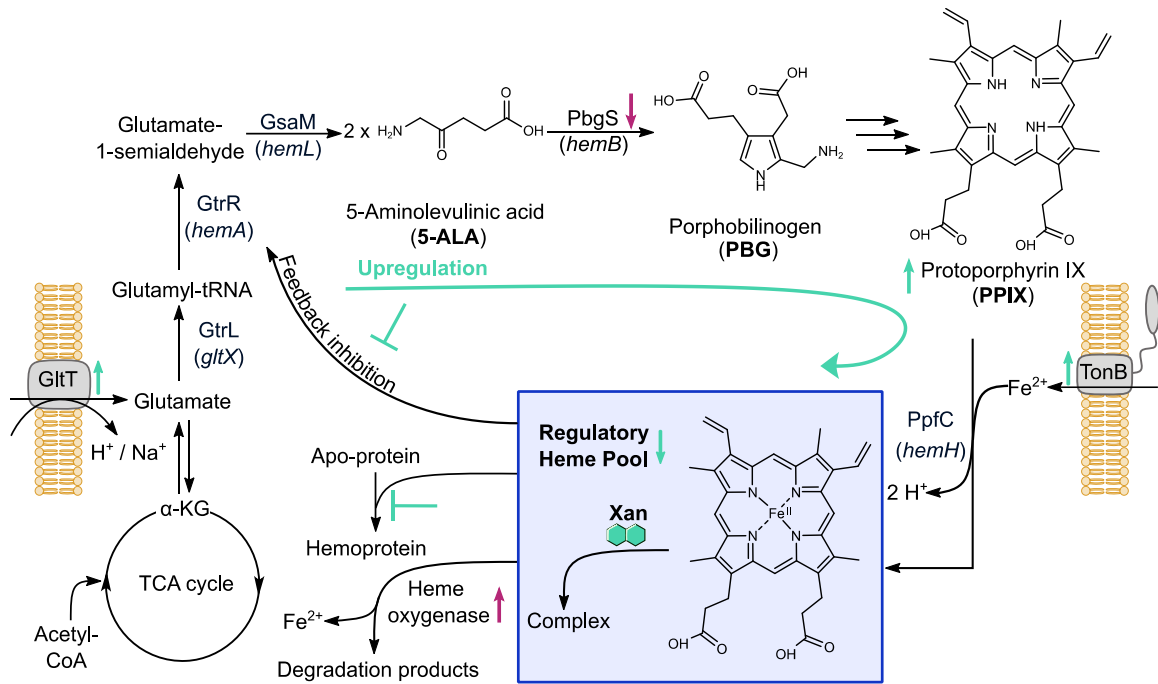


Figure II-16: Dysregulation of heme biosynthesis by Xan. Hypothesis of Xan's MoA is based on experimental evidence within this study. Full proteome analysis of Xan compared to DMSO-treated *A. baumannii* revealed a putative proton/sodium-glutamate symport protein as well as two TonB-dependent siderophore receptors as significantly upregulated proteins pointing to enhanced demand for heme biosynthesis substrates, glutamate and iron. Extraction of porphyrins of Xan-treated *A. baumannii* validated the accumulation of tetrapyrroles. UV-Vis spectroscopy showed an interaction between hemin and Xan. Further, a reconstitution assay using apoHRP led to the conclusion, that complex formation of Xan with hemin leads to a reduced effective level of RH and thus to an impaired regulatory role of heme. Conceivable consequences are the inability of hemoproteins to acquire heme for their normal metabolic function and uncontrolled biosynthesis by hampered feedback inhibition. In-depth analysis of Xan-resistant isolates showed a shared amino acid mutation P241S in PbgS, which leads to a significant drop in enzyme efficiency and thus counteracts the upregulation by Xan. Further, Xan-resistant colonies upregulate proteins involved in biofilm formation, RND transporters, acetoin metabolism and redox enzymes, protecting cells from oxidative stress, e.g., putative heme oxygenase. Abbreviations include the following: TCA, tricarboxylic acid cycle; α-KG, α-ketoglutarate; GluRS (*gltX*), glutamyl-tRNA synthetase; GtrR (*hemA*), glutamyl-tRNA reductase; GsaM (*hemL*), glutamate-1-semialdehyde-2,1-aminomutase; PbgS (*hemB*), porphobilinogen synthase; PpfC (*hemH*), protoporphyrin IX ferrochelatase. Cellular effects induced by Xan treatment are shown by green arrows, while effects of resistance formation are indicated by red arrows.

2.14. Outlook

Xan exhibits a broad spectrum of activity and, as this study has shown, an unprecedented MoA with low toxicity. These are the perfect requirements for a new lead compound for antibiotic development.

In many experiments the solubility of Xan posed a major limitation, and structural optimisations are needed to improve this property. In order to be able to do so, the binding of Xan to heme needs to be structurally clarified, which can be achieved by a crystal structure of the complex. Further, derivatives of Xan, either with only one isonitrile group or a saturated core structure might help to identify the features important for complex formation. In addition, isonitrile compounds are known for their heme binding, making it conceivable that other representatives of this class of NPs, e.g., MDN-0057, have a comparable MoA. Thus, this functional group might serve as a starting point and common denominator for a structurally diverse set of antibiotic compounds with improved physicochemical properties (e.g. solubility).

In addition, remarkably many compounds of this class are effective against Gram-negative bacteria, which means that they penetrate the outer membrane and enter the cell. This is the major challenge in the search for antibiotics that are effective against Gram-negative pathogens. Therefore, it is important to examine the contribution of the functional group of isonitriles to this process. It is conceivable that isonitriles could possibly enable compounds with exclusively Gram-positive activity to have an effect even on Gram-negative pathogens.

In conclusion, the elucidation of this novel MoA may enable the development of structurally new antibiotic compounds that are urgently needed to combat multi-resistant pathogens.

3. Experimental Section

3.1. Media

Unless otherwise stated B medium (10 g/L casein peptone, 5 g/L NaCl, 5 g/L yeast extract, 1 g/L K_2HPO_4 , pH 7.5) was used for cultivation of all *S. aureus* strains. LB medium (Lysogeny Broth; 10 g/L casein peptone, 5 g/L NaCl, 5 g/L yeast extract, pH 7.5) was used for cultivation of all *S. typhimurium* strains, all *A. baumannii* strains, both *E. coli* strains, and *P. aeruginosa* PAO1. BHB medium (Brain Heart Infusion, 7.5 g/L brain infusion, 10 g/L heart infusion, 10 g/L casein peptone, 5 g/L NaCl, 2.5 g/L Na_2HPO_4 , 2 g/L glucose, pH 7.4) was used for cultivating *L. monocytogenes*, *K. pneumoniae*, *E. faecalis* and *E. faecium*.

For resistance development, *A. baumannii* was cultivated in cation-adjusted Mueller-Hinton broth (17.5 g/L acid hydrolysate of casein, 3 g/L beef extract, 1.5 g/L starch, pH 7.3).

3.2. Stock Solutions

Xan, XanDME, XP and XPP were synthesized as described in section "Chemical Synthesis" and stock solutions were prepared with DMSO as solvent. 1 mM hemin working solution in 0.1 N aqueous NaOH was freshly prepared before use and stored in the dark.

Gentamicin (Gen) and Ciprofloxacin (Cip) stock solutions were prepared in sterile ddH₂O and 0.1 N aqueous HCl, respectively.

3.3. Overnight Cultures

The appropriate medium (5 mL) for cultivation was inoculated (1:1,000) with the desired bacterial cryostock with a sterile pipette tip in a plastic culture tube. The culture was then incubated overnight (14 – 16 h, 37 °C, 200 rpm). A sterile control (medium containing no bacteria) was included each time.

3.4. Minimum Inhibitory Concentration (MIC)

Overnight cultures were diluted 1:10,000 into medium and directly used for the tests. Various dilutions of the compounds in DMSO were prepared and 1 μ L thereof was pipetted in triplicates in 96 well-plates (transparent Nunc 96-well flat bottom, *Thermo Fisher Scientific*), including DMSO only, which served as growth control. Then, 99 μ L of the diluted bacterial suspension were transferred to each well and a sterile control containing only medium was included. Bacteria were incubated for 24 h (37°C, 200 rpm) and the dilution series was analysed for microbial growth, indicated by turbidity. The lowest concentration in the dilution series at which no growth of bacteria could be observed by eye was defined as the minimum inhibitory concentration (MIC) of the compound. MIC values were determined by three independent experiments.

3.5. Metal Chelation Assay

The assay was performed as described by Shapiro *et al.* with slight modifications.⁹⁴ All fluorescence titrations were performed in MeOH on a Dual-FL™ (HORIBA Scientific) using a sub-micro fluorometer cell (open top, *Starna*, catalog number: 16.160F-Q-10/Z15). Briefly, a 12.5 μ M stock solution of Xan (150 μ L; 5% DMSO final concentration) was prepared and an emission spectrum was recorded ($\lambda_{\text{excitation}} = 366$ nm, integration time = 1 s, accumulations = 10). The metal chloride stock solution (125 μ M) was added in 3.75 μ L portions (0.25 eq.), the solution was gently mixed, and an emission

spectrum was recorded after each addition. All experiments were performed in triplicates. An emission spectrum of MeOH with 5% DMSO was used as a blank control and was subtracted from values. A fluorescence titration using only MeOH served as a negative control for metal binding.

3.6. Gel-free ABPP and A/BPP

3.6.1. Culture, labelling, lysis and click-reaction

Preparative ABPP in *A. baumannii* ATCC19606 and *E. coli* K12 with XP

Overnight cultures were diluted 1:100 in LB medium and incubated (37 °C, 200 rpm) until an OD₆₀₀ of 2.0 was reached. Bacterial cells were harvested (6,000 ×g, 4 °C, 15 min), washed with PBS and resuspended in PBS to give a final OD₆₀₀ of 40. This bacterial suspension was split into aliquots of 1 mL and either XP (3 μM, 1% DMSO final concentration) or DMSO (1%) was added, followed by incubation (37 °C, 200 rpm) for 2 h. For competition labelling, cells were treated with Xan (30 μM, 1% DMSO final concentration) for 2 h (37 °C, 200 rpm) before the addition of XP (3 μM, 1% DMSO final concentration). After compound treatment, bacteria were harvested (6,000 ×g, 4 °C, 15 min) and washed with PBS. Cell pellets were resuspended in 0.4% (w/v) SDS in PBS (1 mL) and lysed by sonication (4 × 30 sec, 75% intensity; Sonopuls HD 2070 ultrasonic rod, *Bandelin electronic GmbH*) with cooling breaks on ice. The cell lysate was clarified by centrifugation (20,000 ×g, 30 min, 4 °C), protein concentration was measured using the Pierce BCA Protein assay kit (*Thermo Fisher Scientific, Pierce Biotechnology*) and sample concentrations were adjusted to equal protein amount. Next, 500 μL clear cell lysate (2 mg/mL protein concentration) were subjected to click-reaction (CuAAC) by adding 3 μL biotin azide (10 mM in DMSO), 10 μL tris(2-carboxyethyl) phosphine (TCEP; 52 mM in ddH₂O), 30 μL TBTA ligand (1.667 mM in 80% tBuOH and 20% DMSO) and 10 μL CuSO₄ (50 mM in ddH₂O) and samples were incubated for 1 h at room temperature (RT). Following CuAAC, proteins

were precipitated with ice-cold acetone (4 volumes) at $-20\text{ }^{\circ}\text{C}$ overnight, centrifuged ($16,900 \times g$, $4\text{ }^{\circ}\text{C}$, 15 min) and washed twice with ice-cold methanol (1 mL). Pellets were resuspended in 0.4% (w/v) SDS in PBS (500 μL) at RT by sonication (10% intensity, 10 s; Sonopuls HD 2070 ultrasonic rod, *Bandelin electronic GmbH*). Affinity enrichment was performed with avidin agarose resin (product no. A9207, *Sigma Aldrich*, pre-washed three times with 0.4% (w/v) SDS in PBS (1 mL); $400 \times g$ for 2 min was used to pellet beads; typically, 50 μL of bead slurry was used for enrichment). Samples were added to the resin in LoBind Eppendorf tubes and incubated with agitation for 1 h at RT. To remove unbound proteins, the beads were washed three times with 0.4% (w/v) SDS in PBS (1 mL), two times with 6 M urea (in ddH₂O, 1 mL) and three times with PBS (1 mL). For quantitative mass spectrometric analyses, avidin agarose beads with bound proteins were resuspended in 200 μL denaturation buffer (7 M urea, 2 M thiourea in 20 mM pH 7.5 HEPES buffer). Upon on-bead reduction with TCEP (5 mM) at $37\text{ }^{\circ}\text{C}$ for 1 h, proteins were alkylated using iodoacetamide (IAA, 10 mM) at $25\text{ }^{\circ}\text{C}$ for 30 min and samples were quenched with dithiothreitol (DTT, 10 mM) at RT for 30 min. Samples were diluted with 600 μL triethylammonium bicarbonate (TEAB) buffer (50 mM in ddH₂O) and digested with 1.5 μL trypsin (0.5 $\mu\text{g}/\mu\text{L}$; sequencing grade, modified, *Promega*) at $37\text{ }^{\circ}\text{C}$ overnight under continuous shaking (450 rpm). On the next day, the digestion was stopped by adding formic acid (FA, 10 μL) and the suspension was centrifuged ($17,000 \times g$, 3 min, RT) to pelletize the beads. The supernatant was loaded on 50 mg SepPak C 18 columns (*Waters*) equilibrated with 0.1% trifluoroacetic acid (TFA). The peptides were washed three times with 1 mL 0.1% TFA and 500 μL 0.5% FA. Afterwards, the peptides were eluted three times with 250 μL elution buffer (80% acetonitrile (ACN), 0.5% FA), lyophilized and stored at $-80\text{ }^{\circ}\text{C}$ until further usage. The experiment was performed in $n = 4$ (*E. coli* K12) and in $n = 3$ (*A. baumannii* ATCC19606) independent experiments.

Preparative ABPP in *A. baumannii* ATCC19606 with XPP

Overnight cultures were diluted 1:100 in LB medium and incubated (37 °C, 200 rpm) until an OD₆₀₀ of 3.5 was reached. Bacterial cells were harvested (6,000 ×g, 4 °C, 15 min), washed with PBS and resuspended in PBS to give a final OD₆₀₀ of 40. This bacterial suspension was split into aliquots of 1 mL and either XPP (3 μM, 1% DMSO final concentration) or DMSO (1%) was added, followed by incubation (37 °C, 200 rpm) for 2 h. After treatment, samples were transferred to 6-well plates (flat bottom, *VWR*) and irradiated for 15 min with UV light (UV low-pressure mercury-vapour fluorescent lamp, Philips TL-D 18W BLB, 360 nm maximum). During irradiation a cool pack was placed under the plate. Subsequently, bacteria were harvested (6,000 ×g, 4 °C, 15 min) and washed with PBS. Cell pellets were resuspended in PBS (1 mL) and lysed (3 × 30 s at 6,500 rpm, 30 s cooling breaks on ice after each run; Precellys Glass/Ceramic Kit SK38 2.0 mL tubes; Precellys 24 Homogenizer, *Bertin Technologies*). The cell lysate was clarified by centrifugation (20,000 ×g, 30 min, 4 °C). The soluble fraction was transferred to a new Eppendorf tube. The insoluble fraction was washed twice with PBS and resuspended in PBS (600 μL). Protein concentration was measured using the Pierce BCA Protein assay kit (*Thermo Fisher Scientific, Pierce Biotechnology*) and sample concentrations were adjusted to equal protein amount (soluble fraction, 1 mg/mL; insoluble fraction, 2 mg/mL). Next, 10% (w/v) SDS in PBS was added to 500 μL of adjusted protein samples to get a final concentration of 0.4% (w/v) SDS in PBS. Afterwards, the experimental procedure was analogous to ABPP with XP in *A. baumannii* and *E. coli* as described above. The experiment was performed in *n* = 4 independent experiments.

3.6.2. LC-MS/MS analysis

Before MS measurements, the lyophilized peptides were resolved in 25 μL 1% FA and filtered through 0.22 μm PVDF filters (*Millipore*), which were equilibrated with 300 μL

1% FA. The filtrates were transferred into MS-vials and stored at $-20\text{ }^{\circ}\text{C}$ until the measurements were performed.

Samples were analysed with an UltiMate 3000 nano HPLC system (*Dionex*) using an Acclaim C18 PepMap100 ($75\text{ }\mu\text{m ID} \times 2\text{ cm}$) trap column and an Acclaim PepMap RSLC C18 ($75\text{ }\mu\text{m ID} \times 50\text{ cm}$) separation column coupled to a Q Exactive Plus (*Thermo Fisher*) in EASY-spray setting. Samples were loaded on the trap column and washed with 0.1% TFA, then transferred to the analytical column (buffer A: H_2O with 0.1% FA, buffer B: ACN with 0.1% FA, flow 300 nL/min , gradient 5 to 22% buffer B in 115 min, then to 32% buffer B in 10 min, then to 90% buffer B in 10 min and hold 90% buffer B for 10 min, then to 5% buffer B in 0.1 min and hold 5% buffer B for 9.9 min). Q Exactive Plus was operated in a TOP10 data dependent mode. Full scan acquisition was performed in the orbitrap at a resolution of 140,000 and an AGC target of 3e^6 (maximum injection time of 80 ms) in a scan range of 300 – 1,500 m/z . Monoisotopic precursor selection as well as dynamic exclusion (exclusion duration: 60 s) was enabled. Precursors with charge states of >1 and intensities greater than 1e^5 were selected for fragmentation. Isolation was performed in the quadrupole using a window of 1.6 m/z . Precursors were collected to an AGC target of 1e^5 (maximum injection time of 100 ms) and acquisition was performed at a resolution of 17,500 in a scan range of 200 – 2,000 m/z . Fragments were generated using higher-energy collisional dissociation (HCD, normalised collision energy: 27%) and detected in the orbitrap.

3.6.3. MS data analysis

Raw files were analysed using MaxQuant software (version 1.6.2.10) with the Andromeda search engine. The following settings were applied: fixed modification: carbamidomethylation (cysteine); variable modification: oxidation (methionine), acetylation (*N*-terminus); proteolytic enzyme: trypsin/P; missed cleavages: 2; main search tolerance: 4.5 ppm; MS/MS tolerance: 0.5 Da; false discovery rates: 0.01. The

options "LFQ" and "match between runs" (0.7 min match and 20 min alignment time windows) were enabled; "second peptides" was disabled.⁹⁶ Searches were performed against the UniProt database for *A. baumannii* ATCC19606 (taxid: 575584, 29.06.2020) or *E. coli* K12 (taxid: 83333, 01.07.2020). Statistical analysis of the data was performed using Perseus (version 1.6.13.0).¹⁶⁰ Putative contaminants, reverse peptides and peptides only identified by site were deleted. LFQ intensities were \log_2 -transformed and data was filtered for either three valid values in at least one group (ABPP with XP in *E. coli*, ABPP with XPP in *A. baumannii*) or two valid values in at least one group (ABPP with XP in *A. baumannii*) and missing value imputation was performed over the total matrix. For statistical evaluation, $-\log_{10}(P \text{ values})$ were obtained by a two-sided two sample Student's *t*-test.

3.7. Gel-based ABPP

For labelling of recombinant protein, 100 μL of the protein in PBS (1 μM) were incubated with various concentrations of XP (1% DMSO final concentration) for 1 h at RT. Heat control (h.c.) protein samples were prepared in 1% (w/v) SDS in PBS and were boiled at 95 $^{\circ}\text{C}$ for 20 min prior to the addition of the probe. After compound treatment, the samples were subjected to CuAAC by 2 μL rhodamine azide (10 mM in DMSO), 2 μL TCEP (52 mM in ddH₂O), 6 μL TBTA ligand (1.667 mM in 80% tBuOH and 20% DMSO) and 2 μL CuSO₄ (50 mM in ddH₂O) and incubated for 1 h at RT. One equivalent of 2 \times Laemmli buffer (125 mM Tris-HCl, 20% (v/v) glycerol, 4% (w/v) SDS, 0.005% (w/v) bromphenol blue, 10% (v/v) 2-mercaptoethanol) was added and samples were subsequently analysed by SDS-PAGE (12.5% polyacrylamide gels).

The BenchMark™ Fluorescent Protein Standard (*Thermo Fisher Scientific*) and the Roti®-Mark Standard (*Carl Roth*) were used as size markers. An ImageQuant LAS-4000 image reader (*GE Healthcare*) equipped with a Fujinon VRF43LMD3 lens and a 575DF20 filter (*Fujifilm*) was used for visualization of labelled proteins. Gels were then Coomassie-stained by overnight incubation in staining solution (0.25% (w/v)

Coomassie Brilliant Blue R-250, 9.2% AcOH, 45.4% EtOH), followed by destaining with 10% AcOH, 40% EtOH in ddH₂O.

3.8. Cloning

Table II-3| Plasmids used in the present work.

Plasmid	Description	Cloning method	Source
pDONR 207	Gateway donor vector; <i>rrnB</i> T2, <i>rrnB</i> T1, <i>attP1</i> , <i>ccdB</i> , Cm ^R , <i>attP2</i> , <i>Gen</i> ^R , pUC ori	-	Invitrogen
pDONR 207- <i>abhemB</i> _{wt}	Gateway donor vector; <i>rrnB</i> T2, <i>rrnB</i> T1, <i>attL1</i> , <i>attL2</i> , <i>Gen</i> ^R , pUC ori, gene <i>hemB</i> cloned into <i>attP1</i> and <i>attP2</i> sites of pDONR207	Gateway cloning	This study
pDONR 207- <i>abkatG</i>	Gateway donor vector; <i>rrnB</i> T2, <i>rrnB</i> T1, <i>attL1</i> , <i>attL2</i> , <i>Gen</i> ^R , pUC ori, gene <i>AbkatG</i> cloned into <i>attP1</i> and <i>attP2</i> sites of pDONR207	Gateway cloning	This study
pDONR 207- <i>eckatG</i>	Gateway donor vector; <i>rrnB</i> T2, <i>rrnB</i> T1, <i>attL1</i> , <i>attL2</i> , <i>Gen</i> ^R , pUC ori, gene <i>EckatG</i> cloned into <i>attP1</i> and <i>attP2</i> sites of pDONR207	Gateway cloning	This study
pDest 17	Gateway destination vector; T7 promotor, N-6×His, <i>attR1</i> , Cm ^R , <i>ccdB</i> , <i>attR2</i> , Amp ^R , pBR322 ori	-	Invitrogen
pET-41-K	Gateway destination vector; T7 promotor, <i>lacI</i> , N-6×His, MBP,	-	EMBL

	<i>attR1</i> , Cm ^R , <i>ccdB</i> , <i>attR2</i> , Kan ^R , pBR322 ori		
pET 300	Gateway destination vector; T7 promoter, <i>lacI</i> , N-6×His, <i>attR1</i> , Cm ^R , <i>ccdB</i> , <i>attR2</i> , Amp ^R , pBR322 ori	-	Invitrogen
pDest 17- <i>abhemB</i> _{wt}	Expression vector; <i>attB1</i> , <i>attB2</i> , Amp ^R , T7 promoter, pBR322 ori, N-6×His, gene <i>hemB</i> cloned into <i>attR1</i> and <i>attR2</i> sites of pDest17	Gateway cloning	This study
pET-41-K- <i>abhemB</i> _{wt}	Expression vector; <i>attB1</i> , <i>attB2</i> , Amp ^R , T7 promoter, <i>lacI</i> , pBR322 ori, N-6×His, MBP, gene <i>hemB</i> cloned into <i>attR1</i> and <i>attR2</i> sites of pET-41-K	Gateway cloning	This study
pET 300- <i>abkatG</i>	Expression vector; <i>attB1</i> , <i>attB2</i> , Amp ^R , <i>lacI</i> , T7 promoter, pBR322 ori, N-6×His, gene <i>katG</i> (<i>A. baumannii</i>) cloned into <i>attR1</i> and <i>attR2</i> sites of pET 300	Gateway cloning	This study
pET 300- <i>eckatG</i>	Expression vector; <i>attB1</i> , <i>attB2</i> , Amp ^R , <i>lacI</i> , T7 promoter, pBR322 ori, N-6×His, gene <i>katG</i> (<i>E. coli</i>) cloned into <i>attR1</i> and <i>attR2</i> sites of pET 300	Gateway cloning	This study
pET MBP-1a	Modified pET-24d; T7 promoter, <i>lacI</i> , pBR322 ori, Kan ^R , N-6×His, MBP, TEV site, MCS	-	EMBL

pET MBP-1a- <i>abhemB</i> _{wt}	Expression vector; T7 promoter, <i>lacI</i> , pBR322 ori, Kan ^R , N-6×His, MBP, TEV site, MCS, gene <i>hemB</i> cloned into MCS (NcoI, NotI)	Restriction enzyme-based cloning and ligation	This study
pET MBP-1a- <i>abhemB</i> _{P241S}	Expression vector; T7 promoter, <i>lacI</i> , pBR322 ori, Kan ^R , N-6×His, MBP, TEV site, MCS, gene <i>hemB</i> (P241S) cloned into MCS (NcoI, NotI)	QuikChange site-directed mutagenesis	This study
pVRL2	<i>E. coli</i> - <i>Acinetobacter</i> species shuttle vector, araC-P _{BAD} arabinose-inducible expression cassette; Gen ^R , MCS, origin of replication for <i>A. baumannii</i> (oriAb).	-	Lucidi <i>et al.</i> ¹²⁵
pVRL2- <i>abhemB</i> _{wt}	Expression vector, araC-P _{BAD} arabinose-inducible expression cassette; Gen ^R , MCS, oriAB, gene <i>hemB</i> was cloned into MCS (EcoRI, XbaI)	Restriction enzyme-based cloning and ligation	This study
pVRL2- <i>abhemB</i> _{P241S}	Expression vector, araC-P _{BAD} arabinose-inducible expression cassette; Gen ^R , MCS, oriAB, gene <i>hemB</i> (P241S) was cloned into MCS (EcoRI, XbaI)	Restriction enzyme-based cloning and ligation	This study

3.8.1. Gateway Cloning

For the recombinant expression of porphobilinogen synthase (or 5-aminolevulinic acid dehydratase (PbgS)) (gene: *hemB*, UniProt ID: D0C9T7) wild type, catalase-

peroxidase (gene: *katG*, UniProt ID: D0CAQ1) wild type from *A. baumannii* ATCC19606 (taxid: 575584; *AbCAT*) and catalase-peroxidase (gene: *katG*, UniProt ID: P13029) wild type from *E. coli* K12 (taxid: 83333; *EcCAT*), the Invitrogen™ Gateway™ cloning system (*Thermo Fisher Scientific*) was used. The following primers containing the required *attB* recombination sites were designed (fwd. = forward, rev. = reverse):

Table II-4| Primers used for Gateway cloning. *AttB1*- and *attB2*-sequences are indicated in lower case letters.

Primer	Sequence (5' – 3')
fwd. <i>attB1</i> <i>hemB</i>	ggggacaagtttgtaaaaaagcaggcttt ATGGGGCTACAATACAGCAGT
rev. <i>attB2</i> <i>hemB</i>	ggggaccactttgtacaagaaagctgggtg TTAGTTCATTCCTTGAGTTTTTCAG
fwd. <i>attB1</i> <i>AbkatG</i>	ggggacaagtttgtaaaaaagcaggcttt ATGTCAAACGAATCAAAATGTCCT
rev. <i>attB2</i> <i>AbkatG</i>	ggggaccactttgtacaagaaagctgggtg TTAAGCTAAGTCAAAACGGTCAA
fwd. <i>attB1</i> <i> EckatG</i>	ggggacaagtttgtaaaaaagcaggcttt ATGAGCACGTCAGACGATATC
rev. <i>attB2</i> <i>EckatG</i> primer	ggggaccactttgtacaagaaagctgggtg TTACAGCAGGTCGAAACGGT

The polymerase chain reaction (PCR) was carried out in a CFX96 Real-time System in combination with a C1000 Thermal Cycler (*BioRad*). An overnight culture of *A. baumannii* ATCC19606 or *E. coli* K12 was used as DNA template. The reaction mixtures contained 10 µL GC or HF buffer (*NEB*), 1 µL dNTP (10 mM), 2.5 µL fwd. primer (10 µM), 2.5 µL rev. primer (10 µM), 1 µL overnight culture, 0.5 µL Phusion®

High Fidelity DNA polymerase (*NEB*) and 32.5 μL ddH₂O. After initial denaturation (98 °C, 1 min 50 s), the mixtures underwent 34 cycles of denaturation (98 °C, 10 s), annealing (60 °C, 30 s) and extension (72 °C, 60 s), before a final extension (72 °C, 3 min). The PCR products were purified by the MicroElute® Cycle-Pure Kit (*OMEGA Bio-Tek*) and finally the DNA concentration was measured on an Infinite® M200 Pro microplate reader using a NanoQuant Plate™ (*Tecan Group Ltd.*).

In the BP-reaction the PCR-product is incorporated in the donor vector of choice, here pDONR 207 was used. For this, 1 μL of the PCR-product (100-150 ng), 1 μL of the vector pDONR 207 (150 ng), 6 μL TE-buffer and 2 μL Gateway® BP Clonase® II enzyme mix (*Invitrogen*) were mixed and incubated for 4 h at RT. For transformation, the BP-solution was added to 200 μL of chemically competent *E. coli* TOP10 cells (*Invitrogen*) and incubated for 15 – 30 min on ice. After a 40 – 45 s heat shock at 42 °C the cells were put on ice for another 5 min. Afterwards, the cells were grown for 1 h in 500 μL SOC-medium (2% tryptone, 0.5 % yeast extract, 10 mM NaCl, 2,5 mM KCl, 10 mM MgCl₂, 10 mM MgSO₄ und 20 mM glucose) at 37 °C, plated on LB agar plates supplemented with Gen (7.5 mg/L) and incubated at 37 °C overnight. Single colonies were picked and grown in 5 mL LB medium containing Gen (7.5 mg/L) for 15 h at 37 °C. The plasmid DNA of the cells was isolated using the E.Z.N.A.® Plasmid DNA mini Kit I (*OMEGA Bio-Tek*) according to the manufacturer's protocol and the final DNA concentration was measured as described above. The sequences of resulting plasmids pDONR 207-*abhemB_{wtr}*, pDONR 207-*abkatG* and pDONR 207-*eckatG* were verified *via* Sanger sequencing (*GATC Biotech AG*).

For the LR-reaction, pDONR 207-*abhemB_{wtr}*, pDONR 207-*abkatG* or pDONR 207-*eckatG* (100 – 150 ng) were mixed with destination vectors (150 ng) (Table II-5) and TE buffer was added to a final volume of 8 μL . Afterwards, 2 μL Gateway® LR Clonase® II enzyme mix (*Invitrogen*) was added and mixtures were incubated for 2 h at RT. The

transformation into chemically competent *E. coli* TOP10 cells (*Invitrogen*), the isolation of resulting expression plasmids and verification of their sequences was done as already described for the BP-reaction using the appropriate antibiotic.

Table II-5| Destination vectors used for Gateway cloning with respective selection marker.

Destination vector	Tags	Selection
pET 300	N-6×His	Ampicillin (100 mg/L)
pDest 17	N-6×His	Ampicillin (100 mg/L)
pET- 41-K	N-6×His-MBP	Kanamycin (25 mg/L)

Chemically competent *E. coli* expression strains (*E. coli* BL21(DE3) and *E. coli* Lemo21(DE3)) were transformed with the respective expression plasmid (100 ng) following the protocol as described in the BP-reaction using the appropriate antibiotic or antibiotic combinations (Table II-6).

Table II-6| Combinations of expression vectors and expression strains with respective selection markers prepared in this study.

Vectors	Expression strain	Selection	Genes
pET 300	<i>E. coli</i> BL21(DE3)	Ampicillin (100 mg/L)	<i>abkatG</i> , <i>eckatG</i>
pDest 17	<i>E. coli</i> BL21(DE3)	Ampicillin (100 mg/L)	<i>hemB</i>
	<i>E. coli</i> Lemo21(DE3)	Ampicillin (100 mg/L), Chloramphenicol (30 mg/L)	<i>hemB</i>
pET- 41K	<i>E. coli</i> BL21(DE3)	Kanamycin (25 mg/L)	<i>hemB</i>
	<i>E. coli</i> Lemo21(DE3)	Kanamycin (25 mg/L), Chloramphenicol (30 mg/L)	<i>hemB</i>

3.8.2. Restriction enzyme-based cloning and ligation

Cloning of pET MBP-1a-*abhemB*_{wt} and pET MBP-1a-*abhemB*_{P241S}

In order to install a TEV-cleavage site between the maltose binding protein (MBP) and PbgS, vector pET MBP-1a was used and *hemB* was cloned into this plasmid using standard techniques based on PCR, restriction digest and ligation.

For amplification of *hemB* wt, PCR was performed as described in section "Gateway Cloning" using the primers indicated in Table II-7 and an annealing temperature of 63 °C. After purification, the PCR product as well as plasmid pET MBP-1a (each 1 µg) was digested in CutSmart buffer (*NEB*) at 37 °C for 60 min using 10 units of the restriction enzymes *Nco*I-HF and *Not*I-HF, each. The digested PCR product was purified and DNA concentration was measured as described above. The digested vector was purified by agarose gel electrophoresis on a 1% agarose gel. After extraction using a gel extraction kit (*VWR*, catalog no. 101318-972) according to the manufacturer's instructions, 50 ng of the purified vector and 50 ng of the purified insert were ligated using 1 µL Quick Ligase (*NEB*) in 10 µL of Quick Ligase buffer (*NEB*) in a total volume of 20 µL. The ligation mixture was incubated at 25 °C for 10 min. The transformation in chemically competent *E. coli* TOP10 cells (*Invitrogen*), the isolation of pET MBP-1a-*abhemB*_{wt} and the verification of the sequence was performed as already described for the BP-reaction using kanamycin (25 mg/L).

To exchange proline 241 for serine in PbgS, the QuikChange site-directed mutagenesis system (*Agilent*) was used. The two mismatching primers (fwd. *hemB* P241S, rev. *hemB* P241S) were designed with the QuikChange Primer Design program (*Agilent*) and were used for PCR (Table II-7). The plasmid pET MBP-1a-*abhemB*_{wt} served as DNA template for the mismatch PCR reaction. According to Phusion manufacturer's protocol, 50 µL PCR reaction mixture were prepared containing 32 µL ddH₂O, 10 µL GC buffer (*NEB*), 1.5 µL fwd. and 1.5 µL rev. primer (10 µM), 1.0 µL dNTPs (10 mM), 1.5 µL DMSO and 2.0 µL template DNA (50 ng/µL). Finally, 0.5 µL Phusion®

High Fidelity DNA polymerase (*NEB*) was added and the PCR reaction was subsequently performed. After initial denaturation (98 °C, 3 min), the mixtures underwent 34 cycles of denaturation (95 °C, 45 s), annealing (60 °C, 30 s) and extension (72 °C, 4 min), before a final extension (72 °C, 7 min). The unmutated parental DNA was removed by digestion of the PCR mixture with the endonuclease *DpnI* (*NEB*), which is specific for methylated and hemimethylated DNA. Therefore, 1.0 µL *DpnI* (*NEB*) as well as 1.0 µL CutSmart® buffer (*NEB*) was added to 8 µL of PCR product and the digestion mixture was incubated for 3 h at 37 °C. The transformation of PCR product into *E. coli* XL1-Blue competent cells, isolation of the resulting plasmid pET MBP-1a-*abh*emB_{P241S} and verification of the mutation P241S was performed as already described for the BP-reaction using kanamycin (25 mg/L).

Table II-7| Primer used for cloning of hemB into pET MBP-1a vector (fwd. = forward, rev. = reverse) and for QuikChange site-directed mutagenesis to insert the mutation P241S. Restriction sites of *NcoI* and *NotI* are underlined and base pairs that were added to avoid shift in codon usage are shown in italic.

Primer name	Sequence (5' – 3')
fwd. MBP-TEV- <i>hemB</i> primer	TAAGCA <u>CCATGG</u> CA ATGGGGCTACAATACAGCAGT
rev. MBP-TEV- <i>hemB</i> primer	TGCTTA <u>GCGGCCGC</u> TTAGTTCATTTCCCTTGAGTTTTTCAGC
fwd. <i>hemB</i> P241S	GCATCACGGAACGAACCATAGAAGCTAGACGCAT
rev. <i>hemB</i> P241S	ATGCGTCTAGCTTCTATGGTTCGTTCCGTGATGC

Cloning of pVRL2-*abhemB*_{wt} and pVRL2-*abhemB*_{P241S}

The vector pVRL2, which was shown to be suitable for gene cloning and expression in *Acinetobacter* species, was generously provided by Paolo Visca.¹²⁵ The genes *hemB*_{wt} and *hemB*_{P241S} were cloned into the pVRL2 expression vector. The genes *hemB*_{wt} and *hemB*_{P241S} were amplified by PCR using pET MBP-1a-*abhemB*_{wt} and pET MBP-1a-*abhemB*_{P241S} as templates, respectively. PCR was performed as described in section "Gateway Cloning" using the primers indicated in Table II-8 and an annealing temperature of 63 °C. PCR products and vector pVRL2 were digested using *EcoRI*-HF and *XbaI* and purified as described in section "Cloning of pET MBP-1a-*abhemB*_{wt} and pET MBP-1a-*abhemB*_{P241S}". Next, 50 ng of the purified vector and 45 ng of the purified insert were ligated using 2 µL T4 Ligase (*NEB*) in T4 Ligase buffer (*NEB*) in a total volume of 20 µL. The ligation mixture was incubated at RT for 4 h. Transformation into TOP10 chemically competent *E. coli* (*Invitrogen*) and the isolation of the plasmids was performed as already described for the BP-reaction using Gen (10 mg/L). The plasmid sequence was verified by *GeneWiz* using pVRL2 sequencing primer (Table II-8).

Table II-8 Primers used for cloning and sequencing of <i>hemB</i> _{wt} and <i>hemB</i> _{P241S} into the pVRL2 vector (fwd. = forward, rev. = reverse). Restriction sites of <i>EcoRI</i> and <i>XbaI</i> are underlined.	
Primer name	Sequence (5' – 3')
fwd. pVRL2 <i>hemB</i> primer	TAAGCA <u>GAATTC</u> ATGGGGCTACAATACAGC
rev. pVRL2 <i>hemB</i> primer	TGCTTA <u>TCTAGA</u> TTAGTTCATTCCTTGAGTTTTTCAGC
fwd. pVRL2 sequencing primer	CAACTCTCTACTGTTTCTCCAT
rev. pVRL2 sequencing primer	GACGTTGTAACGACGG

3.9. Catalases-Peroxidases (*AbcCAT*, *EcCAT*)

3.9.1. Overexpression and Purification

To overexpress CATs, a protocol published by Di Gennaro *et al.* was used with modifications.¹⁰³ *E. coli*/BL21(DE3) harbouring either pET300-*abkatG* or pET300-*eckatG* were grown at 37 °C overnight in 20 mL LB medium supplemented with ampicillin (100 mg/L). The next day, 10 mL of the overnight culture were transferred into 1 L LB medium containing ampicillin (100 mg/L) and bacteria were grown at 37 °C to an OD₆₀₀ of 0.4. Then, the gene expression was induced by the addition of IPTG (1 mM) as well as FeCl₂ (250 µM) and the cells were grown for 24 h at 30 °C. Afterwards, bacteria were harvested (6,000 ×g, 4 °C, 30 min) and washed with PBS. The pellets were then resuspended in 20 mL His-lysis buffer (20 mM Tris/HCl, 10 mM imidazole, 150 mM NaCl, 2 mM β-Mercaptoethanol, 0.2% (v/v) NP-40, pH 8.0 in ddH₂O) and lysed by sonication using the following protocol twice: 7 min at 30% intensity, 3 min at 80% intensity (Sonopuls HD 2070 ultrasonic rod, *Bandelin electronic GmbH*). Soluble and insoluble fractions were separated by centrifugation (20,000 ×g, 4 °C, 30 min), the soluble fraction was loaded on a 50 mL Superloop (*GE Healthcare*) and injected into an Äkta Purifier 10 System equipped with UV-detector (UPC-900, P-900, Box-900, Frac-950, *GE Healthcare*). For affinity chromatography a His-Trap HP 5 mL column (*GE Healthcare*) was used, which was equilibrated with wash buffer 1 (20 mM Tris/HCl, 10 mM imidazole, 150 mM NaCl, 2 mM β-Mercaptoethanol, pH 8.0 in ddH₂O; (5 CV)). The column was washed with wash buffer 1 (8 CV), wash buffer 2 (20 mM Tris/HCl, 10 mM imidazole, 1 M NaCl, 2 mM β-Mercaptoethanol, pH 8.0 in ddH₂O; 8 CV) and wash buffer 3 (20 mM Tris/HCl, 40 mM imidazole, 150 mM NaCl, 2 mM β-Mercaptoethanol, pH 8.0 in ddH₂O; 8 CV) and proteins were eluted with elution buffer (20 mM Tris/HCl, 500 mM imidazole, 150 mM NaCl, pH 8.0 in ddH₂O). The protein-containing fractions were pooled and dialyzed in CAT storage buffer (20 mM Tris/HCl, 2 mM Na₂EDTA, pH 7.0 in ddH₂O) overnight, aliquoted and stored at -80 °C. Protein

concentrations were determined on an Infinite® M200 Pro microplate reader using a NanoQuant Plate™ (*Tecan Group Ltd.*) by measuring the absorption at 280 nm. Extinction coefficients of 156,870 and 144,840 $\text{M}^{-1}\text{cm}^{-1}$ were used for *Ab*CAT and *Ec*CAT, respectively.

3.9.2. Catalase Activity Assay

The catalase activity assay kit (catalog no. K773-100, *BioVision*) was used and the assay was performed according to manufacturer's protocol with slight modifications. Hydroxylamine was used as a positive control for CAT inhibition. CAT (25 nM final concentration) was pre-incubated with either Xan or Hydroxylamine for 30 min at RT and the reaction was started by the addition of H_2O_2 (16 μM final concentration). After 15 min at RT, 10 μL of the stop solution and 50 μL of the develop mix (47.7 μL assay buffer, 0.3 μL OxiRed probe, 2 μL HRP) were added to terminate the reaction. After incubation for 10 min, the fluorescence signal ($\lambda_{\text{ex.}} = 535 \text{ nm}$, $\lambda_{\text{em.}} = 587 \text{ nm}$) was measured. Experiments were performed in three independent experiments with two technical replicates each.

3.10. Generation and Sequencing of Xan-resistant *A. baumannii* ATCC19606

3.10.1. Resistant Development Assay

Resistance development assay is based on a procedure previously published by Le *et al.* and Bogdanovich *et al.* with slight modifications.^{67,161} For resistance development by sequential passaging, an overnight culture of *A. baumannii* ATCC19606 in cation-adjusted Mueller-Hinton broth (MHII) was adjusted to an OD_{600} of 2.0 and subsequently diluted 1:100 into MHII medium (1 mL) containing various concentrations of Xan (1% DMSO final concentration), Cip as positive control as well as DMSO (1%) or 0.1 N HCl as growth controls. Bacteria were incubated (37 °C, 200 rpm) and passaged in 20 – 24 h intervals in the presence of various

concentrations of Xan or Cip (0.25, 0.5, 1, 2, 4× MIC). The culture of the second highest concentration that allowed visible growth was adjusted to an OD₆₀₀ of 2.0 and subsequently diluted 1:100 into fresh MHII media (1 mL) containing different concentrations of the respective antimicrobial agent (0.25, 0.5, 1, 2, 4 × MIC). If a shift in MIC levels was observed, the concentrations of the respective antimicrobial were adjusted accordingly for the subsequent passage. This serial passaging was repeated for 10 days and in three independent biological replicates. The growth control, which contained only DMSO, was additionally passaged as a negative control to identify naturally occurring mutations. For this purpose, the growth control was adjusted each day to an OD₆₀₀ of 2.0 and diluted 1:100 into MHII medium (1 mL) containing 1% DMSO.

3.10.2. Preparation of Isolated Clones for Whole Genome Sequencing

For sequencing, clones of Xan-resistant mutants and of the negative control (DMSO) were isolated. For this purpose, tubes with 1 mL of MHII media containing either 25 µM Xan (for resistant mutants) or DMSO (for negative control) were inoculated using the cryostocks of day 11 and incubated overnight (37 °C, 200 rpm). On the next day, bacteria (120 µL) were harvested (7,000 ×g, 10 min, 4 °C), washed once with MHII media to remove excess of Xan and resuspended in 20 µL LB medium. Bacterial suspensions were plated on either LB agar plates supplemented with Xan (8 µM, for resistant mutants) or on LB agar plates (negative control), which were incubated overnight at 37 °C. Three colonies of each independent biological experiment (A-1, A-2, A-3 (replicate A), B-1, B-2, B-3 (replicate B), C-1, C-2, C-3 (replicate C)) and of the negative control were isolated and were subjected to genome sequencing.

3.10.3. Whole Genome Sequencing and Processing

Total bacterial DNA was extracted and purified from *A. baumannii* ATCC19606 (wt) and derivatives using the DNeasy Blood & Tissue kit (*Qiagen*). DNA sequencing

libraries were prepared using the NEBNext Ultrall FS DNA Library kit, and the genomic DNAs were sequenced using MiSeq Reagent Kits v3 (2 × 300bp) on an Illumina MiSeq.

Whole-genome sequencing data are available on the SRA repository under Bioproject number PRJNA639720 with Biosample accession numbers SAMN15248516-SAMN15248528.

Briefly, reads were trimmed based on quality with a Phred quality score cut-off of 30 and reads shorter than 50 nucleotides were discarded. Processed reads were assembled using SPAdes (version 3.11.1) de novo genome assembler software in careful mode.¹⁶² Contigs with a length lower than 200 bp or average coverage lower than 15 were discarded. Average contig coverage was determined by mapping processed reads to the assembled contigs utilizing Bowtie2 (version 2.3.2)¹⁶³ and the per base coverage was determined using SAMtools (version 1.8).¹⁶⁴

Processed reads of derivatives were mapped to the ATCC19606 genome assembly using Bowtie2.¹⁶³ Variants were called using mpileup part of BCFtools (version 1.8).¹⁶⁵ Variants were filtered out by a minimum SNP and INDEL distance of 10 bp, variant quality of 30, coverage of 50, mapping quality of 40 and a Z-score of 1.96.¹⁶⁶

All assemblies were annotated utilizing Prokka genome annotation software (version 1.4).¹⁶⁷

3.11. Porphobilinogen Synthase (PbgS)

3.11.1. Overexpression and Purification of PbgS(wt) in *E. coli*

Overnight cultures of *E. coli* expression strains, whose preparation is described in the section "Cloning", were grown (37 °C, 200 rpm) under respective antibiotic selection. On the next day, 20 mL LB medium containing appropriate antibiotics were

inoculated (1:100) and cells were grown (37 °C, 200 rpm) until an OD₆₀₀ of 0.4 – 0.8 was reached. Protein expression was induced by the addition of 400 µM IPTG and cells were incubated at indicated temperature for 20 h at 150 rpm. On the next day, 5 mL of bacterial culture was harvested by centrifugation (15,000 ×g, 1 min, 4 °C) and cells were resuspended in 200 µL lysis buffer (50 mM NaH₂PO₄, 300 mM NaCl, 10 mM imidazole, pH 8.0). Lysozyme was added to a final concentration of 1 mg/ml followed by incubation on ice for 30 min. Cells were lysed by gently vortexing and lysate was cleared by centrifugation (15,000 ×g, 10 min, 4 °C). The supernatant was transferred into a fresh tube, 20 µL of a 50% slurry of Ni-NTA (*Qiagen*) were added and mixed gently for 30 min at 4 °C. Resins were washed twice with 200 µL wash buffer (50 mM NaH₂PO₄, 300 mM NaCl, 20 mM imidazole, pH 8.0) by centrifugation (1,000 ×g, 10 s, 4 °C) and proteins were eluted with 3 × 20 µL elution buffer (50 mM NaH₂PO₄, 300 mM NaCl, 250 mM imidazole, pH 8.0). Next, 50 µL of each collected fraction were mixed with one equivalent of 2× Laemmli buffer and analysed by SDS-PAGE with Coomassie staining as already described in section “Gel-based ABPP”.

3.11.2. Generation of *A. baumannii* (pVRL2-*abhemB*_{wt}) and (pVRL2-*abhemB*_{P241S})

Competent *A. baumannii* cells were prepared for electrotransformation as previously described.¹²⁵ Briefly, an overnight culture of *A. baumannii* ATCC19606 was used to inoculate 50 mL of pre-warmed LB medium (1:100) and the bacteria were grown for 24 h (37 °C and 200 rpm). Cells were harvested by centrifugation (3,000 ×g, 15 min, 4 °C), washed twice with sterile 10% glycerol (25 mL) at RT, and suspended in 10% glycerol (1.5 mL). Bacterial suspension was split into 50 µL aliquots, which were stored at -80 °C until they were used.

Electroporation was performed in 2 mm electroporation cuvettes (Gene Pulser; *BioRad*) using 300 ng/µL of plasmids pVRL2-*abhemB*_{wt} and pVRL2-*abhemB*_{P241S} as well as 50 µL aliquots of competent *A. baumannii* cells. After pulsing (2.5 kV, 200 Ω, 25 µF),

cells were immediately recovered in 1 mL of pre-warmed SOC medium (2% tryptone, 0.5% yeast extract, 10 mM NaCl, 2.5 mM KCl, 10 mM MgCl₂, 10 mM MgSO₄ und 20 mM glucose) and incubated at 37 °C for 3 h. Transformants were selected on LB agar plates supplemented with Gen (100 mg/L). On the next day, 5 mL LB medium supplemented with Gen (100 mg/L) were inoculated with single colonies and cryostocks were prepared using 600 µL of overnight culture and 400 µL of sterile glycerol.

3.11.3. Overexpression of PbgS(wt) and PbgS(P241S) in *A. baumannii* ATCC19606

Overnight cultures of *A. baumannii* (pVRL2-*abhemB*_{wt}), *A. baumannii* (pVRL2-*abhemB*_{P241S}) and *A. baumannii* (wt) (as control) in LB medium supplemented with Gen (100 mg/L, only for *A. baumannii* harbouring pVRL2 plasmids) were diluted 1:100 into LB medium containing Gen (100 mg/L, only for *A. baumannii* harbouring pVRL2 plasmids) and incubated (37 °C, 200 rpm) until an OD₆₀₀ of 0.7 – 0.8 was reached. Protein expression was induced by adding arabinose (20% in sterile LB medium) to a final concentration of 0.5% and bacteria were incubated for 3.5 h (37 °C, 200 rpm). Bacterial suspensions equivalent to 200 mL with an OD₆₀₀ of 2.0 were harvested (7,000 ×g, 30 min, 4 °C) and washed with PBS. Pellets were resuspended in 20 mL PbgS activity buffer (100 mM Tris/HCl, 1 mM MgCl₂, pH 8.5 in ddH₂O), lysed by sonication (6 × 45 s, 80% intensity, 30 s break on ice, Sonopuls HD 2070 ultrasonic rod, *Bandelin electronic GmbH*) and cell lysate was cleared by centrifugation (20,000 ×g, 30 min, 4 °C). The supernatants were transferred into new tubes, kept on ice and were directly used for the PbgS activity assay as well as for full proteome analysis to quantify overexpressed PbgS(wt) and PbgS(P241S).

3.11.4. PbgS Activity Assay

PbgS activity assay was performed as described by Lentz *et al.* with slight modifications.¹²⁰

The assay was performed in a 96 well-plate (transparent Nunc 96-well flat bottom, *Thermo Fisher Scientific*). Into each well, 45 μL of cell lysate (prepared as described in "Overexpression of PbgS(wt) and PbgS(P241S) in *A. baumannii* ATCC19606") were added and equilibrated at 37 °C for 20 min. To determine K_m and v_{max} , varying concentrations of 5-aminolevulinic acid (5-ALA; 5 μL of 100 \times stock in ddH₂O) were added, reaction mixtures were incubated at 37 °C without shaking and stopped after various time points by the addition of 200 μL of modified Ehrlich's Reagent (1 g *p*-dimethylaminobenzaldehyde in 42 mL acetic acid, 12 mL perchloric acid and 7.3 mL 12% trichloroacetic acid). After another 10 min incubation, the absorption was measured at 555 nm with an Infinite® M200 Pro microplate reader (*Tecan Group Ltd*). Samples without 5-ALA added was used as a negative control and the lysate of *A. baumannii* (wt) (without plasmid) was used to subtract the basal PbgS activity level. For each substrate concentration, the linear range from the progress curves was used to determine the reaction velocity (slope). Michaelis Menten constants K_m and v_{max} were calculated with GraphPad Prism (version 5.03) using non-linear regression. The assay was performed in three independent experiments with two technical replicates each.

In order to test PbgS inhibition by Xan, 0.5 μL of Xan (100 μM final concentration with 1% DMSO) were added to 44.5 μL cell lysate and pre-incubated for 30 min before the activity assay was started by the addition of 5-ALA (100 μM final concentration). The reaction was incubated at 37 °C without shaking for 30 min. The reaction was stopped and the absorption was measured as described above. The assay was performed in two independent experiments with two technical replicates each.

3.12. Whole Proteome Analysis

3.12.1. *A. baumannii* ATCC19606 (wt), *A. baumannii* (pVRL2-*abhemB*_{wt}) and *A. baumannii* (pVRL2-*abhemB*_{P241S})

A volume of 500 μ L of the cell lysates prepared in "Overexpression of PbgS(wt) and PbgS(P241S) in *A. baumannii* ATCC19606", corresponding to protein amounts of 500 μ g, 500 μ g and 250 μ g of *A. baumannii* (pVRL2-*abhemB*_{wt}), *A. baumannii* (pVRL2-*abhemB*_{P241S}) and *A. baumannii* (wt), respectively, was directly used to precipitate proteins with ice-cold acetone (4 volumes) at -20 °C overnight. Afterwards, the experimental procedure was analogous to ABPP with XP in *A. baumannii* and *E. coli* as described above, but without enrichment on avidin beads, using 10 μ L (0.5 μ g/ μ L; sequencing grade, modified, *Promega*) trypsin for digestion. The experiment was performed in $n = 2$ independent experiments.

3.12.2. Xan Treatment of *A. baumannii* ATCC19606 (wt)

A. baumannii ATCC19606 overnight cultures were diluted 1:100 in 20 mL LB medium containing Xan (125 nM, 1% DMSO final concentration) or DMSO (1%). Bacteria were incubated (37 °C, 200 rpm) until an OD₆₀₀ of 2.0, harvested (6,000 \times g, 4 °C, 15 min) and pellets were washed with PBS. Cell pellets were resuspended in 0.4% (w/v) SDS in PBS (1 mL) and lysed (3 \times 6,500 rpm, 30 s, 30 s cooling breaks, liquid nitrogen cooling; Precellys Ceramic Kit CK01L, 2.0 mL tubes; Precellys 24 Homogenizer, *Bertin Technologies*). The supernatants were clarified by centrifugation (20,000 \times g, 30 min, 4 °C) and cell lysates corresponding to protein amount of 250 μ g were precipitated with ice-cold acetone (4 volumes) at -20 °C overnight, centrifuged (16,900 \times g, 4 °C, 15 min) and the pellets were washed twice with ice-cold methanol (1 mL). Protein pellets were air dried and dissolved in 200 μ L denaturation buffer (7 M urea, 2 M thiourea in 0.1 M pH 7.5 Tris/HCl-buffer). Upon reduction with TCEP (5 mM) at 37 °C for 1 h, proteins were alkylated using IAA (10 mM) at 25 °C for 30 min and samples

were quenched with DTT (10 mM) at RT for 30 min. Enzymatic digestion using 1 μ L Lys-C (0.5 ng/ μ L, MS-grade, *Wako*) was first carried out at RT for 2 h, upon which samples were diluted with 600 μ L TEAB buffer (50 mM in ddH₂O) and digested with 10 μ L trypsin (0.5 μ g/ μ L; sequencing grade, modified, *Promega*) at 37 °C overnight under continuous shaking (450 rpm). On the next day, the experimental procedure was analogous to ABPP with XP in *A. baumannii* and *E. coli* as described above. The experiment was performed in $n = 4$ independent experiments.

3.12.3. Xan-Resistant *A. baumannii* ATCC19606 Mutants

For overnight cultures of three Xan-resistant *A. baumannii* mutants (A-3, B-3, C-3), 5 mL of LB medium supplemented with 500 nM Xan were inoculated. Additionally, 5 mL overnight culture of *A. baumannii* ATCC19606 (wt) was prepared in LB medium. On the next day, overnight cultures were diluted 1:100 in 20 mL LB medium and bacteria were incubated (37 °C, 200 rpm) until an OD₆₀₀ of 2.0 was reached. Bacteria were harvested (6,000 \times g, 4 °C, 15 min) and cell pellets were washed with PBS. Afterwards, the experimental procedure was analogous to "Xan treatment of *A. baumannii* ATCC19606 (wt)". The experiment was performed in $n = 4$ independent experiments.

3.12.4. LC-MS/MS Analysis

Samples were analysed with an UltiMate 3000 nano HPLC system (*Dionex*) using an Acclaim C18 PepMap100 (75 μ m ID \times 2 cm) trap column and an Aurora Series Emitter Column with Gen2 nanoZero fitting (75 μ m ID \times 25 cm, 1.6 μ m FSC C18) separation column (both heated to 40 °C) coupled to an Orbitrap Fusion (*Thermo Fisher*) in EASY-spray setting. Samples were loaded on the trap column and washed with 0.1% TFA, then transferred to the analytical column (buffer A: H₂O with 0.1% FA, buffer B: ACN with 0.1% FA, flow 400 nL/min, gradient 5 to 22% buffer B in 115 min, then to 32% buffer B in 10 min, then to 90% buffer B in 10 min and hold 90% buffer B for

10 min, then to 5% buffer B in 0.1 min and hold 5% buffer B for 9.9 min). Orbitrap Fusion was operated in a TOP10 data dependent mode. Full scan acquisition was performed in the orbitrap at a resolution of 120,000 and an AGC target of $2e^5$ (maximum injection time of 50 ms) in a scan range of 300 – 1,500 m/z. Monoisotopic precursor selection as well as dynamic exclusion (exclusion duration: 60 s) was enabled. Precursors with charge states of >1 and intensities greater than $5e^3$ were selected for fragmentation. Isolation was performed in the quadrupole using a window of 1.6 m/z. Precursors were collected to an AGC target of $1e^4$ (maximum injection time of 35 ms) and acquisition was performed at a scan range of 120 – 2,000 m/z. Fragments were generated using higher-energy collisional dissociation (HCD, normalised collision energy: 30%) and detected in the ion trap operating in rapid mode.

3.12.5. MS Data Analysis

Raw files were analysed using MaxQuant software (version 1.6.2.10) with the Andromeda search engine. The settings were applied as described in section “Gel-free Activity-based protein profiling (ABPP) and Affinity-based protein profiling (ABPP)”. Searches were performed against the UniProt database for *A. baumannii* ATCC19606 (taxid: 575584, 29.06.2020). For comparison of LFQ intensities of overexpressed PbgS(wt) and PbgS(P241S) the FASTA file was modified to contain a generic PbgS P241W, in order to exclude mutation-site containing peptides from quantification. Statistical analysis of the data was performed using Perseus (version 1.6.13.0).¹⁶⁰ Putative contaminants, reverse peptides and peptides only identified by site were deleted. LFQ intensities were \log_2 -transformed and data was filtered for two valid values in at least one group (for full proteome analysis of *A. baumannii* (pVRL2-*abhemB*_{wt}), *A. baumannii* (pVRL2-*abhemB*_{P241S} and *A. baumannii* (wt)), for three valid values in each group (for full proteome analysis of Xan treatment of *A. baumannii* ATCC19606 (wt)) and for three valid values in at least one group (for full proteome analysis of Xan-resistant *A. baumannii* ATCC19606 mutants) and a missing value

imputation was performed over the total matrix. For statistical evaluation, $-\log_{10}$ (P values) were obtained by a two-sided two sample Student's t -test.

3.13. UV-Vis Spectroscopy

The assay was performed in a transparent 96-well plate (transparent Nunc 96-well flat bottom, *Thermo Fisher Scientific*) and the final volume was 200 μ L. Hemin (20 μ M final concentration) was incubated with various concentrations of Xan (2% DMSO final concentration), resveratrol (Res) or DMSO (2%) in buffer h (200 mM HEPES, pH 7.0) for 1 h at RT in the dark without shaking. Afterwards, UV-Vis spectrum was recorded with an Infinite® M200 Pro microplate reader (*Tecan Group Ltd.*). The respective compound, Xan or Res, in buffer h served as blank control. The assay was performed in three independent experiments with two technical replicates each.

3.14. Hemin Decomposition

The glutathione (GSH)-mediated destruction assay of hemin was performed as previously described by Wright *et al.* with slight modifications.⁸³ The assay was performed in a 96-well plate (transparent Nunc 96-well flat bottom, *Thermo Fisher Scientific*) with a final volume of 200 μ L per well. Hemin (20 μ M final concentration) was pre-incubated with various concentrations of Xan (1% DMSO final concentration) in buffer h (200 mM HEPES, pH 7.0) for 15 min at 37 °C without shaking. DMSO (1%) was included as positive control for hemin decomposition and a sample without GSH addition was used as a negative control. The assay was started by the addition of GSH to a final concentration of 2 mM and the absorption of hemin at the Soret band (400 nm) was measured with an Infinite® M200 Pro microplate reader (*Tecan Group Ltd.*). To determine hemin decomposition, the decrease in absorption over a period of 7.5 min was calculated and normalised to DMSO-treated samples. The assay was performed in three independent experiment with three technical replicates each.

3.15. Measuring Regulatory Heme (RH)

Experiments to measure regulatory heme (RH) was performed as described by Atamna *et al.* with slight modifications.¹¹⁴

3.15.1. Preparing stock solution of apoHRP

Briefly, 8 mg holoHRP were dissolved in cold ddH₂O (2 mL) and heme was extracted with 40 mL acid acetone (1 ml concentrated HCl (36%) in 40 ml acetone). The pellet was then collected by centrifugation (2,000 ×g, 2 min), and was dissolved in PBS (2 mL). The cycle of extraction was repeated twice and the concentration of apoHRP was determined as described in section "Overexpression and purification of catalases-peroxidases (*AbCAT*, *EcCAT*)" using a molar extinction coefficient at 280 nm of 20,000 M⁻¹cm⁻¹. A stock solution of apoHRP (100 μM) was prepared in PBS and stored in aliquots at -20 °C. To exclude residual HRP activity, the peroxidase TMB substrate solution (*Thermo Fisher Scientific*) was used as described in the following section.

3.15.2. *In vitro* apoHRP Reconstitution Activity Assay

The final assay volume of the reconstitution reactions was 100 μL and PBS was used as buffer. Hemin (5 nM final concentration) was pre-incubated with various concentrations of Xan (1% DMSO final concentration) for 5 – 10 min at RT without shaking in the dark. DMSO (1%) was included as a positive control for reconstitution of the active holoHRP. Afterwards, apoHRP was added to a final concentration of 5 μM and incubated for 10 min at 4 °C without shaking. ApoHRP without hemin added was used as a blank control. To measure the resulting holoHRP activity, 10 μL aliquots were transferred from the reconstitution reaction to a transparent 96-well plate (transparent Nunc 96-well flat bottom, *Thermo Fisher Scientific*), 100 μL TMB substrate solution (*Thermo Fisher Scientific*) were added to the aliquots and absorbance was measured at 650 nm with an Infinite® M200 Pro microplate reader (*Tecan Group*

Ltd.). The assay was performed in four independent experiments with two technical replicates each.

To exclude an inhibition of the active holoHRP by Xan, apoHRP (5 nM final concentration) was pre-incubated with hemin (5 nM final concentration) for 10 min at 4 °C in the dark. Afterwards, Xan was added in various concentrations (1% DMSO final concentration) and reconstitution reactions were incubated for 5 – 10 min at RT in the dark. DMSO (1%) was included as a negative control for inhibition. ApoHRP without hemin added was used as a blank control. The resulting holoHRP activity was measured as described above. The assay was performed in three independent experiments with two technical replicates each.

3.15.3. *In vivo* apoHRP Reconstitution Activity Assay

An overnight culture of *A. baumannii* ATCC19606 was diluted 1:100 into LB medium and incubated (37 °C, 200 rpm) until an OD₆₀₀ of 1.0 was reached. The bacterial suspension was diluted to an OD₆₀₀ of 0.4 and 5 mL aliquots were prepared containing various concentrations of Xan (1% DMSO final concentration) or DMSO (1%). After incubation for 30 min (37 °C, 200 rpm), bacteria were harvested (7,000 ×g, 15 min, 4 °C), washed with PBS and were resuspended in 500 µL PBS. Cells were lysed by sonication (3 × 25 s, 75% intensity; Sonopuls HD 2070 ultrasonic rod, *Bandelin electronic GmbH*) with cooling breaks on ice. Next, lysate was cleared by centrifugation (20,000 ×g, 30 min, 4 °C), protein concentration was measured using the Pierce BCA Protein assay kit (*Thermo Fisher Scientific, Pierce Biotechnology*) and sample concentration was adjusted to 0.15 µg/µL. This lysate was directly used to measure regulatory heme by the reconstitution assay. The final volume of this assay was 100 µL and PBS was used as buffer. Cell lysate (2.5 µg protein) was pre-incubated with apoHRP (10 µM final concentration) for 10 min at 4 °C. Lysate without apoHRP added was used as a blank control. The resulting holoHRP activity was measured as

described above. The assay was performed in three independent experiments with four technical replicates each.

3.16. Porphyrin Quantification

The porphyrin extraction was performed as previously described by Mancini *et al.* with slight modifications.¹⁴⁵ An overnight culture of *A. baumannii* ATCC19606 was diluted 1:100 into LB medium and incubated (37 °C, 200 rpm) until an OD₆₀₀ of 1.0 was reached. The bacterial suspension was diluted to an OD₆₀₀ of 0.4 and 20 mL aliquots were prepared containing 1 μM Xan (1% DMSO final concentration) or DMSO (1%). After incubation for 1 h (37 °C, 200 rpm), bacterial suspensions equivalent to 20 mL with an OD₆₀₀ of 0.5 were harvested (7,000 ×g, 30 min, 4 °C) and washed twice with PBS. Cell pellets were resuspended in 1 mL EtOAc / acetic acid (3:1, v/v) and lysed by sonication (3 × 25 s, 75% intensity; Sonopuls HD 2070 ultrasonic rod, *Bandelin electronic GmbH*) with cooling breaks on ice. Cell debris was removed by centrifugation (18,000 ×g, 20 min, 4 °C) and supernatant was transferred to a new Eppendorf tube. The organic phase was washed twice with H₂O (1 mL), transferred to a new Eppendorf tube and 3 M HCl (100 μL) was added to water-solubilize porphyrins. In order to quantify porphyrins, 100 μL of the aqueous phase were transferred into a black flat bottom 96-well plate (*Greiner*) and the fluorescence spectrum ($\lambda_{\text{ex.}} = 406 \text{ nm}$, $\lambda_{\text{em.}} = 550 - 750 \text{ nm}$) was recorded with an Infinite® M200 Pro microplate reader (*Tecan Group Ltd.*). The experiment was performed in six independent experiments.

3.17. Time-kill Assays

To determine the levels of killing by Xan, time-kill experiments were performed as described previously by Le *et al.*⁶⁷

An overnight culture of *A. baumannii* ATCC19606 was diluted 1:100 into LB medium and bacteria were grown to mid-exponential phase (OD_{600} of 0.3 - 0.7; 37 °C, 200 rpm). Subsequently, cells were diluted to 1×10^7 CFU/mL in LB medium and were split into 3 mL aliquots into culture tubes containing either Xan (4 μ M, 1% DMSO final concentration), DMSO (1%), thiourea (TU) (150 mM) or TU (150 mM) and Xan (4 μ M). Cells were incubated (37 °C, 200 rpm) and serial dilutions were plated on LB agar plates at indicated time points for the determination of viable cells (CFU/mL). Experiments were performed in $n = 4$ (DMSO), $n = 3$ (Xan) and $n = 2$ (TU as well as TU and Xan (4 μ M)) independent biological experiments and CFU enumeration was conducted in four replicates each.

3.18. Checkerboard Assay

Overnight cultures of *A. baumannii* ATCC19606 and *A. baumannii* AB5075 were diluted 1:10,000 into LB medium and were directly used for testing. Various dilutions of Xan and Gen were prepared and 1 μ L of the respective 100 \times stock was pipetted in a 96 well-plate (transparent Nunc 96-well flat bottom, *Thermo Fisher Scientific*). Two to four-fold the MIC of each antibiotic was used as the highest concentration tested. The resulting checkerboard contains each combination of the two test molecules. Each well was inoculated with 99 μ L of the diluted bacterial suspension, and the plates were incubated for 24 h (37 °C, 200 rpm). The lowest concentration in the dilution series at which no growth of bacteria could be observed by eye was defined as the MIC. In order to quantify the interactions between the antibiotics, the following equation was used to determine the fractional inhibitory concentration (FIC) index:

$\Sigma FIC = FIC(Xan) + FIC(Gen)$, where $FIC(Xan)$ is the MIC of Xan in the combination/MIC of Xan alone, and $FIC(Gen)$ is the MIC of Gen in the combination/MIC of Gen alone. The combination is considered synergistic when the ΣFIC is ≤ 0.5 , indifferent when the

Σ FIC is $>0.5 - 4$, and antagonistic when the Σ FIC > 4 .¹⁶⁸ FICs were determined in three (*A. baumannii* ATCC19606) and two (*A. baumannii* AB5075) independent experiments.

3.19. MTT Assay

HeLa cells were grown in DMEM medium (*Sigma Aldrich*) with 10% FBS (*Sigma Aldrich*) and 2 mM glutamine (*Sigma Aldrich*) in 5% CO₂ at 37 °C.

For splitting or passaging, the medium was removed, and cells were washed with 10 mL of PBS. Afterwards, the cells were incubated with 1 mL of Accutase® for 10 min at 37 °C until full detachment. Then, 10 mL of the respective medium were added, mixed thoroughly and 1 mL of this cell-solution was transferred into a new flask. The cell-solution was diluted with medium to a volume of 10 mL.

To evaluate the cytotoxicity, HeLa cells were seeded in 96-well plates at a concentration of 4,000 cells per cavity. After 24 h the growth medium was removed by suction and 100 μ L medium (without FBS) with either DMSO (1%) or Xan (10 μ M, 1% DMSO final concentration) was added. After 24 h exposure at 37 °C and 5% CO₂ 20 μ L Thiazolyl blue tetrazolium bromide (MTT, 5 mg/mL in PBS, *Sigma Aldrich*) were added to the cells and incubated for 4 h to allow the MTT to be metabolized. The medium was removed by suction and the resulting formazan dissolved in 200 μ L DMSO. The optical density was measured with an Infinite® M200 Pro microplate reader (*Tecan Group Ltd.*) at 570 nm and background was subtracted at 630 nm. Absorption values were normalised to DMSO control. Each data set represents six replicates obtained from three independent experiments.

3.20. *Galleria mellonella* Assay

G. mellonella waxworms were purchased from Speedy Worm & Minnesota Muskie Farm Inc., Alexandria, MN. Assays were performed as previously described.^{157,169}

To study Xan's toxicity, a 10 μ L Hamilton syringe was used to inject 5 μ L aliquots of the respective solutions into the hemocoel of each caterpillar *via* the last right proleg and worms were incubated in a petri plate at 37 °C in a humidified incubator. At 24 h intervals, viability was assessed by checking for movement, and worms not exhibiting any movement after prodding with a pipette tip were considered dead and were typically dark brown to black.

For infection, LB medium (2 mL) was inoculated with *A. baumannii* AB5075 and grown shaking at 37°C to an OD₆₀₀ of 0.5. Serial dilutions were prepared in cold PBS, and 1×10^5 cells of *A. baumannii* AB5075 were injected into the hemocoel of *G. mellonella* (200 – 250 mg each) *via* the last left proleg. Worms were incubated in a petri plate at 37 °C in a humidified incubator for 1.5 h. Afterwards, 5 μ L aliquots of Xan solutions were injected into the hemocoel of each caterpillar *via* the last right proleg. Worms were incubated in a petri plate at 37 °C in a humidified incubator and at 24 h intervals, viability was assessed as described above. Bacterial colony counts on LB agar were used to confirm the inoculum.

For all experiments, a control group was included that was inoculated with PBS to monitor for killing due to physical trauma. The reported values represent the averages of $n = 3$ (for toxicity tests) or $n = 1$ (infection) independent experiments with at least 10 worms per group for each experiment.

3.21. Chemical Synthesis

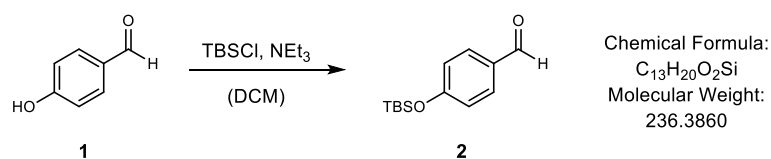
Reagents and solvents were purchased from commercial suppliers (*Sigma Aldrich Co. LLC, Thermo Fisher Scientific Inc., Merck KGaA, TCI Europe GmbH and Alfa Aesar GmbH*) and used as received. Reaction grade or anhydrous solvents (max. 0.01% water content, stored over molecular sieve under an argon atmosphere) were used for all reactions. TLC was performed on precoated silica gel plates (60 F-254, 0.25 mm, *Merck KGaA*) with detection by UV ($\lambda = 254$ and/or 366 nm) and/or by coloration using potassium permanganate (KMnO_4 ; 3.0 g KMnO_4 , 20.0 g K_2CO_3 and 5 mL 5% NaOH in 300 mL ddH₂O) stain and subsequent heat treatment. Flash chromatography was performed on silica gel 60 (0.035 – 0.070 mm, mesh 60 Å, *Merck KGaA*). The solvent compositions reported for all chromatographic separations are on a volume/volume (v/v) basis. Common solvents for chromatography [n-hexane (Hex), ethyl acetate (EtOAc), dichloromethane (DCM) and methanol (MeOH)] were distilled prior to use.

¹H- and proton-decoupled ¹³C- NMR spectra were recorded at the indicated temperature either on a Bruker AVHD-500 or on a Bruker AV-II-500 equipped with cryo probe head. Chemical shifts are reported in delta (δ) units in parts per million (ppm) relative to residual solvent signals [deuterated acetone (acetone-d₆) δ H = 2.05 ppm and δ C = 29.84, 206.26 ppm, CDCl₃ δ H = 7.26 ppm and δ C = 77.16 ppm]. The following abbreviations were used for the assignment of signals: s – singlet, d – doublet, t – triplet, m – multiplet. Coupling constants *J* are given in Hertz [Hz].

HR-MS spectra were recorded in the ESI or APCI mode on an LTQ-FT Ultra (FT-ICR-MS, *Thermo Fisher Scientific*) coupled with an UltiMate 3000 HPLC system (*Thermo Fisher Scientific*).

3.21.1. Synthesis of Xanthocillin X

Xan was prepared in 10 steps from commercially available 4-hydroxybenzaldehyde (1) by following the approach published by Tatsuta *et al.*^{89,90,170}

4-*tert*-Butyldimethylsilyloxybenzaldehyde (2)

A protocol published by Kwong *et al.* was used.¹⁷¹ A solution of *tert*-butyldimethylsilylchloride (18.0 g, 120 mmol, 1.5 eq.) in dry DCM (130 mL) was added dropwise to a solution of 4-hydroxybenzaldehyde (1) (9.75 g, 79.8 mmol, 1.0 eq.) and NEt₃ (16.6 mL, 12.1 g, 120 mmol, 1.5 eq.) in dry DCM (50 mL). The reaction mixture was stirred at RT for 2 h and then quenched with water (100 mL). The organic layer was separated and the aqueous layer was extracted with DCM (3 × 100 mL). The combined organic layers were washed with water (150 mL) and saturated salt solution (150 mL), dried over MgSO₄, filtered, and concentrated *in vacuo*. The crude product was purified by means of flash column chromatography (EtOAc:Hex = 1:20) to afford 4-*tert*-butyldimethylsilyloxybenzaldehyde (2) as a yellow oil (17.7 g, 74.9 mmol, 94%).

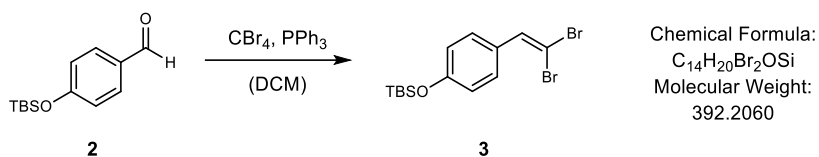
TLC (EtOAc:Hex = 1:20): R_f = 0.35 [UV].

¹H-NMR (500 MHz, CDCl₃): δ [ppm] = 9.87 (s, 1H), 7.78 (d, J = 8.6 Hz, 2H), 6.93 (d, J = 8.6 Hz, 2H), 0.98 (s, 9H), 0.24 (s, 6H).

¹³C-NMR (75 MHz, CDCl₃): δ [ppm] = 190.9, 161.6, 132.0, 130.6, 120.6, 25.7, 18.4, -4.2.

ESI-HR-MS (m/z) [M+H⁺] calcd. for C₁₃H₂₁O₂Si, 237.1305; found, 237.1303.

The NMR and HRMS data match with published data.¹⁷¹

tert-Butyl(4-(2,2-dibromovinyl) phenoxy) dimethylsilane (3)

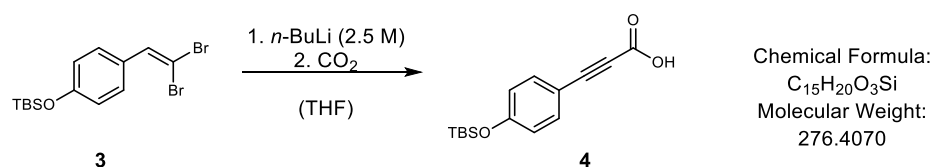
A protocol published by Dixon *et al.* was used.¹⁷² To a mixture of triphenylphosphine (56.6 g, 216 mmol, 3.0 eq.) and carbon tetrabromide (35.8 g, 108 mmol, 1.5 eq.), DCM (170 mL) was added dropwise at 0 °C, followed by stirring for 3 h. Then, compound 2 (17.0 g, 71.9 mmol, 1.0 eq.) was added dropwise, followed by stirring overnight. The reaction mixture was filtered and the filtrate was dry-loaded onto silica. Purification by column chromatography (Hex) afforded *tert*-butyl(4-(2,2-dibromovinyl) phenoxy)-dimethylsilane (3) as a pale-yellow oil (24.6 g, 62.7 mmol, 87%).

TLC (Hex): $R_f = 0.42$ [UV, KMnO₄].

¹H-NMR (300 MHz, CDCl₃): δ [ppm] = 7.47 (d, $J = 8.7$ Hz, 2H), 7.41 (s, 1H), 6.83 (d, $J = 8.7$ Hz, 2H), 1.00 (s, 9H), 0.23 (s, 6H).

¹³C-NMR (75 MHz, CDCl₃): δ [ppm] = 156.2, 136.5, 130.0, 128.5, 120.1, 87.4, 25.8, 18.4, –4.2.

The NMR data match with published data.¹⁷⁰

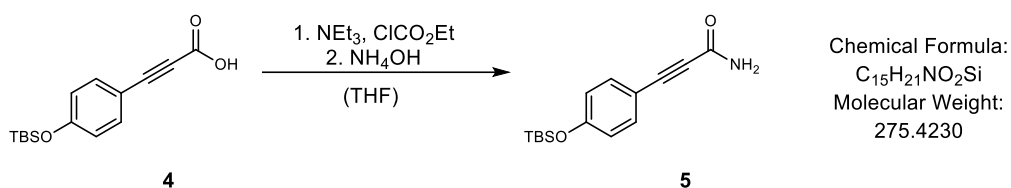
3-(4-*tert*-Butyldimethylsilyloxyphenyl) propionic acid (4)

Compound 3 (3.00 g, 7.65 mmol, 1.0 eq.) was dissolved in THF (45 mL) and a 2.5 mol/L *n*-BuLi (in Hex) solution (7.96 mL, 19.9 mmol, 2.6 eq.) was dropwise added at -78 °C. After stirring for 1 h, crushed dry ice was added while the solution was returned to 0 °C. After stirring for 20 min at 0 °C, water was added and the solution was concentrated under reduced pressure. The residue was diluted with diethyl ether and extracted with water. The obtained aqueous layer was acidified (pH 4) with an aqueous KHSO₄ solution (saturated) and extracted with EtOAc (2 × 20 mL). The obtained organic layer was washed with brine (20 mL), dried over anhydrous MgSO₄, subjected to filtration and concentrated under reduced pressure to give 3-(4-*tert*-butyldimethylsilyloxyphenyl) propionic acid (3) (2.12 g, 7.67 mmol, quant.) as crystals. The crude acid 3 was used without further purification.

¹H-NMR (300 MHz, CDCl₃): δ [ppm] = 7.49 (d, J = 8.6 Hz, 2H), 6.82 (d, J = 8.7 Hz, 2H), 0.98 (s, 9H), 0.22 (s, 6H).

ESI-HR-MS (m/z) [M-H⁺] calcd. for C₁₅H₁₉O₃Si, 275.1109; found, 275.1111.

The ¹H-NMR data match with published data.¹⁷⁰

3-(4-*tert*-Butyldimethylsilyloxyphenyl) propiol amide (5)

Compound 4 (10.9 g, 39.4 mmol, 1.0 eq.) was dissolved in THF (170 mL) and NEt₃ (6.01 mL, 4.39 g, 43.4 mmol, 1.1 eq.) and ethyl chloroformate (7.50 mL, 8.55 g, 78.8 mmol, 2.0 eq.) were added dropwise under cooling with ice followed by stirring for 50 min. Then, an ammonia solution (2 mol/L in methanol, 55.2 mL, 110 mmol, 2.8 eq) was added dropwise, followed by stirring for 20 min at RT. The reaction solution was concentrated under reduced pressure and water was added to the residue, followed by extraction with EtOAc (7 × 30 mL). The combined organic layers were concentrated under reduced pressure and the residue was purified by silica gel column chromatography (Hex:EtOAc = 5:3) to give 3-(4-*tert*-butyldimethylsilyloxyphenyl) propiol amide (5) (8.20 g, 29.8 mmol, 76%) as colourless crystals.

TLC (Hex:EtOAc = 1:1): R_f = 0.51 [UV/KMnO₄].

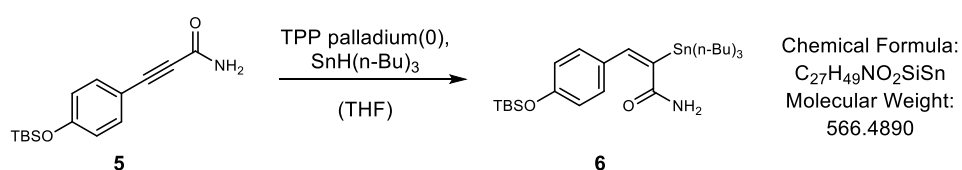
¹H-NMR (300 MHz, CDCl₃): δ [ppm] = 7.43 (d, J = 8.8 Hz, 2H), 6.81 (d, J = 8.8 Hz, 2H), 5.92 (*br. s*, 2H), 0.97 (*s*, 9H), 0.21 (*s*, 6H).

¹³C-NMR (75 MHz, CDCl₃): δ [ppm] = 157.9, 155.5, 134.6, 120.6, 112.6, 87.0, 81.9, 25.7, 18.4, -4.3.

ESI-HR-MS (m/z) [M+H⁺] calcd. for C₁₅H₂₂NO₂Si, 276.1414; found, 276.1414.

The NMR data match with published data.¹⁷⁰

(*E*)-3-(4-*tert*-butyldimethylsilyloxyphenyl)-2-(tributylstannyl) acrylamide (**6**)



Compound **5** (500 mg, 1.82 mmol, 1.0 eq) was dissolved in dry THF (10 mL) in nitrogen atmosphere, and tetrakis(triphenyl)phosphine (TPP) palladium (0) (42.0 mg, 36.3 μ mol, 0.02 eq.) was added under cooling with ice. Then, a THF solution (6 mL) of tri-*n*-butyltin hydride (2.30 mL, 2.48 g, 8.53 mmol, 4.7 eq.) was dropwise added. After stirring for 30 min at 0 °C, carbon tetrachloride (1.40 g, 878 μ L, 9.08 mmol, 5.0 eq.) and potassium fluoride (527 mg, 9.08 mmol, 5.0 eq.) were added to terminate the reaction followed by stirring for 30 min at RT. After filtration, the filtrate was concentrated under reduced pressure and the residue was purified by silica gel column chromatography (Hex:EtOAc = 5:1) to give (*E*)-3-(4-*tert*-butyl-dimethylsilyloxyphenyl)-2-(tributylstannyl)acrylamide (**6**) (653 mg, 1.15 mmol, 63%) as a yellow oil.

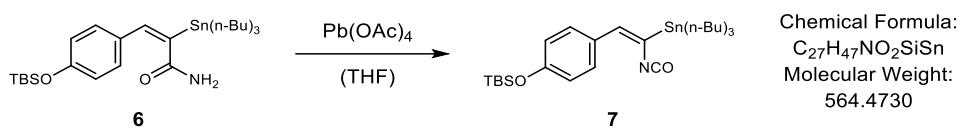
TLC (Hex:EtOAc = 7:1): R_f = 0.41 [UV/ KMnO_4].

¹H-NMR (300 MHz, CDCl_3): δ [ppm] = 7.32 (d, J = 8.5 Hz, 2H), 6.77 (d, J = 8.5 Hz, 2H), 6.57 (s, 1H), 5.20 (s, 2H), 1.60 – 1.51 (m, 6H), 1.36 – 1.31 (m, 6H), 1.13 – 1.00 (m, 6H), 0.97 (s, 9H), 0.90 (m, 9H), 0.19 (s, 6H).

¹³C-NMR (126 MHz, CDCl_3): δ [ppm] = 176.3, 155.9, 141.1, 139.5, 130.0, 129.8, 120.1, 29.0, 27.4, 25.8, 18.4, 13.9, 10.5, –4.3.

The NMR data match with published data.¹⁷⁰

(*E*)-*tert*-butyl(4-(2-isocyanato-2-(tributylstannyl) vinyl) phenoxy) dimethylsilane (7)



Compound 6 (4.00 g, 7.06 mmol, 1.0 eq.) was dissolved in dry THF (72 mL) and lead tetraacetate (3.44 g, 7.77 mmol, 1.1 eq.) was added at RT. After stirring for 45 min, hexane (80 mL) was added, the solution was subjected to filtration with Celite and the filtrate was concentrated under reduced pressure. The residue was purified by silica gel column chromatography (Hex:EtOAc = 50:1) to give (*E*)-*tert*-butyl(4-(2-isocyanato-2-(tributylstannyl) vinyl) phenoxy) dimethylsilane (6) (2.36 g, 4.18 mmol, 59%) as a yellow oil.

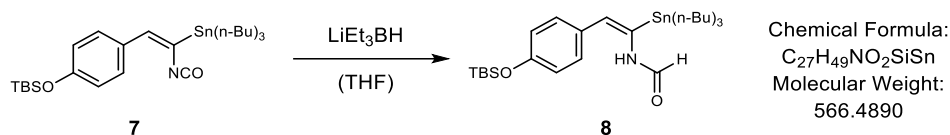
TLC (Hex:EtOAc = 1:50): R_f = 0.54 [UV].

¹H-NMR (500 MHz, CDCl₃): δ [ppm] = 7.54 (d, J = 8.7 Hz, 2H), 6.81 (d, J = 8.7 Hz, 2H), 5.89 (s, 1H), 1.62 – 1.54 (m, 6H), 1.40 – 1.32 (m, 6H), 1.14 – 1.02 (m, 6H), 0.98 (s, 9H), 0.92 (t, J = 7.3 Hz, 9H), 0.20 (s, 6H).

¹³C-NMR (126 MHz, CDCl₃): δ [ppm] = 155.3, 133.7, 130.9, 129.8, 129.1, 124.8, 120.1, 29.0, 27.4, 25.8, 18.4, 13.8, 10.6, –4.2.

The NMR data match with published data.¹⁷⁰

(*E*)-*N*-(2-(4-((*tert*-butyldimethylsilyl)oxy)phenyl)-1-(tributylstannyl)vinyl)formamide (8)



Compound 7 (320 mg, 567 μ mol, 1.0 eq.) was dissolved in dry THF (6 mL) and lithium triethylborohydride in THF (1 M) (590 μ L, 590 μ mol, 1.04 eq.) was dropwise added at -78 $^{\circ}$ C. After 30 min, the reaction mixture was allowed to warm to RT and a saturated aqueous NH₄Cl solution (3 mL) was added to stop the reaction. Celite was added and the solvent was removed under reduced pressure. The resulting residue was purified by silica gel column chromatography (EtOAc:Hex = 1:5) to give (*E*)-*N*-(2-(4-((*tert*-butyldimethylsilyl)oxy)phenyl)-1-(tributylstannyl)vinyl)formamide (8) as a yellow oil (290 mg, 512 μ mol, 90%).

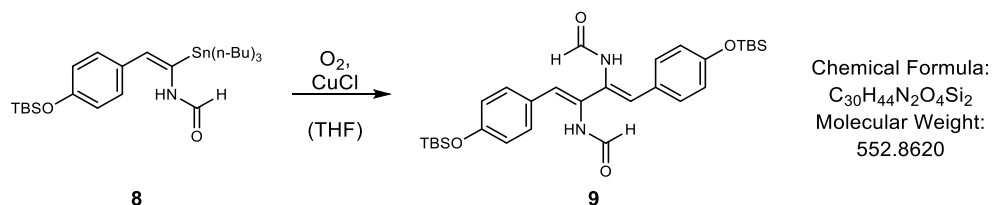
¹H-NMR (400 MHz, CDCl₃): δ [ppm]: = 8.13 (s, 1H), 7.91 (s, 1H), 7.15 (d, J = 8.4 Hz, 2H), 6.87 (d, J = 8.4 Hz, 2H), 5.93 (s, 1H), 1.62 – 1.48 (m, 6H), 1.41 – 1.32 (m, 6H), 1.14 – 0.96 (m, 6H), 0.99 (s, 9H), 0.92 (t, J = 7.3 Hz, 9H), 0.23 (s, 6H).

¹³C-NMR (101 MHz, CDCl₃): δ [ppm] = 159.3, 154.7, 135.6, 129.5, 129.4, 122.8, 120.8, 29.2, 27.5, 25.8, 18.4, 13.9, 12.3, -4.2 .

TLC (EtOAc:Hex = 1:5): R_f = 0.89 [UV, KMnO₄].

The NMR data match with published data.¹⁷⁰

N,N'-((1*Z*,3*Z*)-1,4-bis(4-((*tert*-butyldimethylsilyl) oxy) phenyl) buta-1,3-diene-2,3-diyl)-diformamide (9)



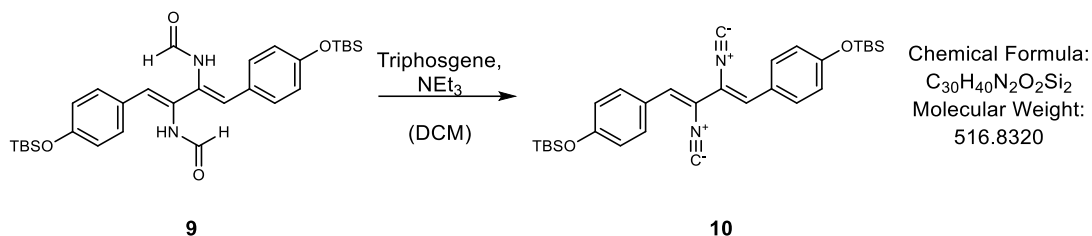
Compound 8 (1.31 g, 2.31 mmol, 1.0 eq.) was dissolved in dry THF (30 mL) in oxygen atmosphere, cooled to 0 °C and CuCl (595 mg, 6.01 mmol, 2.6 eq.) was added. The reaction mixture was vigorously stirred for 3.5 h, filtered, Celite was added and the solvent was removed under reduced pressure. The residue was purified by column chromatography (toluene:acetone = 8:1 → 5:1) to give *N,N'*-((1*Z*,3*Z*)-1,4-bis(4-((*tert*-butyldimethylsilyl) oxy) phenyl) buta-1,3-diene-2,3-diyl)-diformamide (9) (638 mg, 1.15 mmol, quant.) as a yellow powder.

TLC (toluene:acetone = 5:1): $R_f = 0.15$ [UV, $KMnO_4$].

ESI-HR-MS (m/z) [$M+H^+$] calcd. for $C_{30}H_{45}N_2O_4Si_2$, 553.2912; found, 553.2904.

1H -NMR and ^{13}C -NMR: Due to numerous rotamer signals, the product signals could not be assigned. This is in accordance with literature references.¹⁷⁰

(((1*Z*,3*Z*)-2,3-diisocyanobuta-1,3-diene-1,4-diyl) bis(4,1-phenylene)) bis (oxy)) bis (*tert*-butyldimethylsilane) (10)



Compound 9 (226 mg, 409 μmol , 1.0 eq.) was dissolved in dry DCM (3 mL) and NEt_3 (205 μL , 149 mg, 1.47 mmol, 3.6 eq.) was added dropwise at 0 $^\circ\text{C}$. Then, a solution of triphosgene (121 mg, 409 μmol , 1.0 eq.) in DCM (1 mL) and was added dropwise. The reaction mixture was stirred for 1 h at 0 $^\circ\text{C}$, was diluted with EtOAc (3 mL) while it was allowed to warm to RT and poured into a saturated NaHCO_3 solution (5 ml). Extraction with EtOAc was carried out (2 \times 5 mL) and the combined organic layers were concentrated under reduced pressure. The residue was purified by column chromatography (Hex:EtOAc = 20:1) to give (((1*Z*,3*Z*)-2,3-diisocyno-buta-1,3-diene-1,4-diyl) bis(4,1-phenylene)) bis(oxy)) bis(*tert*-butyl-dimethyl-silane) (10) (115 mg, 223 μmol , 54%) as a yellow powder.

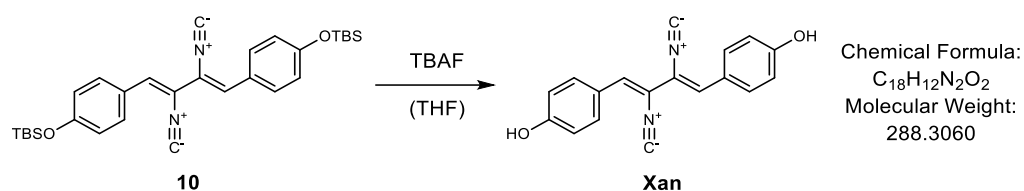
TLC (Hex:EtOAc = 20:1): R_f = 0.73 [UV, KMnO_4].

$^1\text{H-NMR}$ (300 MHz, CDCl_3): δ [ppm]: = 7.73 (d, J = 8.7 Hz, 4H), 7.01 (s, 2H), 6.92 (d, J = 8.7 Hz, 4H), 1.00 (s, 18H), 0.25 (s, 12H).

$^{13}\text{C-NMR}$ (101 MHz, CDCl_3): δ [ppm] = 173.5, 157.9, 131.9, 127.7, 125.5, 120.8, 116.4, 25.8, 18.4, -4.2.

The NMR data match with published data.¹⁷⁰

4,4'-((1Z,3Z)-2,3-diisocyanobuta-1,3-diene-1,4-diyl)diphenol (Xan)



Compound 10 (20.0 mg, 38.7 μ mol, 1.0 eq.) was dissolved in dry THF (1 mL) and the reaction mixture was cooled to 0 °C. Then, *tetra-n*-butylammonium fluoride (TBAF) (1 M in THF) (77.4 μ L, 77.4 μ mol, 2.0 eq.) was slowly added dropwise. The reaction solution was stirred for 10 min at 0 °C and the solution was directly purified by column chromatography (DCM:MeOH = 20:1 + 1% acetic acid) to give Xan (8.80 mg, 30.5 μ mol, 79%) as a yellow powder.

TLC (Hex:EtOAc = 2:1): R_f = 0.27 [UV, KMnO₄].

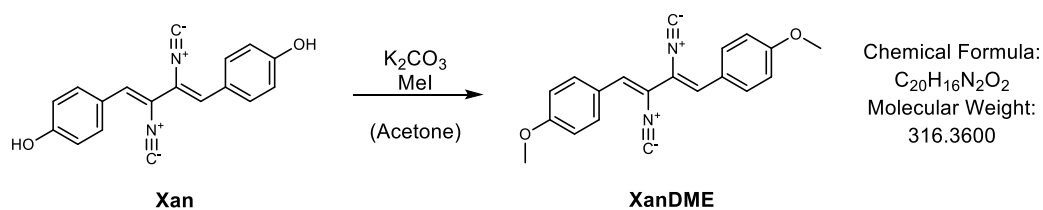
¹H-NMR (500 MHz, Acetone-d₆): δ [ppm] = 9.17 (s, 2H), 7.83 (d, J = 8.7 Hz, 4H), 7.08 (s, 2H), 7.00 (d, J = 8.7 Hz, 4H).

¹³C-NMR (126 MHz, Acetone-d₆): δ [ppm] = 175.0, 160.5, 132.9, 128.4, 124.9, 116.9, 116.6.

ESI-HRMS (m/z): [M-H⁺] calcd. for C₁₈H₁₁N₂O₂, 287.0826; found, 287.0826.

The NMR data of Xan match with published data.^{89,90,170}

3.21.2. Synthesis of Xanthocillin dimethylether (XanDME)



Xan (30.0 mg, 104 μ mol, 1.0 eq) was dissolved in dry acetone (7 mL), the suspension was cooled to 0 °C and K₂CO₃ (30.2 mg, 219 μ mol, 2.1 eq.) as well as methyl iodide (13.6 μ L, 31.0 mg, 219 μ mol, 2.1 eq.) were added. The reaction mixture was stirred at 50 °C and the product formation was controlled *via* ESI-MS. After 2 h the reaction solution was concentrated under reduced pressure and the residue was purified by column chromatography (Hex:EtOAc = 10:1) to obtain XanDME (7.90 mg, 25.0 μ mol, 24%) as green crystals.

TLC (Hex:EtOAc = 5:1): R_f = 0.46 [UV, KMnO₄].

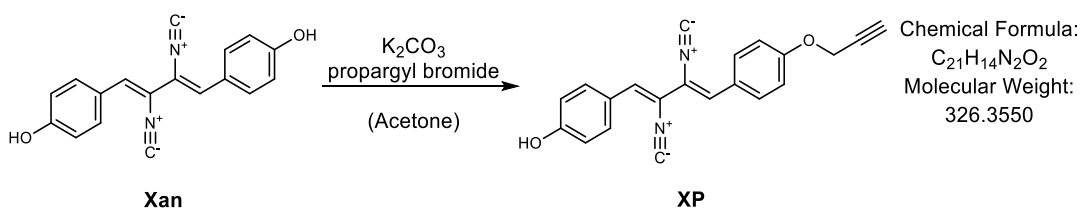
¹H-NMR (500 MHz, Acetone-d₆): δ [ppm] = 7.90 (d, J = 8.8 Hz, 4H), 7.14 (s, 2H), 7.10 (d, J = 8.8 Hz, 4H), 3.90 (s, 6H).

¹³C-NMR (126 MHz, Acetone-d₆): δ [ppm] = 175.1, 162.3, 132.6, 128.4, 125.7, 117.0, 115.3, 55.9.

ESI-HRMS (m/z): [M+H⁺] calcd. for C₂₀H₁₇N₂O₂, 317.1285; found, 317.1283.

The NMR and HRMS data of XanDME match with published data.¹⁷⁰

3.21.3. Synthesis of the Xanthocillin probe (XP)



A protocol published by Lee *et al.* was used with slight modifications.¹⁷³ Xan (17.0 mg, 59.0 μ mol, 1.0 eq) was dissolved in dry acetone (5 mL), the suspension was cooled to 0 °C and K₂CO₃ (8.15 mg, 59.0 μ mol, 1.0 eq.) was added. Then, propargylic bromide solution (9.2 M in toluene) (6.41 μ L, 59.0 μ mol, 1.0 eq.) was added, the reaction mixture was stirred at 50 °C and the product formation was controlled *via* ESI-MS. After 2.5 h the reaction solution was concentrated under reduced pressure and the residue was purified twice by column chromatography (DCM:MeOH = 20:1) to obtain XP (3.60 mg, 11.0 μ mol, 19%) as a light yellow powder. Xan (13.9 mg, 48.2 μ mol, 82%) was re-isolated as a yellow powder.

TLC (DCM:MeOH = 20:1): R_f = 0.18 [UV, KMnO₄].

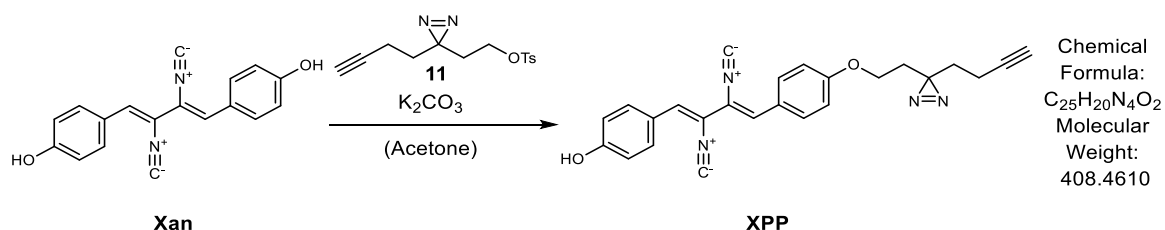
¹H-NMR (500 MHz, Acetone-d₆): δ [ppm] = 9.12 (s, 1H), 7.92 (d, J = 8.8 Hz, 2H), 7.84 (d, J = 8.8 Hz, 2H), 7.17 (d, J = 8.8 Hz, 2H), 7.14 (s, 1H), 7.12 (s, 1H), 7.01 (d, J = 8.8 Hz, 2H), 4.91 (d, J = 2.4 Hz, 2H), 3.15 (t, J = 2.4 Hz, 1H).

¹³C-NMR (126 MHz, Acetone-d₆): δ [ppm] = 175.2, 175.1, 160.6, 160.1, 133.0, 132.6, 128.9, 128.0, 126.6, 124.8, 117.7, 116.9, 116.4, 116.3, 79.3, 77.6, 56.5.

ESI-HRMS (m/z): [M-H⁺] calcd. for C₂₁H₁₃N₂O₂, 325.0983; found, 325.0982.

3.21.4. Synthesis of the Xanthocillin photoprobe (XPP)

Compound 11 was synthesised as previously described.⁹³



The protocol for XP was used with slight modifications. Xan (35.5 mg, 123 μ mol, 1.0 eq) was dissolved in dry acetone (10 mL), the suspension was cooled to 0 °C and K₂CO₃ (17.0 mg, 123 μ mol, 1.0 eq.) was added. Then, compound 11 (36.0 mg, 123 μ mol, 1.0 eq.) was added, the reaction mixture was stirred at 50 °C and the product formation was controlled *via* ESI-MS. After 8 h the reaction solution was concentrated under reduced pressure and the residue was purified by column chromatography (Hex:acetone = 6:1) to give XPP (11.2 mg, 27.4 μ mol, 22%) as a light yellow powder. Xan (17.3 mg, 60.0 μ mol, 49%) was re-isolated.

TLC (Hex:acetone = 4:1): R_f = 0.24 [UV, KMnO₄].

¹H-NMR (500 MHz, Acetone-d₆): δ [ppm] = 9.11 (s, 1H), 7.90 (d, J = 8.8 Hz, 2H), 7.83 (d, J = 8.8 Hz, 2H), 7.14 – 7.08 (m, 4H), 7.00 (d, J = 8.8 Hz, 2H), 4.03 (t, J = 6.2 Hz, 2H), 2.4 (t, J = 2.7 Hz, 1H), 2.11 (td, J = 7.5, 2.7 Hz, 2H), 1.97 (t, J = 6.2 Hz, 2H), 1.75 (t, J = 7.5 Hz, 2H).

¹³C-NMR (126 MHz, Acetone-d₆): δ [ppm] = 175.0, 175.0, 161.0, 160.5, 132.9, 132.6, 128.7, 128.0, 126.0, 124.7, 117.3, 116.8, 116.3, 115.8, 83.6, 70.6, 63.7, 33.3, 33.3, 27.5, 13.6.

ESI-HRMS (m/z): [M-H⁺] calcd. for C₂₅H₁₉N₄O₂, 407.1513; found, 407.1512.

III. Tailored Cofactor Traps for the *in Situ* Detection of Hemithioacetal-Forming Pyridoxal Kinases

Hübner, I.*, Dienemann, J.-N.*, Friederich, J., Schneider, S., Sieber, S. A., Tailored cofactor traps for the *in situ* detection of hemithioacetal-forming pyridoxal kinases. *ACS Chem. Biol.* 2020, 15, 12, 3227–3234.

Contribution:

I.H. and S.A.S. conceived and designed the project. I.H. developed all synthesis strategies and performed IPMS experiments. I.H., J.F. and J.-N.D. synthesised compounds. I.H. and J.-N.D. performed cloning, *in vitro* gel-based labelling experiments and *in situ* labelling (gel- and MS-based). J.-N.D. and J.F. purified recombinant proteins. J.-N.D. performed activity assays. S.S. performed modelling. *I.H. and J.-N.D. contributed equally to this work.

1. Vitamin B₆

Vitamin B₆ is a collective term for three pyridine analogues known as pyridoxal (PL), pyridoxine (PN) and pyridoxamine (PM) (Figure III-1), which are precursors to pyridoxal-5'-phosphate (PLP), a crucial cofactor for PLP-dependent enzymes (PLP-DE). PLP-DEs use PLP to catalyse a number of chemical reactions that are involved in essential cellular processes such as glucose, lipid and amino acid metabolism, as well as the production of heme, nucleotides and neurotransmitters.¹⁷⁴⁻¹⁷⁷ Additionally, PLP represents one of the most versatile cofactors of nature, which is illustrated by the fact that more than 140 different enzymatic activities are PLP-dependent, corresponding to ~4% of all classified activities.¹⁷⁵ These include racemization, transamination, decarboxylation reactions as well as carbon-carbon bond cleavage and formation.¹⁷⁵ Thus, numerous PLP-DEs represent promising drug targets,¹⁷⁷⁻¹⁷⁹ such as alanine racemase for the treatment of bacterial infections.^{180,181} Further, PLP has been shown to be crucial for the virulence and survival of pathogenic bacteria such as *Streptococcus pneumoniae*,¹⁸² *Helicobacter pylori*,¹⁸³ *Mycobacterium tuberculosis*,¹⁸⁴ and *Vibrio cholerae*.¹⁸⁵

Cells are provided with PLP either by endogenous *de novo* biosynthesis or by the uptake of vitamin B₆ from nutrients. While microorganisms are capable of both biosynthesis and uptake, all other organisms depend exclusively on uptake. Additionally, all cells possess a salvage pathway, for the interconversion of the B₆ vitamers. For this, PL, PN, and PM are phosphorylated at the 5'-alcohol by a pyridoxal kinase (PLK) to PLP, PNP and PMP, respectively. Subsequently, PNP and PMP are oxidized by pyridoxine-5'-phosphate oxidase (PNPOx) to PLP (Figure III-1).^{186,187}

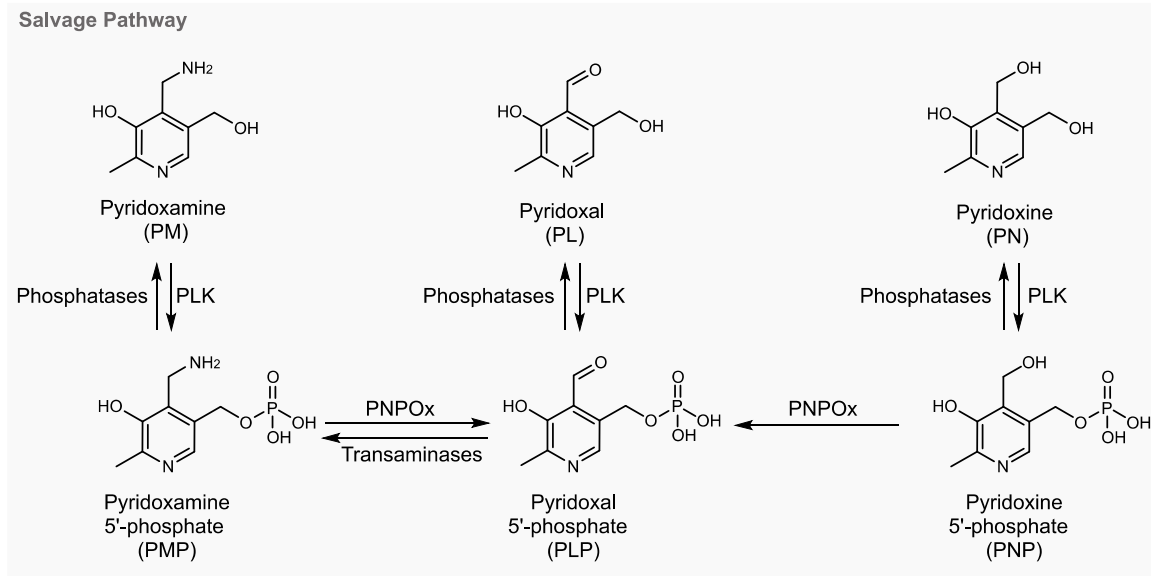


Figure III-1: Salvage pathways for the interconversion of the B₆ vitamins. Pyridoxal kinase (PLK) catalyzes the addition of phosphate from adenosine triphosphate (ATP) to the 5'-alcohol group of PN, PM and PL to form PNP, PMP and PLP, respectively. Pyridoxine 5'-phosphate oxidase (PNPOx) catalyses the oxidation of the 4'-hydroxyl group of PNP or the 4'-amino group of PMP into the aldehyde group of PLP.

While PLP deficiency in cell is suspected to cause several pathologies, too high concentrations are known to be toxic due to the reactive aldehyde group at the 4' position.¹⁸⁶ Thus, the PLP level in the cell must be strictly controlled, which is achieved by the enzymes PLK and PNPOx.¹⁸⁶ It has been shown that this regulation can be manipulated by inhibition of the PLK using small molecules. This resulted in PLP deficiency, manifested by headaches, agitation, convulsions, unconsciousness, paralysis and even death, demonstrating the importance of these enzymes for cells. One example for an inhibitor is ginkgotxin, which binds to the pyridoxal binding pocket of the human PLK (*h*PLK) with a reported K_i of 0.4 μM .¹⁸⁸

For a long time, it was believed that a single PLK was responsible for the phosphorylation of B₆ vitamers in cells, but a study by Winkler *et al.* challenged this hypothesis. An *Escherichia coli* strain with both a mutation in the PLK gene (*pdxK*) and an inactive *de novo* biosynthesis can grow on PL, leading to the discovery of a second PLK encoded by the gene *pdxY*, hereafter referred to as *EcPLK*.^{189–191} While the PLK (*pdxK*) is able to catalyse the phosphorylation of all three B₆ vitamins, the *EcPLK* is only able to convert PL, with a very low activity compared to the PLK (*pdxK*) (less than 1% of PLK activity). The crystal structure of *EcPLK* showed that in one monomer PL within the active site is covalently bound as a hemithioacetal to cysteine (Cys) 122, which is located in the flexible lid region.¹⁸⁹ Interestingly, this covalent PL catalysis is not limited to *EcPLK*, but was subsequently discovered in several strains, such as *Pseudomonas aeruginosa* and *Staphylococcus aureus*.^{192,193}

In *S. aureus*, the corresponding PLK was coincidentally discovered in a study to unravel cellular targets of the NP rugulactone. An enzyme encoded by *thiD* (ThiD1, UniProt-ID: A0A0H2XGZ0) was identified as the target protein.¹⁹⁴ ThiD1 was previously predicted to be involved in the thiamine biosynthesis, yet this enzyme did not cluster with any of the thiamine biosynthesis genes. In fact, a closer examination of the *S. aureus* genome discovered an additional protein annotated as *thiD* (ThiD2, UniProt ID: A0A0H2XGE7) located in the thiamine biosynthesis operon. Experiments with the recombinantly expressed ThiD1 enzyme showed significant activity not only in phosphorylation of the predicted substrate, 4-amino-5-hydroxymethyl-2-methylpyrimidine (HMP, the substrate of ThiD2 in the thiamine signalling pathway), but also of PL and PN.¹⁹³ In addition, metabolome studies with a ThiD1 transposon mutant showed elevated extracellular PL levels, suggesting that this enzyme plays an important role in PL phosphorylation in the cell, which is why the protein ThiD1 was reclassified as a PLK (*SaPLK*).^{193,194} Detailed mechanistic studies showed that this enzyme, similar to *EcPLK*, has a nucleophilic Cys residue (Cys110) in its flexible lid

region, which forms a covalent hemithioacetal with the PL 4'-aldehyde group (Figure III-2). Co-crystal structures showed that the lid shields the substrate pocket from bulk solvent and the corresponding hemithioacetal intermediate precisely positions PL for deprotonation of the 5'-alcohol, facilitated by an active site Cys (Cys214). Subsequently, the deprotonated alcohol attacks the γ -phosphate of ATP. Mutation of the lid Cys (C110A) completely abolished the activity, which demonstrates the importance of the covalent PL binding for the catalysis of this enzyme. A BLAST analysis showed that Cys110 is conserved in numerous homologous enzymes of Gram-positive bacteria, including *Enterococcus faecalis*, where the same C110A mutation led to a loss of PL turnover. Furthermore, these PLKs all have a reactive Cys as base in the active site and were therefore defined as a new class, namely the dual-Cys (one in the lid, one in the active site) PLKs (CC-PLKs).¹⁹³ Sequence alignments of these Gram-positive and Gram-negative PLKs containing lid Cys showed that corresponding lid Cys in Gram-negative enzymes is positioned five residues upstream compared to *Sa*PLK (Supplementary Figure 5).^{189,192} Furthermore, these PLKs in Gram-negative bacteria, such as *Ec*PLK or *P. aeruginosa* PLK (*Pa*PLK), bear an aspartate (Asp) in the active site and not, like the Gram-positive PLKs, a Cys. Therefore, the class of lid Cys containing PLKs was expanded to CD-PLK (Cys in the lid, Asp in the active site).^{189,192}

Interestingly, CD- and CC-PLKs seem to be absent in humans, which makes this class particularly interesting for antimicrobial drug development. However, the function and distribution of these enzymes in bacteria is still poorly understood. Surprisingly, studies on the catalytic mechanism of *Pa*PLK suggested that the Cys residue in the lid is not directly involved in PL phosphorylation.¹⁹² Therefore, sequence alignments of putative PLKs without detailed biochemical studies appear to be insufficient to predict the catalytic mechanism of these enzymes.^{192,195}

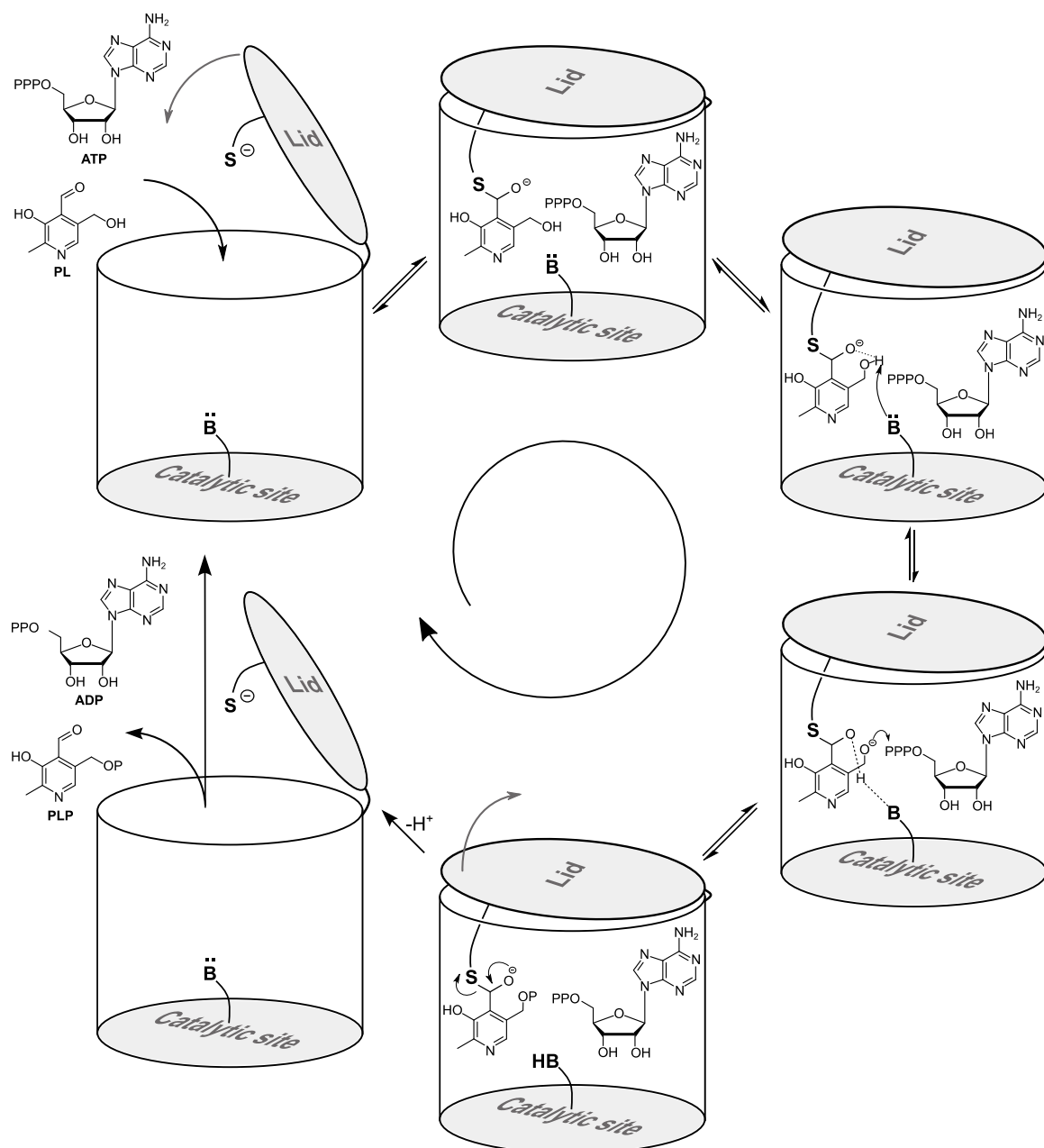


Figure III-2: Proposed mechanism for PL turnover by CC-PLKs. Upon binding of PL and ATP in the active site, the flexible lid closes and the Cys forms a hemithioacetal with PL. The intramolecular hydrogen bond network lowers pK_a of 5'-PL alcohol and catalytic base completes its deprotonation. The deprotonated 5'-alcohol then attacks the γ -phosphate of bound ATP and the hemithioacetal subsequently collapses. Finally, the flexible lid resumes its dynamic state and releases PLP and ADP.

2. Results and Discussion

In this work, a tool was developed to identify PLKs that use a hemithioacetal as an intermediate in catalysis. Probes for chemical proteomics were designed, which aim to react selectively with these PLKs, if a reactive Cys is involved in the catalysis. Therefore, the core scaffold of pyridoxal was equipped with an electrophilic warhead instead of the aldehyde, which allowed irreversible trapping of the nucleophilic attack of the lid Cys. In addition, these probes were modified with an alkyne handle, which enabled whole proteome mining for CC- and CD-PLKs. Upon protein binding, these probes could be functionalized with either rhodamine or biotin azide *via* click-chemistry to facilitate visualization by SDS-PAGE or identification of targeted proteins by LC-MS/MS analysis after enrichment on avidin beads. (Figure III-3). Although it is known that the *Sa*PLK tolerates various PL derivatives, the probes were developed step by step and always directly biologically evaluated.

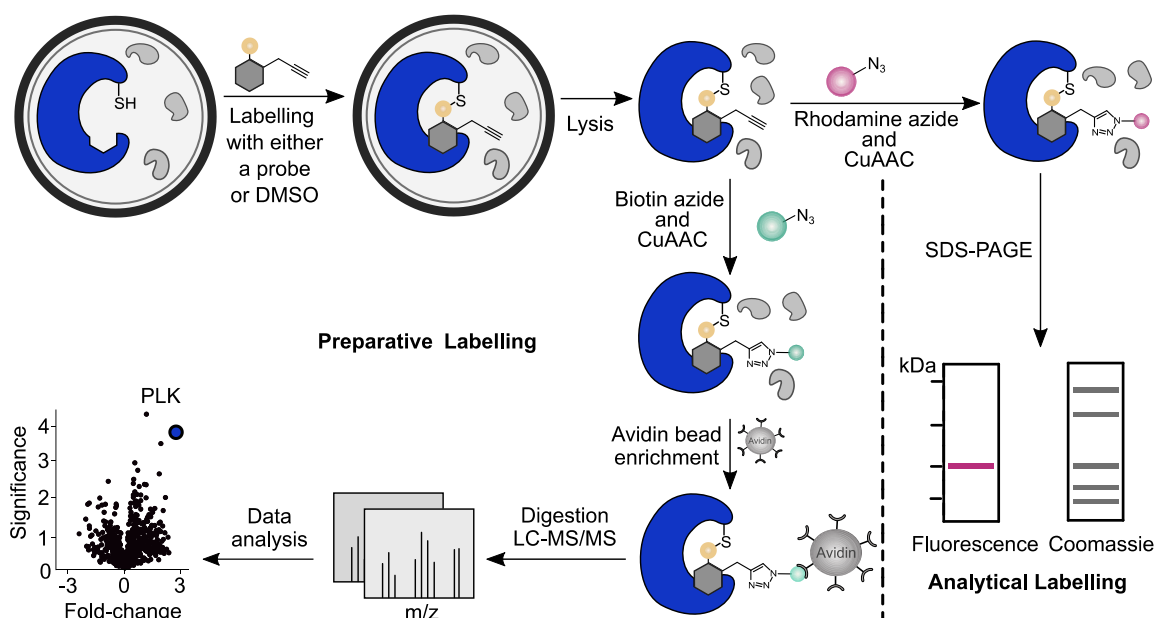
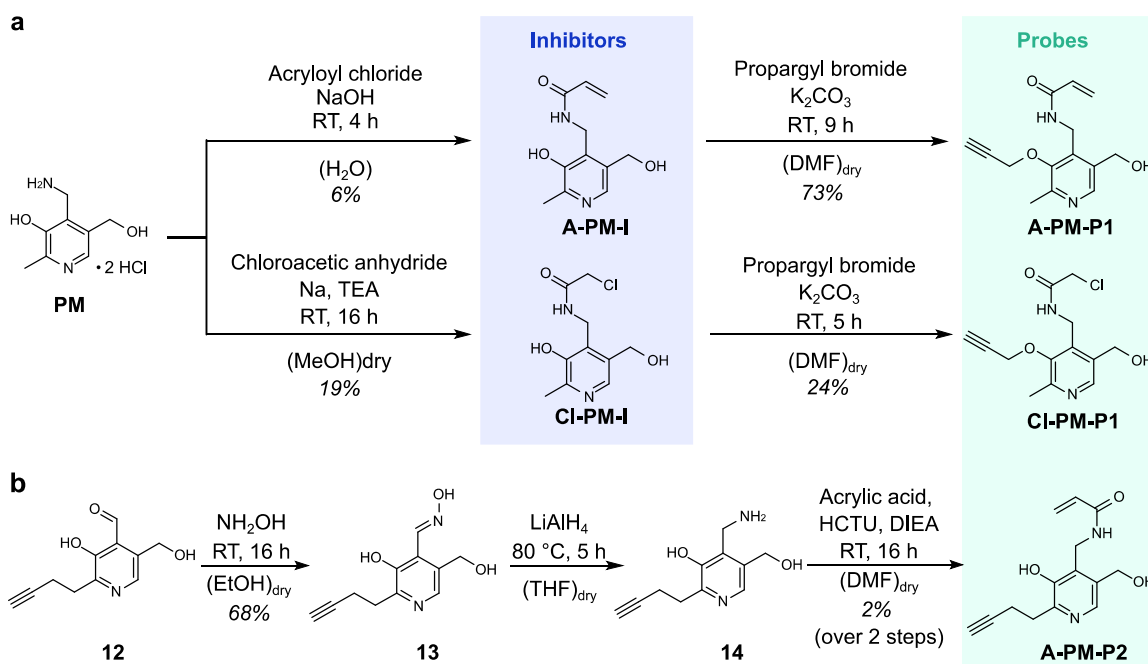


Figure III-3: Schematic experimental workflow for target identification by activity-based protein profiling (ABPP). After incubation of intact cells with a probe or DMSO, cells were lysed and samples subjected to copper-catalysed azide-alkyne cycloaddition (CuAAC) to attach rhodamine (analytical labelling) or biotin (preparative labelling) for

downstream analysis. For analytical labelling, samples were analysed via SDS-PAGE. For preparative studies, labelled proteins were enriched on avidin beads, enzymatically digested and analysed by LC-MS/MS.

2.1. Synthesis and Biological Evaluation of Inhibitors and Probes

First, the 4'-aldehyde of PL was replaced by an electrophilic Michael-acceptor moiety by acylation of PM using acryloyl chloride, thereby obtaining the inhibitor A-PM-I (Scheme III-1a).¹⁹⁶ Subsequently, the ability of the inhibitor A-PM-I to covalently modify recombinant *Sa*PLK was demonstrated *via* intact protein mass spectrometry (IPMS). In fact, while the wild type (wt) protein was completely modified overnight by A-PM-I (100 equivalents), treatment of the C110A mutant under the same conditions showed only 25% labelling (Figure III-4a). This confirmed the lid Cys as the primary binding site of the inhibitor, which was a requirement for the application of the intended probes for lid Cys containing PLK mining.



Scheme III-1: Synthesis of inhibitors A-PM-I and Cl-PM-I as well as the corresponding probes A-PM-P1, Cl-PM-P1 and A-PM-P2. (A) A-PM-I and Cl-PM-I were synthesised by acylation of PM as has already been described by *Ueda et al.*¹⁹⁶ and *Cravatt*,¹⁹⁷ respectively. Probes A-PM-P1 and Cl-PM-P1 were synthesised by propargylation of inhibitors A-PM-I and Cl-PM-I, respectively. (B) Synthesis of A-PM-P2. Compound 12 was synthesised as described by

*Hoegl et al.*¹⁹⁸ Compound 12 was converted to oxime 13,¹⁹⁹ which was subsequently reduced by LiAlH₄ and acylated using acrylic acid to yield A-PM-P2.²⁰⁰

Encouraged by the IPMS data, corresponding probe molecules were designed by attaching the alkyne handle *via* either the 3'-alcohol (A-PM-P1) or the 2'-methyl group (A-PM-P2). Probe A-PM-P1 was synthesised by alkylation of the 3'-alcohol of inhibitor A-PM-I with propargyl bromide (Scheme III-1a). To obtain the probe A-PM-P2, the alkylation strategy described by *Hoegl et al.* was used to synthesize 2'-propargylated PL derivative 12.¹⁹⁸ An excess of hydroxylamine was then added to 12 in order to obtain the corresponding oxime 13,¹⁹⁹ which was reduced with LiAlH₄ to yield the amine 14.²⁰⁰ In the last step, the coupling to acrylic acid was performed, resulting in A-PM-P2 (Scheme III-1b).

To test A-PM-P1 and A-PM-P2, the recombinant proteins *Sa*PLK wt and *Sa*PLK C110A were incubated with the respective probe and then subjected to click-chemistry, in which rhodamine azide was attached to the alkyne residues, thus enabling analysis *via* SDS-PAGE. The stronger labelling of *Sa*PLK wt for A-PM-P1 demonstrates the preference of *Sa*PLK wt for this probe. In accordance with the IPMS data, the mutant protein showed a significantly weaker labelling for A-PM-P1, which was also independent of heat inactivation of the protein, indicating non-specific probe binding (Figure III-4b). The preference of *Sa*PLK for A-PM-P1 can be explained by using the co-crystal structure of *Sa*PLK in complex with the native PL cofactor (PDB: 4C5L)¹⁹³ as a basis for computational modelling. Fitting the probes into the structure visualized that the alkyne handle at the 3'-hydroxyl group of A-PM-P1 points into an open space next to the β -hairpin and Val142. For probe A-PM-P2, however, steric clashes with the first β -strand and the propargylated 2'-substituent of A-PM-P2 were predicted (Figure III-4c). It is important to note, that the preference for attaching the alkyne tag to the 3'-hydroxyl group was not limited to *Sa*PLK as comparable results were obtained *via*

gel-based labelling experiments for recombinant *E. faecalis* PLK (*E*PLK), another confirmed CC-PLK (Figure III-4d).¹⁹³

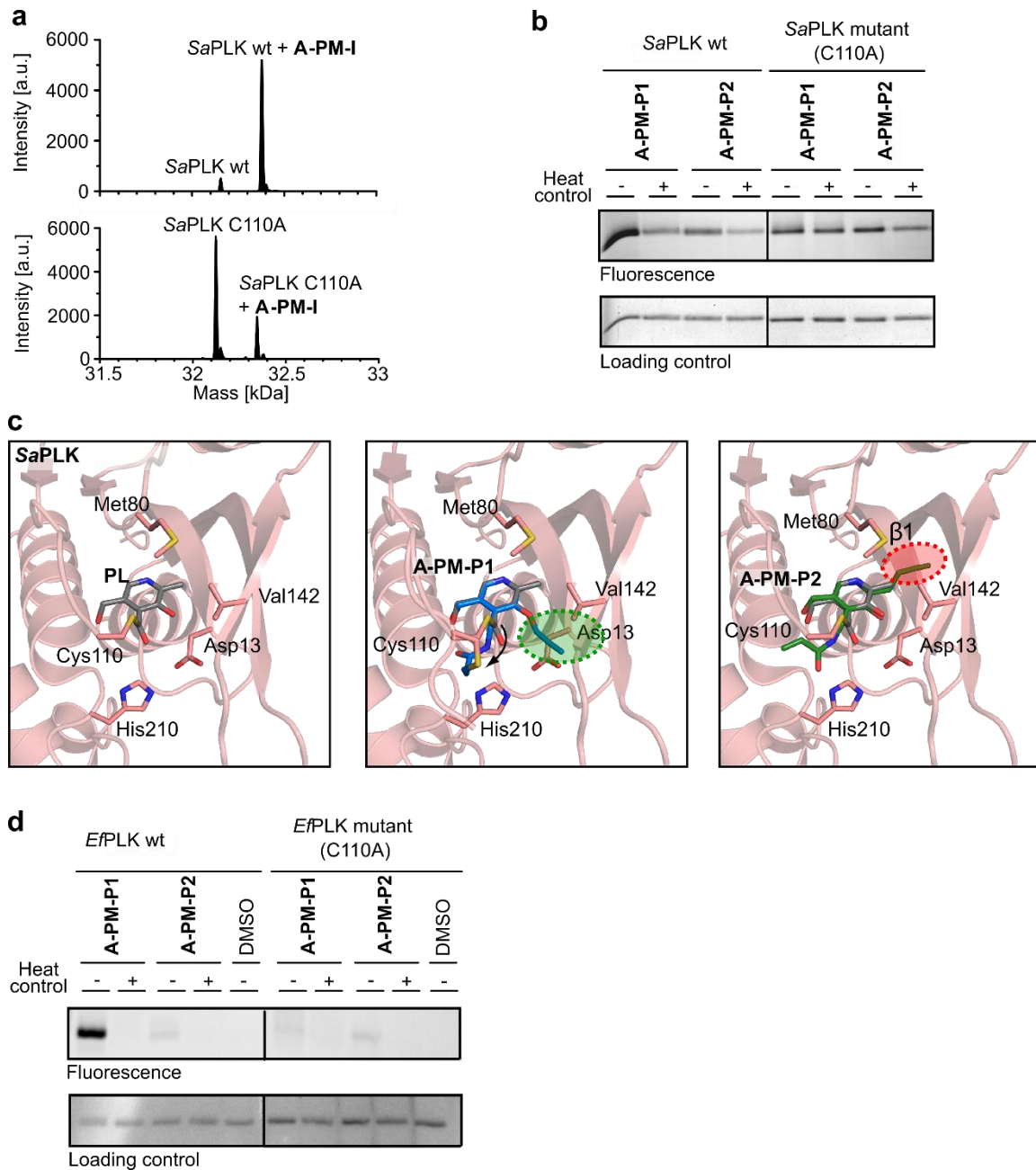


Figure III-4: Evaluation experiments of inhibitor A-PM-I and probes A-PM-P1 and A-PM-P2. a) Mass spectra of intact *Sa*PLK wt and *Sa*PLK C110A after incubation with A-PM-I (100 eq.) for 24 h. b) Gel-based labelling of recombinant *Sa*PLK. Wild type and mutant enzymes were incubated with probes (10 eq.) for 24 h, subjected to click-reaction and analysed *via* SDS-PAGE. c) Close-up view of the PL-binding site of *Sa*PLK (*thiD*, PDB code: 4C5L, pink).¹⁹³ The left panels present the respective binding sites with PL (gray stick model) as previously obtained by co-crystallization.¹⁹³ The structures of A-PM-P1 (blue stick model, middle panel) and A-PM-P2 (green stick model,

right panel) have been modeled into the available X-ray crystal structures using atoms of the covalently bound PL as reference points. The alkyne handle positioned at the 3'-OH group in A-PM-P1 can slot next to the β -hairpin and Val142 (middle panel), as indicated by the green circle. Consequently, the arrow indicates the conformational change of the lid loop and its lid Cys110 to react with the warhead of the accommodated probe. In contrast, the alkyne moiety positioned at the 2'-methyl group in A-PM-P2 clashes with the first β -strand in *Sa*PLK (right panel), highlighted by the red circle. d) Gel-based labelling of recombinant *E*PLK. *E*PLK wt and *E*PLK C110A were incubated with probes (10 eq.) for 24 h, subjected to click-reaction and analysed *via* SDS-PAGE.

Based on these results, the probe set was expanded. Since acrylamide is known to be a weak electrophile and relatively unreactive toward thiols, it is of high interest to examine whether a more reactive warhead might lead to more efficient PLK labelling. For this purpose, the Michael acceptor was replaced by a chloroacetamide (CI-PM-I).²⁰¹ Similar to A-PM-I, the synthesis started with PM, which was acylated using chloroacetic anhydride (Scheme III-1a). The corresponding probe, CI-PM-P1, was obtained by subsequent propargylation of the 3'-alcohol of CI-PM-I.

With these new compounds at hand, the inhibitors A-PM-I and CI-PM-I were first compared using an activity assay. Previous experiments have shown that the lid Cys is the primary binding site for these compounds, which is essential for PL phosphorylation. The concentration dependent inhibition of *Sa*PLK and *E*PLK activity after incubation with A-PM-I and CI-PM-I supported these results, indicating binding of these compounds to the active site with subsequent covalent attachment to Cys110 (Figure III-5a and b). Furthermore, the elevated reactivity of CI-PM-I resulted in stronger inhibition compared to A-PM-I. In contrast, ginkgotoxin (4'-*O*-methylpyridoxine), a *h*PLK inhibitor, did not inhibit *Sa*PLK highlighting the importance of the Cys reactive warheads.

A higher reactivity may result in a lower selectivity. Therefore, the next step was to investigate the selectivity of all probes by labelling lysates of *S. aureus* with spiked-in *Sa*PLK wt. And indeed, a comparison between all probes revealed that although the

probe CI-PM-P1 labelled *Sa*PLK more strongly than the Michael-acceptor probes, significantly more off-target proteins were addressed (Figure III-5c). This clearly demonstrated the enhanced but nonspecific reactivity of CI-PM-P1 compared to A-PM-P1 and A-PM-P2, which almost exclusively labelled the spiked-in *Sa*PLK. Noteworthy, the longer incubation time of 24 h proved to be beneficial in order to enhance *Sa*PLK engagement. Similar results were obtained when the probes were incubated with intact *S. aureus* cells; while the probe A-PM-P1 showed only one other band besides *Sa*PLK, CI-PM-P1 displayed a strong background labelling (Figure III-5d).

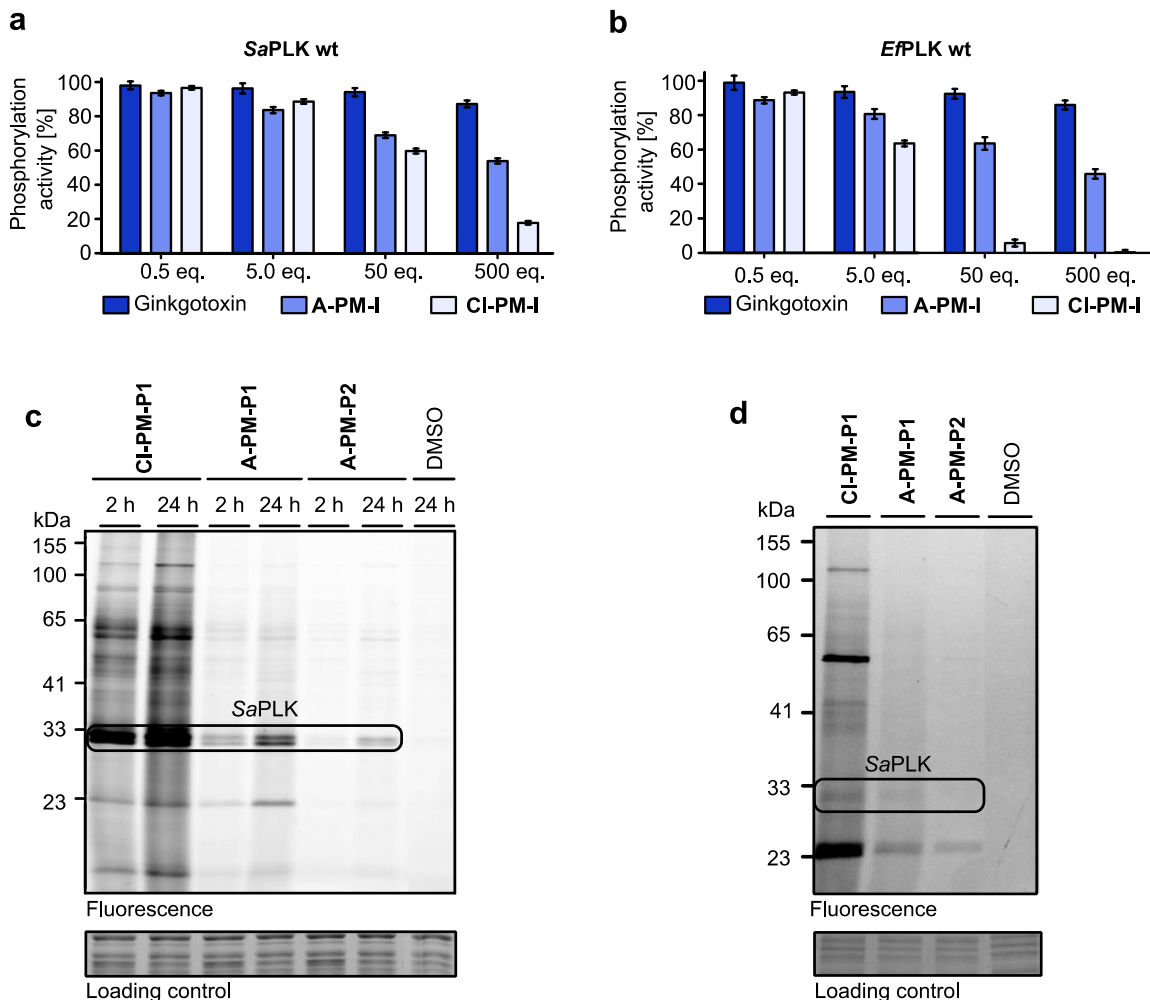


Figure III-5: Evaluation of Cys-reactive warhead of inhibitors A-PM-I and CI-PM-I as well as probes A-PM-P1, A-PM-P2 and CI-PM-P1. a) Influence of compounds A-PM-I, CI-PM-I and ginkgotxin on *Sa*PLK phosphorylation activity. Activity was measured after incubation for 2 h at 25 °C ($n = 3$ independent experiments per group; data represent the mean \pm SEM). b) Influence of the compounds A-PM-I, CI-PM-I and ginkgotxin on *E*PLK phosphorylation

activity. Activity was measured after incubation for 2 h at 25 °C ($n = 3$ independent experiments per group; data represent the mean \pm SEM). c) Comparison of probes in spike-in studies with recombinant *Sa*PLK (1 μ M) in *S. aureus* lysate after 2 h and 24 h incubation time. Samples were analysed via SDS-PAGE. d) Comparison of *in situ* labelling of intact *S. aureus* cells using all probes (200 μ M, 24 h) visualized by SDS-PAGE and fluorescence detection.

2.2. *In situ* Profiling in Gram-positive Bacteria

To assess the application of the probes for the identification of CC-PLKs, preparative ABPP was performed. For this purpose, intact *S. aureus* and *E. faecalis* cells were incubated with individual probes for 24 h, lysed, clicked to biotin azide and enriched on avidin beads. After digestion, peptides were analysed *via* label-free LC-MS/MS analysis. Remarkably, the A-PM-P1 probe was able to enrich both *Sa*PLK and *Ef*PLK selectively (Figure III-6a and d), which is in agreement with the gel-based labelling experiments. In addition, profile plots of the LFQ data revealed a dose-dependent enrichment of the two CC-PLKs (Figure III-6c and f).

As already expected from the crystal structure and gel-based labelling experiments, probe A-PM-P2 could neither enrich *Sa*PLK nor the *Ef*PLK, which proved this probe to be unsuitable for CC-PLK mining (Figure III-6b and e). Unsurprisingly, the increased reactivity of CI-PM-P1 caused high background labelling (Supplementary Figure 7) thus confirming the results of gel-based spike-in studies with recombinant *Sa*PLK. Notably, many of these background binders (>58%) are proteins with medium or highly reactive Cys, explaining the enrichment of these with CI-PM-P1.²⁰²

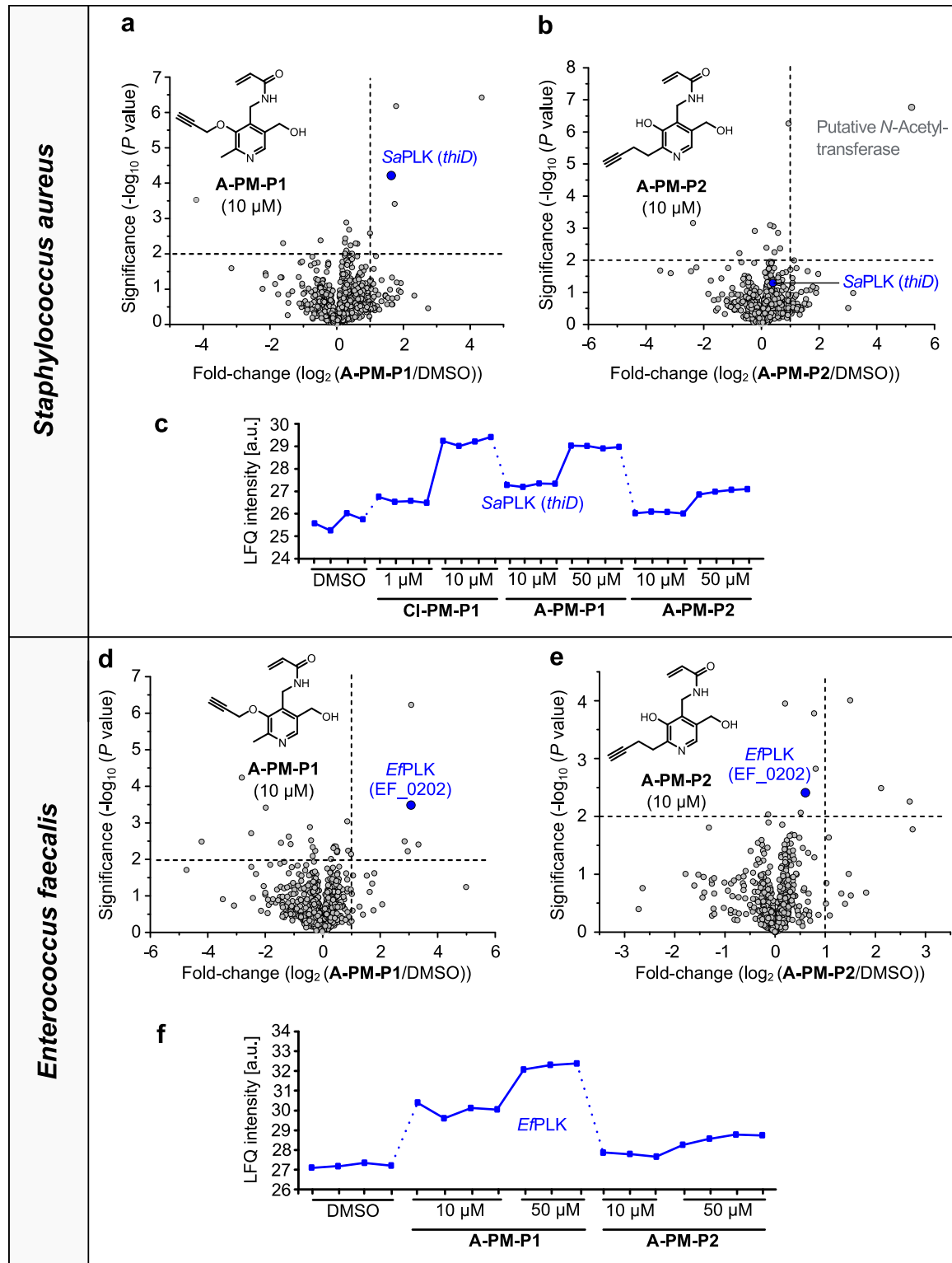


Figure III-6: Target identification of probes in intact *S. aureus* and *E. faecalis*. The volcano plots show enrichment of proteins after treatment (24 h) of *S. aureus* cells with a) A-PM-P1 (10 μM) or b) A-PM-P2 (10 μM) on a \log_2 scale. The vertical and horizontal threshold lines represent a \log_2 enrichment ratio of 1 and a $-\log_{10}(P \text{ value})$ of 2 (two-sided two-sample *t*-test, $n = 4$ independent experiments per group), respectively. Supplementary Figure 7 contains volcano plot for CI-PM-P1. c) Profile plot representation of proteomic data showing LFQ intensities of SaPLK after

treatment of intact *S. aureus* with CI-PM-P1 (1 μ M and 10 μ M), A-PM-P1 (10 μ M and 50 μ M) and A-PM-P2 (10 μ M and 50 μ M) ($n = 4$ independent experiments per group). Further, the volcano plots show enrichment of proteins after treatment (24 h) of *E. faecalis* cells with d) A-PM-P1 (10 μ M) or e) A-PM-P2 (10 μ M) on a \log_2 scale. The vertical and horizontal threshold lines represent a \log_2 enrichment ratio of 1 and a $-\log_{10}$ (P value) of 2 (two-sided two-sample t -test, $n = 4$ independent experiments per group), respectively. f) Profile plot representation of proteomic data showing LFQ intensities of *Ef*PLK after treatment of intact *E. faecalis* with A-PM-P1 (10 μ M and 50 μ M) and A-PM-P2 (10 μ M and 50 μ M) ($n = 4$ independent experiments per group).

Together with the preceding gel-based labelling experiments, the proteomic data showed that the probe A-PM-P1 selectively enriches CC-PLKs from intact cells by covalent attachment to the lid Cys C110. Thus it can be used as a reliable *in situ* tool for the detection of Gram-positive CC-PLKs.

2.3. *In situ* Profiling in Gram-negative Bacteria

In Gram-negative bacteria, the significance of the lid Cys has not yet been clarified and contradictory data exists. A co-crystal structure of the *E. coli* enzyme revealed a covalent bond with PL, albeit in only one of the two monomers, suggesting that the Cys is important for PL phosphorylation. In contrast, the lid Cys mutant of the corresponding enzyme in *P. aeruginosa* remains active in phosphorylation assays, implying that it is dispensable for catalysis.

The probes can be used to experimentally consolidate these divergent reports on CD-PLKs. The reactivity and accessibility of lid Cys were assessed by incubating recombinant proteins *Ec*PLK and *Pa*PLK with the two probes A-PM-P1 and A-PM-P2. Labelling was subsequently analysed by fluorescent SDS-PAGE. Surprisingly, A-PM-P1, the probe tailored for CC-PLK, could not mark either protein (Figure III-7a and b). In contrast, the probe A-PM-P2 showed very strong labelling of both enzymes, which is absent in the respective mutants. This confirms the lid Cys as the primary binding site of A-PM-P2 and also suggests that this amino acid residue is important for catalysis.

The preference of these enzymes for the probe A-PM-P2 can be explained using the *E. coli* co-crystal structure, which revealed different accessibility compared to *Sa*PLK. While free space is available at the 2'-methyl group, restricted access is visible at the 3'-OH group (Figure III-7c).

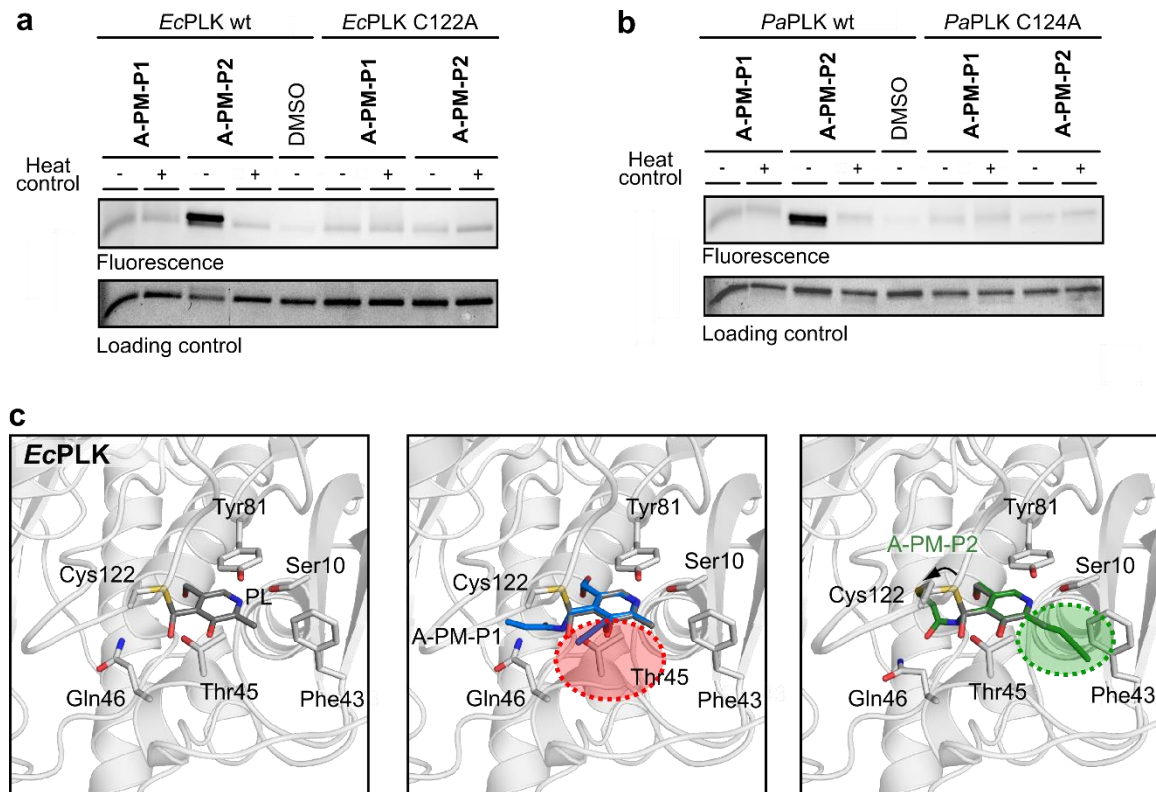


Figure III-7: Evaluation of probes of CD-PLK profiling. Gel-based labelling experiments using recombinant a) *Ec*PLK and b) *Pa*PLK. Wild type and mutant enzymes were incubated with probes (10 eq.) for 24 h and analysed *via* SDS-PAGE. c) Close-up view of the PL-binding site of Gram-negative *Ec*PLK (*pdxY*, PDB code: 1TD2, gray).¹⁸⁹ The left panels present the respective binding sites with PL (gray stick model) as previously obtained by co-crystallization.¹⁸⁹ The structures of A-PM-P1 (blue stick model, middle panel) and A-PM-P2 (green stick model, right panel) have been modeled into the available X-ray crystal structures using atoms of the covalently bound PL as reference points. A-PM-P1 clashes with Thr45 located at the small-helix-loop secondary structural element (middle panel, red circle) while A-PM-P2 fits well into the binding pocket. Conformational change as well as covalent engagement with the lid Cys122 is indicated by the arrow (right panel).

Next, the enzymatic activity of wild type and mutant proteins was evaluated in order to investigate the importance of lid Cys for phosphorylation activity. However, in accordance with previous literature reports, turnover of the purified protein in buffer

was found to be slow.²⁰³ By using the lysate of *E. coli*, expressing the corresponding recombinant proteins, a significantly higher phosphorylation activity was achieved. The *E. coli* cell lysate lacking recombinant PLK expression were used as a control to subtract the basal PLK activity level. A PLP turnover rate of 57 μM PLP/h was determined for overexpressed *Ec*PLK wt, which was reduced by 50% for the corresponding mutant (Figure III-8a). This is in perfect agreement with the results of the co-crystal structure of *E. coli*, where PL was covalently bound in only every other monomer. The *Pa*PLK wt showed a 3-fold reduced turnover compared to the *E. coli* wt enzyme. Remarkably, the corresponding *Pa*PLK lid mutant completely lacked the enzymatic activity, highlighting the importance of this residue for catalysis.

To demonstrate the applicability of these probes for *in situ* experiments and to identify CD-PLKs, intact *E. coli* cells were incubated with the probes A-PM-P1 and A-PM-P2 and target proteins were analysed after enrichment using LC-MS/MS with label-free quantification (Figure III-8b). Importantly, *Ec*PLK has been strongly enriched with A-PM-P2 and in a concentration-dependent manner as demonstrated by the LFQ intensity profile plot (Figure III-8c). Additionally, several proteins with reactive Cys, such as thioredoxin-like proteins and enzymes known for PL or PLP binding, such as aromatic amino acid aminotransferase (*tyrB*) and *E. coli* PLK (*pdxK*, kinase without lid Cys), were among the hits. As anticipated from the gel-based labelling experiments, A-PM-P1 was not able to enrich the *Ec*PLK (Figure III-8d).

In summary, two probes A-PM-P1 and A-PM-P2 were developed with tailored performance in different bacteria types. The probe A-PM-P1 can be used to screen for further representatives of CC-PLKs in Gram-positive bacteria, while A-PM-P2 is suitable for the identification of CD-PLKs in Gram-negative bacteria.

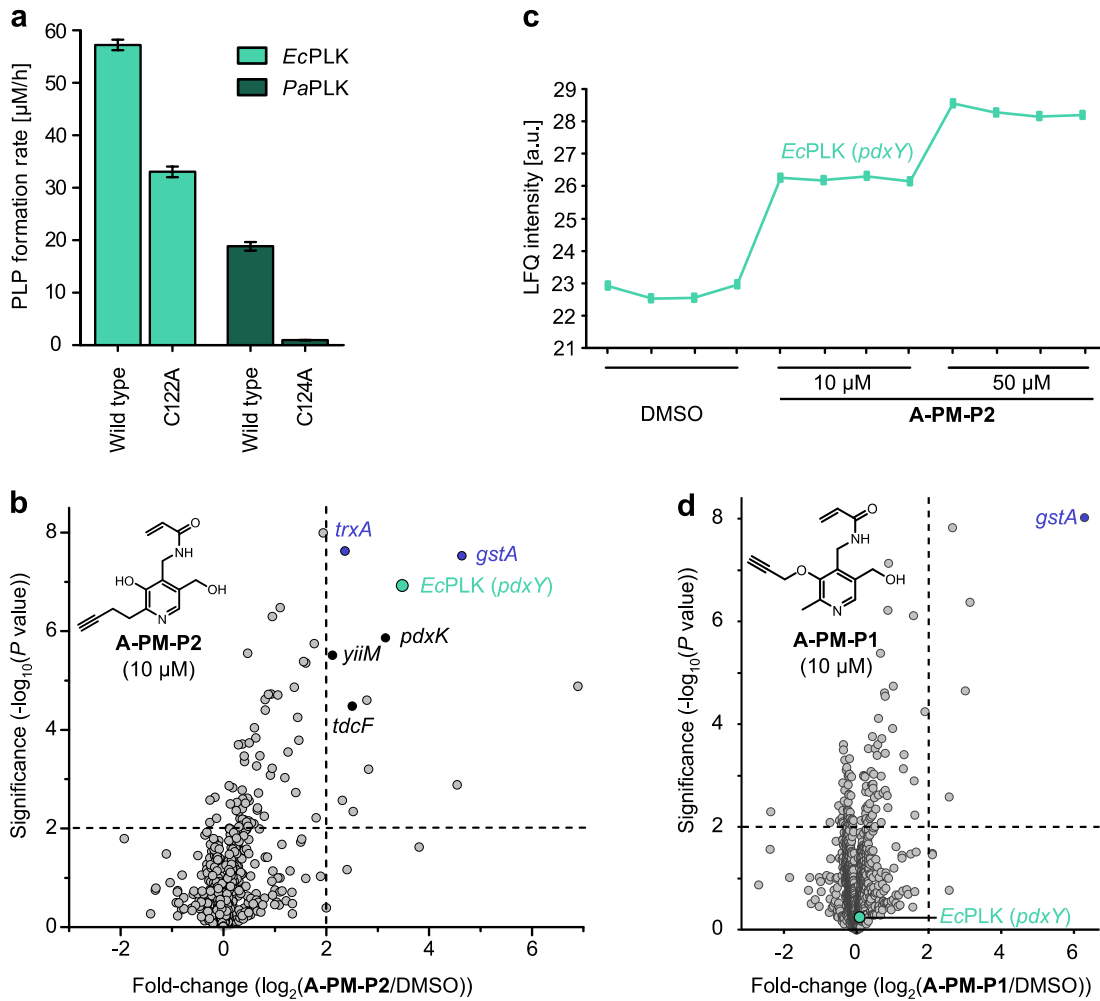


Figure III-8: Target identification by chemical proteomic profiling. a) PL phosphorylation activity assay of Gram-negative PLKs was performed in cell lysate of an *E. coli* expression strain after overexpression of proteins ($n = 3$; data represent the mean \pm SEM). Further, the volcano plots show enrichment of proteins after treatment (24 h) of *E. coli* cells with b) A-PM-P2 (10 μ M, *E. coli* K12) or d) A-PM-P1 (10 μ M, *E. coli* 536) on a \log_2 scale. The vertical and horizontal threshold lines represent a \log_2 enrichment ratio of 2 and a $-\log_{10}(P \text{ value})$ of 2 (two-sided two-sample t -test, $n = 4$ independent experiments per group), respectively. The green dot represents the target protein, EcPLK (UniProt IDs for *pdxY* in *E. coli* K12 and *E. coli* 537 are P77150 and Q0THJ1, respectively and proteins share 99% sequence identity). Black dots represent PLP associated enzymes and blue dots represent proteins of the thioredoxin-like superfamily (assignment according to UniProtKB).²⁰⁴ c) Profile plot representation of proteomic data showing Lfq intensities of EcPLK after treatment of intact *E. coli* cells with A-PM-P2 (10 μ M and 50 μ M) ($n = 4$ independent experiments per group).

2.4. Conclusion and Outlook

Pyridoxal kinases are important enzymes for supplying the cell with the essential cofactor PLP. Recently, several PLKs with a Cys in their lid region were discovered and

Gram-positive PLKs and Gram-negative PLKs were referred to as CC-PLKs and CD-PLKs, respectively. However, the Cys reactivity for the formation of hemithioacetals and their importance for catalytic turnover was largely unknown.

Within the scope of this work, probes were developed that selectively target Gram-positive or Gram-negative PLKs. The reactive Cys in the lid was validated as the primary binding site of these compounds, which was irreversibly trapped by the electrophilic groups, thus allowing enrichment and identification by LC-MS/MS. Importantly, the lid Cys of all wt enzymes in this study were modified by the respective tailored probes highlighting their important role in catalysis, which was confirmed by the corresponding activity assays. This approach contributed to elucidate the contradictory role of this amino acid residue in CD-PLKs.

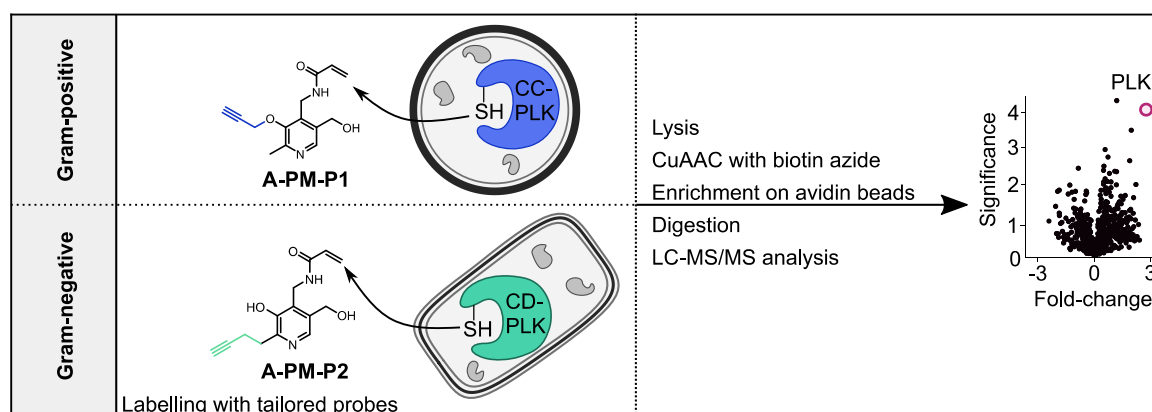


Figure III-9: This study developed tailored probes for CC-PLK and CD-PLK mining. Probes A-PM-P1 and A-PM-P2 selectively target Gram-positive and Gram-negative PLKs, respectively and can be used to identify further representatives of this PLK subclass family.

Thus, the probes represent suitable tools to further decipher these PLK subclasses in other bacterial cells with yet unknown function. Since this kinase class does not exist in humans, they are of great interest as potential antibiotic targets.

One example might be a homologous protein encoded by *thiD* (UniProt ID: P9WG77) in *Mycobacterium tuberculosis*, with a Cys two residues downstream compared to *Sa*PLK. This protein is annotated as a HMP kinase and is thought to be essential.^{181,205} A compound based on the HMP scaffold and with an acrylamide as a reactive group could potentially inhibit this enzyme, thus possibly resulting in antibiotic activity.

3. Experimental Section

3.1. Bacterial Cultures

The bacterial strains *S. aureus* USA 300 LAC JE2, *E. faecalis* V583, *E. coli* K12 and *P. aeruginosa* PAO1 were cultivated as described in section “Media” and “Overnight Cultures”.

For pre-cultures, 5 mL of the respective media were inoculated with bacteria and were grown for 7 h (200 rpm, 37 °C).

3.2. Cloning of Pyridoxal Kinases

Recombinant PLK (*pdxY*) proteins of *E. coli* K12 (UniProt ID: P77150) and *P. aeruginosa* PAO1 (UniProt ID: Q9HT57) were constructed to carry an *N*-terminal His₆-tag. The Invitrogen™ Gateway™ cloning system (*Thermo Scientific*) was used following the manufacturer’s cloning protocol (as already described in detail in section “Gateway Cloning”). Primers for wild type (wt) genes were designed to carry *attB1* or *attB2* sequences (Table III-1) to shuffle the respective PCR products into donor vector pDONR201^{Kan} (pDONR201_*Ec*PLK_wt, pDONR201_*Pa*PLK_wt) and destination vector pET300^{Amp} (pET300_*Ec*PLK_wt, pET300_*Pa*PLK_wt).

Table III-1| Primers used for Gateway cloning and QuikChange site-directed mutagenesis. *AttB1*- and *attB2*-sequences are indicated in lower case.

Primer name	DNA sequence (5' → 3')
<i>E. coli pdxY</i> wt fwd w/ <i>attB1</i>	ggggacaagttgtacaaaaagcaggcttt ATGATGAAAAATATTCTCGCTATCC
<i>E. coli pdxY</i> wt rev w/ <i>attB2</i>	ggggaccacttgtacaagaaagctgggtg TCAGAGCTTTGTTGCGCT
<i>E. coli pdxY</i> C122A fwd	GTCATCCGGAAAAAGGCGCTATCGTTGCACCGGGTG
<i>E. coli pdxY</i> C122A rev	CACCCGGTGCAACGATAGCGCCTTTTCCGGATGAC

<i>P. aeruginosa pdxY</i> wt fwd w/ <i>attB1</i>	ggggacaagttgtacaaaaagcaggcttt ATGCCACGTACGCCCCAC
<i>P. aeruginosa pdxY</i> wt rev w/ <i>attB2</i>	ggggaccactttgtacaagaaagctgggtg CTAAAGGCGCACTGCGTCGAA
<i>P. aeruginosa pdxYC124A</i> fwd	CCCGGAAAAAGGCGCCATCGTGGCCCCG
<i>P. aeruginosa pdxYC124A</i> rev	CGGGGCCACGATGGCGCCTTTTTCCGGG

Plasmids carrying a point mutation in the respective PLK gene (pET300_*Ec*PLK_C122A, pET300_*Pa*PLK_C124A) were obtained using the QuikChange II site-directed mutagenesis protocol (*Agilent*) with the respective pET300 wt plasmids as DNA templates. The primer sequences (Table III-1) were designed using QuikChange Primer Design (*Agilent*). After amplification of the desired plasmid containing the respective point mutation by PCR using Phusion HF Polymerase, the wt plasmids were digested by *DpnI* and the remaining mutant plasmids were transformed into chemically competent *E. coli* XL1-Blue, which were subsequently plated on LB agar supplemented with appropriate antibiotic (Table III-2). Single colonies were picked and grown in 5 mL LB medium containing appropriate antibiotic. On the next day, plasmid DNA was isolated using E.Z.N.A. Plasmid mini Kit I (*OMEGA Bio-Tek*) according to the manufacturer's protocol. The plasmid concentration was measured on an Infinite® M200 Pro microplate reader using a NanoQuant Plate™ (*Tecan Group Ltd.*) and the sequences were verified by DNA sequencing (*Genewiz*). Plasmids (Table III-2) were transformed into chemically competent *E. coli* BL21(DE3) cells for protein expression.

Table III-2| Plasmids used or prepared in this study.

Plasmid	Gene – UniProt ID	Antibiotic (final concentration)	Source
pDONR201	empty	Kanamycin (25 µg mL ⁻¹)	<i>Invitrogen</i>
pET300	empty	Ampicillin (100 µg mL ⁻¹)	<i>Invitrogen</i>

pDONR201_ <i>Ec</i> PLK_wt	<i>pdxY</i> – P77150	Kanamycin (25 µg mL ⁻¹)	This study
pET300_ <i>Ec</i> PLK_wt	<i>pdxY</i> – P77150	Ampicillin (100 µg mL ⁻¹)	This study
pET300_ <i>Ec</i> PLK_C122A	<i>pdxY</i> – P77150	Ampicillin (100 µg mL ⁻¹)	This study
pDONR201_ <i>Pa</i> PLK_wt	<i>pdxY</i> – Q9HT57	Kanamycin (25 µg mL ⁻¹)	This study
pET300_ <i>Pa</i> PLK_wt	<i>pdxY</i> – Q9HT57	Ampicillin (100 µg mL ⁻¹)	This study
pET300_ <i>Pa</i> PLK_C124A	<i>pdxY</i> – Q9HT57	Ampicillin (100 µg mL ⁻¹)	This study

3.3. Protein Overexpression and Purification

For protein overexpression, 1 L LB medium containing 100 µg mL⁻¹ ampicillin was inoculated (1:100) with overnight cultures of the corresponding expression strains and grown to an OD₆₀₀ of 0.6 (37 °C, 200 rpm). To induce protein overexpression, isopropyl-1-thio-β-D-galactopyranoside (IPTG) was added (*Ec*PLK wt: 1mM, *Ec*PLK C122A: 1mM, *Pa*PLK wt: 10 µM, *Pa*PLK C124A: 10 µM) and bacteria were incubated under the following conditions: *Ec*PLK wt: 22h, 25 °C; *Ec*PLK C122A: 22h, 18 °C; *Pa*PLK wt: 22h, 18 °C, *Pa*PLK C124A: 22h, 18 °C. Bacteria were harvested (6,000 g, 10 min, 4 °C), washed with PBS and resuspended in 30 mL lysis buffer (20 mM HEPES, 10 mM imidazole, 150 mM NaCl, 2 mM β-mercaptoethanol (β-ME), 0.2% (v/v) NP-40, pH 8.0 in ddH₂O). Lysis was performed by sonication repeating the following protocol twice: 7 min at 30% intensity, 3 min at 80% intensity (Sonopuls HD 2070 ultrasonic rod, *Bandelin electronic GmbH*). The supernatant was cleared (18,000 g, 30 min, 4 °C) and transferred into a Superloop (*GE Healthcare*) for loading onto a 5 mL pre-equilibrated HisTrap HP column (*GE Healthcare*) installed at an ÄKTA Purifier 10 FPLC system equipped with an UV-detector (UPC900, P900, Box 900, Frac950, *Thermo Fisher*). The column was washed using the following buffers: Wash buffer 1 (40 mL; 20 mM HEPES, 10 mM imidazole, 150 mM NaCl, 2 mM β-ME, pH 8.0 in ddH₂O), wash buffer 2 (40 mL; 20 mM HEPES, 10 mM imidazole, 1 M NaCl, 2 mM β-ME, pH 8.0 in ddH₂O)), wash buffer 3 (40 mL, 20 mM HEPES, 40 mM imidazole, 150 mM NaCl, 2 mM β-ME, pH 8.0 in ddH₂O), and the protein was eluted with elution buffer (25 mL, 20 mM HEPES,

500 mM imidazole, 150 mM NaCl, 2 mM β -ME, pH 8.0 in ddH₂O). Fractions containing proteins were pooled and concentrated using ultra-centrifugal filters (Amicon, 10 kDa cut-off). Next, preparative size-exclusion chromatography was performed using a 120 mL pre-equilibrated Superdex column (HiLoad 16/60 Superdex 75 or 200 prep grade, *GE Healthcare*) and SEC buffer (1.5 column volumes, 50 mM HEPES, 250 mM NaCl, pH 8.0 in ddH₂O). Homodimeric protein fractions were pooled, concentrated and protein concentration was measured on an Infinite[®] M200 Pro microplate reader with a NanoQuant plate (*Tecan Group Ltd.*) using the following extinction coefficients: *Ec*PLK wt: $\epsilon = 29,910 \text{ M}^{-1} \text{ cm}^{-1}$; *Ec*PLK C122A: $\epsilon = 29,910 \text{ M}^{-1} \text{ cm}^{-1}$; *Pa*PLK wt: $\epsilon = 26,930 \text{ M}^{-1} \text{ cm}^{-1}$; *Pa*PLK C124A: $\epsilon = 26,930 \text{ M}^{-1} \text{ cm}^{-1}$.

The proteins (*Ec*PLK wt: 1.6 mM, *Ec*PLK C122A: 586 μM , *Pa*PLK wt: 332 μM , *Pa*PLK C124A: 496 μM) were stored at $-80 \text{ }^\circ\text{C}$ in SEC buffer.

N-terminally STREPII-tagged *Sa*PLK wt (*sav0580*, *S. aureus* Mu50, with TEV site) and *Sa*PLK C110A as well as *Ef*PLK wt (*EF_0202*, *E. faecalis* V583) and *Ef*PLK C110A were prepared as previously described.¹⁹³

3.4. Intact Protein Mass Spectrometry (IPMS)

Recombinant protein was diluted in PBS to a concentration of 1 μM , compound was added to a final concentration of 100 μM and samples were incubated overnight at RT without shaking. Proteins were analysed on a LTQ FT Ultra[™] mass spectrometer (*Thermo Scientific*) equipped with electrospray ionization (ESI) source operated in positive ionization mode coupled to a Dionex Ultimate 3000 HPLC system (*Thermo Scientific*). Intact protein spectra were deconvoluted by the Thermo Xcalibur software 2.2 (*Thermo Scientific*).

3.5. Activity-based Protein Profiling

3.5.1. Labelling of Recombinant Protein

Recombinant PLK was diluted in 50 μ L K-buffer (50 mM HEPES, 50 mM KCl, 10 mM $MgCl_2$, pH 7.9 in ddH₂O) or *S. aureus* lysate (1 mg mL⁻¹ protein in PBS) as background to a final concentration of 1 μ M. For heat control samples, SDS was added to a final concentration of 0.4% (w/v) and the solution was heated (95 °C, 30 min). Next, various concentrations of the probes were added (50 \times stock, 2% final concentration DMSO) or DMSO (negative control) and samples were incubated for 24 h (if not stated differently) without shaking at RT. Afterwards, the samples were subjected to click-reaction and analysed by SDS-PAGE as already described in section "Gel-based ABPP".

3.5.2. Analytical *in situ* Labelling

Pre-cultures of *S. aureus* were used to inoculate 50 mL B-media and bacteria were grown to stationary phase (OD₆₀₀ of 7.6, 12 h). The cells were harvested (5,000 \times g, 10 min, 4 °C) and washed with PBS (15 mL; 5,000 \times g, 10 min, 4 °C). The pellet was resuspended in PBS to a final OD₆₀₀ of 40. The bacterial suspension was split into aliquots of 200 μ L and either a probe (200 μ M, 2% final concentration DMSO) or DMSO was added. The cultures were incubated (24 h, 25 °C, 800 rpm) and harvested by centrifugation (5,000 \times g, 10 min, 4 °C). The pellet was washed with PBS (2 \times 0.5 mL) and resuspended in 200 μ L 0.4% (w/v) SDS in PBS. The cells were lysed by bead disruption (Precellys 24 Homogenizer, *Bertin Technologies*) using the following cycle three times: 30 sec at 6,500 rpm, with 20 sec cooling break using liquid nitrogen air flow. The lysed cells were transferred to Eppendorf tubes and centrifuged (16,000 \times g, 30 min, RT). Next, 50 μ L of supernatant were subjected to click-reaction analysed by SDS-PAGE as already described in section "Gel-based ABPP".

3.5.3. Preparative *in situ* Labelling

Preparation of MS samples

Pre-cultures of *S. aureus*, *E. faecalis* and *E. coli* were used to inoculate fresh media and bacteria were grown to stationary phase (*S. aureus*: OD₆₀₀ of 8.0, 12 h; *E. faecalis*: OD₆₀₀ of 2.0, 6 h; *E. coli*: OD₆₀₀ of 3.0, 6 h). The cells were harvested (5,000 ×g, 10 min, 4 °C) and washed with PBS (15 mL; 5,000 ×g, 10 min, 4 °C). Pellets were resuspended in PBS to a final OD₆₀₀ of 40. This bacterial suspension was split into aliquots of 1 mL and either a probe (final concentrations indicated in corresponding figures, 1% final concentration of DMSO) or DMSO was added. The cultures were incubated (24 h, 25 °C, 800 rpm) and harvested by centrifugation (5,000 ×g, 10 min, 4 °C). The pellets were washed with PBS (2 × 1 mL) and resuspended in 1 mL 0.4% (w/v) SDS in PBS for lysis. *E. coli* samples were lysed by sonication (3 × 20 s, 80%, Sonopuls HD 2070 ultrasonic rod, *Bandelin electronic GmbH*) with cooling breaks on ice. *E. faecalis* and *S. aureus* samples were transferred into 2 mL lysis tubes for bead disruption (Precellys 24 Homogenizer, *Bertin Technologies*) using the following cycle three times: 30 sec at 6,500 rpm, with 20 sec cooling break using liquid nitrogen air flow. The lysed cells were transferred to Eppendorf tubes and lysate was cleared (16,000 ×g, 30 min, RT). Protein concentration was measured using the Pierce BCA Protein assay kit (*Thermo Fisher Scientific, Pierce Biotechnology*) and sample concentrations were adjusted to equal protein amounts (1–2 mg mL⁻¹) in a total volume of 500 µL. Next, click-reaction and protein enrichment on avidin beads followed by reduction, alkylation and quenching was performed as described in section "Gel-free ABPP and A/BPP".

The samples were digested by Lys-C (1 µL, 0.5 µg µL⁻¹, *Wako*) for 2 h (RT, 450 rpm) and diluted with TEAB (50 mM, 600 µL). Trypsin (1.5 µL, 0.5 µg µL⁻¹ in 50 mM acetic acid, *Promega*) was added to digest the samples for 16 h (37 °C, 450 rpm). On the next day, the reaction was stopped by acidification using formic acid (FA, 10 µL, final

pH below 3.0). Desalting and filtration of the samples was performed as described in section "Gel-free ABPP and A β PP".

LC-MS/MS Measurement

MS-measurement of *S. aureus* and *E. faecalis* samples was performed on a Q Exactive Plus instrument equipped with an electrospray easy source (*Thermo Fisher*) coupled to an Ultimate 3000 Nano-HPLC (*Thermo Fisher*). Samples were loaded on a 2 cm Acclaim C18 PepMap100 trap column (particles 3 μm , 100 \AA , inner diameter 75 μm , *Thermo Fisher*) with 0.1% (v/v) TFA and separated on a 50 cm PepMap RSLC C18 column (particles 2 μm , 100 \AA , inner diameter 75 μm , *Thermo Fisher*) constantly heated to 50 $^{\circ}\text{C}$. The gradient was run from 5-32% (v/v) acetonitrile, 0.1% (v/v) formic acid during a 152 min method (7 min 5%, 105 min to 22%, 10 min to 32%, 10 min to 90%, 10 min wash at 90%, 10 min equilibration at 5%) at a flow rate of 300 nL min^{-1} .

MS-measurement of *E. coli* samples was performed on a slightly different setup. The Q Exactive Plus instrument was equipped with a Nanospray Flex ion source (ES071, *Thermo Fisher*) and separation of peptides was performed at a flow rate of 400 nL min^{-1} on a 25 cm Aurora Series emitter C18 column (AUR2-25075C18A, particles 1.6 μm , inner diameter 75 μm , *Ionoptics*) constantly heated to 40 $^{\circ}\text{C}$.

MS data on the Q Exactive Plus instrument was acquired with the following parameters: survey scans (m/z 300-1,500) were acquired at a resolution of 140,000 and the maximum injection time was set to 80 ms (AGC target value $3e^6$). Data-dependent HCD fragmentation scans of the 10 most intense ions of the survey scans were acquired at a resolution of 17,500, maximum injection time was set to 100 ms (AGC target value $1e^5$). The isolation window was set to 1.6 m/z . Unassigned and singly charged ions were excluded for measurement and the dynamic exclusion of peptides enabled for 60 s. The lock-mass ion 445,12002 from ambient air was used for real-time mass calibration on the Q Exactive Plus.

MS Data Analysis

Data were acquired using Xcalibur software (version 4.1.31.9, *Thermo Fisher*) and MaxQuant (version 1.6.1.0) was used to analyze the obtained raw files of the label-free quantification with Andromeda.²⁰⁶ The following settings were applied: variable modifications: oxidation (methionine), acetylation (*N*-terminus); fixed modifications: carbamidomethylation (cysteine); proteolytic enzyme: trypsin/P; missed cleavages: 2; "No fractions", "LFQ", "Requantify" and "Match between runs" were enabled; "Second Peptide" was disabled. Searches were performed against the following FASTA files from UniProtKB: *S. aureus* USA300 (taxon identifier: 367830, downloaded: 1 April 2019), *E. faecalis* V583 (taxon identifier: 226185, downloaded: 1 April 2019), *E. coli* K12 (taxon identifier: 83333, downloaded: 7 April 2020) and *E. coli* 536 (taxon identifier: 362663, downloaded: 21 June 2019).²⁰⁴

Perseus (version 1.6.2.3) was used for statistical analysis of MS data.¹⁶⁰ Putative contaminants, reverse peptides and peptides only identified by site were deleted. LFQ intensities were \log_2 -transformed and data was filtered for at least 3 valid values in at least one group. Missing values imputation over the total matrix was performed and annotations derived from UniProtKB were added.²⁰⁴ For statistical evaluation, $-\log_{10}(P$ values) were obtained by a two-sided two sample Student's *t*-test.

3.6. PLK Inhibition Assay

A previously published kinase activity assay was performed with slight modifications.²⁰⁷ Briefly, 110 μ L K-Buffer (50 mM HEPES, 50 mM KCl, 10 mM MgCl_2 , pH 7.9 in ddH₂O) containing 2 μ M recombinant protein (*Sa*PLK wt and *Ef*PLK wt) was pre-incubated (2 h, 25 °C, 200 rpm) with 1.1 μ L compound (final concentration: 1 μ M – 1 mM, 1% final concentration DMSO) or DMSO in a 96-well flat bottom transparent plate. To start the activity assay, 98 μ L of the pre-incubated samples were added to 1 μ L ATP (250 mM in K-buffer, final concentration 2.5 mM) and 1 μ L PL (200 mM in K-

buffer, final concentration 2 mM) and the absorption at 388 nm was recorded (45 minutes, 25 °C, intervals of 75 seconds) using an Infinite® M200 Pro microplate reader (*Tecan Group Ltd.*). The slope of the curve in the linear range was obtained *via* linear regression using *Prism 5.03 (GraphPad)*. Values were normalised to DMSO-treated samples (100% activity) and samples without recombinant protein (negative controls, 0% activity). The assay was performed in three independent experiments with three technical replicates each.

3.7. PLK Activity Assay in Lysate

Kinase activity was determined in cell lysate of expression strains for *E. coli* and *P. aeruginosa* PLK wild types and mutants. *E. coli* BL21 (DE3) without plasmid was used as a negative control to identify the basal PLK activity level. For overexpression, LB medium containing 100 µg mL⁻¹ ampicillin (for negative control without antibiotic) was inoculated (1:100) with overnight cultures of the corresponding expression strains and grown to an OD₆₀₀ of 0.6 (37 °C, 200 rpm). To induce protein overexpression, IPTG was added to a final concentration of 10 µM and bacteria were incubated under the following conditions: *E. coli* BL21(DE3): 3 h, 37 °C, *Ec*PLK (wt and C122A): 3 h, 37 °C, *Pa*PLK (wt and C124A): 22h, 18 °C. Cultures were harvested (6,000 ×g, 10 min, 4 °C), washed with PBS and resuspended in K-buffer (50 mM HEPES, 50 mM KCl, 10 mM MgCl₂, pH 7.9 in ddH₂O) to a calculated OD₆₀₀ of 40. Lysis was performed by sonication (3 min, 80%, Sonopuls HD 2070 ultrasonic rod, *Bandelin electronic GmbH*) on ice. The supernatant was cleared by centrifugation (18,000 ×g, 30 min, 4 °C), was split into aliquots and stored at -80 °C. The concentration of overexpressed PLK in lysate was determined semi-quantitatively. For that, varying concentrations of recombinant *E. coli* PLK wt were loaded on a gel and gray values of protein bands were measured using ImageJ (Supplementary Figure 6a and b). A calibration curve was calculated, which was used to determine the concentration of overexpressed PLK in lysates (Supplementary Figure 6c).

For the assay, lysates were diluted in K-buffer to a final concentration of 5 μM overexpressed PLK (98 μL final volume) and were incubated with 1 μL ATP (250 mM in K-buffer, final concentration 2.5 mM) and 1 μL PL (100 mM in K-buffer, final concentration 1 mM) at 37 $^{\circ}\text{C}$. Over a time period of 16 h, the absorption at 388 nm was recorded every 15 minutes on a Tecan Infinite M200Pro microplate reader (*Thermo Fisher*). The slope of the curves in the linear range was determined *via* linear regression using *Prism 5.03 (GraphPad)*. Using the PLP extinction coefficient ($\epsilon = 5444 \text{ M}^{-1} \text{ cm}^{-1}$), slope values were transformed into PLP formation rates per hour. Samples containing lysate of untransformed *E. coli* BL21 (DE3) were included as negative controls and values were subtracted from the formation rates of PLK overexpression strains. The obtained rates indicate the PLK phosphorylation activity of 5 μM overexpressed PLK as PLP formation rate per hour. The assay was performed in three independent experiments with three technical replicates each.

3.8. Computational Modeling

Atomic models for A-PM-P1 and A-PM-P2 were generated with JLigand²⁰⁸ and regularized with AceDRG.²⁰⁹ Modeling of A-PM-P1 and A-PM-P2 in the PL binding site in the *Sa*PLK¹⁹³ and *Ec*PLK¹⁸⁹ X-ray crystal structures using the PL atoms of the pyridine ring as reference was carried out in Coot.²¹⁰ Structural figures were prepared in PyMOL (*Schrödinger*).

3.9. Chemical Synthesis

Chemicals

Chemicals with reagent or higher grade as well as dry solvents were purchased from *Sigma Aldrich*, *TCl Europe*, *VWR*, *Roth* and *Alfa Aesar*, and were used without any further purification. Solvents of technical grade were distilled prior to use. Air- or moisture-sensitive reactions were carried out in flame-dried reaction flasks under an argon atmosphere.

Analytical thin layer chromatography

Analytical thin layer chromatography was performed on aluminium-coated TLC silica gel plates (silica gel 60, F₂₅₄, *Merck KGaA*). For visualization, UV light ($\lambda = 254$ nm), KMnO₄-stain (3.0 g KMnO₄, 20 g K₂CO₃ and 5 mL 5% NaOH in 300 mL ddH₂O), CAM (5.0 g Cer-(IV)-sulfate, 25 g ammoniummolybdate and 50 mL concentrated sulphuric acid in 450 mL water) or ninhydrine (10 g ninhydrine in 300 mL ethanol) with subsequent heat treatment (ca. 250 °C) were used. Column chromatography was carried out using silica gel [40-63 μ m (Si 60), *Merck KGaA*].

Mass-Spectrometry

High-resolution mass spectra (HRMS) were obtained using an LTQ-FT Ultra (*Thermo Fisher*) equipped with an ESI ion source. Data were visualized and processed using Xcalibur 2.2 (*Thermo Fisher*). Low-resolution mass spectra were recorded on an MSQ Plus instrument (*Thermo Fisher*) equipped with a Dionex Ultimate 3000 separation module (*Thermo Fisher*). Data were visualized and processed using Chromeleon 7.2.7 (*Thermo Fisher*).

High Pressure Liquid Chromatography

Purification by preparative, reversed-phase HPLC was performed using a *Waters* 2545 quaternary gradient module equipped with a *Waters* 2998 photodiode array detector and fraction collector on a *YMC* Triart C18 column (250 × 10 mm, 5 μm). Gradients are listed in the Table III-3 using ddH₂O and HPLC-grade acetonitrile as the mobile phase.

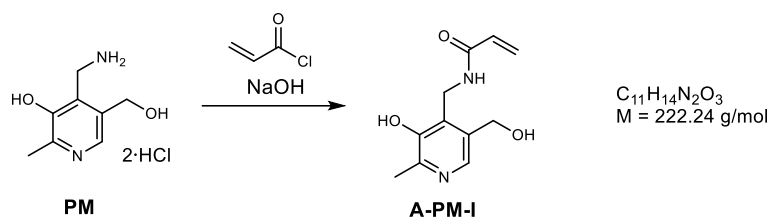
Table III-3 Gradients used for HPLC purifications.					
Method A			Method B		
t [min]	%-H ₂ O	%-ACN	t [min]	%-H ₂ O	%-ACN
0	98	2	0	98	2
1	80	20	1	98	2
7	60	40	12	60	40
8	2	98	13	2	98
9	2	98	14	2	98
11	98	2	15	98	2
13	98	2	17	98	2

NMR-Spectroscopy

¹H-NMR experiments were conducted on Avance-III HD (300, 400 or 500 MHz) NMR systems (*Bruker Co.*) at RT. using deuterated solvents. Chemical shifts are given in parts per million (ppm) and residual proton signals of deuterated solvents (CDCl₃ δ = 7.26 ppm, MeOD-*d*₄ δ = 4.87 ppm, DMSO-*d*₆ δ = 2.50 ppm, D₂O δ = 4.79 ppm) were used as internal reference. Coupling constants (*J*) are given in Hertz (Hz). For assignment of signal multiplicities, the following abbreviations were used: *br s* – broad singlet, *s* – singlet, *d* – doublet, *dd* – doublet of doublets, *ddd* – doublet of doublet of doublets, *t* – triplet, *td* – triplet of doublets, *q* – quadruplet and *m* – multiplet. ¹³C-NMR spectra were measured on Avance-III HD NMR systems (*Bruker Co.*) with deuterated solvents. Chemical shifts were referenced to the residual

solvent peak as an internal standard (CDCl_3 $\delta = 77.16$ ppm, $\text{MeOD-}d_4$ $\delta = 49.00$ ppm, $\text{DMSO-}d_6$ $\delta = 39.52$ ppm). Spectra were processed using MestReNova (*Mestrelab Research*).

3.9.1. Synthesis of Inhibitor A-PM-I



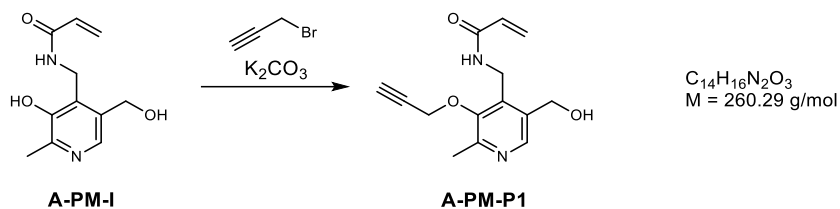
This synthesis was performed according to the protocol published by *Ueda et al.*¹⁹⁶ Briefly, pyridoxamine dihydrochloride (PM) (350 mg, 1.45 mmol, 1.0 eq.) was dissolved in 5 mL of water. Next, NaOH (480 μ L, 30% in H₂O) was added slowly and the solution was stirred for 5 min. Afterwards, acryloyl chloride (140 μ L, 157 mg, 1.74 mmol, 1.2 eq.) was added and the reaction mixture was stirred for 4 h at RT. followed by extraction with EtOAc (3 \times 10 mL). The aqueous phase was neutralized using 2 N HCl and extracted with EtOAc (3 \times 10 mL). The combined organic layers were dried over MgSO₄ and the solvent was removed under reduced pressure. The residue was dissolved in 5 mL of dry EtOH, HCl_(g) was passed through the solution and the product was precipitated by the addition of diethyl ether (20 mL). The product was washed with diethyl ether (2 \times 10 mL) and the remaining solvent was removed under reduced pressure to obtain the product A-PM-I (25.7 mg, 90.0 μ mol, 6%).

¹H-NMR (500 MHz, D₂O): δ [ppm] = 8.12 (s, 1H), 6.31 - 6.25 (m, 2H), 5.81 (dd, J = 9.2 Hz, 2.3 Hz, 1H), 4.89 (s, 2H), 4.62 (s, 2H), 2.63 (s, 3H).

¹³C-NMR (126 MHz, D₂O): δ [ppm] = 169.2, 153.4, 143.5, 139.5, 137.6, 129.6, 128.63, 128.6, 58.4, 34.8, 14.7.

ESI-HR-MS (m/z) [M+H⁺] calcd. for C₁₁H₁₅N₂O₃, 223.1077; found, 223.1077.

3.9.2. Synthesis of Probe A-PM-P1



A-PM-I (87.0 mg, 400 μ mol, 1.0 eq.) was dissolved in 4 mL of dry DMF and potassium carbonate (57.0 mg, 410 μ mol, 1.0 eq.) was added. After stirring for 15 min at RT, propargyl bromide (30.0 μ L, 47.0 mg, 400 μ mol, 1.0 eq.) was added dropwise. The mixture was stirred at RT for 9 h. The solvent was removed under reduced pressure and the crude product was purified by column chromatography (DCM:MeOH = 10:1) yielding A-PM-P1 (63.9 mg, 245 μ mol, 73%) as a yellow oil.

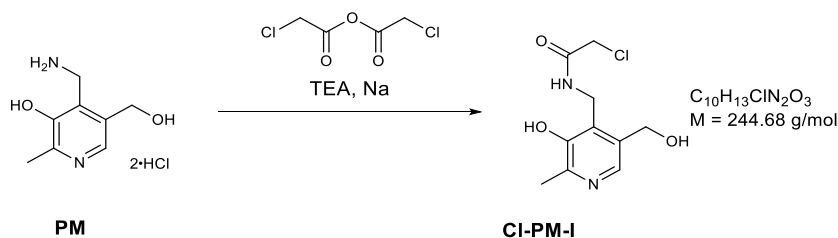
TLC (DCM:MeOH = 10:1): R_f = 0.34 [UV].

$^1\text{H-NMR}$ (500 MHz, $\text{DMSO-}d_6$): δ [ppm] = 8.26 (s, 1H), 6.23 (dd, J = 17.1 Hz, 10.1 Hz, 1H), 6.10 (dd, J = 17.1 Hz, 2.2 Hz, 1H), 5.59 (dd, J = 10.1 Hz, 2.3 Hz, 1H), 5.32 (t, J = 5.3 Hz, 1H), 4.67 (d, J = 2.4 Hz, 2H), 4.54 (d, J = 5.0 Hz, 2H), 4.44 (d, J = 5.2 Hz, 2H), 3.64 (t, J = 2.4 Hz, 1H), 2.54 (s, 1H), 2.46 (s, 3H).

$^{13}\text{C-NMR}$ (126 MHz, $\text{DMSO-}d_6$): δ [ppm] = 164.4, 151.2, 150.8, 144.0, 137.2, 135.1, 131.3, 125.7, 79.2, 79.0, 61.0, 58.4, 33.9, 19.7.

ESI-HR-MS (m/z) [$\text{M}+\text{H}^+$] calcd. for $C_{14}H_{17}N_2O_3$, 261.1233; found, 261.1233.

3.9.3. Synthesis of Inhibitor Cl-PM-I



This synthesis was performed as previously published.¹⁹⁷ To a solution of PM dihydrochloride (154 mg, 640 μ mol, 1.0 eq.) in anhydrous methanol (20 mL) at RT, sodium metal (33.8 mg, 1.47 mmol, 2.3 eq.) and triethylamine (232 μ L, 1.66 mmol, 2.6 eq.) were added. Next, chloroacetic anhydride (383 mg, 1.47 mmol, 2.3 eq.) was added and the mixture was stirred at RT for 22 h. The crude reaction mixture was concentrated *in vacuo* and purified by preparative TLC (20 \times 20 cm, UV₂₅₄, 2 mm) using EtOAc/Hex (10/1). Fractions detected by UV light were scratched from the glass surface and the product was dissolved in methanol. The suspension was cooled to 0 $^{\circ}$ C, filtered and concentrated *in vacuo* to obtain Cl-PM-I (29.9 mg, 122 μ mol, 19%) as an ocher-colored oil.

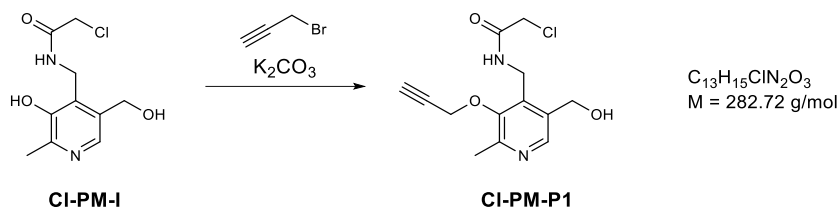
TLC (EtOAc:Hex = 10:1): R_f = 0.08 [UV].

$^1\text{H-NMR}$ (500 MHz, CDCl_3): δ [ppm] = 9.26 (*br s*, 1H), 7.88 (*s*, 1H), 7.85 (*br s*, 1H), 4.76 (*s*, 2H), 4.50 (*d*, J = 6.7 Hz, 2H), 4.07 (*s*, 2H), 2.51 (*s*, 3H).

$^{13}\text{C-NMR}$ (101 MHz, CDCl_3): δ [ppm] = 169.2, 150.9, 150.4, 139.5, 132.4, 130.1, 62.3, 42.2, 36.2, 19.8.

ESI-HR-MS (m/z) [$\text{M}+\text{H}^+$] calcd. for $\text{C}_{10}\text{H}_{14}\text{ClN}_2\text{O}_3$, 245.0687; found, 245.0687.

3.9.4. Synthesis of Probe Cl-PM-P1



Cl-PM-I (19.3 mg, 78.9 μ mol, 1.0 eq.) was dissolved in anhydrous DMF (1 mL) before K_2CO_3 (10.9 mg, 78.9 μ mol, 1.0 eq.) was added. The suspension was stirred at RT for 15 min. Propargyl bromide (80% in toluene, 8.50 μ L, 78.9 μ mol, 1.0 eq.) was added dropwise and the suspension was stirred at RT for 5 h. Brine (5 mL) was added and the aqueous phase was extracted with EtOAc (3 \times 10 mL). The combined organic phases were washed with brine (5 \times 30 mL), dried over Na_2SO_4 and concentrated *in vacuo*. The crude product was purified by column chromatography (EtOAc:Hex = 10:1 \rightarrow DCM:MeOH 10:1) to obtain Cl-PM-P1 (5.30 mg, 19.0 μ mol, 24%) as an ochre-colored solid.

TLC (DCM:MeOH = 10:1): R_f = 0.14 [UV].

1H -NMR (500 MHz, $CDCl_3$): δ [ppm] = 8.29 (s, 1H), 7.61 (*br s*, 1H), 4.75 (s, 2H), 4.70 (d, J = 6.4 Hz, 2H), 4.69 (d, J = 2.4 Hz, 2H), 4.03 (s, 2H), 2.59 (t, J = 2.4 Hz, 1H), 2.55 (s, 3H).

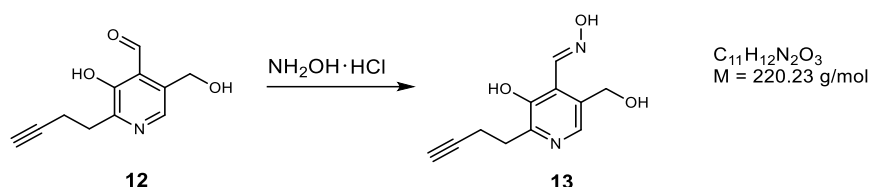
^{13}C -NMR (126 MHz, Methanol- d_4): δ [ppm] = 168.8, 153.8, 153.0, 145.3, 140.4, 136.3, 79.3, 78.3, 62.1, 60.6, 43.1, 36.1, 19.6.

ESI-HR-MS (m/z) [$M+H^+$] calcd. for $C_{13}H_{16}ClN_2O_3$, 283.0844; found, 283.0843.

3.9.5. Synthesis of Probe A-PM-P2

2-(But-3-yn-1-yl)-3-hydroxy-5-(hydroxymethyl) isonicotinaldehydeoxime (13)

Compound 12 was synthesised according to Hoegl *et al.*¹⁹⁸



The formation of oxime 13 was adapted from Dale *et al.*¹⁹⁹ Compound 12 (126 mg, 420 μmol , 1.0 eq.) was dissolved in 18 mL of dry EtOH and hydroxylamine hydrochloride (115 mg, 1.66 mmol, 4.0 eq.) was added. The solution was stirred at RT for 49 h, the solvent was removed under reduced pressure and the crude compound was purified by HPLC using method A, yielding compound 13 (62.5 mg, 284 μmol , 68%) as a pale-yellow solid.

TLC (MeOH:DCM = 1:10): $R_f = 0.45$ [UV].

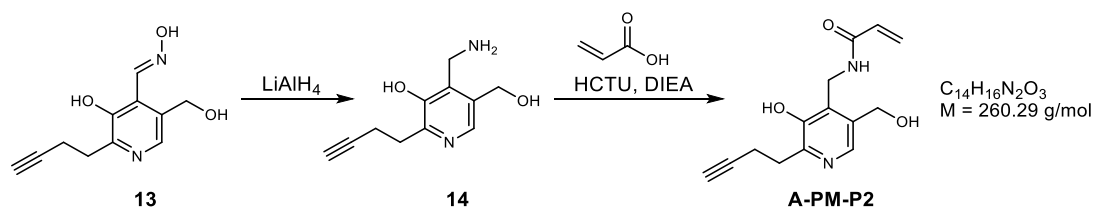
HPLC: $t_R = 6.4$ min (Method A).

$^1\text{H-NMR}$ (300 MHz, $\text{DMSO-}d_6$): δ [ppm] = 12.14 (*br s*, 1H), 10.80 (*br s*, 1H), 8.60 (*s*, 1H), 8.02 (*s*, 1H), 5.32 (*s*, 1H), 4.60 (*d*, $J = 4.1$ Hz, 2H), 2.97 (*t*, $J = 7.6$ Hz, 2H), 2.71 (*t*, $J = 2.6$ Hz, 1H), 2.57 (*dt*, $J = 7.6$ Hz, 2.6 Hz, 2H).

$^{13}\text{C-NMR}$ (75 MHz, $\text{DMSO-}d_6$): δ [ppm] = 149.6, 148.2, 147.9, 139.1, 132.7, 120.2, 84.3, 71.1, 58.7, 30.5, 16.0.

ESI-HR-MS (m/z) [$\text{M}+\text{H}^+$] calcd. for $\text{C}_{11}\text{H}_{13}\text{N}_2\text{O}_3$, 221.0920; found, 221.0920.

N-((2-(But-3-yn-1-yl)-3-hydroxy-5-(hydroxymethyl) pyridine-4-yl) methyl) acrylamide
(A-PM-P2)



A protocol published by Müller *et al.* was used to reduce compound 13.²⁰⁰ Compound 13 (100 mg, 450 μmol , 1.0 eq.) was dissolved in 7 mL dry THF under argon and LiAlH_4 (320 μL , 2.4 M in THF, 29.2 mg, 770 μmol , 1.7 eq.) was added slowly at 0 °C. Upon stirring at RT for 1 h, the temperature was increased to 80 °C and the mixture was stirred for 5 h. Next, 1 N HCl (15 mL) was added, the solvent was removed under reduced pressure and crude amine 14 was directly used for the next step.

Acrylic acid (30.0 μL , 450 μmol , 1.0 eq.), DIEA (120 μL , 680 μmol , 1.5 eq.) and HCTU (281.3 mg, 680 μmol , 1.5 eq.) were dissolved in 2 mL DMF at 0 °C under argon and the solution was stirred for 2 h. Amine 14 dissolved in 7 mL DMF was slowly added at 0 °C and the mixture was stirred overnight. Next, the solvent was removed under reduced pressure and the residue was dissolved in EtOAc (30 mL). The organic phase was washed with 30 mL 1 N NaOH, 20 mL saturated $\text{NaHCO}_{3(\text{aq})}$ solution and 20 mL brine. The combined aqueous phases were neutralized and extracted with EtOAc (7 \times 10 mL). The solvent of the combined organic phases was removed under reduced pressure. The crude product was purified by HPLC using method B followed by column chromatography (3% MeOH/DCM \rightarrow 5% MeOH/DCM) yielding A-PM-P2 (2.17 mg, 8.33 μmol , 2% over two steps) as a yellow oil.

TLC (MeOH:DCM = 1:10): $R_f = 0.47$ [UV, KMnO_4].

HPLC: $t_R = 5.4$ min (Method B).

$^1\text{H-NMR}$ (500 MHz, Methanol- d_4): δ [ppm] = 8.00 (s, 1H), 6.35 - 6.25 (m, 2H), 5.74 (dd, J = 9.5 Hz, 2.5 Hz, 1H), 4.76 (s, 2H), 4.55 (s, 2H), 3.07 (t, J = 7.6 Hz, 2H), 2.58 (td, J = 7.6 Hz, 2.6 Hz, 2H), 2.20 (t, J = 2.7 Hz, 1H).

$^{13}\text{C-NMR}$ (126 MHz, Methanol- d_4): δ [ppm] = 169.7, 152.8, 149.7, 138.2, 137.1, 134.7, 130.5, 128.6, 83.8, 70.3, 60.6, 35.6, 32.3, 17.8.

ESI-HR-MS (m/z) [$\text{M}+\text{H}^+$] calcd. for $\text{C}_{14}\text{H}_{17}\text{N}_2\text{O}_3$, 261.1234; found, 261.1232.

IV. Bibliography

1. Fleming, A. The discovery of penicillin. *Br. Med. Bull.* 2, 4–5 (1944).
2. Neill, J. O. ' . Antimicrobial Resistance: Tackling a crisis for the health and wealth of nations. (2014).
3. CDC. Antibiotic resistance threats in the United States, 2019. Atlanta, GA: U.S. Department of Health and Human Services, CDC; 2019.
4. Ventola, C. L. The antibiotic resistance crisis: part 1: causes and threats. *P T* 40, 277–83 (2015).
5. Bartlett, J. G., Gilbert, D. N. & Spellberg, B. Seven ways to preserve the miracle of antibiotics. *Clin. Infect. Dis.* 56, 1445–1450 (2013).
6. Xu, X. *et al.* Synergistic combination of two antimicrobial agents closing each other's mutant selection windows to prevent antimicrobial resistance. *Sci. Rep.* 8, 1–7 (2018).
7. Brown, D. G., Lister, T. & May-Dracka, T. L. New natural products as new leads for antibacterial drug discovery. *Bioorganic Med. Chem. Lett.* 24, 413–418 (2014).
8. Lewis, K. Platforms for antibiotic discovery. *Nat. Rev. Drug Discov.* 12, 371–387 (2013).
9. Schaenzer, A. J. & Wright, G. D. Antibiotic resistance by enzymatic modification of antibiotic targets. *Trends Mol. Med.* 26, 768–782 (2020).
10. Ramirez, M. S. & Tolmasky, M. E. Aminoglycoside modifying enzymes. *Drug Resist. Updat.* 13, 151–171 (2010).
11. Poole, K. Efflux pumps as antimicrobial resistance mechanisms. *Ann. Med.* 39, 162–176 (2007).
12. Lambert, P. A. Bacterial resistance to antibiotics: Modified target sites. *Adv. Drug Deliv. Rev.* 57, 1471–1485 (2005).
13. Fernandes, R., Amador, P. & Prudêncio, C. β -Lactams. *Rev. Med. Microbiol.* 24, 7–17 (2013).
14. Bycroft, B. W. & Shute, R. E. The molecular basis for the mode of action of beta-lactam antibiotics and mechanisms of resistance. *AAPS J.* 2, 3–14 (1985).
15. Sanders, C. C. Mechanisms responsible for cross-resistance and dichotomous resistance among the quinolones. *Clin. Infect. Dis.* 32, S1–S8 (2001).
16. Kohanski, M. A., Dwyer, D. J. & Collins, J. J. How antibiotics kill bacteria: From

- targets to networks. *Nat. Rev. Microbiol.* 8, 423–435 (2010).
17. Walkenhorst, W. F. Using adjuvants and environmental factors to modulate the activity of antimicrobial peptides. *Biochim. Biophys. Acta - Biomembr.* 1858, 926–935 (2016).
 18. Lakemeyer, M., Zhao, W., Mandl, F. A., Hammann, P. & Sieber, S. A. Thinking outside the box—novel antibacterials to tackle the resistance crisis. *Angew. Chem. Int. Ed.* 57, 14440–14475 (2018).
 19. Leclercq, R. Mechanisms of resistance to macrolides and lincosamides: Nature of the resistance elements and their clinical implications. *Clin. Infect. Dis.* 34, 482–492 (2002).
 20. Newman, D. J. & Cragg, G. M. Natural products as sources of new drugs over the 30 years from 1981 to 2010. *J. Nat. Prod.* 75, 311–335 (2012).
 21. McGuire, J. M. *et al.* Ilotycin, a new antibiotic. *Schweiz. Med. Wochenschr.* 82, 1064–1065 (1952).
 22. Debono, M. *et al.* A21978C, a complex of new acidic peptide antibiotics: Isolation, chemistry, and mass spectral structure elucidation. *J. Antibiot.* 40, 761–77 (1987).
 23. Margalith, P. & Beretta, G. Rifomycin. XI. taxonomic study on *Streptomyces mediterranei* nov. sp. *Mycopathol. Mycol. Appl.* 13, 321–330 (1960).
 24. Robbel, L. & Marahiel, M. A. Daptomycin, a bacterial lipopeptide synthesized by a nonribosomal machinery. *J. Biol. Chem.* 285, 27501–27508 (2010).
 25. Vydrin, A. F., Shikhaleev, I. V., Makhortov, V. L., Shcherenko, N. N. & Kolchanova, N. V. Component composition of gentimacin sulfate preparations. *Pharm. Chem. J.* 37, 448–450 (2003).
 26. Rodriguez, M. *et al.* Fast determination of underivatized gentamicin C components and impurities by LC-MS using a porous graphitic carbon stationary phase. *Anal. Bioanal. Chem.* 407, 7691–7701 (2015).
 27. Morrison, K. C. & Hergenrother, P. J. Natural products as starting points for the synthesis of complex and diverse compounds. *Nat. Prod. Rep.* 31, 6–14 (2014).
 28. Lipinski, C. A., Lombardo, F., Dominy, B. W. & Feeney, P. J. Experimental and computational approaches to estimate solubility and permeability in drug discovery and development settings. *Adv. Drug Deliv. Rev.* 64, 4–17 (2012).

29. O'Shea, R. & Moser, H. E. Physicochemical properties of antibacterial compounds: Implications for drug discovery. *J. Med. Chem.* 51, 2871–2878 (2008).
30. Nikaido, H. Preventing drug access to targets: Cell surface permeability barriers and active efflux in bacteria. *Semin. Cell Dev. Biol.* 12, 215–223 (2001).
31. Benedetto Tiz, D., Kikelj, D. & Zidar, N. Overcoming problems of poor drug penetration into bacteria: Challenges and strategies for medicinal chemists. *Expert Opin. Drug Discov.* 13, 497–507 (2018).
32. Gray, D. A. & Wenzel, M. Multitarget approaches against multiresistant superbugs. *ACS Infect. Dis.* 6, 1346–1365 (2020).
33. Pagès, J. M., James, C. E. & Winterhalter, M. The porin and the permeating antibiotic: A selective diffusion barrier in Gram-negative bacteria. *Nat. Rev. Microbiol.* 6, 893–903 (2008).
34. Cunningham, M. L., Kwan, B. P., Nelson, K. J., Bensen, D. C. & Shaw, K. J. Distinguishing on-target *versus* off-target activity in early antibacterial drug discovery using a macromolecular synthesis assay. *J. Biomol. Screen.* 18, 1018–1026 (2013).
35. Schenone, M., Dančík, V., Wagner, B. K. & Clemons, P. A. Target identification and mechanism of action in chemical biology and drug discovery. *Nat. Chem. Biol.* 9, 232–240 (2013).
36. Kubota, K., Funabashi, M. & Ogura, Y. Target deconvolution from phenotype-based drug discovery by using chemical proteomics approaches. *Biochim. Biophys. Acta - Proteins Proteomics* 1867, 22–27 (2019).
37. Farha, M. A. & Brown, E. D. Strategies for target identification of antimicrobial natural products. *Nat. Prod. Rep.* 33, 668–680 (2016).
38. Jana, B., Baker, K. R. & Guardabassi, L. *Antimicrobial Peptides*. 1548, (Springer New York, 2017).
39. Cotsonas King, A. & Wu, L. Macromolecular synthesis and membrane perturbation assays for mechanisms of action studies of antimicrobial agents. *Curr. Protoc. Pharmacol.* 47, 1–23 (2009).
40. Singh, M. P. *et al.* Mechanistic studies and biological activity of bioxalomycin α_2 , a novel antibiotic produced by *Streptomyces viridodiataticus* subsp.

- "litoralis" LL- 31F508. *Antimicrob. Agents Chemother.* 38, 1808–1812 (1994).
41. Ling, L. L. *et al.* A new antibiotic kills pathogens without detectable resistance. *Nature* 517, 455–459 (2015).
 42. Cuatrecasas, P., Wilchek, M. & Anfinsen, C. B. Selective enzyme purification by affinity chromatography. *Proc. Natl. Acad. Sci.* 61, 636–643 (1968).
 43. Curtis, S. J. & Strominger, J. L. Purification of penicillin-binding protein 2 of *Escherichia coli*. *J. Bacteriol.* 145, 398–403 (1981).
 44. Kam, C. M., Abuelyaman, A. S., Li, Z., Hudig, D. & Powers, J. C. Biotinylated isocoumarins, new inhibitors and reagents for detection, localization, and isolation of serine proteases. *Bioconjug. Chem.* 4, 560–567 (1993).
 45. Abuelyaman, A. S., Powers, J. C., Hudig, D. & Woodard, S. L. Fluorescent derivatives of diphenyl [1-(*N*-peptidylamino)alkyl]phosphonate esters: Synthesis and use in the inhibition and cellular localization of serine proteases. *Bioconjug. Chem.* 5, 400–405 (1994).
 46. Walker, B. *et al.* The synthesis, kinetic characterization and application of a novel biotinylated affinity label for cathepsin B. *Biochem. J.* 283, 449–453 (1992).
 47. Liu, Y., Patricelli, M. P. & Cravatt, B. F. Activity-based protein profiling: The serine hydrolases. *Proc. Natl. Acad. Sci. U. S. A.* 96, 14694–14699 (1999).
 48. Greenbaum, D., Medzihradszky, K. F., Burlingame, A. & Bogoy, M. Epoxide electrophiles as activity-dependent cysteine protease profiling and discovery tools. *Chem. Biol.* 7, 569–581 (2000).
 49. Speers, A. E., Adam, G. C. & Cravatt, B. F. Activity-based protein profiling in vivo using a copper(I)-catalyzed azide-alkyne [3 + 2] cycloaddition. *J. Am. Chem. Soc.* 125, 4686–4687 (2003).
 50. Padwa, A. 1,3-Dipolar cycloaddition chemistry. *J. Heterocyc. Chem.* 23, 1899 (1986).
 51. Rostovtsev, V. V., Green, L. G., Fokin, V. V. & Sharpless, K. B. A stepwise Huisgen cycloaddition process: Copper(I)-catalyzed regioselective "ligation" of azides and terminal alkynes. *Angew. Chem. Int. Ed.* 41, 2596–2599 (2002).
 52. Kolb, H. C., Finn, M. G. & Sharpless, K. B. Click chemistry: Diverse chemical function from a few good reactions. *Angew. Chem. Int. Ed.* 40, 2004–2021 (2001).

53. Lewis, W. G. *et al.* Click chemistry in situ: Acetylcholinesterase as a reaction vessel for the selective assembly of a femtomolar inhibitor from an array of building blocks. *Angew. Chem. Int. Ed.* 41, 1053–1057 (2002).
54. Dalton, S. E. & Campos, S. Covalent small molecules as enabling platforms for drug discovery. *ChemBioChem* 21, 1080–1100 (2020).
55. Dubinsky, L., Krom, B. P. & Meijler, M. M. Diazirine based photoaffinity labeling. *Bioorganic Med. Chem.* 20, 554–570 (2012).
56. Pan, S. *et al.* A suite of “minimalist” photo-crosslinkers for live-cell imaging and chemical proteomics: Case study with BRD4 inhibitors. *Angew. Chemie* 129, 11978–11983 (2017).
57. Li, Z. *et al.* Design and synthesis of minimalist terminal alkyne-containing diazirine photo-crosslinkers and their incorporation into kinase inhibitors for cell- and tissue-based proteome profiling. *Angew. Chem. Int. Ed.* 52, 8551–8556 (2013).
58. Eirich, J., Orth, R. & Sieber, S. A. Unraveling the protein targets of vancomycin in living *S. aureus* and *E. faecalis* cells. *J. Am. Chem. Soc.* 133, 12144–12153 (2011).
59. Koteva, K. *et al.* A vancomycin photoprobe identifies the histidine kinase VanSsc as a vancomycin receptor. *Nat. Chem. Biol.* 6, 327–329 (2010).
60. Kleiner, P., Heydenreuter, W., Stahl, M., Korotkov, V. S. & Sieber, S. A. A whole proteome inventory of background photocrosslinker binding. *Angew. Chem. Int. Ed.* 56, 1396–1401 (2017).
61. Doitsidou, M., Jarriault, S. & Poole, R. J. Next-generation sequencing-based approaches for mutation mapping and identification in *Caenorhabditis elegans*. *Genetics* 204, 451–474 (2016).
62. Metzker, M. L. Sequencing technologies the next generation. *Nat. Rev. Genet.* 11, 31–46 (2010).
63. Kram, K. E. *et al.* Adaptation of *Escherichia coli* to long-term serial passage in complex medium: Evidence of parallel evolution. *mSystems* 2, 1–12 (2017).
64. Andersson, D. I., Hughes, D. & Kubicek-Sutherland, J. Z. Mechanisms and consequences of bacterial resistance to antimicrobial peptides. *Drug Resist. Updat.* 26, 43–57 (2016).
65. Zhou, J. *et al.* Selection of antibiotic-resistant bacterial mutants: Allelic diversity

- among fluoroquinolone-resistant mutations. *J. Infect. Dis.* 182, 517–525 (2000).
66. Smith, P. A. *et al.* Optimized arylomycins are a new class of Gram-negative antibiotics. *Nature* 561, 189–194 (2018).
 67. Le, P. *et al.* Repurposing human kinase inhibitors to create an antibiotic active against drug-resistant *Staphylococcus aureus*, persists and biofilms. *Nat. Chem.* 12, 145–158 (2020).
 68. Rothe, W. Das neue Antibiotikum Xanthocillin. *Dtsch. Medizinische Wochenschrift* 79, 1080–1081 (1954).
 69. Beiersdorf, R. & Ahrens, W. Untersuchungen über die antibakteriellen und pharmakodynamischen Eigenschaften des neuen Antibiotiums Xanthocillin. *Pharmazie* 8, 796–801 (1953).
 70. Bettley, F. R. Xanthocillin cream for local treatment. *BMJ* 1, 1226–1227 (1959).
 71. Storch, H. Beiträge zur antiallergischen Wirkung von *Apis mellifica*. *Allg. Homöopathische Zeitung* 200, 85–86 (1955).
 72. World Health Organization. *Global Antimicrobial Resistance and Use Surveillance System (GLASS) Report*. *Who* (2020).
 73. Shang, Z. *et al.* Chemical profile of the secondary metabolites produced by a deep-sea sediment-derived fungus *Penicillium commune* SD-118. *Chinese J. Oceanol. Limnol.* 30, 305–314 (2012).
 74. Takatsuki, A., Tamura, G. & Arima, K. New antiviral antibiotics; Xanthocillin X mono- and dimethylether, and methoxy-xanthocillin X dimethylether. *J. Antibiot.* 21, 676–680 (1968).
 75. Tsunakawa, M. *et al.* Bu-4704, a new member of the xanthocillin class. *J. Antibiot.* 46, 687–688 (1993).
 76. Tacconelli, E. *et al.* Discovery, research, and development of new antibiotics: the WHO priority list of antibiotic-resistant bacteria and tuberculosis. *Lancet Infect. Dis.* 18, 318–327 (2018).
 77. Isshiki, K. *et al.* A new antibiotic indisocin and *N*-methylindisocin. *J. Antibiot.* 40, 1195–1198 (1987).
 78. Wang, L. *et al.* Diisonitrile natural product SF2768 functions as a chalkophore that mediates copper acquisition in *Streptomyces thioluteus*. *ACS Chem. Biol.* 12, 3067–3075 (2017).

79. Di Blasio, B. *et al.* Axisonitrile-3, axisothiocyanate-3 and axamide-3. Sesquiterpenes with a novel spiro[4,5]decane skeleton from the sponge *Axinella cannabina*. *Tetrahedron* 32, 473–478 (1976).
80. Miyaoka, H. *et al.* Antimalarial activity of kalihinol A and new relative diterpenoids from the okinawan sponge, *Acanthella* sp. *Tetrahedron* 54, 13467–13474 (1998).
81. Galli, U., Tron, G. C., Purghè, B., Grosa, G. & Aprile, S. Metabolic fate of the isocyanide moiety: Are isocyanides pharmacophore groups neglected by medicinal chemists? *Chem. Res. Toxicol.* 33, 955–966 (2020).
82. Sun, J. Z., Chen, K. S., Yao, L. G., Liu, H. L. & Guo, Y. W. A new kalihinol diterpene from the hainan sponge *Acanthella* sp. *Arch. Pharm. Res.* 32, 1581–1584 (2009).
83. Wright, A. D. *et al.* Inhibition of heme detoxification processes underlies the antimalarial activity of terpene isonitrile compounds from marine sponges. *J. Med. Chem.* 44, 873–885 (2001).
84. Daub, M. E., Prudhomme, J., Ben Mamoun, C., Le Roch, K. G. & Vanderwal, C. D. Antimalarial properties of simplified kalihinol analogues. *ACS Med. Chem. Lett.* 8, 355–360 (2017).
85. Zhu, M. *et al.* Diisonitrile-mediated reactive oxygen species accumulation leads to bacterial growth inhibition. *J. Nat. Prod.* 83, 1634–1640 (2020).
86. Itoh, J. *et al.* MK4588, a new antibiotic related to xanthocillin. *J. Antibiot.* 43, 456–461 (1990).
87. Chang, C. W. J. *et al.* Kalihinol-A, a highly functionalized diisocyano diterpenoid antibiotic from a sponge. *J. Am. Chem. Soc.* 106, 4644–4646 (1984).
88. Fattorusso, E., Magno, S., Mayol, L., Santacroce, C. & Sica, D. Isolation and structure of axisonitrile-2. A new sesquiterpenoid isonitrile from the sponge *Axinella cannabina*. *Tetrahedron* 30, 3911–3913 (1974).
89. Yamaguchi, T., Miyake, Y., Miyamura, A., Ishiwata, N. & Tatsuta, K. Structure-activity relationships of xanthocillin derivatives as thrombopoietin receptor agonist. *J. Antibiot.* 59, 729–734 (2006).
90. Tatsuta, K. & Yamaguchi, T. The first stereoselective total synthesis of antiviral antibiotic, xanthocillin X dimethylether and its stereoisomer. *Tetrahedron Lett.* 46, 5017–5020 (2005).

91. Corey, E. J. & Fuchs, P. L. A synthetic method for formyl→ethynyl conversion. *Tetrahedron Lett.* 13, 3769–3772 (1972).
92. Baumgarten, H. E., Smith, H. L. & Staklis, A. Reactions of amines. XVIII. Oxidative rearrangement of amides with lead tetraacetate. *J. Org. Chem.* 40, 3554–3561 (1975).
93. He, D. *et al.* Quantitative and comparative profiling of protease substrates through a genetically encoded multifunctional photocrosslinker. *Angew. Chem. Int. Ed.* 56, 14521–14525 (2017).
94. Shapiro, J. A., Morrison, K. R., Chodisetty, S. S., Musaev, D. G. & Wuest, W. M. Biologically inspired total synthesis of Ulbactin F, an iron-binding natural product. *Org. Lett.* 20, 5922–5926 (2018).
95. Knight, D., Dimitrova, D. D., Rudin, S. D., Bonomo, R. A. & Rather, P. N. Mutations decreasing intrinsic β -lactam resistance are linked to cell division in the nosocomial pathogen *Acinetobacter baumannii*. *Antimicrob. Agents Chemother.* 60, 3751–3758 (2016).
96. Cox, J. *et al.* Accurate proteome-wide label-free quantification by delayed normalization and maximal peptide ratio extraction, termed MaxLFQ. *Mol. Cell. Proteomics* 13, 2513–2526 (2014).
97. Baba, T. *et al.* Construction of *Escherichia coli* K-12 in-frame, single-gene knockout mutants: The Keio collection. *Mol. Syst. Biol.* 2, (2006).
98. Yamazaki, Y., Niki, H. & Kato, J. Profiling of *Escherichia coli* chromosome database. *Methods in Molecular Biology* 385–389 (Humana Press, Inc., 2008).
99. Goodall, E. C. A. *et al.* The essential genome of *Escherichia coli* K-12. *MBio* 9, 1–18 (2018).
100. Gallagher, L. A. *et al.* Resources for genetic and genomic analysis of emerging pathogen *Acinetobacter baumannii*. *J. Bacteriol.* 197, 2027–2035 (2015).
101. Altschul, S. F., Gish, W., Miller, W., Myers, E. W. & Lipman, D. J. Basic local alignment search tool. *J. Mol. Biol.* 215, 403–410 (1990).
102. Altschul, S. *et al.* Gapped BLAST and PSI-BLAST: A new generation of protein database search programs. *Nucleic Acids Res.* 25, 3389–3402 (1997).
103. Di Gennaro, P., Bargna, A., Bruno, F. & Sello, G. Purification of recombinant catalase-peroxidase HPI from *E. coli* and its application in enzymatic

- polymerization reactions. *Appl. Microbiol. Biotechnol.* 98, 1119–1126 (2014).
104. Switala, J. & Loewen, P. C. Diversity of properties among catalases. *Arch. Biochem. Biophys.* 401, 145–154 (2002).
 105. Vogler, A. Coordinated isonitriles. *Organic Chemistry*, 217–233 (1971).
 106. Agarwala, R. *et al.* Database resources of the national center for biotechnology information. *Nucleic Acids Res.* 46, D8–D13 (2018).
 107. Frankenberg, N., Moser, J. & Jahn, D. Bacterial heme biosynthesis and its biotechnological application. *Appl. Microbiol. Biotechnol.* 63, 115–127 (2003).
 108. Kumar, A. Glutamyl-transfer RNA: At the crossroad between chlorophyll and protein biosynthesis. *Trends Plant Sci.* 1, 371–376 (1996).
 109. Shemin, D. & Russell, C. S. δ -Aminolevulinic acid, its role in the biosynthesis of porphyrins and purines. *J. Am. Chem. Soc.* 75, 4873–4874 (1953).
 110. Dailey, H. A. *et al.* Prokaryotic heme biosynthesis: Multiple pathways to a common essential product. *Microbiol. Mol. Biol. Rev.* 81, 1–62 (2017).
 111. Choby, J. E. & Skaar, E. P. Heme synthesis and acquisition in bacterial pathogens. *J. Mol. Biol.* 428, 3408–3428 (2016).
 112. Li, T., Bonkovsky, H. L. & Guo, J. Structural analysis of heme proteins: Implications for design and prediction. *BMC Struct. Biol.* 11, 13 (2011).
 113. Ponka, P. Cell biology of heme. *Am. J. Med. Sci.* 318, 241–256 (1999).
 114. Atamna, H., Brahmabhatt, M., Atamna, W., Shanower, G. A. & Dhahbi, J. M. ApoHRP-based assay to measure intracellular regulatory heme. *Metallomics* 7, 309–321 (2015).
 115. Jahn, D., Michelsen, U. & Söll, D. Two glutamyl-tRNA reductase activities in *Escherichia coli*. *J. Biol. Chem.* 266, 2542–8 (1991).
 116. Jones, A. M. & Elliott, T. A purified mutant Hema protein from *Salmonella enterica* serovar typhimurium lacks bound heme and is defective for heme-mediated regulation *in vivo*. *FEMS Microbiol. Lett.* 307, 41–47 (2010).
 117. Wang, L., Elliott, M. & Elliott, T. Conditional stability of the Hema protein (Glutamyl-tRNA reductase) regulates heme biosynthesis in *Salmonella typhimurium*. *J. Bacteriol.* 181, 1211–1219 (1999).
 118. Breinig, S. *et al.* Control of tetrapyrrole biosynthesis by alternate quaternary forms of porphobilinogen synthase. *Nat. Struct. Biol.* 10, 757–763 (2003).

119. Mitchell, L. W., Volin, M., Martins, J. & Jaffe, E. K. Mechanistic implications of mutations to the active site lysine of porphobilinogen synthase. *J. Biol. Chem.* 276, 1538–1544 (2001).
120. Lentz, C. S. *et al.* WALADin benzimidazoles differentially modulate the function of porphobilinogen synthase orthologs. *J. Med. Chem.* 57, 2498–2510 (2014).
121. Heinemann, I. U. *et al.* Structure of the heme biosynthetic *Pseudomonas aeruginosa* porphobilinogen synthase in complex with the antibiotic alaremycin. *Antimicrob. Agents Chemother.* 54, 267–272 (2009).
122. Jarret, C. *et al.* Inhibition of *Escherichia coli* porphobilinogen synthase using analogs of postulated intermediates. *Chem. Biol.* 7, 185–196 (2000).
123. Madeira, F. *et al.* The EMBL-EBI search and sequence analysis tools APIs in 2019. *Nucleic Acids Res.* 47, W636–W641 (2019).
124. Dhanasekaran, S., Chandra, N. R., Sagar, B. K. C., Rangarajan, P. N. & Padmanaban, G. δ -Aminolevulinic acid dehydratase from *Plasmodium falciparum*. *J. Biol. Chem.* 279, 6934–6942 (2004).
125. Lucidi, M. *et al.* New shuttle vectors for gene cloning and expression in multidrug-resistant *Acinetobacter* species. *Antimicrob. Agents Chemother.* 62, 1–19 (2018).
126. Lentz, C. S. *et al.* A selective inhibitor of heme biosynthesis in endosymbiotic bacteria elicits antifilarial activity *in vitro*. *Chem. Biol.* 20, 177–187 (2013).
127. Frankenberg, N. *et al.* High resolution crystal structure of a Mg^{2+} -dependent porphobilinogen synthase. *J. Mol. Biol.* 289, 591–602 (1999).
128. Bollivar, D. W. *et al.* *Rhodobacter capsulatus* porphobilinogen synthase, a high activity metal ion independent hexamer. *BMC Biochem.* 5, 1–12 (2004).
129. Wrenbeck, E. E., Azouz, L. R. & Whitehead, T. A. Single-mutation fitness landscapes for an enzyme on multiple substrates reveal specificity is globally encoded. *Nat. Commun.* 8, 15695 (2017).
130. Coleman, C. S., Stanley, B. A. & Pegg, A. E. Effect of mutations at active site residues on the activity of ornithine decarboxylase and its inhibition by active site-directed irreversible inhibitors. *J. Biol. Chem.* 268, 24572–24579 (1993).
131. Yoon, E. J. *et al.* Contribution of resistance-nodulation-cell division efflux systems to antibiotic resistance and biofilm formation in *Acinetobacter*

- baumannii*. *MBio* 6, 1–13 (2015).
132. Vestergaard, M., Nøhr-Meldgaard, K. & Ingmer, H. Multiple pathways towards reduced membrane potential and concomitant reduction in aminoglycoside susceptibility in *Staphylococcus aureus*. *Int. J. Antimicrob. Agents* 51, 132–135 (2018).
 133. Dekic, S., Hrenovic, J., van Wilpe, E., Venter, C. & Goic-Barisic, I. Survival of emerging pathogen *Acinetobacter baumannii* in water environment exposed to different oxygen conditions. *Water Sci. Technol.* 80, 1581–1590 (2019).
 134. Deng, W. L., Chang, H. Y. & Peng, H. L. Acetoin catabolic system of *Klebsiella pneumoniae* CG43: Sequence, expression, and organization of the *aco* operon. *J. Bacteriol.* 176, 3527–3535 (1994).
 135. Tomaras, A. P., Dorsey, C. W., Edelmann, R. E. & Actis, L. A. Attachment to and biofilm formation on abiotic surfaces by *Acinetobacter baumannii*: Involvement of a novel chaperone-usher pili assembly system. *Microbiology* 149, 3473–3484 (2003).
 136. Choi, A. H. K., Slamti, L., Avci, F. Y., Pier, G. B. & Maira-Litrán, T. The *pgaABCD* locus of *Acinetobacter baumannii* encodes the production of poly- β -1-6-*N*-acetylglucosamine, which is critical for biofilm formation. *J. Bacteriol.* 191, 5953–5963 (2009).
 137. Xiao, Z. & Xu, P. Acetoin metabolism in bacteria. *Crit. Rev. Microbiol.* 33, 127–140 (2007).
 138. Tolner, B., Ubbink-Kok, T., Poolman, B. & Konings, W. N. Characterization of the proton/glutamate symport protein of *Bacillus subtilis* and its functional expression in *Escherichia coli*. *J. Bacteriol.* 177, 2863–2869 (1995).
 139. Noinaj, N., Guillier, M., Barnard, T. J. & Buchanan, S. K. TonB-dependent transporters: Regulation, structure, and function. *Annu. Rev. Microbiol.* 64, 43–60 (2010).
 140. Atamna, H. & Ginsburg, H. Heme degradation in the presence of glutathione. *J. Biol. Chem.* 270, 24876–24883 (1995).
 141. Sinclair, P. R., Gorman, N. & Jacobs, J. M. Measurement of heme concentration. *Curr. Protoc. Toxicol.* 00, 8.3.1–8.3.7 (1999).
 142. Quiroz-Segoviano, R. I. Y. *et al.* On tuning the fluorescence emission of

- porphyrin free bases bonded to the pore walls of organo-modified silica. *Molecules* 19, 2261–2285 (2014).
143. Huang, W., Liu, Q., Zhu, E. Y., Shindi, A. A. F. & Li, Y. Q. Rapid simultaneous determination of protoporphyrin IX, uroporphyrin III and coproporphyrin III in human whole blood by non-linear variable-angle synchronous fluorescence technique coupled with partial least squares. *Talanta* 82, 1516–1520 (2010).
 144. Shepherd, M. & Dailey, H. A. A continuous fluorimetric assay for protoporphyrinogen oxidase by monitoring porphyrin accumulation. *Anal. Biochem.* 344, 115–121 (2005).
 145. Mancini, S. & Imlay, J. Bacterial porphyrin extraction and quantification by LC/MS/MS Analysis. *Bio-Protocol* 5, 1–4 (2015).
 146. Kwon, S. J., De Boer, A. L., Petri, R. & Schmidt-Dannert, C. High-level production of porphyrins in metabolically engineered *Escherichia coli*. Systematic extension of a pathway assembled from overexpressed genes involved in heme biosynthesis. *Appl. Environ. Microbiol.* 69, 4875–4883 (2003).
 147. Mike, L. A. *et al.* Activation of heme biosynthesis by a small molecule that is toxic to fermenting *Staphylococcus aureus*. *Proc. Natl. Acad. Sci. U. S. A.* 110, 8206–8211 (2013).
 148. Zhang, J., Kang, Z., Chen, J. & Du, G. Optimization of the heme biosynthesis pathway for the production of 5-aminolevulinic acid in *Escherichia coli*. *Sci. Rep.* 5, 8584 (2015)
 149. Morales, E. H. *et al.* Accumulation of heme biosynthetic intermediates contributes to the antibacterial action of the metalloid tellurite. *Nat. Commun.* 8, 15320 (2017).
 150. Salas, J. R., Jaber-Douraki, M., Wen, X. & Volkova, V. V. Mathematical modeling of the “inoculum effect”: Six applicable models and the MIC advancement point concept. *FEMS Microbiol. Lett.* 367, 1–12 (2020).
 151. Dewachter, L., Herpels, P., Verstraeten, N., Fauvart, M. & Michiels, J. Reactive oxygen species do not contribute to O₂gE*-mediated programmed cell death. *Sci. Rep.* 6, 1–8 (2016).
 152. Vestergaard, M. *et al.* Novel pathways for ameliorating the fitness cost of gentamicin resistant small colony variants. *Front. Microbiol.* 7, 1–12 (2016).

153. Anderson, S. E., Sherman, E. X., Weiss, D. S. & Rather, P. N. Aminoglycoside heteroresistance in *Acinetobacter baumannii* AB5075. *mSphere* 3, 1–12 (2018).
154. Tsai, C. J. Y., Loh, J. M. S. & Proft, T. *Galleria mellonella* infection models for the study of bacterial diseases and for antimicrobial drug testing. *Virulence* 7, 214–229 (2016).
155. Junqueira, J. *et al.* Recent advances in the use of *Galleria mellonella* model to study immune responses against human pathogens. *J. Fungi* 4, 128 (2018).
156. Wojda, I. Immunity of the greater wax moth *Galleria mellonella*. *Insect Sci.* 24, 342–357 (2017).
157. Peleg, A. Y. *et al.* *Galleria mellonella* as a model system to study *Acinetobacter baumannii* pathogenesis and therapeutics. *Antimicrob. Agents Chemother.* 53, 2605–2609 (2009).
158. Thöny-Meyer, L. Biogenesis of respiratory cytochromes in bacteria. *Microbiol. Mol. Biol. Rev.* 61, 337–376 (1997).
159. Ramsey, M., Hartke, A. & Huycke, M. The physiology and metabolism of *Enterococci*. in *Enterococci: From Commensals to Leading Causes of Drug Resistant Infection* 1–55 (2014).
160. Tyanova, S. *et al.* The Perseus computational platform for comprehensive analysis of (prote)omics data. *Nat. Methods* 13, 731–740 (2016).
161. Bogdanovich, T., Ednie, L. M., Shapiro, S. & Appelbaum, P. C. Antistaphylococcal activity of ceftobiprole, a new broad-spectrum cephalosporin. *Antimicrob. Agents Chemother.* 49, 4210–4219 (2005).
162. Bankevich, A. *et al.* SPAdes: A new genome assembly algorithm and its applications to single-cell sequencing. *J. Comput. Biol.* 19, 455–477 (2012).
163. Langmead, B. & Salzberg, S. L. Fast gapped-read alignment with Bowtie 2. *Nat. Methods* 9, 357–359 (2012).
164. Li, H. *et al.* The sequence alignment/map format and SAMtools. *Bioinformatics* 25, 2078–2079 (2009).
165. Li, H. A statistical framework for SNP calling, mutation discovery, association mapping and population genetical parameter estimation from sequencing data. *Bioinformatics* 27, 2987–2993 (2011).
166. Kaas, R. S., Leekitcharoenphon, P., Aarestrup, F. M. & Lund, O. Solving the

- problem of comparing whole bacterial genomes across different sequencing platforms. *PLoS One* 9, 1–8 (2014).
167. Seemann, T. Prokka: Rapid prokaryotic genome annotation. *Bioinformatics* 30, 2068–2069 (2014).
 168. Odds, F. C. Synergy, antagonism, and what the checkerboard puts between them. *J. Antimicrob. Chemother.* 52, 1 (2003).
 169. Tipton, K. A., Dimitrova, D. & Rather, P. N. Phase-variable control of multiple phenotypes in *Acinetobacter baumannii* strain AB5075. *J. Bacteriol.* 197, 2593–2599 (2015).
 170. Tatsuta, K. Alpha-substituted vinyltin compound. 23–27 (2009).
 171. Kwong, C. K. W., Huang, R., Zhang, M., Shi, M. & Toy, P. H. Bifunctional polymeric organocatalysts and their application in the cooperative catalysis of Morita-Baylis-Hillman reactions. *Chem. - A Eur. J.* 13, 2369–2376 (2007).
 172. Dixon, L. I. *et al.* Unprecedented regiochemical control in the formation of aryl[1,2-a]imidazopyridines from alkynyliodonium salts: Mechanistic insights. *Org. Biomol. Chem.* 11, 5877–5884 (2013).
 173. Lee, B. *et al.* Design, synthesis and biological evaluation of photoaffinity probes of antiangiogenic homoisoflavonoids. *Bioorganic Med. Chem. Lett.* 26, 4277–4281 (2016).
 174. Salvo, M. L., Budisa, N. & Contestabile, R. PLP-dependent enzymes: A powerful tool for metabolic synthesis of non-canonical amino acids. *Beilstein Bozen Symp. Mol. Eng. Control* 27–66 (2013).
 175. Percudani, R. & Peracchi, A. A genomic overview of pyridoxal-phosphate-dependent enzymes. *EMBO Rep.* 4, 850–854 (2003).
 176. Schneider, G., Käck, H. & Lindqvist, Y. The manifold of vitamin B₆ dependent enzymes. *Structure* 8, 1–6 (2000).
 177. Eliot, A. C. & Kirsch, J. F. Pyridoxal phosphate enzymes: Mechanistic, structural, and evolutionary considerations. *Annu. Rev. Biochem.* 73, 383–415 (2004).
 178. Kappes, B., Tews, I., Binter, A. & MacHeroux, P. PLP-dependent enzymes as potential drug targets for protozoan diseases. *Biochim. Biophys. Acta - Proteins Proteomics* 1814, 1567–1576 (2011).
 179. Amadasi, A. *et al.* Pyridoxal 5-phosphate enzymes as targets for therapeutic

- agents. *Curr. Med. Chem.* 14, 1291–1324 (2007).
180. Strominger, J. L., Ito, E. & Threnn, R. H. Competitive inhibition of enzymatic reactions by oxamycin. *J. Am. Chem. Soc.* 82, 998–999 (1960).
 181. Sassetti, C. M., Boyd, D. H. & Rubin, E. J. Genes required for mycobacterial growth defined by high density mutagenesis. *Mol. Microbiol.* 48, 77–84 (2003).
 182. El Qaidi, S. *et al.* The vitamin B₆ biosynthesis pathway in *Streptococcus pneumoniae* is controlled by pyridoxal 5'-phosphate and the transcription factor PdxR and has an impact on ear infection. *J. Bacteriol.* 195, 2187–2196 (2013).
 183. Grubman, A. *et al.* Vitamin B₆ is required for full motility and virulence in *Helicobacter pylori*. *MBio* 1, 1–9 (2010).
 184. Dick, T., Manjunatha, U., Kappes, B. & Gengenbacher, M. Vitamin B₆ biosynthesis is essential for survival and virulence of *Mycobacterium tuberculosis*. *Mol. Microbiol.* 78, 980–988 (2010).
 185. Kelly, R. C. *et al.* The *Vibrio cholerae* quorum-sensing autoinducer CAI-1: Analysis of the biosynthetic enzyme CqsA. *Nat. Chem. Biol.* 5, 891–895 (2009).
 186. Di Salvo, M. L., Contestabile, R. & Safo, M. K. Vitamin B₆ salvage enzymes: Mechanism, structure and regulation. *Biochim. Biophys. Acta - Proteins Proteomics* 1814, 1597–1608 (2011).
 187. Richts, B., Rosenberg, J. & Commichau, F. M. A survey of pyridoxal 5'-phosphate-dependent proteins in the gram-positive model bacterium *Bacillus subtilis*. *Front. Mol. Biosci.* 6, (2019). doi: 10.3389/fmolb.2019.00032.
 188. Kästner, U., Hallmen, C., Wiese, M., Leistner, E. & Drewke, C. The human pyridoxal kinase, a plausible target for ginkgotoxin from *Ginkgo biloba*. *FEBS J.* 274, 1036–1045 (2007).
 189. Safo, M. K. *et al.* Crystal structure of the pdxY protein from *Escherichia coli*. *J. Bacteriol.* 186, 8074–8082 (2004).
 190. Safo, M. K. *et al.* Crystal structure of pyridoxal kinase from the *Escherichia coli* pdxK Gene: Implications for the classification of pyridoxal kinases. *J. Bacteriol.* 188, 4542–4552 (2006).
 191. Yang, Y., Tsui, H. C. T., Man, T. K. & Winkler, M. E. Identification and function of the pdxY gene, which encodes a novel pyridoxal kinase involved in the salvage

- pathway of pyridoxal 5'-phosphate biosynthesis in *Escherichia coli* K-12. *J. Bacteriol.* 180, 1814–1821 (1998).
192. Kim, M. Il & Hong, M. Crystal structure and catalytic mechanism of pyridoxal kinase from *Pseudomonas aeruginosa*. *Biochem. Biophys. Res. Commun.* 478, 300–306 (2016).
193. Nodwell, M. B., Koch, M. F., Alte, F., Schneider, S. & Sieber, S. A. A subfamily of bacterial ribokinases utilizes a hemithioacetal for pyridoxal phosphate salvage. *J. Am. Chem. Soc.* 136, 4992–4999 (2014).
194. Nodwell, M. B., Menz, H., Kirsch, S. F. & Sieber, S. A. Rugulactone and its analogues exert antibacterial effects through multiple mechanisms including inhibition of thiamine biosynthesis. *ChemBioChem* 13, 1439–1446 (2012).
195. Park, J., Burns, K., Kinsland, C. & Begley, T. P. Characterization of two kinases involved in thiamine pyrophosphate and pyridoxal phosphate biosynthesis. *Society* 186, 1571–1573 (2004).
196. Ueda, T., Nakaya, K., Nagai, S., Sakakibara, J. & Murata, M. Synthese of dihydrodioxepinopyridines, dihydrodioxocinopyridines, and a dihydrooxazepinopyridine. *Chem. Pharm. Bull. (Tokyo)*. 38, 19–22 (1990).
197. Cravatt, B. F. Compositions and methods of modulating immune response. (2017).
198. Hoegl, A. *et al.* Mining the cellular inventory of pyridoxal phosphate-dependent enzymes with functionalized cofactor mimics. *Nat. Chem.* 10, 1234–1245 (2018).
199. Dale, T. J., Sather, A. C. & Rebek, J. Synthesis of novel aryl-1,2-oxazoles from ortho-hydroxyaryloximes. *Tetrahedron Lett.* 50, 6173–6175 (2009).
200. E. Müller, T. & Pleier, A.-K. Intramolecular hydroamination of alkynes catalysed by late transition metals. *J. Chem. Soc. Dalt. Trans.* 583 (1999). doi:10.1039/a808938h
201. Backus, K. M. *et al.* Proteome-wide covalent ligand discovery in native biological systems. *Nature* 534, 570–574 (2016).
202. Zanon, P. R. A., Lewald, L. & Hacker, S. M. Isotopically labeled desthiobiotin azide (isoDTB) tags enable global profiling of the bacterial cysteinome. *Angew. Chem. Int. Ed.* 59, 2829–2836 (2020).
203. Di Salvo, M. L., Hunt, S. & Schirch, V. Expression, purification, and kinetic

- constants for human and *Escherichia coli* pyridoxal kinases. *Protein Expr. Purif.* 36, 300–306 (2004).
204. Consortium, T. U. UniProt: A worldwide hub of protein knowledge. *Nucleic Acids Res.* 47, D506–D515 (2019).
205. Sasseti, C. M., Boyd, D. H. & Rubin, E. J. Comprehensive identification of conditionally essential genes in mycobacteria. *Proc. Natl. Acad. Sci. U. S. A.* 98, 12712–12717 (2001).
206. Cox, J. & Mann, M. MaxQuant enables high peptide identification rates, individualized p.p.b.-range mass accuracies and proteome-wide protein quantification. *Nat. Biotechnol.* 26, 1367–1372 (2008).
207. Scott, T. C. & Phillips, M. A. Characterization of *Trypanosoma brucei* pyridoxal kinase: purification, gene isolation and expression in *Escherichia coli*. *Mol. Biochem. Parasitol.* 88, 1–11 (1997).
208. Lebedev, A. A. *et al.* JLigand: A graphical tool for the CCP 4 template-restraint library. *Acta Crystallogr. Sect. D Biol. Crystallogr.* 68, 431–440 (2012).
209. Long, F. *et al.* AceDRG: A stereochemical description generator for ligands. *Acta Crystallogr. Sect. D Struct. Biol.* 73, 112–122 (2017).
210. Emsley, P., Lohkamp, B., Scott, W. G. & Cowtan, K. Features and development of Coot. *Acta Crystallogr. Sect. D* 66, 486–501 (2010).
211. Wang, N., Ozer, E. A., Mandel, M. J. & Hauser, A. R. Genome-wide identification of *Acinetobacter baumannii* genes necessary for persistence in the lung. *MBio* 5, 1–8 (2014).
212. Sievers, F. *et al.* Fast, scalable generation of high-quality protein multiple sequence alignments using Clustal Omega. *Mol. Syst. Biol.* 7, 539 (2011).

V. Appendix

Supplementary Table 1| Table gives detailed information on proteins above the set threshold from the ABPP experiments (Figure II-4). To determine essentiality, a transposon mutant library generated by Gallagher *et al.* was used.¹⁰⁰ For that, BLAST search was performed to assign homologous proteins in *A. baumannii* AB5075 (Program version BLASTP 2.10.1+, search limited to *A. baumannii* AB5075 (taxid:1116234), the resulting query coverage and percent identity are listed).^{101,102}

#	Uniprot ID (ATCC19606)	Protein	Order Locus Name (AB5075)	Query coverage	Percent identity	Essentiality	Competition
1	D0C6E6	Transcriptional regulator, HxlR family	ABUW_1714	100%	99%	No	Yes
2	D0C997	Copper-resistance protein, CopA family	ABUW_3228	100%	97%	No	No
3	D0CB00	3-ketoacyl-CoA thiolase	ABUW_3573	100%	100%	No	No
4	D0CDE0	Acetyl-CoA acetyltransferase	ABUW_0638	100%	99%	No	Yes
5	D0CBN6	Uncharacterized protein	ABUW_1015	100%	76%	No	No
6	D0C6H5	UDP-3-O-acylglucosamine N-acyltransferase	ABUW_1743	100%	100%	Yes	No
7	D0CAQ1	Catalase-peroxidase	ABUW_3469	100%	100%	No	Yes
8	D0CA28	Putative betaine-aldehyde dehydrogenase	ABUW_2942	100%	100%	No	No
9	D0CAP3	3-isopropylmalate dehydratase large subunit	ABUW_3463	93%	100%	No	No
10	D0CCP3	Pyridine nucleotide-disulfide oxidoreductase	ABUW_0299	100%	100%	No	No
11	D0CDA9	Uncharacterized protein	ABUW_0607	100%	98%	No	No

Supplementary Table 2| Resistance development during serial passaging in the presence of sub-MIC concentrations of antimicrobials. Ciprofloxacin (Cip) served as positive control. For Xan and Cip, the highest concentrations tested were 25 μM (100 fold MIC) and 800 μM (~ 100-fold MIC), respectively. The table contains all individual data from $n = 3$ independent experiments.

Day	Xan			Cip		
	Replicate A MIC [μM]	Replicate B MIC [μM]	Replicate C MIC [μM]	Replicate A MIC [μM]	Replicate B MIC [μM]	Replicate C MIC [μM]
1	0.25	0.25	0.25	16	8	8
2	0.50	0.50	0.5	64	32	16
3	1	0.5	0.5	128	32	64
4	1	1	1	500	128	64
5	2	2	2	>800	>500	256
6	2	2	2	>800	>800	500
7	>8	>8	>8	>800	>800	800
8	>25	>25	25	>800	>800	800
9	>25	>25	>25	>800	>800	>800
10	>25	>25	>25	>800	>800	>800
11	>25	>25	>25	>800	>800	>800

upstream gene variant			efflux RND transporter periplasmic adaptor subunit	-	-	-	+	+	+	-	-	-	-	-	-
disruptive inframe deletion	His174_Val177del	<i>acrR</i>	HTH-type transcriptional regulator AcrR	-	-	-	-	-	-	-	-	-	+	-	-
synonymous variant	His339His		5-(carboxyamino)imidazole ribonucleotide synthase	-	-	+	-	-	-	-	-	-	-	-	-
upstream gene variant		<i>grpE</i>	nucleotide exchange factor GrpE	-	-	-	+	-	-	-	-	-	-	-	-
downstream gene variant			helix-turn-helix domain-containing protein	-	-	-	+	+	-	-	-	-	-	-	-
downstream gene variant			helix-turn-helix domain-containing protein	-	-	-	+	-	-	-	-	-	-	-	-

Supplementary Table 4| Table containing detailed information on proteins upregulated in full proteome analysis of Xan-resistant mutants. For uncharacterized proteins, BLAST search was used to assign homologous proteins in *A. baumannii* AB5075 (Program version BLASTP 2.10.1+, search limited to *A. baumannii* AB5075 (taxid:1116234), query coverage and percent identity are listed), which has a higher annotation rate than *A. baumannii* ATCC19606.^{101,102}

Function	Proteins	UniProt ID (ATCC19606)	BLAST Search	Query Coverage	Percent Identity	Gene name (AB5075)
Acetoin metabolism	Acetoin:2,6-dichlorophenolindophenol oxidoreductase, alpha subunit	D0C7E8	-			
	Dihydrolipoyl dehydrogenase	D0C7E5	-			
	TPP-dependent acetoin dehydrogenase complex, E1 component, beta subunit	D0C7E7	-			
Redox enzyme	Uncharacterized protein	D0CAC1	Heme oxygenase-like protein	98%	99%	ABUW_3351
	Catalase	D0C8B2	-			
	Uncharacterized protein	D0C8B3	Heme oxygenase-like protein (Iron-containing redox enzyme family protein)	99%	99%	ABUW_2437
RND transporter	Efflux transporter, RND family, MFP subunit	D0CF95	-			
	RND transporter, HAE1/HME family, permease protein	D0CF96	-			
Biofilm formation	Fimbrial usher protein	D0C5T3	-			
	Protein CsuC	D0C5T2	-			
	Protein CsuE	D0C5T4	-			
	Spore Coat Protein U domain protein	D0C5T1	-			
	Poly-beta-1,6 N-acetyl-D-glucosamine export porin PgaA	D0C5Z9	-			
	Poly-beta-1,6-N-acetyl-D-glucosamine N-deacetylase PgaB	D0C600	-			

	Putative alpha,alpha-trehalose-phosphate synthase (UDP-forming)	D0C9J2	-			
	Trehalose 6-phosphate phosphatase	D0C9J3	-			
	Hep/Hag repeat protein	D0C9I2	-			
	OmpA family protein	D0C9I3	-			
	DUF4142 domain-containing protein	D0CFS8	-			
	FMN-dependent oxidoreductase, nitrilotriacetate monooxygenase family	D0C858	-			
	Oxidoreductase, short chain dehydrogenase/reductase family protein	D0C8B1	-			
	Reverse transcriptase domain-containing protein	D0CBF4	-			
	Rhs element Vgr protein	D0C9Y7	-			
	Transcriptional regulator, TetR family	D0C7Z9	-			
	Transcriptional regulator, TetR family	D0CAC2	-			
	Uncharacterized protein	D0C5R3	DUF2171 domain-containing protein	100%	100%	ABUW_1466
	Uncharacterized protein	D0C5R4	hypothetical protein	96%	99%	not found
	Uncharacterized protein	D0C692	DNA breaking-rejoining protein	100%	98%	ABUW_1659
	Uncharacterized protein	D0C8B0	Uncharacterized protein	100%	98%	ABUW_2434
	Uncharacterized protein	D0C8B6	hypothetical protein	100%	99%	ABUW_2440
	Uncharacterized protein	D0C9C4	no significant similarity found	-	-	-
	Uncharacterized protein	D0C9Y0	Rhs element Vgr protein, putative	11%	47 %	ABUW_2817
	Uncharacterized protein	D0CAU6	Chaperone modulatory protein CbpM (MerR HTH regulatory family protein)	100%	100%	ABUW_3516
	Uncharacterized protein	D0CE49	No significant similarity found	-	-	-
	Uncharacterized protein	D0CE50	No significant similarity found	-	-	-
	Uncharacterized protein	D0CFS7	17 kDa surface antigen	100%	96%	ABUW_2678

Supplementary Table 5| Table containing detailed information on proteins downregulated in full proteome analysis of Xan-resistant colonies. For uncharacterized proteins, BLAST search was used to assign homologous proteins in *A. baumannii* AB5075 (Program version BLASTP 2.10.1+, search limited to *A. baumannii* AB5075 (taxid:1116234), query coverage and percent identity are listed), which has a higher annotation rate than *A. baumannii* ATCC19606.^{101,102}

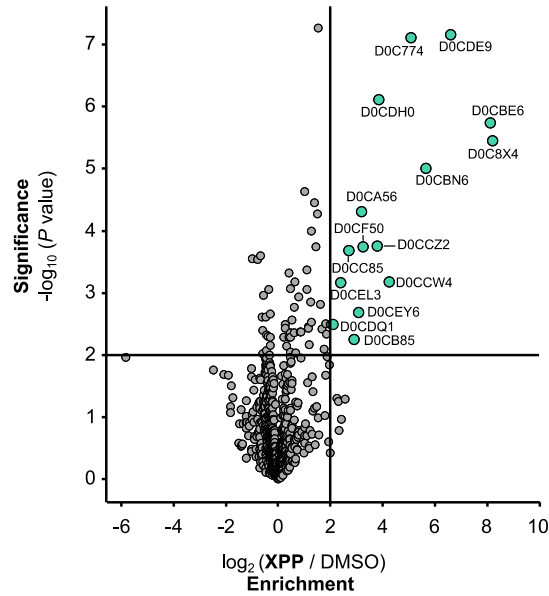
Proteins	UniProt ID (ATCC19606)	BLAST Search	Query Coverage	Percent Identity	Gene name (AB5075)
Toxin-antitoxin system, toxin component, Bro domain protein	D0C5H6	-			
Phosphomethylpyrimidine synthase	D0CB46	-			
Uncharacterized protein	D0CC98	Uncharacterized protein	100%	44%	ABUW_0742
Uncharacterized protein	D0CCB7	Uncharacterized protein	82%	54%	ABUW_1278
Uncharacterized protein	D0CCD2	Uncharacterized protein	83%	58%	ABUW_0781
Uncharacterized protein	D0CCD3	No significant similarity found			
Sulfate ABC transporter, sulfate-binding protein	D0CCM4	-			
Protein PilG	D0CDH8	-			
Uncharacterized protein	D0CDU2	Putative tail fiber	59%	66%	ABUW_0790
Uncharacterized protein (Fragment)	D0CDU3	Uncharacterized protein	100%	89%	ABUW_0791
Uncharacterized protein	D0CED4	Uncharacterized protein	31%	54%	ABUW_2662
Metallo-beta-lactamase domain protein	D0CF44	-			
Cytochrome b562	D0CG11	-			

Supplementary Table 6 | Table containing detailed information on proteins downregulated in full proteome analysis of Xan versus DMSO-treated *A. baumannii*. For uncharacterized proteins, BLAST search was used to assign homologous proteins *A. baumannii* AB5075 (Program version BLASTP 2.10.1+, search limited to *A. baumannii* AB5075 (taxid:1116234), query coverage and percent identity are listed), that has a higher annotation rate than *A. baumannii* ATCC19606.^{101,102}

#	Proteins	UniProt ID (ATCC19606)	BLAST Search	Query Coverage	Percent Identity	Gene name (AB5075)
1	Uncharacterized protein	D0CC95	hypothetical protein	100%	99%	ABUW_1256
2	Uncharacterized protein	D0CC98	hypothetical protein	100%	44%	ABUW_0742
3	Toxin-antitoxin system, toxin component, Bro domain protein	D0C5H6				
4	Uncharacterized protein	D0CDH3	YegP family protein	99%	100%	ABUW_0673
5	Transporter, branched chain amino acid: cation symporter (LIVCS) family protein	D0C8S3				
6	Aspartate racemase	D0C5W2				
7	Uncharacterized protein	D0CCB7	hypothetical protein	82%	54%	ABUW_1278
8	5-oxoprolinase subunit A	D0C8S2				
9	Uncharacterized protein	D0C8S0	5-oxoprolinase/urea amidolyase family protein	100%	97%	ABUW_2604
10	Metallo-beta-lactamase domain protein	D0CF44				
11	Cytochrome d ubiquinol oxidase, subunit II	D0C6M3				
12	Type VI secretion system lysozyme-related protein	D0C8P2				
13	Diacylglycerol kinase catalytic domain protein	D0CBD5				
14	Uncharacterized protein (Fragment)	D0C8P6	hypothetical protein	100%	100%	ABUW_2581
15	Uncharacterized protein	D0C773	hypothetical protein	100%	99%	not found

16	Molybdate ABC transporter, periplasmic molybdate-binding protein	D0C793				
17	Fumarylacetoacetase	D0CFD2				
18	Uncharacterized protein	D0CD61	hypothetical protein	100%	98%	ABUW_0514
19	Conserved TM helix	D0C9F9				
20	Putative hydrolyase	D0C8S1				

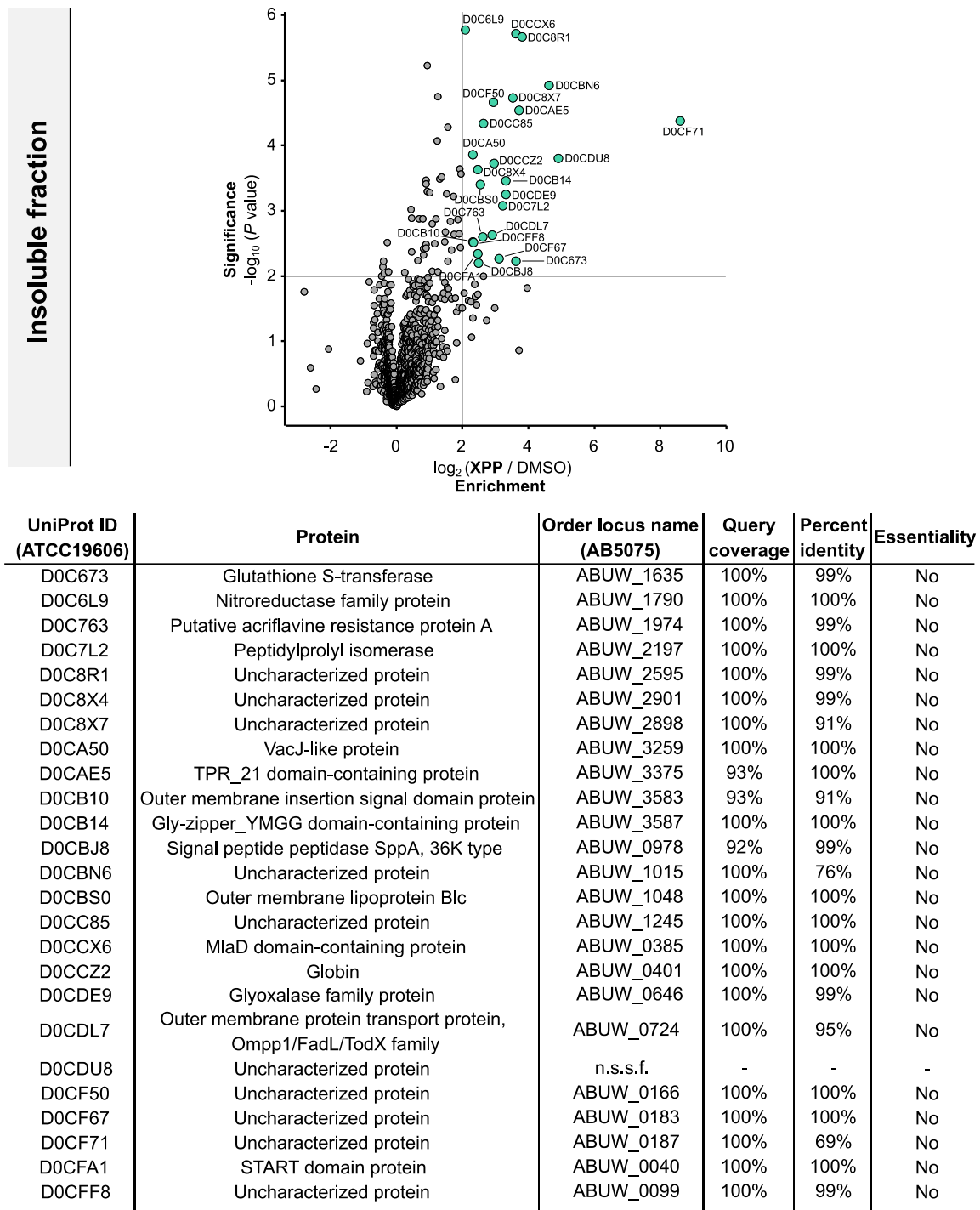
Soluble fraction



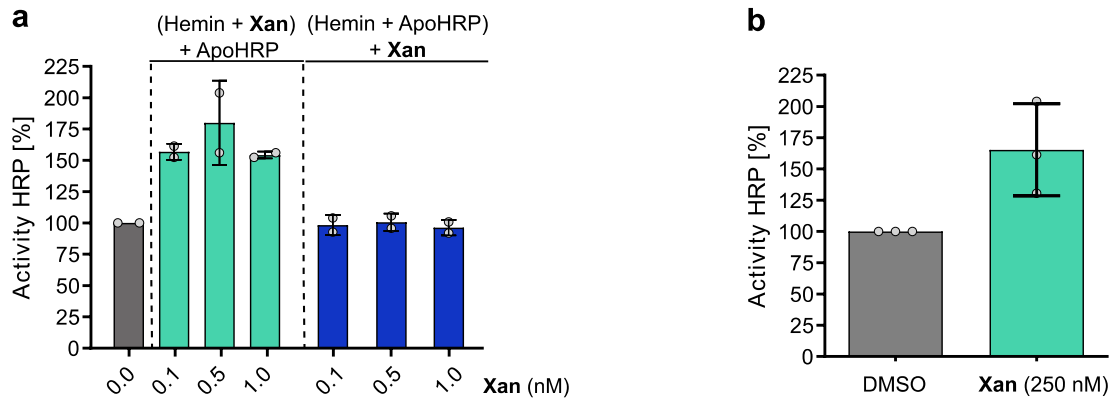
UniProt ID ATCC19606	Protein	Order locus name (AB5075)	Query coverage	Percent identity	Essentiality
D0C774	Catalase domain-containing protein	ABUW_2059	100%	98%	No
D0C8X4	Uncharacterized protein	ABUW_2901	100%	99%	No
D0CA56	Organic hydroperoxide resistance protein OhrB	ABUW_3265	100%	99%	No
D0CB85	Outer membrane porin, OprD family	ABUW_3685	100%	100%	No
D0CBE6	SCP2 domain-containing protein	ABUW_0927	100%	100%	No
D0CBN6	Uncharacterized protein	ABUW_1015	100%	76%	No
D0CC85	Uncharacterized protein	ABUW_1245	100%	100%	No
D0CCW4	Uncharacterized protein	A1S_3112 *	98%	100%	No*
D0CCZ2	Globin	ABUW_0401	100%	100%	No
D0CDE9	Glyoxalase family protein	ABUW_0646	100%	99%	No
D0CDH0	Putative toxin-antitoxin system, toxin component	ABUW_0667	100%	100%	No
D0CDQ1	Efflux pump membrane transporter	ABUW_0843	100%	100%	No
D0CEL3	Transcriptional regulator, Fur family	ABUW_3741	97%	100%	No
D0CEY6	Uncharacterized protein	n.s.s.f.	-	-	-
D0CF50	Uncharacterized protein	ABUW_0166	100%	100%	No

Supplementary Figure 1: Target identification by chemical proteomic profiling in *A. baumannii* ATCC19606 using XPP in soluble fraction. The volcano plot shows enrichment of proteins after treatment of *A. baumannii* cells with XPP (3 μ M) compared with DMSO on a \log_2 scale. The vertical and horizontal threshold lines represent a \log_2 enrichment ratio of 2 and a $-\log_{10}(P \text{ value})$ of 2 (two-sided two-sample *t*-test, $n = 4$ independent experiments per group), respectively. Table gives detailed information on proteins above the set threshold from the A β PP experiments. To determine essentiality, the transposon mutant library generated by Gallagher *et al.* was used.¹⁰⁰ For that, BLAST search was performed to assign homologous proteins in *A. baumannii* AB5075 (Program version BLASTP 2.10.1+, search limited to *A. baumannii* AB5075 (taxid:1116234), the resulting query coverage and percent identity are listed).^{101,102} * Essential gene list published by Wang *et al.* was used to determine essentiality and BLAST search was limited to *A. baumannii* ATCC17978 (taxid: 400667, program version BLASTP 2.10.1+, query coverage and percent identity are listed).²¹¹ Proteins, for which BLAST search did not find any proteins significantly similar

to proteins in *A. baumannii* AB5075 or *A. baumannii* ATCC17978 (no significant similarity found – n.s.f.), cannot be categorized according to essentiality.



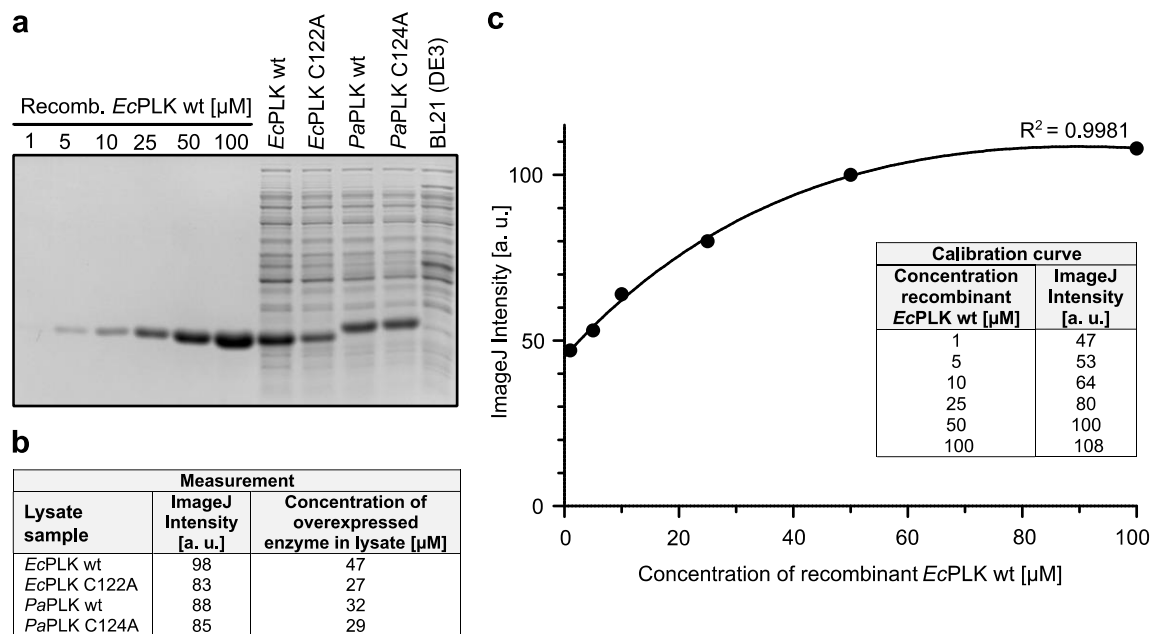
Supplementary Figure 2: Target identification by chemical proteomic profiling in *A. baumannii* ATCC19606 using XPP in insoluble fraction. A/BPP experiment using XPP in *A. baumannii* ATCC19606 in insoluble fraction. The volcano plot shows enrichment of proteins after treatment of *A. baumannii* cells with XPP (3 μ M) compared with DMSO on a \log_2 scale. The vertical and horizontal threshold lines represent a \log_2 enrichment ratio of 2 and a



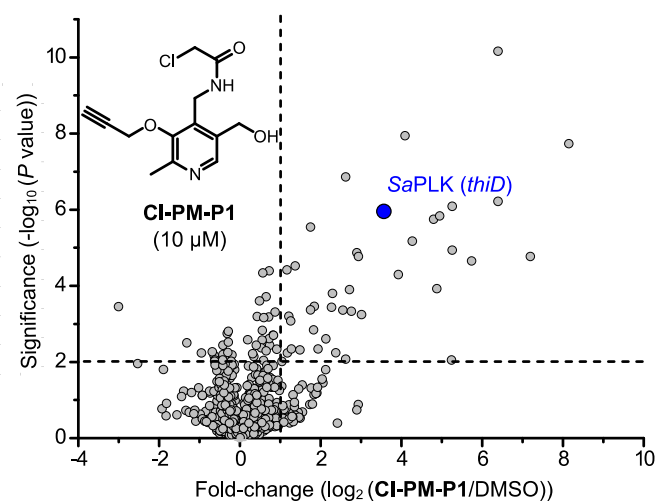
Supplementary Figure 4: *In vitro* activity assay of reconstituted holoHRP in the presence of sub-equivalent concentrations of Xan compared to hemin. a) Hemin (5 nM) was pre-incubated with either Xan (green bars) or apoHRP (blue, 5 μ M) followed by addition of apoHRP (5 μ M) or Xan, respectively and activity of holoHRP was subsequently measured. Averaged technical duplicates were normalised to the respective DMSO-treated samples and values represent mean \pm s.d. of independent experiments ($n = 2$). b) Reconstitution activity assay of holoHRP in *A. baumannii* cell lysate after treatment of intact cells with either 250 nM Xan or DMSO for 30 min. Cell lysates (2.5 μ g protein) were pre-incubated with apoHRP (final concentration 10 μ M) for 10 min at 4 $^{\circ}$ C and the activity of resulting holoHRP was measured. Lysates without apoHRP added were used as blank control. Averaged technical quadruplicates were normalised to the respective DMSO-treated samples and value represents mean \pm s.d. of independent experiments ($n = 3$).

<i>Staphylococcus aureus</i> A0A0H2XGZ0	-MALKKVLTIAGSDTSAGAGMQADLKTQELDT-----YGMVALTAIVTMDK-DTWSH	51
<i>Enterococcus faecalis</i> Q839G7	---MEKVLTIAGSDSTGGAGIQADLKTFFEEYGV-----FGFSSLTSIVTMDPTIGWSH	50
<i>Bacillus subtilis</i> P39610	-MSMHKALTIAGSDSSGGAGIQADLKTQEKV-----YGMALTIVVAMPDNNNSWNH	52
<i>Listeria monocytogenes</i> Q8Y971	-MTIKKTLTIAGSDSSGGAGLQADLKTFFEEYGT-----YGFSAITTIIVTMDPDNNWAH	52
<i>Escherichia coli</i> P77150	--MMKNLILAIQSHVVYGHAGNSAAEFPMRRLGANVWPLNTVQFSNHT-----QYG-KWTF	52
<i>Pseudomonas aeruginosa</i> Q9HT57	MPRTPHLLAIQSHVVYGHAGNSAAVFPQRIGINWVPLNTVQFSNHT-----QYG-RWTF	54
<i>Vibrio vulnificus</i> Q8D4Q2	---MQGILSIQSHVYAGHAGNSAVFPQRMGFVWPIHTVQFSNHT-----QYQEGWTF	52
<i>Salmonella typhimurium</i> Q8ZPM8	---MKNLILAIQSHVVYGHAGNSAAEFPMRRLGANVWPLNTVQFSNHT-----QYG-KWTF	51
<i>Homo sapiens</i> O00764	MEEECRVLSIQSHVIRGYVGNRAATFPLQVLGFEIDAVNSVQFSNHT-----GYA-HWKG	54
	: . . . * : : . . . *	
<i>Staphylococcus aureus</i> A0A0H2XGZ0	DVTPLPMD-VFEKQLETALS-IGPDAIKTGLMGTTEEIIKRAGEVVEASN----AQYFVVD	105
<i>Enterococcus faecalis</i> Q839G7	EVTELPET-LLEKQLISVFAGGPPVAALKTGMMGNEQNIKMASKYIKQEK----IQKVVVD	105
<i>Bacillus subtilis</i> P39610	QVFPIDTD-TTRAQLATITDGIQVDAMKTGMLPTVDIIELAAKTIKEKQ----LKNVVVD	107
<i>Listeria monocytogenes</i> Q8Y971	GVTPIDAQ-LVREQLKTIILSGGPPVAMKTGMLGSEIIEIKATREAIKDYD----LKNVVVD	107
<i>Escherichia coli</i> P77150	CVMPPSHLTEIVQGIATDKLHTCDAVLSGYLGSAAEQGEHILGIVRQVKAANPQAKYFCD	112
<i>Pseudomonas aeruginosa</i> Q9HT57	QVLPPEIGIPALVDGIAGIGELGNCDAVLSGYLGSAAQGRAILDVVARLQANPRALYLCD	114
<i>Vibrio vulnificus</i> Q8D4Q2	RAFSAADDISELVRGLNINIGALEKCAQVLTGYQGSAAEQCLAVEETVTKVQKQANPDALYVCD	112
<i>Salmonella typhimurium</i> Q8ZPM8	CVMPPSHLTEIVQGIADIGQLAHCDAVLSGYLGSAAEQGEHILGIVRQVKAANPQAKYFCD	111
<i>Homo sapiens</i> O00764	QVLNSDELQLEYELR-LNNMKNKYDYVLTGYTRDKSFLAMVVDIVQELKQNPRLVYVCD	113
 : : * *	
	Lid-Cys	
<i>Staphylococcus aureus</i> A0A0H2XGZ0	PVMVCKGEDE---VLNPGNTEAMIKYLLPKATVVTNPLFEAGQLSGLGKLNIEDMKKAA	162
<i>Enterococcus faecalis</i> Q839G7	PVIACKGTAQ---ILQPKSVEGLKNDLPLALVATPNLIEAGILSGLGEISSVAEMEEAA	162
<i>Bacillus subtilis</i> P39610	PVMVCKGANE---VLYPEHAQALREQLAPLATVITPNLFEASQLSGMDELKTVDDMIEAA	164
<i>Listeria monocytogenes</i> Q8Y971	PVMVCKGEDE---LIQPENAEAIRDLLLPKATITTPNLFEEAGQLSGLGKLTLLDDMKAAA	164
<i>Escherichia coli</i> P77150	PVMGHPEKGC---IVAPGVAEFHVRHGLPASDI IAPNLEVELEILCEH-AVNNVEEAVLAA	168
<i>Pseudomonas aeruginosa</i> Q9HT57	PVMGHPEKGC---IVAPEVDFLLEEAADVLYLCPNQLLELDSFCDR-QPNSLADCVEMA	170
<i>Vibrio vulnificus</i> Q8D4Q2	PVMGAPDKGC---IVAPGIAENLNLNRLMPMADVIVPNQFELSQFAEM-EIHTLDDAI IAC	168
<i>Salmonella typhimurium</i> Q8ZPM8	PVMGHPEKGC---IVAPGVAEFHVRYPALPASDI IAPNLELELEILSKH-SVNNVDDAVQAA	167
<i>Homo sapiens</i> O00764	PVLGDKWDGEGSMVPEDDLVPVYKEKVVPLADIITPNQFEAELLSGR-KIHSQEEALRVM	172
	** : : : * * * *	
<i>Staphylococcus aureus</i> A0A0H2XGZ0	TIIFDKGAQHVIIKGGKAL--DQDKSYDLYYDGQTFYQ-----LTTDMFQ---QSYNHG	211
<i>Enterococcus faecalis</i> Q839G7	KRIVQMGAKHVVVVGGHRL--AGEKALDLFYDGHTAHL-----LENELYP---TDYNHG	211
<i>Bacillus subtilis</i> P39610	KKIHALGAQYVVITGGGKL--KHEKAVDVLVDGETAEV-----LESEMID---TPYTHG	213
<i>Listeria monocytogenes</i> Q8Y971	KKIIELGAKYVVIKGGKAL--ESDKAIDLVDYDGKEFTI-----YEVEKIS---PSHNHG	213
<i>Escherichia coli</i> P77150	RELIAQGPQLVVLVKHLARAGYSRDRFEMLLVTADEAWH-----ISRPLVDFG--MRQPVG	221
<i>Pseudomonas aeruginosa</i> Q9HT57	RSLLRGPRAILVHNLNYPGKAGDTFEMLLVAADQAWH-----LQRPLLAFP---RQPVG	222
<i>Vibrio vulnificus</i> Q8D4Q2	QRALAKGPKVVLVVKHLYC--LSDESFNMLLATQEGTYL-----AKRPHFEFA---KAPVG	218
<i>Salmonella typhimurium</i> Q8ZPM8	RELIAQGPQLVVLVKHLARAGYSRDRFEMLLVTAQEAWH-----ISRPLVDFG--SRQPVG	220
<i>Homo sapiens</i> O00764	DMLHSMGPDVTVVITSSDLPSPQGSNYLIVLGSQRRRNPAGSVVMERIMDIRKVDVAVFG	232
	* : : : : * *	
	Base	
<i>Staphylococcus aureus</i> A0A0H2XGZ0	AGCTFAAATTAYLANGSKPKEAVIS--AKAFVASAIKNGWKMNDVFGVPDHDGAYNR----	265
<i>Enterococcus faecalis</i> Q839G7	AGCTFSAAITAGLAKGYSVLEAVTL--AKKFVAAAIAKHGIQVNPVYGVHVVHGHAYTH----	265
<i>Bacillus subtilis</i> P39610	AGCTFSAAVTAELAKGAEVKEAIYA--AKEFTAAIKESFPNLQYVGPPTKHSALRL----	267
<i>Listeria monocytogenes</i> Q8Y971	AGCTFAAATAGLAKGLTVEGAVAK--AKDFVTAIAKGGFALNEFIVVHGHAYNR----	267
<i>Escherichia coli</i> P77150	VGDVTSGLLVKLLQGGATLQE-----ALEHVTAAVYEIMVTTKAMQE-----	263
<i>Pseudomonas aeruginosa</i> Q9HT57	VGLASGLFSLRLLGLDGLRN-----AFEFTHGAAVHEVLELLELQACGS-----	264
<i>Vibrio vulnificus</i> Q8D4Q2	AGDLISAI FTAGLLKGWTPKQ-----AFQCHDACYGVLNATYQAGE-----	260
<i>Salmonella typhimurium</i> Q8ZPM8	VGDVTSGLLVKLLQGGATLQO-----ALEHVTAAVYEMIMATKTMQE-----	262
<i>Homo sapiens</i> O00764	TGDLFAA-----MLLAWTHKHPNPKVACERTVSTLHHVLRQTIQCAKAQAGEGVRPSPM	287
	* : : *	
<i>Staphylococcus aureus</i> A0A0H2XGZ0	-----IEHIDVEVTEV-----	276
<i>Enterococcus faecalis</i> Q839G7	-----AEQMRMKA-----	274
<i>Bacillus subtilis</i> P39610	-----NQQS-----	271
<i>Listeria monocytogenes</i> Q8Y971	-----AENR-----	271
<i>Escherichia coli</i> P77150	-YELQVVAQDRIAKPEHYFSATKL-----	287
<i>Pseudomonas aeruginosa</i> Q9HT57	-YELELVRAQDRIAHPRVRFDAVRL-----	288
<i>Vibrio vulnificus</i> Q8D4Q2	-WELQTIAAQQEFVEPSKHFPLEEVTLKTFE	290
<i>Salmonella typhimurium</i> Q8ZPM8	-YELQVVAQDRIANPEHYFSATRL-----	286
<i>Homo sapiens</i> O00764	QLELRMVQSKRDIEDPEIVVQATVLE-----	312

Supplementary Figure 5: Multiple sequence alignment of putative PL kinases highlighting lid cysteines (Cys) (green) and catalytic bases Cys (C) and Asp (D) (blue) using Clustal O (1.2.4).²¹² Sequences of *S. aureus* USA300 (UniProt ID: A0A0H2XGZ0, SaPLK), *E. faecalis* V583 (UniProt ID: Q839G7, EfPLK), *B. subtilis* 168 (UniProt ID: P39610), *L. monocytogenes* EGD-e (UniProt ID: Q8Y971), *E. coli* K12 (UniProt ID: P77150, EcPLK), *P. aeruginosa* PAO1 (UniProt ID: Q9HT57, PaPLK), *V. vulnificus* CMCP6 (UniProt ID: Q8D4Q2), *S. typhimurium* LT2 (UniProt ID: Q8ZPM8) and *Homo sapiens* (UniProt ID: O00764, hPLK) were aligned.



Supplementary Figure 6: Determining the concentration of overexpressed PLKs in lysate using ImageJ. a) Gel containing varying concentrations of recombinant *EcPLK wt* as well as overexpressed PLK lysates. b) Gray values for recombinant enzyme bands were analysed using ImageJ and a calibration curve was calculated. c) Calibration curve was used to determine the protein concentration of PLKs in lysates.



Supplementary Figure 7: The volcano plots show enrichment of proteins after treatment (24 h) of *S. aureus* cells with CI-PM-P1 (10 μM) on a \log_2 scale. The vertical and horizontal threshold lines represent a \log_2 enrichment ratio of 1 and a $-\log_{10}(P \text{ value})$ of 2 (two-sided two-sample *t*-test, $n = 4$ independent experiments per group), respectively.